1996

Air mixing criteria for ceiling slot-ventilated agricultural enclosures

Hsin Yu
Iowa State University

INFORMATION TO USERS

This manuscript has been reproduced from the microfilm master. UMI films the text directly from the original or copy submitted. Thus, some thesis and dissertation copies are in typewriter face, while others may be from any type of computer printer.

The quality of this reproduction is dependent upon the quality of the copy submitted. Broken or indistinct print, colored or poor quality illustrations and photographs, print bleedthrough, substandard margins, and improper alignment can adversely affect reproduction.

In the unlikely event that the author did not send UMI a complete manuscript and there are missing pages, these will be noted. Also, if unauthorized copyright material had to be removed, a note will indicate the deletion.

Oversize materials (e.g., maps, drawings, charts) are reproduced by sectioning the original, beginning at the upper left-hand corner and continuing from left to right in equal sections with small overlaps. Each original is also photographed in one exposure and is included in reduced form at the back of the book.

Photographs included in the original manuscript have been reproduced xerographically in this copy. Higher quality 6" x 9" black and white photographic prints are available for any photographs or illustrations appearing in this copy for an additional charge. Contact UMI directly to order.

UMI

A Bell & Howell Information Company
300 North Zeeb Road, Ann Arbor MI 48106-1346 USA
313/761-4700 800/521-0600

Air mixing criteria for ceiling slot-ventilated agricultural enclosures

by

Hsin Yu

A dissertation submitted to the graduate faculty
in partial fulfillment of the requirement for the degree of
DOCTOR OF PHILOSOPHY

Department: Agricultural and Biosystems Engineering
Major: Agricultural Engineering
Major Professor: Steven J. Hoff

Iowa State University
Ames, Iowa
1996

Graduate College
Iowa State University

This is to certify that the doctoral dissertation of

Hsin Yu

has met the dissertation requirements of Iowa State University

Signature was redacted for privacy.

Major Professor

Signature was redacted for privacy.

For the Major Department

Signature was redacted for privacy.

For the Graduate College

TABLE OF CONTENTS

LIST OF FIGURES

LIST OF TABLES

NOMENCLATURE

SYMBOLS

a = degree of turbulence of the air

A = area (m^2)

A_0, A_1 = experimentally determined coefficients

Ar = Archimedes number defined as $\frac{\beta g h (T_f - T_d)}{U_d^2}$

Ar_c = corrected Archimedes number defined as $\frac{C_d g b h W H (T_w - T_d)}{(546 + T_w + T_d) Q^2}$

Ar_w = wall jet Archimedes number defined as $\frac{\beta g (T_f - T_d) H L_p}{h U_d^2}$

b = diffuser length (m)

C = throw constant of free plane jet

C_d = discharge coefficient

C_w = throw constant of plane wall jet

d = hydraulic diameter of plane wall jet defined as $\frac{2bh}{b+h}$ (m)

D = hydraulic diameter defined as $\frac{2WH}{W+H}$ (m)

Eu = Euler number defined as $\frac{2\Delta P}{\rho U^2}$

Fr = Froude number defined as $\frac{U}{\sqrt{gL}}$

g = gravitational acceleration rate (m/s^2)

h = diffuser width (m)

H = room height (m)

I_o = jet momentum function defined by Kaul et al. (1975) ($kg/m^2\text{-}s^2$)

J = jet momentum number defined as $\frac{QU_d}{gV}$

K = turbulent kinetic energy (m^2/s^2)

K_{rm} = ratio of maximum velocity at reverse flow to maximum velocity at end wall

L = room length (m)

L_p = penetration distance defined by Adre and Albright (1994), see Figure 3.4 (m)

L_{pn} = penetration distance defined by Kaul et al. (1975), see Figure 3.4 (m)

L_{max} = maximum penetration distance (m)

m = mixing number defined as $\frac{h}{D} \approx 0.2$

n = geometry scale ratio of prototype to model

P = thermodynamic pressure (Pa)

Pe = Peclet number defined as $\frac{UL}{\alpha}$

Pr = Prandtl number defined as $\frac{\alpha}{\nu}$

q = heat transfer rate (w)

Q = ventilation rate (m^3/s)

Q_e = entrainment (m^3/s)

Re = Reynolds number, defined as $\frac{hU_d}{\nu}$

Rm = inlet jet momentum ratio defined as $\frac{hU_d^2}{L+H}$ (m^2/s^2)

T, t = mean temperature and fluctuation component (°C)

ΔT = $T_f - T_d$ (°C)

TI = turbulent intensity

U, u = mean air velocity and fluctuation component (m/s)

V = room volume (m^3)

W = room depth (m)

x = horizontal distance from inlet wall (m)

x_o = the additional distance to the virtual origin of jet (m)

y = vertical distance from solid boundary (m)

$y_{1/2}$ = vertical distance at which airspeed is one half maximum airspeed (m)

GREEK SYMBOLS

α = thermal diffusion coefficient, (m^2/s)

β = thermal expansion coefficient defined as $\frac{1}{(T_f + T_d)/2}$, (1/K)

δ_{i2} = kronecker delta function($\delta_{i2} = 1$ if i= 2 and $\delta_{i2} = 0$ if i≠2)

η = ratio of y to $y_{1/2}$

λ = bulk viscosity (N s/m^2)

ν = kinematic viscosity, (m^2/s)

μ = dynamic viscosity (N s/m^2)

ρ = density of air, (kg/m^3)

∇ = divergence

SUBSCRIPTS

b = pig body

c = characteristic scales

d = diffuser

e = entrainment

f = floor

i, j = indices representing direction of coordinates (i, j = 1,2,3, referring to longitudinal, vertical and lateral coordinates)
jt = jet throw
m = model
max = maximum
mean = mean of floor region
o = outside of room
p = prototype
rm = maximum at reverse flow
w = wall
∞ = ambient

SUPERSCRIPTS

* = non-dimensionlized variable
$\bar{}$ = denotes average component

ABSTRACT

The use of a scale-model is an effective technique to predict the performance of ventilation in full-scale prototypes. Many criteria have been proposed to simulate the behavior of airflow between scale-model and prototype. Because of the inconsistent results of past proposed similarity criteria, more validation work is needed to clarify the conflicts.

Dimensional analysis using both the Buckingham Pi method and manipulating the governing differential equations was used to theoretically establish similarity parameters. Only partially similarity was reached since conflicts exist between proposed similarity parameters.

Experiments of two scale models were conducted to study airflow similarity in ceiling slot-ventilated agricultural enclosures using different similarity criteria. The evaluation of similarity between scale-model and prototype included validation of penetration distance, airflow pattern, airspeed field, and temperature field using methods that included smoke visualization, airspeed field measurement, and temperature field measurement.

The studies focused on the Reynolds number (Re) and inlet jet momentum ratio (Rm) as the similitude criteria for isothermal airflow, and Archimedes number (Ar) for nonisothermal airflow. The experimental results offer better agreement using Rm than using Re as the similitude criterion for isothermal airflow. Ar is an appropriate similitude criterion when the nonisothermal airflow pattern exhibits two-circulation airflow behavior. After the airflow is

increased resulting in a single-circulation airflow, Rm associated with a similar heat load becomes the better similitude criteria.

Future studies including improvement of the evaluation method, more complete investigation of the enclosure, variation of scale dimension and configuration layout, and better control of the experimental environment are recommended.

CHAPTER 1. INTRODUCTION

In a modern technological society, people spend more than 90% of their time in an artificial environment such as a dwelling, workplace, or transport vehicle (Awbi, 1991). Ventilation is an important technique to regulate the room environment and produce an appropriate micro-climate for the occupant's thermal comfort and indoor air quality. The behavior of ventilated airflow inside an enclosure influences air distribution, the thermal environment, and contaminant concentration. In most mechanically ventilated rooms, air-jets are used to mix inlet air with room air. The air-jet performance determines the distribution of thermal energy, moisture, and fresh air into a room (Awbi, 1991).

A free jet is one where air enters an air space without a solid boundary to disturb air -jet development. A wall jet is bounded by a surface on one side and parallel to the surface. The air-jet that occurs in a ceiling slot-ventilated enclosure is a wall jet and is also influenced by enclosure walls. The characteristics of an enclosed wall jet have been studied using prototype buildings, scale-models (similitude), and numerical simulation.

Prototype buildings. A prototype study investigates room air behavior using full-scale buildings. The advantages of a prototype study include true geometric conditions, true response, and the results can be used immediately. The disadvantages of a prototype study are that the results can only be used in identical buildings, the room is generally large and not convenient to modify or control, and the costs can be high.

Scale-model study. Scale-model studies investigate the behavior of airflow in scaled enclosures to predict the performance of room air in the full-scale prototype. The use of a scale-model affords advantages in time, expense, and control of variables. The validity of prediction from scale-model results has been questioned (Bodman, 1976) and may relate to the absence of validation in the full-scale prototype (Timmons, 1984).

Numerical simulation. Numerical simulation uses mathematical models to simulate the physical performance of airflow. This method is the most convenient and describes in detail the airflow phenomenon. Mathematical models require experimental data for verification, but a wide array of physical situations can be modeled.

Scale-model studies are practical for simulating the behavior of a prototype and can be used to validate a numerical simulation. Similitude, or the relation between a scale-model and prototype, is an important issue when using scale-models.

Complete similitude of the airflow field between scale-model and prototype must satisfy geometric similitude, kinematic similitude, dynamic similitude, thermal similitude, and all boundary conditions (Shepherd, 1965; Baturin, 1972; Szucs, 1980; Awbi, 1991; Zhang et al., 1991).

Moog (1981) described that a precise mathematical model was impossible for the extremely complex micro-structure of room air flow. Model tests would always be required if the dimensional uncertainty was not given and no precise mathematical-physical prediction model was established. Only partial similarity between scale-model and prototype could be

satisfied for most of the realistic problems because most of the dimensionless parameters affecting performance have equal importance.

Previous research has shown that Reynolds number (Re), inlet jet momentum number (J), and inlet jet momentum ratio (Rm) can be used as similitude criteria for isothermal conditions with the Archimedes number (Ar) added for nonisothermal airflow (Adre and Albright, 1991). However, these similitude criteria have been proposed as inappropriate in some past research (Zhang, 1991; Adre and Albright, 1994; Liu et al., 1995) and thus more validation work is needed to help clarify this dilemma.

CHAPTER 2. OBJECTIVES

This dissertation attempts to clarify past proposals for similitude criteria to be used between a scale-model and a prototype for both isothermal and nonisothermal conditions using both theoretical arguments and experimental data using 1:3 and 1:6 scale-model enclosures. This study was limited to a slot-ventilated enclosure using air as the fluid medium.

The objective of this study was to investigate similitude criteria of airflow between a scale-model and prototype ceiling slot-ventilated enclosure for both isothermal and nonisothermal conditions. The sub-objectives were to:

1. Validate the Reynolds number (Re) or inlet jet momentum ratio (Rm) as the similitude criteria for isothermal conditions, and
2. Prove or disprove the use of Archimedes number (Ar) as an acceptable nonisothermal similitude criterion.

The ultimate purpose of this research was to develop guidelines when using scale-models for assessing prototype behavior in slot-ventilated livestock facilities. The desire was to be able to predict airflow patterns, temperature distribution, and airspeed distribution, especially within the animal occupied zone (AOZ).

CHAPTER 3. LITERATURE REVIEW

This chapter describes previous research regarding the principles of room air diffusion, airflow characteristics in an enclosure, and scale-model studies for both isothermal and nonisothermal airflow. The literature cites current understanding of the airflow characteristics within an enclosure and the methods used to validate similitude criteria between a scale-model and prototype.

3.1. Principles of Room Air Diffusion

Room air diffusion is dependent upon air-jet performance. Understanding the principles of air-jets would be helpful in understanding room air-flow behavior. The following sections describe common air-jet nomenclature.

3.1.1. Classification of air-jets

Air-jets have been extensively studied due to their importance in mechanical ventilation systems. The classification of air-jets describes how air is supplied to a room. Various types of diffusers and other factors such as room geometry and size, air-jet trajectory, and the thermal environment all combine to affect room airflow (Awbi, 1991; ASHRAE, 1993; Li et al., 1993). The classification of air-jets depends on many of the conditions listed above. A summary of air-jet classifications are given below:

Free jet : the air-jet is discharged into a large open space without any surrounding obstructions such as walls or ceilings.

Attached jet: the air-jet is attached to a surface such as a wall (wall jet) or ceiling (ceiling jet).

Confined jet: the air-jet is issued into a room confined by solid boundaries and is influenced by reverse flow created by the air-jet itself. The confined jet has also been referred to as an enclosed jet (Szucs, 1980).

Isothermal jet: the temperature of the supplied air-jet is equal to the temperature of the ambient room air that the air-jet penetrates.

Nonisothermal jet: the air-jet is at an initial temperature that differs from the temperature of ambient air that the air-jet penetrates.

Submerged Jet: the air-jet is issued spreading through a medium at rest (Abramovich, 1963).

Depending on the diffuser type, air-jets can be further classified as:

Compact jets: air-jets that exit from grilles, nozzles or round openings, square openings, or rectangular openings with small aspect ratios (i.e. length/width ratio). These jets are considered axisymmetric and three-dimensional.

Linear jets: air-jets that exit from slots or rectangular openings with large aspect ratios. Linear air-jets have two-dimensional characteristics and have also been called plane jets.

Radial jets: air-jets that exit from diffusers where the axial flow from a cylindrical chamber is deflected in all 360 degrees.

Incomplete radial jets: air-jets that exit from grilles having diverging vanes.

Conical jets: air-jets that exit from a cone-type or regulated multi-diffuser.

Swirling jets: air-jets that exit from diffusers where a vortex can form.

3.1.2. Jet expansion zones

After an air-jet exits from an opening, four zones or regions generally form and these have been identified and studied. The zones of a typical linear, free jet are shown in Figure 3.1 (Awbi, 1991).

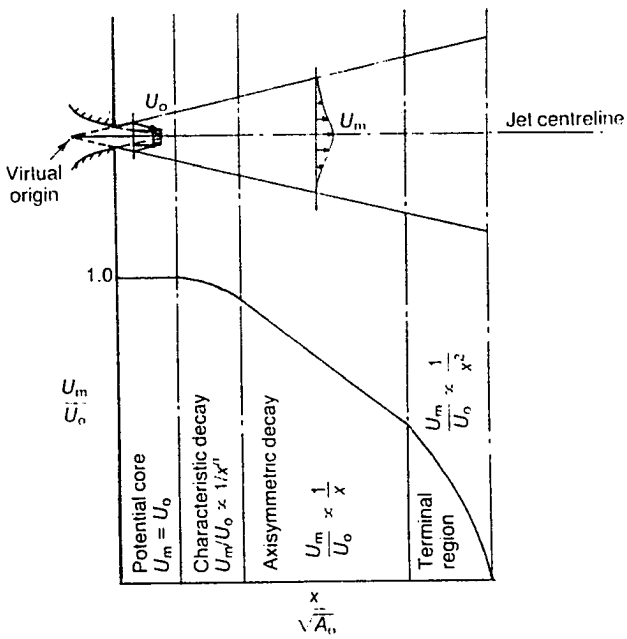

Figure 3.1. The description of four jet expansion regions (Awbi, 1991).

Potential core region. A short length immediately downstream of the opening where mixing of the air-jet and ambient room air is not complete. The length depends on the type of opening and the turbulence of the air supply but usually extends 5 to 10 equivalent opening diameters. The maximum velocity within this region remains unchanged.

Characteristic decay region. The shear layer penetrates to the core of the air-jet producing a velocity profile. The extent of this region depends on, among other factors, the type of opening, aspect ratio, and initial flow turbulence. The centerline velocity decreases gradually as:

$$\frac{U_{max}}{U_d} \propto \frac{1}{x^n} \qquad (3.1)$$

This region can be neglected for circular or square openings because the peak airspeed decay is rapid (Awbi, 1991).

Axisymmetric decay region. This is the fully developed flow region. It is the predominant region for low aspect ratio openings and can extend to about 100 equivalent diameters at which point the maximum airspeed is reduced to a terminal velocity. The point of terminal velocity is defined as the "air-jet throw". The centerline velocity in the axisymmetric decay region decreases inversely with the distance from opening as:

$$\frac{U_{max}}{U_d} \propto \frac{1}{x} \qquad (3.2)$$

This region is not significant for high aspect ratio openings because the peak airspeed decay is similar to the characteristic decay region.

Terminal region. A zone of rapid diffusion where the velocity profile degenerates and where the air-jet disappears within a few equivalent diameters.

The potential core and characteristic decay regions dominate linear, free jet performance. The potential core and axisymmetric decay regions dominate compact, free jet performance. The characteristic decay region is usually very small when the aspect ratio is close to unity.

3.1.3. Linear attached jets

The air-jet that exits from a ceiling slot-ventilated enclosure is defined as a linear attached jet because it is bounded by a flat surface and the diffuser has a large aspect ratio. Commonly, this air-jet is referred to as a plane wall jet. The air-jet is two-dimensional with only a potential core and a characteristic decay region (Awbi, 1991) as show in Figure 3.2. As the air-jet exits from the inlet, a shear layer develops on the fluid side due to the "no-slip" condition at the solid boundary (Rajaratnam, 1976). A boundary layer develops on the wall side. The potential core region is consumed when the boundary and shear layers meet. Beyond this region, a fully developed flow in the characteristic decay region is established (Rajaratnam, 1976).

3.1.4. Velocity profiles of plane wall air-jets

Rajaratnam (1976) expressed the non-dimensional velocity profile of a turbulent plane wall jet by the empirical expression

$$\frac{U}{U_{max}} = 1.48\eta^{1/2}[1 - \mathrm{erf}(0.68\eta)] \qquad (3.3)$$

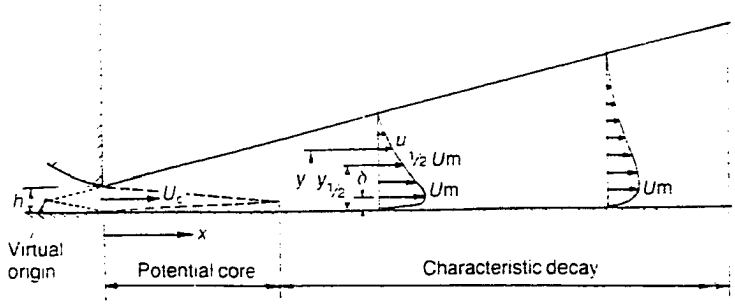

Figure 3.2. Schematic of a plane wall jet (Awbi, 1991).

where $\eta = y / y_{1/2}$ and $y_{1/2} = 0.068(x - 10h)$.

Schwarz and Cosart (1961) described this profile as:

$$\frac{U}{U_{max}} = \exp[-0.937(\eta - 0.14)^2] \qquad (3.4)$$

Awbi (1991) concluded that Rajaratnam's (1976) equation (3.3) gave better agreement with experimental data.

3.1.5. Centerline velocity of plane wall air-jets

Previous studies (Sigalla, 1958; Myers et al., 1963) concluded that the peak velocity decay of a plane wall jet was similar to the plane free jet. The peak velocity decay in the streamwise direction was caused mainly by entrainment from the surrounding air and was unaffected by the

shear (viscous) stress at the wall (Adre and Albright, 1994). The plane wall centerline velocity decay was defined as (Adre and Albright, 1994):

$$\frac{U_{max}}{U_d} = C_w\sqrt{\frac{h}{x}} \tag{3.5}$$

where C_w was usually referred to as the throw constant (Awbi, 1991) given by

$$C_w = \sqrt{2}CC_d \tag{3.6}$$

The value of C was the peak velocity decay coefficient for a plane free jet and suggested by Tennekes and Lumley (1972) as 2.7, and C_d was the diffuser discharge coefficient that depends on the inlet configuration. Because the plane wall jet has only one free shear boundary resulting in less entrainment, Tuve (1953) found the maximum velocity of the plane wall jet was greater than that of a plane free jet by a factor of the square root of two.

Rajaratnam (1976) described the velocity decay for a plane wall jet by averaging the curves from different experimental data sources resulting in the following:

$$\frac{U_{max}}{U_d} = 3.50\sqrt{\frac{h}{x}} \tag{3.7}$$

which has a similar form as equation (3.5).

3.1.6. Entrainment ratio

The entrainment ratio (Q_e/Q_d) for a plane wall jet was determined by Rajaratnam (1976) as:

$$\frac{Q_e}{Q_d} = 0.248\sqrt{\frac{x}{h}} \tag{3.8}$$

with an entrainment velocity (i.e. the vertical component at the air-jet boundary) of:

$$U_e = 0.035U_{max} \qquad (3.9)$$

The concept of entrainment and entrainment velocity is shown in Figure 3.3.

3.1.7. Turbulence characteristics

In an air-jet, the region near the diffuser may be laminar flow with turbulent flow existing downstream of the air-jet. The essential characteristics of turbulent motion is the random turbulence fluctuation (Pai, 1954). Turbulent motion is composed of eddies varying in size and frequency. The turbulent parameters relevant to ventilation studies are described below (Hanzawa et al., 1987; Awbi, 1991; White, 1991).

Time-average velocity:

The instaneous velocity can be expressed as:

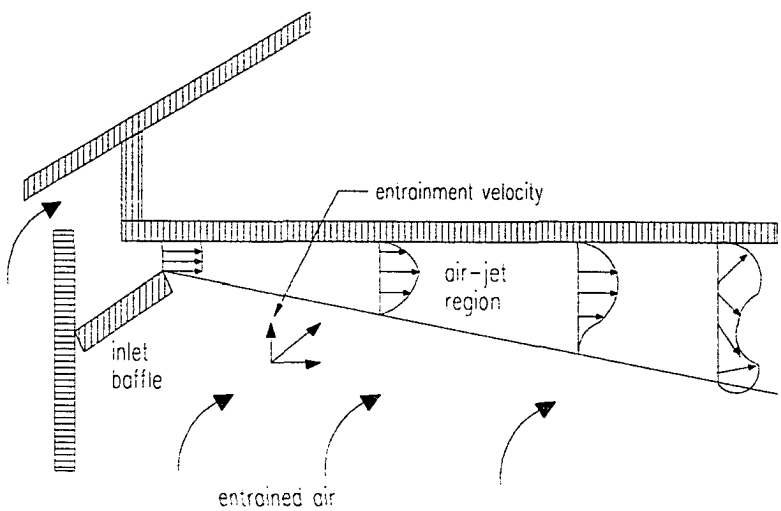

Figure 3.3. The concept of entrainment and entrainment velocity.

$$U = \bar{U} + u \tag{3.10}$$

where

U = instantaneous velocity, m/s

$\bar{U}$ = time-average velocity, m/s

u = velocity fluctuation from the average, m/s

the time-average velocity represents the average velocity over a specified time interval, t, as:

$$\bar{U} = \frac{1}{t}\int_0^t U dt \tag{3.11}$$

Turbulent intensity:

The turbulent intensity can be expressed as:

$$TI = \frac{\sqrt{\overline{uu}}}{\bar{U}} \tag{3.12}$$

where $\sqrt{\overline{uu}}$ is the standard deviation of the velocity which is equal to the root-mean-square of the fluctuating velocity.

Turbulent energy spectrum:

The turbulent energy spectrum can be expressed as:

$$\overline{uu} = \int_0^\infty E(f) df \tag{3.13}$$

where f is the frequency of fluctuation and E(f) is the energy density spectrum of u. The turbulent energy spectrums defines the kinetic energy of turbulence over a distinct range of frequencies.

Length scale of turbulence:

The length scale of turbulence can be expressed as:

$$L = \frac{\overline{U}E(f)}{4\overline{uu}} \tag{3.14}$$

and represents the average size of the largest eddies (Hinze, 1975).

Turbulent kinetic energy:

The turbulent kinetic energy can be expressed as:

$$K = \frac{1}{2}\overline{u_j u_j} \tag{3.15}$$

where u_j represents the velocity components of fluctuation in Cartesian coordinates.

Zhang (1991) showed that the turbulent intensity at the diffuser was significantly higher than the 4-5% used in many numerical simulations of room air motion. Similar results have been reported in previous studies (Rajaratnam, 1976). The turbulent kinetic energy in the floor of room ventilation flows was significantly smaller compared to the diffuser jet region (Zhang, 1991).

3.1.8. Air-jet throw

ASHRAE Handbook of Fundamentals (ASHRAE, 1993) defines the air-jet throw as the distance from the diffuser where the maximum velocity in the air-jet reaches a terminal velocity of 0.25 m/s for all diffusers except for ceiling slot diffusers, where the terminal velocity was proposed as 0.5 m/s.

3.2. Airflow Characteristics in an Enclosure

The air supplied into a ventilated room as a plane wall jet that is influenced by surrounding solid boundaries is called a confined jet. The theoretical and experimental investigations of confined plane wall jets is much more difficult than the plane free jet (Szucs, 1980). Airflow patterns, air-jet penetration distance, air-jet trajectory, and airspeed in the occupied zone for both isothermal and nonisothermal conditions are affected by the physical confinement of a plane wall jet.

3.2.1. Airflow patterns

3.2.1.1. Isothermal conditions

Kaul et al. (1975) studied the principles that govern the control of the environment in livestock houses through prototype and scale-model tests. Their results for isothermal airflow showed that airflow patterns related to the inlet jet momentum, and that the minimum inlet jet momentum function that produced a stable three-dimensional eddy (rotary airflow) was $I_o \geq 0.01$ kg/m^2-s^2. Tests were conducted for geometric ratios between prototype and scale-model of 1:1 to 1:6.

Timmons et al. (1980) studied air movement in slot-ventilated enclosures both experimentally and numerically. They concluded that the airflow pattern was independent of Re above a threshold value of about 3800. Air-jet attachment to a solid boundary, termed the "Coanda effect", was found to disappear as the enclosure length shortened and/or the distance from the bottom of the inlet to the adjacent wall increased.

Timmons (1984) derived the values of threshold Re in different enclosures and found there was a proportional relationship between threshold Re and test room size.

Jin and Ogilvie (1990) identified three airflow zones which represented three types of airflow patterns in an empty 1:2 scale-model. They varied the inlet air velocity and inlet height (width) and found that the near-floor airspeed profiles were similar in form to a plane wall jet that exits along a ceiling. The three zones were defined as the stagnant airflow zone (the mean floor airspeed remained below 0.1 m/s); the rotary airflow zone (air movement was fully rotary along the room perimeter), and the intermediate zone (the mean floor airspeed was greater than 0.1 m/s). These zones were distinguished and determined using a non-linear least squares method.

Adre and Albright (1994) reported that a threshold Rm existed between model and prototype where the airflow pattern remained unchanged for increasing airflow rates in three different enclosures. Similar results were verified by Yu and Hoff (1994).

3.2.1.2. Nonisothermal conditions

Randall and Battams (1979) conducted stability criteria for airflow patterns in livestock buildings using a prototype building with heated cylinders simulating pigs. They proposed an inlet corrected Archimedes number (Ar_c) to describe the relative influence of buoyant forces on the air-jet. Their results showed that the air-jet remained horizontal for Ar_c less than 30 and fell immediately to the floor when it was greater than 75. The airflow patterns were stable, and rotary, with an opposite rotation for both regions. Intermediate Ar_c values

caused unstable airflow patterns. Berckmans et al. (1993) validated the criterion of Ar_c defined by Randall and Battams (1979) in ventilating commercial livestock buildings. They concluded that the Ar_c criterion was valid for applying to both the direction of the air-jet on entry and the trajectory of the air-jet further from the inlet.

Barber et al. (1982) suggested that design criteria for inlets should use Ar_c to predict air-jet trajectory as proposed by Randall and Battams (1979) and that a dimensionless inlet jet momentum number ($J \geq 0.00075$) derived from the inlet jet momentum (Kaul et al. 1975), should be used to predict air mixing.

Leonard and McQuitty (1986a) used the Ar_c proposed by Randall and Battams (1979) to design a livestock ventilation system and measured the air-jet trajectory in a test room using smoke visualization and a temperature recording grid. They concluded that the airflow patterns were in agreement with the Ar_c and that the tendency of air-jets to fall related linearly to the Ar_c for any given inlet. The possibility of using the outlet temperature instead of the heated surface temperature in the definition of the Ar_c was confirmed. The relation between the Ar_c and the air-jet trajectory was not quantified.

Leonard and McQuitty (1986b) used the Ar_c as the criteria for the control of cold ventilation air-jets. They concluded that when the Ar_c was less than 50, satisfactory airflow patterns were established in most agricultural ventilation systems.

Leonard and McQuitty (1988) studied air mixing in a mechanically ventilated room using a test room under nonisothermal conditions. A measurement of temperature variation within the room was used to represent air mixing. Their results showed that an Ar_c of

approximately 5 based on room temperature resulted in good air mixing. This value corresponds to an inlet momentum number (J)=0.013 which is higher than a J=0.00075 proposed for isothermal conditions (Barber et al., 1982).

Wang and Ogilvie (1994a) investigated airflow patterns in slot-ventilated rooms under nonisothermal conditions using a test room where the room height could be varied. A wall jet Archimedes number (Ar_w) was defined and proposed as the criterion describing airflow patterns. The Ar_w was about 40 before the air-jet extended to the midpoint of the room and was about 110 for fully rotary airflow. A significant lag phenomenon was found in the study where once a fully rotary airflow pattern was created, the inlet velocity could be decreased significantly without changing the airflow pattern with the Ar_w increased to about 240.

Zhang (1991) described this lag phenomenon in a study of the relation between the horizontal air-jet penetration and the diffuser air velocity for nonisothermal airflow. It was concluded that extra momentum was needed to overcome the existing airflow pattern before a new flow pattern could be formed. The critical Ar defined as the condition where the air-jet fell on entry was found for nonisothermal airflow. The airflow behavior agreed with numerical and experimental results presented by Nielsen et al. (1979)

3.2.2. Air-jet penetration

Air-jet penetration has been used to express airflow patterns quantitatively. The definition of air-jet penetration has differed as shown in Figure 3.4. Kaul et al. (1975) defined air-jet penetration as the distance from the inlet wall on the floor where the incoming

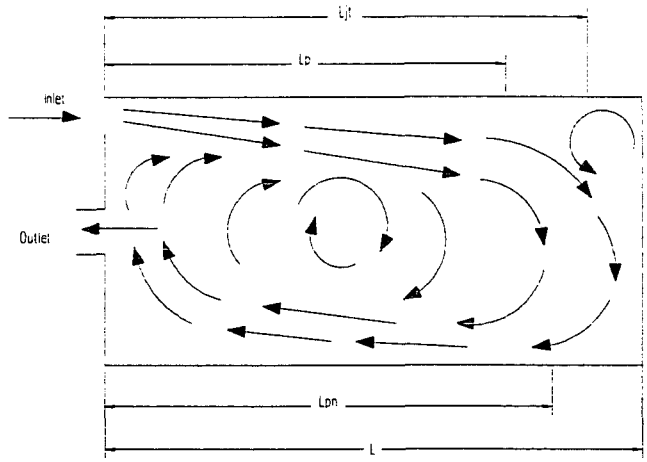

Figure 3.4. The definition of air-jet penetration distance.
L_p: Adre and Albright (1994) definition.
L_{pn}: Kaul et al. (1975) definition.
L_{jt}: Jet throw

air-jet impinged. Adre and Albright (1994) defined air-jet penetration as the distance from the inlet wall where the wall jet separated from the ceiling. Air-jet throw, which represents the maximum distance the air-jet extends into the enclosure, is related to air-jet penetration distance (Nevins, 1976).

Kaul et al. (1975) asserted that a sufficiently large air-jet momentum would extend into the room no further than 3H (H= room height) even when the enclosure length was greater than 3H in isothermal airflow. Leonard and McQuitty (1988) found that the air-jet with a large inlet momentum extended to the full length of the room which was 3.8H. Forthmann (1934) proposed that the air-jet penetration distance could be 5.3H in deep enclosures (i.e. large H). Nielsen (1976) found air-jet penetrations of 4H to 4.5H in a long enclosure and

found that it was independent of the inlet Re between 2400 and 9300 (Adre and Albright, 1994).

Timmons (1984) compared airflow patterns and air-jet attachment lengths in a scale-model and a prototype. The results showed that the value of a threshold Re was different for different enclosures and there was a proportional relationship between the required threshold Re and the physical size of the ventilated enclosure. The threshold Re was defined as the Re where an unchanging fully-rotary airflow pattern was established.

Adre and Albright (1994) theoretically analyzed air-jet penetration distance as a function of inlet jet momentum ratio (Rm) for isothermal airflow in a ceiling slot-ventilated enclosure. Yu and Hoff (1994) derived similar description of penetration distance as a function of Rm in a ceiling slot-ventilated enclosure as Adre and Albright's (1994) result. Threshold inlet jet momentum ratios were presented. Adre et al. (1995) derived a universal expression of air-jet penetration distance based on previous work for both isothermal and nonisothermal airflow.

Awbi and Setrak (1986) derived an expression for plane wall jet penetration distance as a function of the inlet slot height (h) and room length (L) as follows:

$$\frac{L_{max}}{h} = 0.52\left(\frac{L}{h}\right)^{1.09} \qquad (3.16)$$

3.2.3. Air-jet trajectory

Kaul et al. (1975) measured the path of incoming air-jets in both prototype and scale-model farm buildings and showed that the Ar can be used for predicting air-jet trajectory for nonisothermal conditions.

Berckmans et al. (1993) derived the relations between the inlet corrected Archimedes number (Ar_c) and the direction or final path of the air-jet. Various authors (Koestel, 1955; Regenscheit, 1959, cited by Mullejans, 1966; Mullejans, 1966; Baturin, 1972) have proposed formula for the incoming air-jet trajectory as a function of the Ar for nonisothermal plane wall jets.

3.2.4. Airflow characteristics in the occupied zone

Albright (1989) stated that the desired near-floor airspeeds in adult animal housing was 0.2 to 0.4 m/s. The maximum average airspeed in the occupied zone for human comfort has been specified as 0.15 m/s in winter and 0.25 m/s in summer (ASHRAE Standards as specified in Awbi, 1991).

Ogilvie et al. (1990) studied floor air speeds for different swine ventilation systems. Experiments confirmed that jet momentum number (J) correlated well with floor air speed for various building configurations. Correlated equations and inlet design conditions were presented.

Jin and Ogilvie (1992) found a good correlation between the velocity in the occupied region with the inlet parameters as long as the room airflow patterns stayed in the fully rotary condition. An empirical equation of mean floor velocity in the floor region (0-0.6 m above the floor) as a function of the inlet jet momentum number at the inlet was derived.

Wang and Ogilvie (1994b) investigated floor velocity distribution in slot-inlet ventilated buildings under isothermal and nonisothermal conditions using a test room of varied height.

Their results confirmed the previous analysis (Jin and Ogilvie, 1992) indicating that maximum floor velocity could be determined by the inlet jet momentum ratio (Rm) under isothermal conditions. They found that floor velocity was a function of both the inlet jet momentum and thermal buoyancy for nonisothermal conditions.

The maximum air velocity in the return flow (occupied zone) might occur at a distance of 2/3 L from the inlet in ceiling slot-ventilated enclosures (Nielsen, 1988). The ratio of maximum air velocity in the return flow (U_{rm}) to the wall jet velocity at a distance x=L from the opening (U_L) was derived as:

$$\frac{U_{rm}}{U_L} = K_{rm} \tag{3.17}$$

where K_{rm} was found to be a weak function of room and inlet geometry and was assumed to be 0.7 as a rough estimate (Nielsen et al., 1978). Combined with the equation of centerline velocity (equation (3.5) with $x=x+x_o$) results in:

$$\frac{U_{max}}{U_d} = C_w \sqrt{\frac{h}{x + x_o}} \tag{3.18}$$

The maximum floor airspeed can than be expressed as:

$$U_{rm} = C_w K_{rm} U_d \sqrt{\frac{h}{L + x_o}} \tag{3.19}$$

3.3. Scale-Model Studies for Isothermal Airflow

Pattie and Milne (1966) used a 1:10 scale-model building with various air inlet systems including combinations of ducts, holes, and slots to predict airflow patterns in a poultry

house. Airflow patterns were measured by both hot-wire anemometry and chemical smoke. They used the Reynolds number as the similitude criteria and tested Re of 0.20, 0.65 and 0.91. Their results showed no significant variation of airflow pattern and air velocity distribution between scale-model and prototype. They also found that the ventilation airflow pattern and airflow velocity distribution was governed by the configuration of the air inlet.

Smith and Hazen (1968) used 1:2 and 1:4 scale-models to test similitude theory and to predict the inlet airflow characteristics for two-dimensional, steady, incompressible, and isothermal flow. Measuring velocity profiles in the air-jet showed that, with geometric similarity between inlets and dynamic similarity using the Reynolds number, resulted in geometric similarity of the air-jet velocity profiles. Only the velocity data for Reynolds number greater than 4500 was used for this study.

Rajaratnam (1976) provided a theoretical relation between variables for turbulent plane wall jets in unconfined and isothermal conditions using dimensional analysis. The normalized maximum velocity, thickness of air-jet, and the skin-friction coefficient were related as a function of inlet Reynolds number. Experimental results generally showed that if the Reynolds number was greater than 1×10^4, then the relation with Reynolds number was small representing the threshold condition.

Timmons (1984) studied a series of small, intermediate and prototype slot ventilated enclosures to reaffirm the validity of using scale-models to predict airflow patterns in prototype cases with two-dimensional, steady, incompressible, and isothermal flow. It was found that the threshold Reynolds number (Re), above which the dimensionless velocities

and airflow patterns were independent of Re, was dependent and proportional to the dimensional size of the model. It was also found that the size of recirculatory areas could be predicted by geometric similarity of outlet locations. The relationship between the threshold Re and the size of model was not quantified. The changing threshold Re with model size was verified by Zhang (1991). Zhang (1991) concluded that room size was affecting overall room airflow turbulence.

Zhang et al. (1991) investigated similitude criteria both theoretically and experimentally using a prototype and a 1:4 scale-model for isothermal airflow. Theoretical analysis indicated that the Reynolds number and boundary conditions including dimensionless velocity, turbulence stress, and pressure at the diffuser inlet were the only similarity parameters of importance. They also showed that the air velocity profile at the diffuser had a significant effect on air-jet momentum and room air motion when the room airflow was not fully turbulent. Differences of inlet air velocity profiles between the scale-model and prototype resulted in higher dimensionless inlet jet momentum for the scale-model even though the inlet Reynolds number was the same. A proper scaling method based on the similarity of inlet jet momentum in addition to the Reynolds number was proposed to account for differences between inlet air velocity profiles was suggested for future studies.

Recently, Adre and Albright (1994) determined criterion for establishing similar two-dimensional isothermal airflow patterns in slotted-inlet ventilated enclosures. Tests were conducted both analytically and experimentally using 1:5 and 1:10 scale-models to represent the prototype and scale-model, respectively. Several inlet/outlet configurations were tested.

The inlet Reynolds number (Re) and the inlet jet momentum number (J) were found inappropriate to predict airflow pattern behavior in the prototype but the ratio of inlet jet momentum to the momentum loss due to shear along the enclosure walls, denoted as inlet jet momentum ratio (Rm), was claimed to be the appropriate scaling criteria for airflow pattern similarity. Yu and Hoff (1994) verified the inlet jet momentum ratio concept for isothermal airflow similarity in a ceiling slot-ventilated enclosure using 1:3 and 1:6 models to represent prototype and scale-model, respectively. Questions were raised regarding the use of a dimensional parameter (Rm) as a scaling criteria.

Liu et al. (1995) compared three ventilation criteria (Reynolds number (Re), jet momentum number (J), and jet momentum ratio (Rm)) analytically under isothermal conditions. Reynolds number (Re) was found to be the correct similitude criterion based on a dimensional analysis and the Navier-Stokes equation. They concluded that previous research that showed the inappropriateness of Reynolds number as the similitude criterion might be the result of experimental error such as the failure of similarity in turbulence boundary conditions at the inlet and other outside influences.

Most recently, Rousseau and Albright (1996) proposed the Euler number as an alternative kinematic similarity criterion for slot-ventilated enclosures to remove the anomaly in the use of Reynolds number as a kinematic similarity criterion based on theoretical considerations and experimental observations.

3.4. Scale-Model Studies for Nonisothermal Airflow

Mullejans (1966) applied the similarity principle to the differential equations governing nonisothermal airflow, and found the parameters governing similarity between scale-model and prototype. He showed that the Reynolds number, Archimedes number, and Peclet number were the governing dimensionless parameters. Neglecting the effects of molecular friction on flow and molecular heat transfer on energy exchange, a simplified scaling model was derived relating the Ar. He used three geometrically similar rooms with linear dimensions in the ratio of 1:3:9 and provided nonisothermal conditions using heated walls. The experimental results showed that airflow patterns were clearly dominated by the Ar and independent of Re even for low-turbulence conditions (i.e. Re<100). The airflow approximated that of isothermal airflow at and below a critical value of Ar. The critical Ar varied with the geometrical scale and was approximated as $Ar(bh/D^2) \leq 40$. Fully turbulent airflow was found for inlet Re>1500.

Baturin (1972) studied scale-model theory and the rules associated with distorted models for industrial ventilation and variations in fluid density. Fluid densities were altered using either nonisothermal flow or a different fluid in isothermal flow. The scaling criteria should be based on Ar provided that the Re is in the turbulent fluid region (i.e., Re>2320 or Re >10000).

Penzes, as reported in Szucs (1980), examined nonisothermal airflow in a large domed sports hall. The similitude criteria used was Ar and either dimensionless heat generation (for the zone above the stand) or dimensionless heat loss (for the zone under the dome) with Re of

the inlet always at and above 2350. The Froude number (Fr) and Peclet number (Pe) were found not to be important for their study.

Yao et al. (1986) studied a neutral-pressure swine barn with a 1:12 scale-model and summer ventilation data in low turbulent flow. The effects of internal heat load and obstructions were compared. It was concluded that Ar was maintained as the undistorted similitude parameter and Re was neglected as a distorted parameter since air movement was believed relatively independent of Re within the enclosures, but Re became important in higher speed flow. Christianson et al. (1988) validated the above similitude modeling approach by comparing the pig-level air velocity between the 1:12 scale-model and prototype. The scale-model overpredicted velocity by approximately 3 times if based on Ar and underestimated it by 17 times if based on Re. They concluded that Ar should be more important than Re in low velocity flow conditions for nonisothermal airflow.

Fissore and Liebecq (1991) derived the parameters for predicting velocity distribution and temperature gradients in the occupied zone using a 1:3 scale-model. They studied the effects of Ar, inlet velocities, slot inlet length, and building length. They developed a simple empirical model using Ar for cases where the Re remained above a critical value of 1850 (Fissore and Liebecq, 1990). The results were validated using measurements of temperature and velocity in the prototype and scale-model.

Zhang et al. (1993) conducted similitude modeling for predicting room air motion for nonisothermal airflow. They investigated similitude modeling using both theoretical and experimental techniques using a prototype and 1:4 scale-model. A new scaling method was

derived based on the relative deviation of the Ar from a critical Ar. The critical Ar was that at which the air-jet fell immediately after entering the building. They found that the critical Ar decreased as the scale-model size decreased. The new scaling criteria was a compromise between the Ar and Re. The results showed good agreement between scale-model and prototype. The model slightly overpredicted mean air velocity and underpredicted turbulent intensity and turbulent kinetic energy. A compensation coefficient accounting for the effect of temperature difference was suggested to improve the scaling model.

3.5. Summary

3.5.1. Classification of air-jets

1. The air diffusion system in a ceiling slot-ventilated enclosure is a confined (enclosed) plane wall jet with zones primarily consisting of a potential core region and a characteristic decay region (Figure 3.2).

2. The air-jet characteristics of a plane wall jet are summarized in Table 3.1.

Table 3.1 Characteristics of a plane wall jet

Nomenclature	Notation	Main section	Reference
Velocity profiles	$\frac{U}{U_{max}}$	$1.48\eta^{1/2}[1-\mathrm{erf}(0.68\eta)]$	Rajaratnam, 1976
Centerline velocity	$\frac{U_{max}}{U_d}$	$3.50\sqrt{\frac{h}{x}}$	Rajaratnam, 1976
		$2.48\sqrt{\frac{h}{x}}$	Adre and Albright, 1994 (see Note 1)
Entrainment ratio	$\frac{Q_e}{Q_d}$	$0.248\sqrt{\frac{x}{h}}$	Rajaratnam, 1976

Note 1. $C_w = \sqrt{2}CC_d = 2.48$ from equation (3.6), where C=2.7 and C_d=0.65 (assumed).

3.5.2. Airflow characteristics in an enclosure

1. The critical values to determine airflow patterns in isothermal and nonisothermal airflow are summarized in Tables 3.2 and 3.3. The critical dimensional/nondimensional parameters used to distinguish airflow patterns are different. The variations differ due to differences in air-jet configurations and test room size. Each of the parameters presented represent possible similitude guidelines between a scale-model and prototype.

2. The expression of air-jet penetration distance and air-jet trajectory are summarized in Tables 3.4 and 3.5. Tables 3.4 and 3.5 show that the airflow patterns were determined roughly by air-jet throw in an enclosure first, and more precise equations of penetration distance and air-jet trajectory were derived later. The possible similitude criteria were Rm

Table 3.2. Summary of the critical value to determine the airflow pattern in slot-ventilated enclosures under isothermal condition.

References	Unstable or fall in entry	Fully rotary	Inlet/outlet position	Configuration of test room
Kaul et al., 1975	$I_0<0.01$ kg/m^2s^2		same wall	L/H=1 and L/H=6
Timmons, 1980		Re>3800	opposite wall	1×1×0.5m
Timmons, 1984		Re>2500 Re>4600 Re>54000	opposite wall	1×W×0.5m 2.44×W×1.22m 7.72×W×2.05m
Jin and Ogilvie, 1990	$hU_d^{1.65} \le 0.046$	$hU_d^{2.5} \ge 0.136$	same wall	4.8×4×3m
Adre and Albright, 1994		Rm=0.052 Rm=0.043 Rm=0.012	opposite wall same wall duel inlet, one outlet	in both of 1×0.6×0.25m and 2×1.2×0.5m
Yu and Hoff, 1994		Rm=0.01	duel inlet, duel outlet	in both of 3.65×2.42×0.9m 1.83×1.21×0.45m

Table 3.3. Summary of the critical value to determine the airflow pattern in slot-ventilated enclosures under nonisothermal condition.

References	Unstable or fall in entry	Fully rotary	Inlet/outlet position	Configuration of test room
Randall and Battams, 1979	Ar_c>75	Ar_c<30	both inlet, central ceiling outlet	7.6×3.1×2.1m
Leonard and McQuitty, 1986a	Ar_c>50 Ar_c>40		top inlet position lower inlet position	7.2×5.4×1.9m
Zhang, 1991	Ar<0.023 Ar<0.0127		in opposite wall	18×W×8ft 4.5×W×2ft
Wang and Ogilvie, 1994a		creative: Ar_w<110 maintainable: Ar_w<240	in same wall	4.9×3.8× (2.6-3.2)m

Table 3.4. Summary expressions for air-jet throw and penetration distance

Conditions	Expressions	References
Isothermal	$L_{jt} \leq 5.3H$	Forthmann, 1934
Isothermal	$L_{jt} \leq 3H$	Kaul et al., 1975
Isothermal	L_{jt}=4H to 4.5H	Nielsen, 1976
Isothermal	L_{jt}<3.8H	Leonard and McQuitty, 1986a
Isothermal	$\frac{L_p}{h} = 0.52(\frac{L}{h})^{1.09}$	Awbi and Setrak, 1986
Isothermal	$\frac{L_p}{L} = \frac{L_{max}/L}{A_1 \exp(-A_0\sqrt{Rm})+1}$	Adre and Albright, 1994
Isothermal and non-isothermal	$\frac{L_p}{L} = \frac{L_{max}/L}{A_1 \exp(-A_0(\sqrt{Rm} - \frac{1}{\tan\theta}\sqrt{\frac{h}{L+H}}\sqrt{g\beta\Delta T_d h})+1}$	Adre et al., 1995

Table 3.5. Summary expressions for air-jet trajectory

Conditions	Expressions	References
Non-isothermal	$\frac{y}{h} = 0.4\sqrt{m}Ar(\frac{x}{h})^{2.5}$	Regenscheit, 1959 cited by Mullejans, 1966
Non-isothermal	$\frac{y}{h} = Ar\sqrt{\frac{T_d}{T_o}}\frac{0.226}{a^2}(a\frac{x}{h}+0.205)^{2.5}$	Baturin, 1972

and Ar from an-evaluation of air-jet penetration distance. The similitude criteria of nonisothermal airflow were Ar and geometric similarity from the expressions describing air-jet trajectory.

3. The airflow characteristics in the occupied zone are summarized in Table 3.6. The air velocity in the occupied zone may be used as an evaluation criteria for similitude between a scale-model and prototype.

3.5.3. Scale-model studies for isothermal airflow

1. Reynolds number has been widely used (Pattie and Milne, 1966; Smith and Hazen, 1968; Albright, 1976; Timmons and Bangnman, 1981; Timmons, 1984; Yao et al., 1986; Jin and

Table 3.6. Summary of expressions of air velocity in occupied zone

Conditions	Expressions	Data information	References
Isothermal	$U_{mean} = A_0 + A_1(J)^n$	Average 10 locations at 0.3m above the floor	Ogilvie et al., 1990
Isothermal	$U_{max} = C_w K_{rm} U_d \sqrt{\frac{h}{L + x_o}}$	Maximum floor velocity at 2/3L from inlet wall	Nielsen et al., 1988
Isothermal	$U_{mean} = A_0 J^{A_1}$	Average 80 positions horizontally and up to 0.62m above the floor vertically	Jin and Ogilvie, 1992
Isothermal	$U_{max} = 4.55 Rm^{0.5}$	Maximum floor velocity measured from 0.02m to 0.6m above the floor at x=0.5L	Wang and Ogilvie, 1994b
Isothermal and non-isothermal	$U_{max/mean} = A_0 \sqrt{Rm} + A_1(H\Delta T)^n$	Mean floor velocity measured from 0.02m to 0.6m above the floor at x=0.25L, 0.5L, and 0.75L by averaging 18 to 45 points	Wang and Ogilvie, 1994b

Ogilvie, 1992) as the similarity criterion for isothermal airflow in enclosures, but experimental results do not always show that Reynolds number is the appropriate similitude criterion (Zhang et al., 1991; Adre and Albright, 1992; Yu and Hoff, 1994).

2. Most experiments with high values of Re may be beyond the threshold Re resulting in self-similar airflow which is independent of the Reynolds number.

3. Re is the explicit similarity parameter based on an analytical analysis for isothermal airflow, but boundary conditions must be matched especially with non-fully developed turbulent flow (Zhang et al., 1991; Szucs, 1980).

4. Inlet jet momentum ratio (Rm) was validated as the appropriate similarity criterion through recent experiments (Adre and Albright, 1992; Yu and Hoff, 1994), but Rm is a dimensional parameter and the theory surrounding its derivation need further investigation.

3.5.4. Scale-model studies for nonisothermal airflow

1. Archimedes number has been widely used as the similitude criterion for nonisothermal conditions as long as the Reynolds number is maintained at and above a threshold level (Baturin, 1972; Szucs, 1980; Fissore and Liebecq, 1991).

2. The similarity criterion describing airflow patterns has been shown to be Archimedes number and independent of Reynolds number (Mullejans, 1966). Recent studies do not agree with this finding and a new scaling method has been proposed (Zhang et. al., 1993).

3. Most experimental data describing airflow patterns has been qualitative using visualization techniques without precise quantitative data.

CHAPTER 4. THEORETICAL CONSIDERATIONS

4.1. Overall Description of Airflow Field Parameters

As mentioned in the previous chapter, airflow inside a slot-ventilated enclosure is a confined plane wall jet. The air-jet is two-dimensional if the inlet aspect ratio (inlet length to inlet width) is larger than 20 (Forthmann, 1934) or conservatively 40 (Awbi, 1991).

The working fluid for this research was air treated as an incompressible fluid with constant viscosity. For the isothermal experiments, the variation of potential energy and pressure difference was comparably small resulting in a nearly constant fluid density through the flow field. For airflow with airspeeds less than 100 m/s (Mach number less than 0.3), the assumption of incompressibility is appropriate (Anderson et al., 1984).

There was significant fluid density changes due to temperature differences for the nonisothermal experiments. During the nonisothermal experiments, gravity forces are comparable to inertial and viscous forces and thus could not be neglected in low-speed flow (White, 1991). The viscosity is highly temperature-dependent for nonisothermal liquid flow conditions, thus the approximation of constant viscosity was inappropriate. For this experiment, the viscosity of air was only moderately temperature-dependent and the approximation of constant viscosity was an acceptable assumption even in nonisothermal airflow (White, 1991).

The characteristics of air-jet flow have been summarized by Albertson et al. (1950) and Pai (1954). The fluid discharged from an air-jet opening was assumed as being discharged at a constant velocity, was inviscid, and incompressible.

Turbulence is established in the interaction region between the incoming air-jet and the room air due to shear forces between the rapidly moving air-jet and the relatively still room air. A lateral mixing process is generated within the air-jet as the air-jet decelerates. Fluid from the ambient region is constantly being entrained within the air-jet. As a result, the constant-velocity core region of the air-jet decreases in the lateral direction, whereas both the airflow rate and the transverse width of the jet increase gradually along the downstream direction from the air-jet opening. The kinetic energy associated with the incoming air-jet is transferred to kinetic energy of turbulence within this process and the air-jet becomes fully turbulent (Albertson et al., 1950; Smith, 1965).

Turbulence is generated mainly in the interaction region between the air-jet and surrounding room air, although turbulence is also produced due to solid boundaries. The established temperature gradients also initiated turbulence close to the heat source (Zhang, 1991). Turbulence occurs in the bulk room space with a large amplitude and a small frequency, and best described as large eddy motion (Mullejans, 1966). The molecular transport process and molecular heat transfer terms are relatively unimportant compared with the turbulent transport phenomenon (Mullejans, 1966).

4.2. Similitude Criteria

Szucs (1980) defined similitude as the process where two systems (phenomenon) have corresponding characteristics (features, parameters) and connected by bi-unique (one-to-one) mappings (representations). The physical characteristics between a scale-model and prototype should be linked with unique transformation functions. Complete similitude of turbulent plane wall air-jets diffused into a slot-ventilated enclosure under isothermal or nonisothermal conditions requires geometric similitude, kinematic similitude, dynamic similitude, thermal similitude, and similar boundary conditions (Shepherd, 1965; Awbi, 1991; Baturin, 1972; Szucs, 1980; Zhang, 1991). Each is described below.

Geometric similitude. Requires that all linear-dimension ratios are equal including all angles and shapes between the scale-model and prototype. The scale factor of geometry is always greater than one for the prototype relative to the reduced scale-model.

Kinematic similitude. Requires that all ratios of all corresponding velocities and accelerations are the same everywhere between the geometrically similar scale-model and prototype.

Dynamic similitude. Requires that all ratios of forces causing airflow motion are similar everywhere. The forces affecting air-jet performance include inertial forces, viscous forces, pressure forces, and buoyant forces.

Thermal similitude. Requires that the temperature and heat flows remain similar. Thermal similitude is achieved only when the modes of heat transfer by conduction, convection, and radiation are identical between scale-model and prototype.

Boundary conditions. Similarity of boundary conditions must be present in addition to the above criteria to reach complete similitude. Similar boundary conditions include geometric, hydrodynamic, and thermal conditions at all solid boundaries of the scale-model and prototype. Geometric conditions require geometrically similar dimensions at all boundaries. Hydrodynamic conditions are achieved by accurately scaling the flow boundaries including the air supply opening, exhaust outlet, and roughness of all surfaces. Similar hydrodynamic conditions assure similar airflow patterns and turbulence levels at the boundaries of the enclosure. Thermal conditions require equality of dimensionless heat flux at all boundaries to generate similar fluid temperature distributions in the enclosure. However, even with this requirement, the temperature distribution might not be similar close to solid boundaries due to the complexity of heat transfer processes (Awbi, 1991).

In addition to the stated similarity criteria, the physical properties of air such as thermal conductivity and specific heat should be considered as factors affecting similitude between a scale-model and prototype. The source of heat, moisture, vapors, and gases should be similar in arrangement, production, and form (Baturin, 1972).

4.3. Similitude Analysis

The traditional method for investigating similitude requirements uses dimensional analysis and the Buckingham Pi theorem. Only a knowledge of the variables related to the problem of interest are required. The risk with this method is that if one or more important variables are neglected, serious mistakes of scale-model design could result (Young, 1994).

A more sophisticated method of similitude analysis is derived from the governing differential equations and the associated initial and boundary conditions. This method gives the necessary Pi terms directly and is a more rigorous statement of similitude, but requires more knowledge and analysis of the nature of the problem (Shepherd, 1965). Both methods are developed as related to this research and are given in the following two sections.

4.3.1. Dimensional analysis and the Buckingham Pi theorem

This method develops (n-m) dimensionless Pi (Π) terms, where n independent variables are related to the problem using m basic independent dimensional units. The result from a dimensional analysis does not specify the relationships between Pi-terms but does provide information for conducting experiments using scale-models. The functional relation between Pi-terms needs to be determined experimentally (Shepherd, 1965; Fox and McDonald, 1973).

4.3.1.1. Procedures for deriving similitude parameters (Fox and McDonald, 1973)

Step 1. List all the parameters involved

Consider clearly the parameters that govern the phenomenon of the problem. Additional parameters would make related dimensionless groups to be extraneous experimentally. The governing variables could be selected by grouping the variables into four groups representing geometry, material properties, external effects, and other miscellaneous factors as described below (Young, 1994).

Geometry. The prototype shape, represented by lengths and angles describe the geometric characteristics which affect air motion in an enclosure. These include the inlet width of the plane wall jet, the enclosure height, and the enclosure length.

Material properties. The response of a system depends on the applied external forces and these are influenced by material properties involved in the system. The viscosity of the fluid, gravity, specific heat, and thermal conductivity are examples of material properties.

External effects. The external effects represent any variable which produces a change in the system. External effects include all forces applied to the system, and any pressure, velocity, heat flux, or temperature changes.

Others. Other variables may need to be considered which may not fall into the above three categories. One example of this would be time.

Step 2. Select a set of basic dimensions

Select a minimum set of basic dimensions that can describe all other variables identified in Step 1. The use of mass (M), length (L), time (t), or force (F) are common. Length (L) and time (t) are the simplest set for mechanical phenomenon. In thermal or electrical phenomenon, temperature and heat energy should be considered as basic dimensions. Five basic dimensions are required if transformation from thermal to mechanical energy exist (Murphy, 1950).

Step 3. Determine the Pi terms

Pi terms are derived from the above basic dimensions. A method commonly used for producing Pi terms is the method of repeating variables. This method establishes a

dimensionless Pi term by dividing one of the involved parameters (non-repeating variables) by the product of the repeating variables (basic dimensions), each raised to an exponent that would make the combination of terms dimensionless. Repeating the above step for each of the remaining non-repeating variables produces all required Pi terms.

Step 4. Check each group obtained

The only restriction of this technique is that all Pi terms should be independent and dimensionless (Murphy, 1950). The groups determined from step 3 should meet this requirement.

Step 5. Set the similitude model

The functional relation between dimensionless Pi terms represents the similitude model. The similitude expressions of dependent Pi terms between scale-model and prototype are prediction equations, and the similitude expressions of independent Pi terms are specified as modeling laws, also called similarity requirements, or scale-model design conditions (Young, 1994).

4.3.1.2. Similitude parameters using the Buckingham Pi theorem

Isothermal airflow. For isothermal airflow, dimensionless parameters are derived to predict the behavior of steady, incompressible, and two-dimensional room ventilation airflow. For example, the velocity field can be described as (Murphy, 1950; Smith and Hazen, 1968):

$$\frac{U(x,y)}{U_d} = f\left(\frac{U_d h}{\nu}, \frac{L_j}{h}\right) \qquad (4.1)$$

Equation (4.1) indicates that similitude requires the same Reynolds number ($\frac{U_d h}{\nu}$) between scale-model and prototype and a similar ratio of geometric length (L_j) to inlet slot height (h).

Nonisothermal airflow. Yao et al. (1986) derived the similitude variables to describe airspeed and temperature in a neutral-pressure swine grower barn using dimensional analysis. A series of 17 non-repeating independent variables were found (Table 4.1) and

Table 4.1. Similitude variables describing pig thermal environment. (Yao, et al., 1986)

Number[1]	Description	Symbol	Dimensions[2]
1	Velocity at any point	U	Lt^{-1}
2	Temperature at any point	T	T
3	Inlet velocity	U_d	Lt^{-1}
4	Inlet characteristic dimension	h	L
5	Room length	L	L
6	Room width	W	L
7	Wall surface area	A_w	L
8	Air density	ρ	ML^{-3}
9	Air viscosity	μ	$ML^{-1}t^{-1}$
10	Gravitational acceleration	g	Lt^{-2}
11	Air expansion coefficient	β	T^{-1}
12	Ventilation heat loss	q	Ht^{-1}
13	Mean room to inlet air temp difference	ΔT	T
14	Coef of conv and rad heat trans	h_b	$HL^{-2}t^{-1}T^{-1}$
15	Mean pig body surface to room temp	ΔT_b	T
16	Pig body surface area	A_b	L^2
17	Pig body diameter	D_b	L
18	Coef of conv heat trans at wall	h_w	$HL^{-2}t^{-1}T^{-1}$
19	Mean temp difference wall to room	ΔT_w	T

Note 1. The first two variables are the dependent variables; all others are independent variables.
Note 2. Dimensions are: length (L), time (t), mass (m), temperature (T) and energy (H).

5 basic dimensions including mass (M), length (L), time (t), temperature (T), and thermal energy (H) were used. A series of similitude Pi terms were derived as shown in Table 4.2. There results (Yao et al., 1986) showed that along with geometric similarity, the Archimedes number (Ar) and Reynolds number (Re) needed to be similar as well, however, the Ar and Re can not be satisfied simultaneously. They suggested using Ar and geometric similarity, while distorting Re similarity. The end result was partial similarity between scale-model and prototype.

Table 4.2. Similitude Pi terms determined by Yao, et al. (1986)

Number	Description	Condition between model (m) and prototype (p)
π_i	U / U_d	
π_i	$T / \Delta T$	
π_1	h/L	$h_m = \frac{h_p}{n}$
π_2	$\rho U_d L / \mu$	Distorted
π_3	U_d^2 / gL	$U_{d,m} = \sqrt{n} U_{d,p}$
π_4	$\Delta T_w / \Delta T$	Distorted
π_5	$\beta \Delta T$	$\Delta T_w = \Delta T_p$
π_6	D_b / L	Distorted
π_7	$h_b \Delta T_b D_b \sqrt{A_b} / q$	$(h_b D_b \sqrt{A_b})_m = (h_b D_b \sqrt{A_b})_p$
π_8	A_b / L^2	Distorted
π_9	$\Delta T_b / \Delta T$	$\Delta T_{b,m} = \Delta T_{b,p}$
π_{10}	W / L	$W_m = W_p / n$
π_{11}	$h_w \Delta T_w L W / q$	$(h_w \Delta T_w)_m = (h_w \Delta T_w)_p$
π_{12}	A_w / L^2	$A_{w,m} = A_{w,p} / n^2$

4.3.2. Similitude parameters from the governing differential equations

An alternative approach for obtaining similitude parameters is developed from the non-dimensionalized governing equations (usually differential equations) to get the scale factors maintaining similitude between scale-model and prototype (Young, 1994).

4.3.2.1. Procedures of deriving similitude parameters (Young, 1994)

Step 1. Specify or develop the equations (usually differential equations) governing the phenomenon of the problem.

Step 2. Express the dependent and independent variables in dimensionless form using appropriate definitions for characteristic length, time, pressure, and velocity for the system.

Step 3. Rewrite the governing equations from step 1 in terms of the dimensionless variables until only dimensionless groups appear in the governing equations. Boundary and initial conditions must also be expressed in dimensionless form. The dimensionless groups that arise from this procedure correspond to the Pi terms that would be obtained from a dimensional analysis using the Buckingham Pi theorem.

4.3.2.2. Governing equations of isothermal airflow

The governing equations describing isothermal airflow should be thoroughly investigated to get a precise form of the governing parameters. The parameters of mean airspeed $(\overline{U})$, pressure $(\overline{P})$, and turbulent stress in isothermal airflow are governed by the following equations with the assumptions of steady-state, incompressible, and constant viscosity fluid.

Continuity equation:

$$\frac{\partial \overline{U}_j}{\partial x_j} = 0 \tag{4.2}$$

Momentum equation:

$$\rho \overline{U}_j \frac{\partial \overline{U}_i}{\partial x_j} = \delta_{i2}\rho g - \frac{\partial \overline{P}}{\partial x_i} + \mu \frac{\partial^2 \overline{U}_i}{\partial x_j \partial x_j} - \rho \frac{\partial}{\partial x_j}(\overline{u_i u_j}) \tag{4.3}$$

The continuity equation represents mass conservation through the air control volume with assumptions of incompressible flow. The momentum equation describes the momentum balance applied to a fluid passing through a control volume and includes the body force, the pressure gradient, molecular viscosity, and turbulent stresses. The momentum loss due to dissipation were considered negligible due to the constant density assumption. Nondimensionalizing the above incompressible Reynolds equation by the following characteristic scales:

$$x_i^* = \frac{x_i}{L_c} \tag{4.4}$$

$$P^* = \frac{\overline{P}}{P_o - P_d} \tag{4.5}$$

$$U_i^* = \frac{\overline{U}_i}{U_c} \tag{4.6}$$

$$u_i^* = \frac{u_i}{U_c} \tag{4.7}$$

results in the following nondimensional governing equations:

Continuity equation:

$$\frac{\partial U_j^*}{\partial x_j^*} = 0 \tag{4.8}$$

Momentum equation:

$$U_j^* \frac{\partial U_i^*}{\partial x_j^*} = \delta_{i2} \frac{1}{Fr^2} - \frac{Eu}{2} \frac{\partial P^*}{\partial x_i^*} + \frac{1}{Re} \frac{\partial^2 U_i^*}{\partial x_j^* \partial x_j^*} - \frac{\partial}{\partial x_j^*} (\overline{u_i u_j})^* \tag{4.9}$$

with boundary conditions as:

1. $U_i^* = 0$ at $y^* = 0$ and $y^* = H/L$.

2. The inlet and outlet openings and enclosure surfaces between scale-model and prototype should be hydrodynamically similar with properly scaled geometry and surface roughness.

The continuity equation results indicated only a change of variables but no dimensionless parameters were derived. The nondimensional momentum equation indicates that similarity between scale-model and prototype will exist from the distribution of dimensionless mean airspeed, pressure, and turbulent stress. Complete similarity requires that the two be geometrically similar including similar boundary conditions, the same Froude number (Fr), the same Euler number (Eu), and the same Reynolds number (Re).

4.3.2.3. Governing equations of nonisothermal airflow

The parameters of nonisothermal turbulent airflow includes mean airspeed ($\overline{U}$), mean temperature ($\overline{T}$), pressure ($\overline{P}$), and turbulence stress. The governing equation was derived using the Reynolds equations with assumptions of steady state, partly incompressible (i.e.

based on the Boussinesq approximation), constant viscosity, negligible body force, and no internal momentum or volumetric heat production.

Continuity equation:

$$\frac{\partial \overline{U}_j}{\partial x_j} = 0 \tag{4.10}$$

Momentum equation:

$$\rho \overline{U}_j \frac{\partial \overline{U}_i}{\partial x_j} = \delta_{i2} \rho g - \frac{\partial \overline{P}}{\partial x_i} + \mu \frac{\partial^2 \overline{U}_i}{\partial x_j \partial x_j} - \frac{\partial}{\partial x_j} (\overline{\rho u_i u_j}) \tag{4.11}$$

Energy equation:

$$\overline{U}_j \frac{\partial \overline{T}}{\partial x_j} = \alpha \frac{\partial^2 \overline{T}}{\partial x_j \partial x_j} - \frac{\partial}{\partial x_j} (\overline{u_j t}) \tag{4.12}$$

The above equations were simplified by applying the Boussinesq approximation (Kays and Crawford, 1980) for nonisothermal buoyant ventilation flow. The approximation included two parts as:

1. All variable-property effects were neglected in the above equations, except for density in the momentum equation.

2. The density difference term was simplified as

$$\rho_\infty - \rho = \rho \beta (T - T_\infty) \tag{4.13}$$

The continuity equation and energy equation were simplified assuming incompressible flow. The energy equation was derived from the First Law of Thermodynamics applied to a fluid passing through a fixed control volume by the mechanisms of heat and work. The pressure term and dissipation term of the energy equation was neglected with the

assumptions of low-speed flow defined as velocities less then 30% of the speed of sound (White, 1991). The dissipation term from the momentum equation could be neglected because of the effect of the coefficient of bulk viscosity (λ) is negligible except in the study of the structure of shock waves and the absorption and attenuation of acoustic waves (Anderson et al., 1984).

The characteristic scales for nondimensionalizing the above Reynolds equations were as follows:

$$x_i^* = \frac{x_i}{L_c} \tag{4.14}$$

$$U_i^* = \frac{\overline{U}_i}{U_c} \tag{4.15}$$

$$u_i^* = \frac{u_i}{U_c} \tag{4.16}$$

$$T^* = \frac{\overline{T} - T_d}{T_f - T_d} \tag{4.17}$$

$$t^* = \frac{t}{T_f - T_d} \tag{4.18}$$

$$P^* = \frac{\overline{P}}{P_o - P_d} \tag{4.19}$$

Substituting the characteristic scales into the governing equations, results in the following nondimensional equations:

Continuity equation:

$$\frac{\partial U_j^*}{\partial x_j^*} = 0 \tag{4.20}$$

Momentum equation:

$$U_j^* \frac{\partial U_i^*}{\partial x_j^*} = \delta_{i2} \frac{1}{Fr^2} - \delta_{i2} Ar T^* - \frac{Eu}{2} \frac{\partial P^*}{\partial x_i^*} + \frac{1}{Re} \frac{\partial^2 U_i^*}{\partial x_j^* \partial x_j^*} - \frac{\partial}{\partial x_j^*} (\overline{u_i u_j})^* \tag{4.21}$$

Energy equation

$$U_j^* \frac{\partial T^*}{\partial x_j^*} = \frac{1}{Pe} \frac{\partial^2 T^*}{\partial x_j^* \partial x_j^*} - \frac{\partial}{\partial x_j^*} (\overline{u_j t})^* \tag{4.22}$$

with the following boundary conditions:

1. $U_i^* = 0$ at $y^* = 0$ and $y^* = H/L$

2. $T^* = 1$ at $y^* = 0$ and $T^* = 0$ at $y^* = H/L$

3. The inlet and outlet openings and enclosure surfaces should be hydrodynamically similar and the thermal conditions should be similar as well.

No dimensionless parameters were derived from the continuity equation. Several dimensionless parameters resulted from the momentum and energy equations including the Fr, Ar, Re, Eu, and Pe numbers. Complete similitude requires that all the similarity parameters associated with geometric similarity and boundary conditions be satisfied between scale-model and prototype.

4.3.3. Similitude parameters

The dimensionless similitude parameters derived from both the dimensional analysis approach and the governing differential equation approach for both isothermal and nonisothermal conditions are described below.

(1) Froude number

$$Fr = \frac{U_c}{\sqrt{gL_c}} \tag{4.23}$$

The Fr represents the ratio of inertial to gravitational forces. Similarity requires that:

$$(\frac{U_c}{\sqrt{gL_c}})_m = (\frac{U_c}{\sqrt{gL_c}})_p \tag{4.24}$$

With $g_m = g_p$, results in a relation between diffuser airspeed as:

$$\frac{U_{c,m}}{U_{c,p}} = \frac{\sqrt{L_{c,m}}}{\sqrt{L_{c,p}}} = \sqrt{\frac{1}{n}} \tag{4.25}$$

(2) Archimedes number

$$Ar = \frac{\beta g L_c (T_f - T_d)}{U_c^{\,2}} \tag{4.26}$$

where $\beta = 1 / T$ for perfect gases. The Ar represents the ratio of buoyant to inertial forces and could also be expressed as $Re^2 Gr$. Similarity requires that:

$$[\frac{\beta g L_c (T_f - T_d)}{U_c^{\,2}}]_m = [\frac{\beta g L_c (T_f - T_d)}{U_c^{\,2}}]_p \tag{4.27}$$

With $g_m = g_p$, results in:

$$[\frac{\beta g L_c (T_f - T_d)}{U_c^2}]_m = [\frac{\beta g L_c (T_f - T_d)}{U_c^2}]_p \qquad (4.28)$$

If the temperature field is set equal, then $\beta_m = \beta_p$ and $(T_f - T_d)_m = (T_f - T_d)_p$, resulting in a relation between diffuser airspeed as:

$$\frac{U_{c,m}}{U_{c,p}} = \frac{\sqrt{L_{c,m}}}{\sqrt{L_{c,p}}} = \sqrt{\frac{1}{n}} \qquad (4.29)$$

which is the same as equation (4.25).

(3) Euler number

$$Eu = \frac{P_o - P_d}{\frac{1}{2}\rho U_c^2} \qquad (4.30)$$

The Eu represents the ratio of pressure to momentum forces. Similarity requires that:

$$(\frac{P_o - P_d}{\frac{1}{2}\rho U_c^2})_m = (\frac{P_o - P_d}{\frac{1}{2}\rho U_c^2})_p \qquad (4.31)$$

If the same working fluid between scale-model and prototype is used, then $\rho_m = \rho_p$ and the relation simplifies to:

$$(\frac{P_o - P_d}{U_c^2})_m = (\frac{P_o - P_d}{U_c^2})_p \qquad (4.32)$$

If the pressure difference between inlet and outlet are the same between scale-model and prototype, the relation further simplifies to:

$$U_{c,m} = U_{c,p} \tag{4.33}$$

(4) Reynolds number

$$Re = \frac{\rho U_c L_c}{\mu} \tag{4.34}$$

The Re represents the ratio of inertial to viscous forces. Similarity between scale-model and prototype requires that:

$$(\frac{\rho U_c L_c}{\mu})_m = (\frac{\rho U_c L_c}{\mu})_p \tag{4.35}$$

If the same working fluid between scale-model and prototype is used, then $\rho_m = \rho_p$ and $\mu_m = \mu_p$, resulting in the following requirement between diffuser airspeeds:

$$\frac{U_{c,m}}{U_{c,p}} = \frac{L_{c,p}}{L_{c,m}} = n \tag{4.36}$$

where n is the scale between prototype and scale-model.

(5) Peclet number

$$Pe = \frac{U_c L_c}{\alpha} \tag{4.37}$$

The Pe represents dimensionless heat transfer and could also be expressed as Re Pr. Similarity requires that:

$$(\frac{U_c L_c}{\alpha})_m = (\frac{U_c L_c}{\alpha})_p \tag{4.38}$$

If the same working fluid between scale-model and prototype is used, then $\alpha_m = \alpha_p$ resulting in the following requirement between diffuser airspeeds:

$$\frac{U_{c,m}}{U_{c,p}} = \frac{L_{c,p}}{L_{c,m}} = n \qquad (4.39)$$

The scaling velocity is the same as equation (4.36). This result implies that the Prandtl number (Pr) is satisfied between the scale-model and prototype if the same working fluid is used.

4.4. Scaling Model

4.4.1. Isothermal airflow

The similarity analysis indicates that the similarity parameters for isothermal airflow were geometry, Fr, Eu, and Re between scale-model and prototype. The Froude number is important for compressible flow and for motions with free liquid-vapor surfaces in the flow (Schlichting, 1979). The isothermal airflow in a slot-ventilated enclosure was considered as a homogeneous fluid without free liquid-vapor surfaces, thus the Froude number could be neglected (Zhang, 1991).

The remaining similarity parameters require higher inlet velocities in the scale-model based on Re but the same inlet airspeed between scale-model and prototype based on Eu.

Rousseau and Albright (1996) stated an anomaly in the use of Reynolds number as a kinematic similarity criterion for scale modeling of slot-ventilated enclosures. They suggested that pressure losses between the inlet and outlet dominated the overall airflow

patterns within the enclosure based on the experimental results of Timmons (1979), which showed pressure loss remained constant above the threshold inlet Re. On the other hand, above a certain threshold value, Re had a negligible effect on the governing equation compared with Eu using an order of magnitude analysis.

Eu ($=2\Delta P / \rho U^2$) becomes an alternative kinematic similarity criterion instead of Re. The results also justified the concept of using Rm ($= U_d^2 h / (L + H)$) as the similarity criterion (Adre and Albright, 1994). However, the viscosity term should not be neglected for low-Reynolds number flow because of the expansion of the air-jet region caused by the discontinuous airspeed and viscous effects in this region.

4.4.2. Nonisothermal airflow

Complete similarity for nonisothermal airflow requires geometric similarity between the scale-model and prototype with similar boundary conditions and equal Fr, Ar, Eu, Re, and Pe numbers. Only partial similarity is reached with scale-model studies because of the conflict between these similarity requirements. A distorted model is usually unavoidable. Using the predominant undistorted parameters as the similarity requirement is usually used to study regions of interest (e.g. the occupied zone) in the prototype (Zhang, 1991).

If air is used as the working fluid in both the scale-model and prototype, and the same thermal environment is maintained ($(T_f - T_d)_m = (T_f - T_d)_p$), then the same air properties such as $\rho_m = \rho_p$, $\nu_m = \nu_p$, $\alpha_m = \alpha_p$, $\beta_m = \beta_p$ exist (Baturin, 1972). With consistent air

properties , the Prandtl number will be satisfied and the governing similitude parameters become the Eu, Re, Ar, and Fr numbers. Recall also that the kinematic similitude requirement between scale-model and prototype was the same based on either the Fr or Ar number.

Based on the similitude parameters presented in section 4.3.3, the Re requires a higher inlet airspeed in the scale-model and the Eu requires the same inlet airspeed in the scale-model. The Ar and Fr on the other hand require lower inlet airspeeds in the scale-model. Some reports state that air movement in slot-ventilated enclosures with air-jet ventilation is affected mainly by thermal buoyancy and independent of the Re when examined at higher ranges (Re>1850) (Baturin, 1972; Szucs, 1980; Yao et al., 1986; Christianson et al., 1988; Fissore and Liebecg, 1991) or lower ranges (Re<100) (Mullejans, 1966). For small Ar, airflow approximates isothermal flow (Mullejans, 1966). The critical value of Ar depends on the geometrical conditions between the scale-model and prototype (Zhang, 1991).

Randall and Battams (1979) postulated a corrected Archimedes number (Ar_c) which accounted for the properties of aperture and room size to describe airflow patterns in livestock buildings. The air-jet remains horizontal as would an isothermal jet when $Ar_c<30$, and falls after entry due to the dominant buoyant forces when $Ar_c>75$.

Perfect thermal similarity is difficult to obtain due to the complex modes of heat transfer phenomena at the enclosures boundaries. However, satisfactory thermal similarity could be obtained between the heated scale-model and prototype by assuring geometric similarity, proportionately reducing the wall thickness and conductivity of the scale-model, and

operating the heat input proportional to the square of the linear size reduction scale factor as (Parczewski and Renzi, 1963):

$$\frac{q_p}{q_m} = n^2 \tag{4.40}$$

where q_p and q_m represent the total input heat rate for the prototype and scale-model, respectively. The factors q_p and q_m imply that the unit heat flux is equal between scale-model and prototype.

Fluid motion in buoyant air-jets is generally governed by pressure, inertial, buoyant, and viscous forces. The local characteristics of the flow are determined by the relative magnitude of these forces at each point. The overall characteristics are determined by the strength of the forces at the air-jet source and by the ambient conditions (Chen and Rodi, 1980). Chen and Rodi (1980) concluded that for very small velocities or large temperature differences, the air-jet flow performance in a ventilated room was solely dominated by the Ar. As the airflow rate increased or the heat load decreased, the airflow was more like isothermal airflow and depended on the Re or Eu. The critical value to distinguish the dominant parameters may depend on the specific structure of airflow conditions, such as enclosure dimensions, geometric configurations, and the amount of heat flux.

4.5. Summary

1. The studied ceiling slot-ventilated flow is a steady-state, incompressible, and constant-viscosity airflow for isothermal conditions. Compressibility existed for nonisothermal

conditions in the momentum equation and this was treated using the Boussinesq approximation.

2. Complete similarity requires geometric similitude, kinematic similitude, dynamic similitude, thermal similitude, and similar boundary conditions between scale-model and prototype.

3. Complete similarity of isothermal airflow requires similar geometry, Re, Eu, and boundary conditions. Ar, Fr, and Pe numbers are added requirements for nonisothermal airflow.

4. Only partial similarity can be achieved due to conflicts between similarity requirements. The airflow characteristics are determined by the relative magnitude of governing forces at different airflow conditions. The critical values to distinguish different airflow characteristics should be investigated to determine the dominant forces and similarity parameters for such airflow conditions.

5. In isothermal airflow, a question still exists whether airflow motion is governed by pressure forces or viscous forces implying that either the Eu or Re are possible similarity parameters depending upon the airflow conditions.

6. In nonisothermal airflow, Ar has been validated as the similarity criterion even though other dimensionless parameters have been distorted. When the airflow rate increases or the heat load decreases, nonisothermal airflow approaches isothermal airflow and therefore will be governed by a different similarity parameter.

CHAPTER 5. MATERIALS AND METHOD

5.1. Experimental Facilities

Two geometrically similar scale models representing a 1:3 and 1:6 scale-model of a prototype swine grower barn located at the Iowa State University Swine Nutrition and Management Research Center were used to study airflow parameters between a prototype and scale-model. The airflow patterns, air-jet penetration distance, and variations in velocity and temperature fields were measured using airflow visualization, airspeed measurements, and temperature measurements.

5.1.1. The test chambers

The test chambers used are shown in Figure 5.1. The slot inlet width used was the same as the width of the enclosure (W). The inlet aspect ratio was much larger than 20 and as a result, the airflow was treated as a two-dimensional wall jet without the effect of side walls (Forthmann, 1934).

The dimensions of the two models are shown in Figure 5.2. The scale models were made from 12.7 mm thick (1/2 inch) plywood. The inner surface of the models were sanded and painted black. The front wall was made of Plexiglas to accommodate airflow visualization. Access holes were placed on the top ceiling along a cross line between the inlet wall and the end wall at intervals of 20 mm, except for the area between the inlet and a distance of 33 h

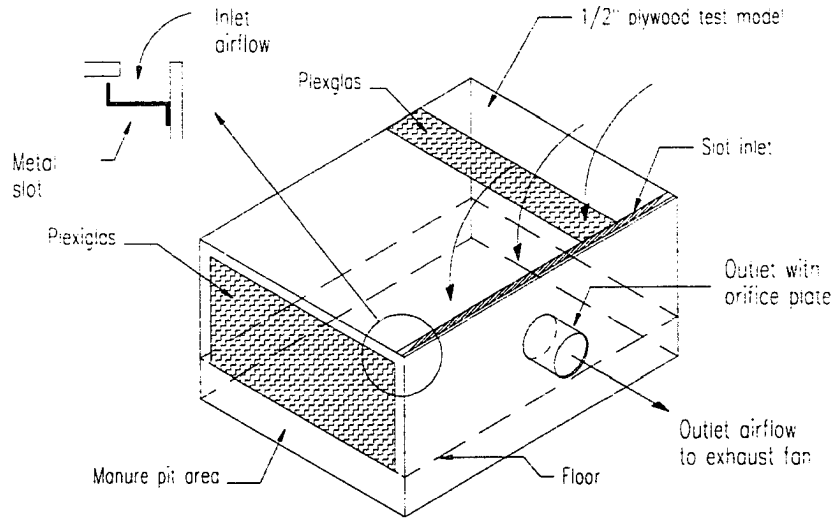

Figure 5.1. The scheme of experimental scale-model.

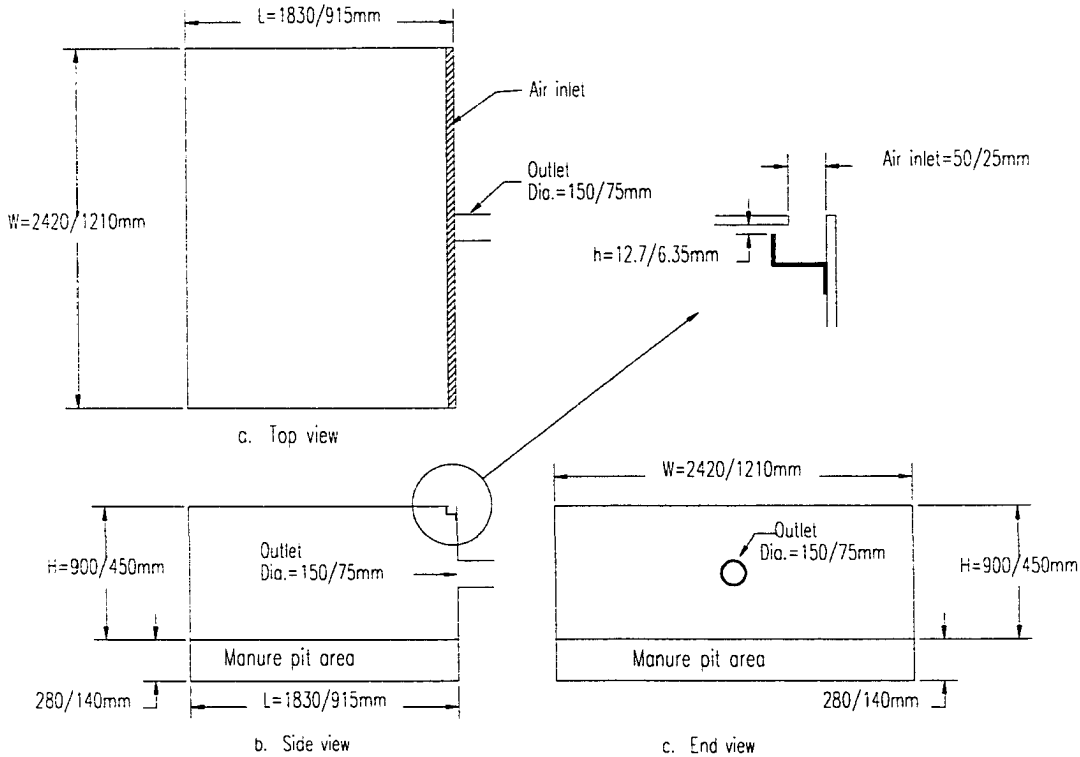

Figure 5.2. Dimensions (scale= 1:3/scale= 1:6) of scale-models in different views.

from the inlet where a continuous access slot was constructed to discretize air-jet development near the inlet (Figure 5.3).

A portion of the top ceiling was fabricated with Plexiglas which extended along the length of both models for illuminating purposes. Circular exhaust ports were provided on the inlet wall as shown in Figure 5.2. A 75 mm diameter hole was used for the 1:6 model and a 150 mm diameter hole was used for the 1:3 model.

Duct work was constructed and fitted between the circular exhaust hole and an exhaust fan of 1:3 model (Model 3C507A; Dayton Electric MFC, Co.) and 1:6 model (Model K8L; Kanalflakt, Inc.). Calibrated orifice plates were used to select desired airflow rates through each model. A micromanometer (Model 1430; Dwyer Instruments, Inc.) was used to measure the pressure difference across the orifice to determine airflow rate (Figure 5.4). The models were insulated with 88.9 mm (3 1/2 inches) of fiberglass insulation to reduce heat conduction loss for the nonisothermal airflow experiments.

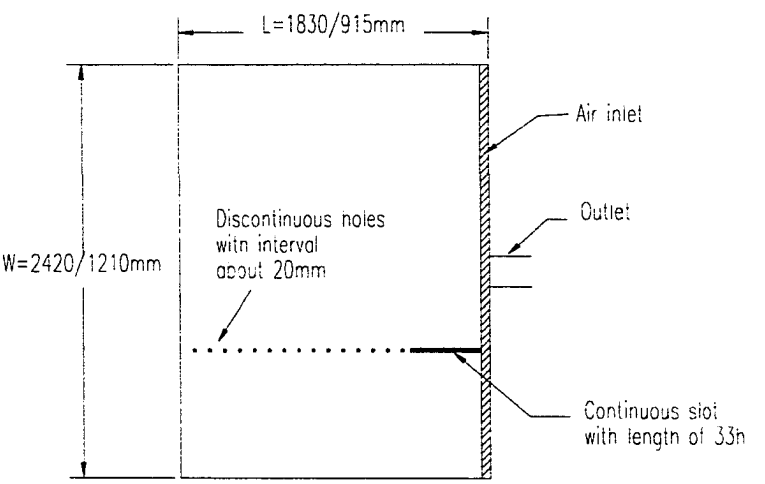

Figure 5.3. The plane-view layout of access holes on the top ceiling of test models.

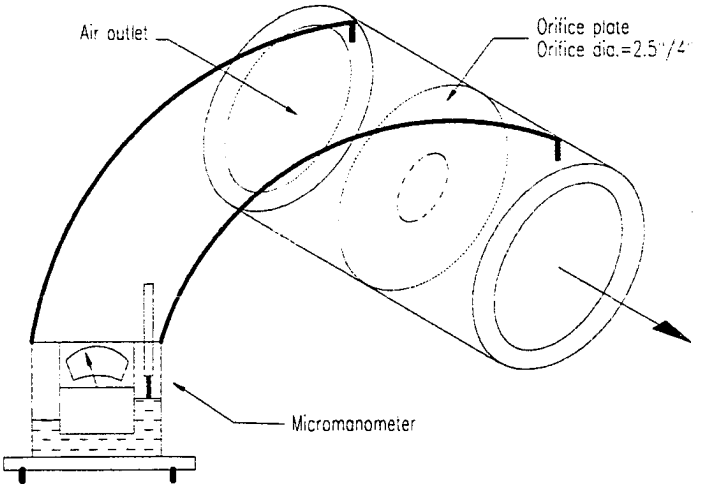

Figure 5.4. Orifice plate and micromanometer used to measure pressure difference.

5.1.2. Heating system

The floor of both models was fitted with insulated silicone rubber heat panels (Model SRFG 442/2 and 1242/2; OMEGA Engineering, Inc.) that occupied 58% of the floor area to simulate animal surface temperature (Figure 5.5). The power density was 2.5 W/in^2 and was controlled by miniature microprocessor temperature controllers (Model CN9000; OMEGA Engineering, Inc.) with an accuracy of $\pm$ 0.5° C using a PID control mode. The maximum operating temperature of the heaters was 120° C.

5.1.3. Airflow visualization

Airflow patterns were visualized using titanium tetrachloride (Model 15-049; E. Vernon Hill, Inc.). The chemical was introduced at the inlet and illuminated by 300 Watt

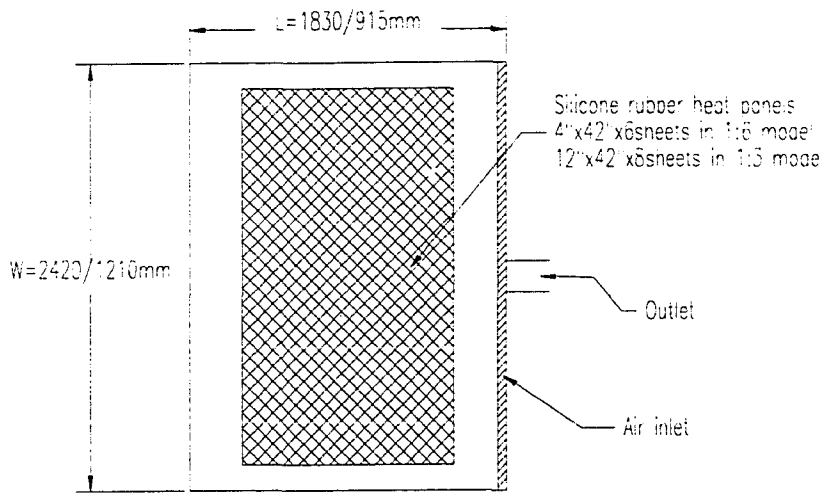

Figure 5.5. The top-view layout of rubber heating panels.

photocopy lamps. A light box focused light along the longitudinal axis as shown in Figure 5.6. The bright light combined with the black inner surfaces allowed for photographing of air movement by both camera and camcorder.

5.1.4. Airspeed measurement

Airspeed was measured using an omni-directional hot-film anemometer (Model 8470; TSI, Inc.). A portable data acquisition system (Model CR10; Campbell Scientific, Inc.) was used to collect data (Figure 5.7). The acquiring period for each measurement was 180s and the sampling frequency was set at 16Hz. The average value over time, at a point, was used for analysis and presentation.

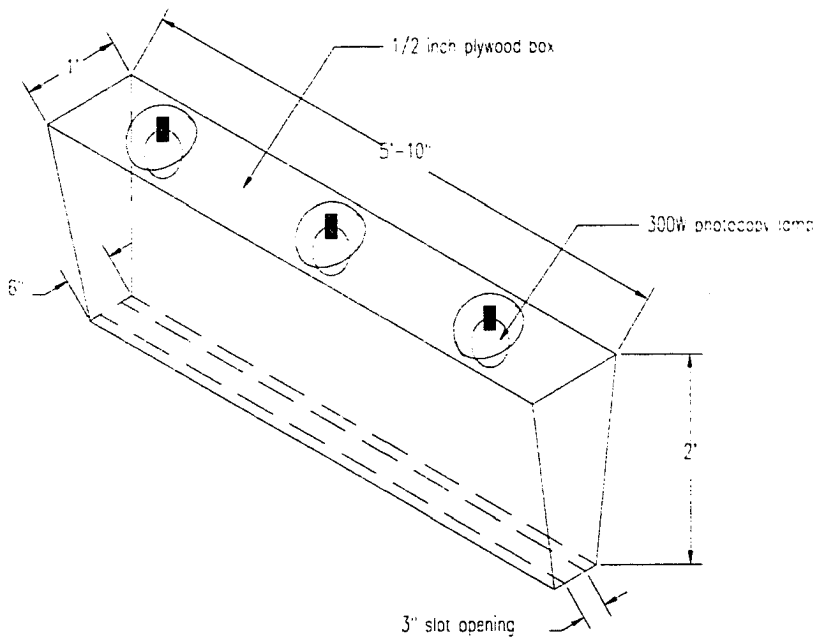

Figure 5.6. Scheme of light box

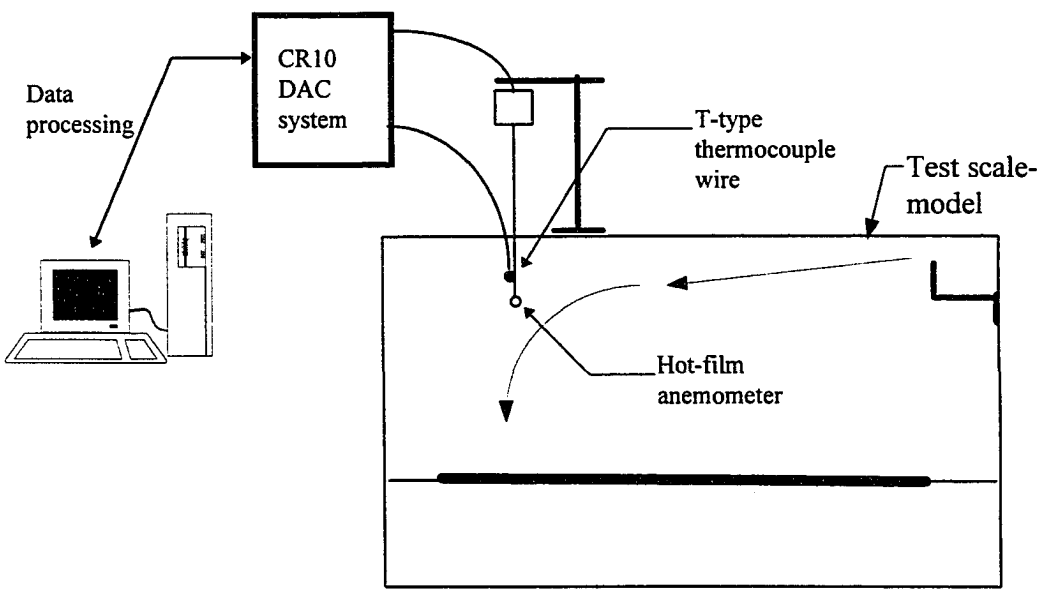

Figure 5.7. Communication link between data acquisition system and measurement field.

5.1.5. Temperature measurement

The temperature field was measured using T-type thermocouples connected to the same data acquisition system as the airspeed measurement.

5.2. Measurements and Method

5.2.1. Airflow patterns

Airflow patterns were measured using airflow visualization and by quantifying the measured peak airspeed trajectory along the longitudinal axis of the air-jet. Airflow visualization allowed for a qualitative image of the airflow patterns. Peak airspeed was measured along the ceiling and floor by a series of velocity measurements in the vertical direction (i.e. downward from the ceiling or upward from the floor) at increments of 2 to 10 cm. The connected peak airspeed positions along the ceiling and floor was used to describe the air-jet trajectory which was used in conjunction with airflow visualization to described airflow patterns.

5.2.2. Air-jet penetration

The air-jet penetration described in this research was defined as the distance from the inlet wall to where the wall air-jet separated from the ceiling. The air-jet penetration distance was measured using axial velocity measurements at a point located 5 mm beneath the ceiling. The separation of the wall jet was defined when the decay of axial velocity fell below 0.1

m/s. The air-jet penetration distance was determined by moving the anemometer back and forth at least two iterations to ensure accuracy of the measurement.

The inlet airflow rate was initialized at a small rate and increased gradually to avoid the lag phenomenon found for confined airflow (Zhang, 1991). The air-jet penetration distance was also confirmed qualitativeiy using airflow visualization and measurements of peak airspeed trajectories.

5.2.3. Airspeed field

5.2.3.1. Measurement scheme

The airspeed field was measured to verify kinematic similarity. The measurement scheme used a non-uniform grid from 0.1 L to 0.9 L horizontally at 0.2 L intervals and from the floor to ceiling vertically at 2 cm to 10 cm intervals (Figure 5.8). The measured points near the ceiling and floor regions were more closely spaced. This information was used to discretize the peak velocity profile, air-jet trajectory, and the velocity distribution in the room. Approximately 65 to 100 points per run was collected for each model. The above measurements were repeated twice for each unique airflow condition.

5.2.3.2. Sampling period

The sampling period was fixed at 180 seconds per collection point to ensure accurate time-averaged results for turbulent airflow (Thorshauge, 1982). This sampling period was

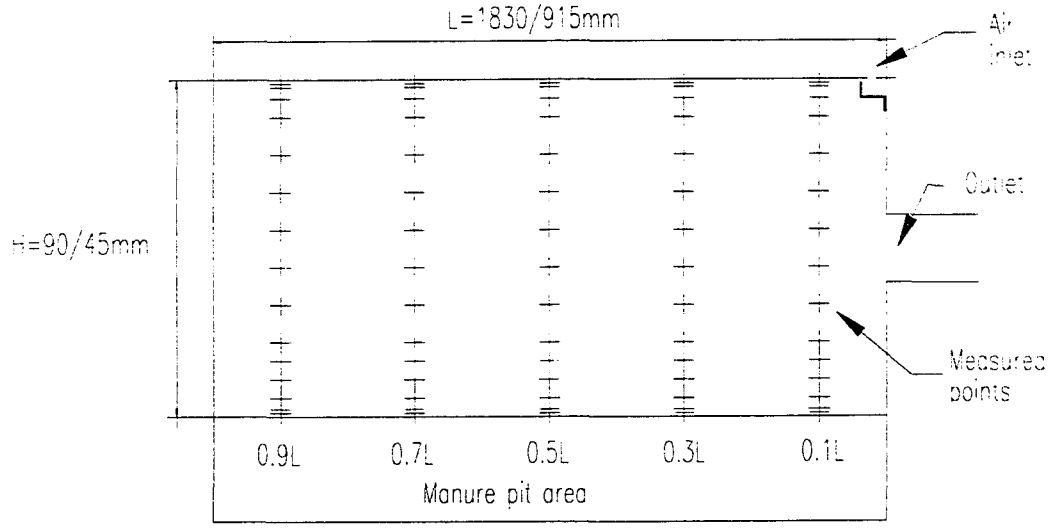

Figure 5.8. The scheme of measurements of velocity and temperature field.

much longer than was used in previous similar studies (Zhang, 1991; Adre and Albright, 1994).

5.2.3.3. Sampling rate

The sampling rate needs to be high enough to capture turbulent velocity fluctuations. The sampling frequency should be at least twice the highest frequency of the turbulent velocity fluctuation according to the Nyquist sampling theorem (Franklin et al., 1990). The sampling rate used in this experiment was 16 Hz and the velocity fluctuation components with higher frequencies were considered to be negligible because of the small amount of kinetic energy associated with those components.

5.2.4. Temperature field

The measurement scheme for quantifying the temperature field was the same as that shown in Figure 5.8. Thermocouple wire was attached to the hot-film anemometer and simultaneous measurements of both airspeed and temperature were made at each point.

5.3. Experimental Plan

The experiment was separated into isothermal and nonisothermal tests. Each is described below.

5.3.1. Isothermal tests

For isothermal airflow, the air-jet penetration distance was tested initially to study variations of airflow patterns for both slot-ventilated enclosures (1:3 and 1:6). The specific airflow pattern was validated by airflow visualization and use of the peak airspeed trajectory. Airflow rates between the minimum jet momentum (described below) and the threshold airflow rate were tested to verify the velocity in both enclosures.

The minimum jet momentum to produce a stable rotary airflow pattern within a confined enclosure has been suggested to be 0.01 kg/m^2s^2 (Kaul et al., 1975). This implies that the minimum airflow rates required were 12 and 69 cfm for the 1:6 and 1:3 scale-models, respectively. Because the airflow field has been shown to be independent of the airflow rate when beyond a threshold value, the airflow patterns and velocity fields should be self-similar (Timmons, 1984) without the need for further validation beyond the threshold value.

The threshold value varies with the scale of the model. The threshold maximum airflow rate was found by using air-jet penetration distance measurements. The airflow rate for similitude verification of the velocity fields was derived between these critical values by comparing the Re and Rm as the similarity criteria. Recall that the Rm is related to the Eu and has been proposed as an acceptable similarity criteria for isothermal airflow (Adre and Albright, 1994).

5.3.2. Nonisothermal tests

The experimental plan for nonisothermal tests was similar to that for the isothermal tests except that the airflow rates tested were adjusted based on variations in heat loads. The related similarity criteria include the Ar, Re, and Rm.

5.3.2.1. Heat loads

The floor of the scale-model and prototype were maintained at a constant temperature to simulate the heat gains from animals in the occupied zone. The temperature differences (ΔT) between the heated floor panel and the inlet air-jet were set at 10°C,40°C, and 60°C in different tests to simulate the physical thermal environment of a swine grower barn located in Ames, Iowa, ventilated during the winter. The actual temperature difference between the estimated pig's surface temperature of 33° C and the winter design outside air temperature of −24° C was 57° C. The choice of 60° C represented the extreme condition of winter.

5.3.2.2. Airflow rates

The airflow rates used for the nonisothermal tests was determined using results from the air-jet penetration distance tests. Air-jet penetration showed the approximate critical values of airflow rate for both the threshold fully rotary airflow condition and the case where the air-jet fell immediately after entry to the ventilated space. Airflow rates between the above critical values were chosen to validate similitude of the velocity and temperature fields between scale-model and prototype.

CHAPTER 6. RESULTS AND DISCUSSION

The experimental results are discussed separately as isothermal and nonisothermal airflow. The objectives of the experiments conducted were to evaluate basic physical features of airflow in confined enclosures where wall-jets are used to provide air-mixing. Ideally, it would be desirable to study prototypes in the laboratory using scale-models, and do so with confidence. The ultimate objective then was, in the process of studying basic physical features of air motion, to find guidelines for using similitude parameters that give the best agreement between scale-model and prototype. Please note that Rm, the inlet jet momentum ratio, is cited throughout this section. The units on Rm are m^2/s^2.

6.1. Isothermal Airflow

The similitude criteria required between a scale-model and prototype were stated in Chapter 4. The similarity requirements include geometric similitude, kinematic similitude, dynamic similitude, and similar boundary conditions. Geometric similitude is based on the precise scaling of both scale-model and prototype in all linear dimensions. Geometric similitude combined with dynamic similitude must combine to yield kinematic similarity, which ensures that similar airspeeds will exist in all dimensions of the flow field (Young, 1992).

The most significant similitude evaluation technique between the scale-model and prototype are measurements of the airspeed field. Airflow patterns provide information on

relative airflow motion and are the result of relative forces acting on the enclosed air-jet. Thus the evaluation of isothermal similitude for this research between scale-model and prototype focused on airflow patterns and the airspeed field in ceiling slot-ventilated enclosures.

The similitude parameters for isothermal airflow were shown to be the Reynolds number (Re) and Euler number (Eu). It was previously shown (Chapter 4) that the Euler number could be represented by the inlet jet momentum ratio (Rm) as proposed by Adre and Albright (1994). Thus the parameters that need to be validated as similarity requirements for isothermal airflow were the Reynolds number (Re) and the inlet jet momentum ratio (Rm).

The experimental procedures for isothermal airflow included air-jet penetration distance, airflow pattern, and the airspeed field. The method of airflow visualization and airspeed measurement were used in both the scale-model and prototype enclosures.

6.1.1. Air-jet penetration distance

Air-jet penetration distance is a quantitative method used to describe the airflow pattern in ceiling slot-ventilated enclosures. The range of airflow rates with the corresponding values of Re and Rm used to evaluate air-jet penetration distance are shown in Table 6.1. The maximum rate for each enclosure represents a level that exceeds the threshold Re for fully rotary airflow. The minimum rate for each enclosure represents a level far lower than that required for a stable airflow pattern as suggested by Kaul et al. (1975). The maximum and minimum rates thus bracketed the range of expected airflow patterns in each enclosure.

Table 6.1. Isothermal airflow test condition ranges for testing penetration distance.

Test		Q, cfm	U_d, m/s	ΔT,°C	Re	Rm
Prototype	Max.	362	5.56	0	4442	0.1400
	Min.	16	0.25	0	199	0.0003
Scale-model	Max.	87	5.32	0	2124	0.1300
	Min.	4	0.26	0	104	0.0003

The air-jet penetration distance for both enclosures showed that as Re (Figure 6.1) and Rm (Figure 6.2) increase, air-jet penetration distance varies positively and remains constant above a threshold maximum value. As shown in Figure 6.2, air-jet penetration distance plotted against Rm followed the same curve for both the scale-model and prototype.

The threshold value indicated that the airflow patterns were independent to further increases in Re or Rm and agrees with past research (Timmons, 1984). When the air-jet penetration distance reaches the maximum value, the airflow pattern becomes fully rotary and does not change with increases in the airflow rate. The threshold air-jet penetration distance was an important quantitative index used to validate similitude between the scale-model and prototype.

The maximum penetration distance was approximately 0.84 L in both enclosures which equates to 1.73 H. Adre and Albright's (1994) experiment resulted in a maximum penetration distance of 0.64 L when the inlet was located on the same wall as the outlet, as is the current situation. The difference in measured maximum penetration distance between Adre and Albright (1994) and this research may have resulted from differences in outlet configurations. The outlet configuration in Adre and Albright's (1994) experiment was a long slot outlet of about 1/4 cross room area of the enclosure. A circular exhaust outlet of

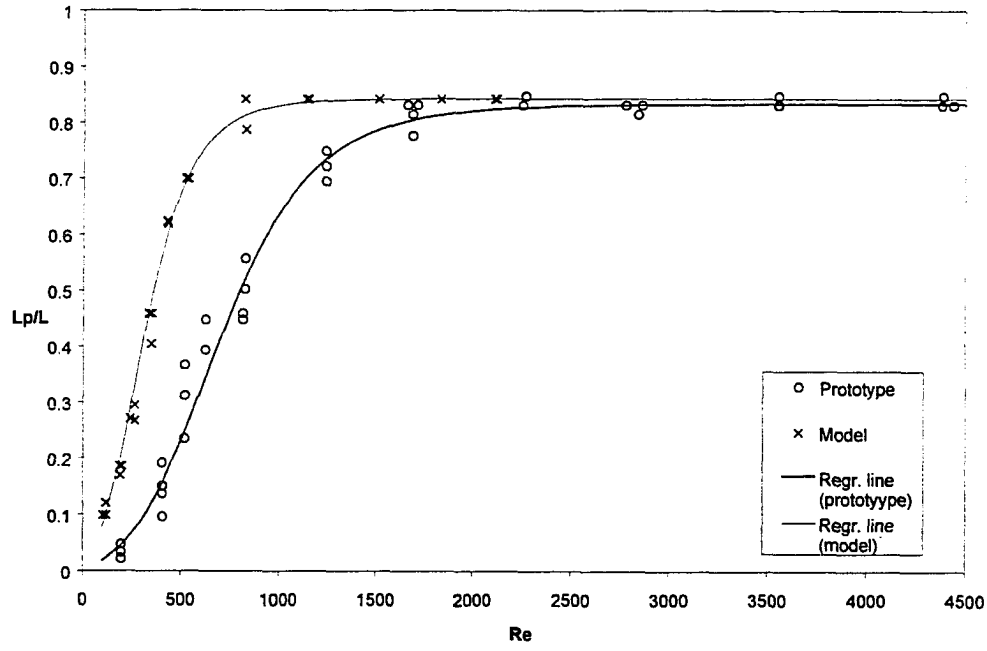

Figure 6.1. Normalized penetration distance as a function of Reynolds number (Re).

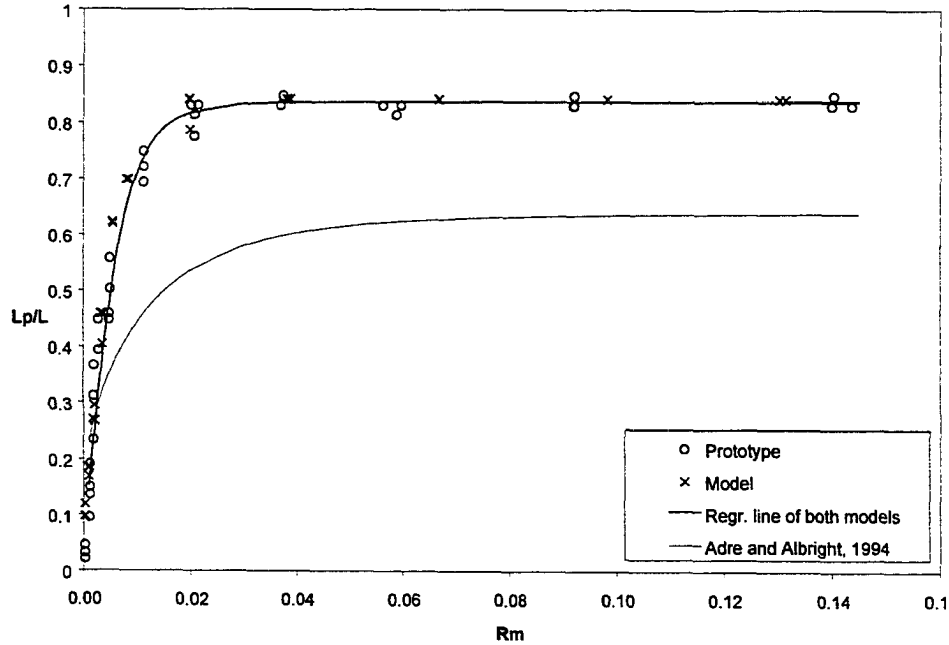

Figure 6.2. Normalized penetration distance as a function of inlet jet momentum number (Rm).

about 1/120 cross room area of the model was used in this project. In addition, Adre and Albright (1994) used a slightly different approach for quantifying air-jet penetration. They primarily used airflow visualization to quantify air-jet penetration. This study used an airspeed of ≤ 0.1 m/s to quantify air-jet penetration as was described in section 5.2.2.

The plots of air-jet penetration distance suggest that Rm is the appropriate similitude criteria for establishing similar airflow patterns. The results agree with the study of Adre and Albright (1994). The threshold value of Re is about 950 (scale-model) and 1900 (prototype) to reach 98% threshold penetration distance. The equations describing air-jet penetration (L_p) for the scale-model as a function of Re is as follows:

$$\frac{L_p}{L} = \frac{0.84}{205e^{-0.30\sqrt{Re}} + 1} \tag{6.1}$$

where r^2=0.98; and for the prototype is:

$$\frac{L_p}{L} = \frac{0.84}{450e^{-0.23\sqrt{Re}} + 1} \tag{6.2}$$

where r^2=0.96. The threshold value of Rm is about 0.02 to reach 98% threshold penetration distance in both models and the equation describing air-jet penetration (L_p) was as follows:

$$\frac{L_p}{L} = \frac{0.84}{20.18e^{-47.29\sqrt{Rm}} + 1} \tag{6.3}$$

where r^2=0.92. Equation 6.3 can be used to predict air-jet penetration distance and the threshold value of Rm which results in a fully rotary airflow pattern for isothermal conditions.

6.1.2. Airflow patterns

Airflow patterns were measured using air-jet trajectory measurements and airflow visualization. Air-jet trajectories between scale-model and prototype were compared using Re and Rm similitude parameters.

The airflow pattern within ceiling slot-ventilated enclosures has been classified into three categories as shown in Figure 6.3 (Jin and Ogilvie, 1990). Several proposals have been made in the past for describing transitions between these three airflow patterns. Table 6.2 describes some of these and the corresponding airflow rates required for the current scale-model and prototype. For this research project, the critical values derived from the air-jet penetration distance test (Section 6.1.1) and Kaul et al.'s (1975) results were used. Therefore, for the chambers studied, it was assumed that transition from stagnant to intermediate zone airflow occurred at 12 and 69 cfm for the scale-model and prototype, respectively, and from intermediate to fully rotary zone airflow at 33 and 134 cfm, respectively. All future references to airflow pattern "expectations" use these airflow rate guidelines.

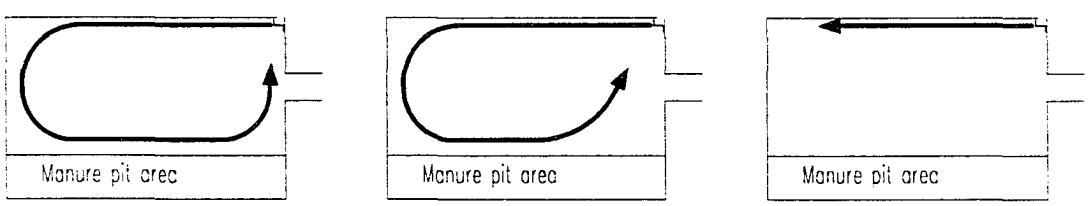

Figure 6.3. Categories of airflow pattern for isothermal condition (Jin and Ogilvie, 1990).

Table 6.2. The critical airflow rates proposed for various isothermal airflow patterns for ceiling slot-ventilated enclosures.

Airflow pattern category	Airflow rate of prototype, cfm	Airflow rate of model, cfm	Formula	Reference
Critical values to divide stagnant zone and intermediate zone	69	12	I_o=0.01 kg/m^2-s^2	Kaul et al., 1975
	56	54	$hU_d^{1.65}$=0.046	Jin and Ogilvie, 1990
Critical values to divide intermediate zone and rotary airflow zone	134	33	Rm=0.02	Penetration distance test
	168	142	$hU_d^{2.5}$=0.136	Jin and Ogilvie, 1990

Airflow patterns were measured using two techniques. Air-jet trajectories were used to provide quantitative evidence for the air-jet path near the ceiling and floor regions. Finally, airflow visualization was used to provide additional support for air-jet trajectory data.

6.1.2.1. Air-jet trajectory measurement

Several airflow rates were chosen around the critical airflow rates shown in Table 6.2 to encompass the anticipated stagnant and fully rotary airflow zones as shown in Figure 6.3. The test conditions used are shown in Table 6.3. The peak airspeed trajectories for each test were used to quantify the airflow pattern. Figures 6.4 and 6.5 show the air-jet peak airspeed trajectory along the ceiling and floor for the prototype (Figure 6.4) and scale-model (Figure 6.5).

Fully rotary airflow zone. The trajectories in both physical models were similar when the airflow rate was beyond the threshold value for fully rotary airflow (IP1, IP2, IM1, IM2) which was determined using the air-jet penetration test results (Section 6.1.1). Higher

Table 6.3. Test conditions of trajectory measurement for isothermal airflow.

Test	Q,cfm	U_d,m/s	ΔT,°C	Re	Rm	Anticipated airflow zone
IP1[1]	205	3.14	0	2512	0.0460	Fully rotary
IP2	142	2.18	0	1745	0.0222	Fully rotary
IP3	70	1.08	0	863	0.0054	Intermediate airflow
IP4	35	0.54	0	435	0.0014	Stagnant zone
IP5	19	0.29	0	234	0.0004	Stagnant zone
IM1	52	3.22	0	1287	0.0483	Fully rotary
IM2	35	2.14	0	854	0.0212	Fully rotary
IM3	18	1.14	0	454	0.0060	Intermediate airflow
IM4	9	0.57	0	228	0.0015	Stagnant zone
IM5	4	0.24	0	97	0.0003	Stagnant zone

Note 1. I=isothermal, P=prototype, M=scale-model, 1=test 1.

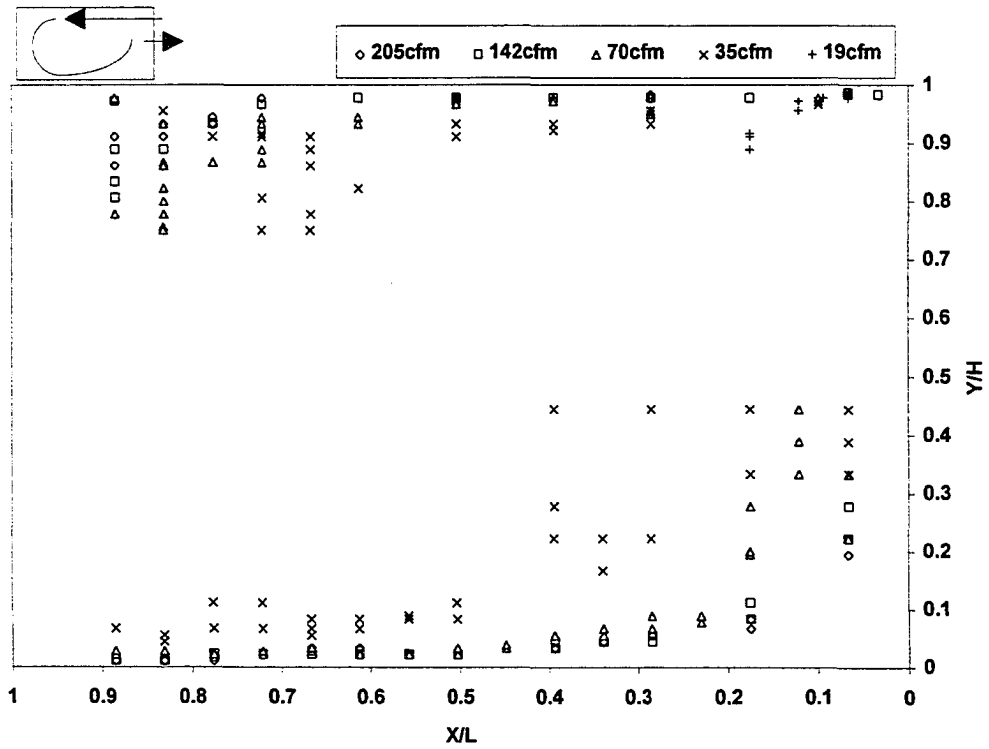

Figure 6.4. Peak airspeed trajectory of isothermal air-jet along prototype's surface.

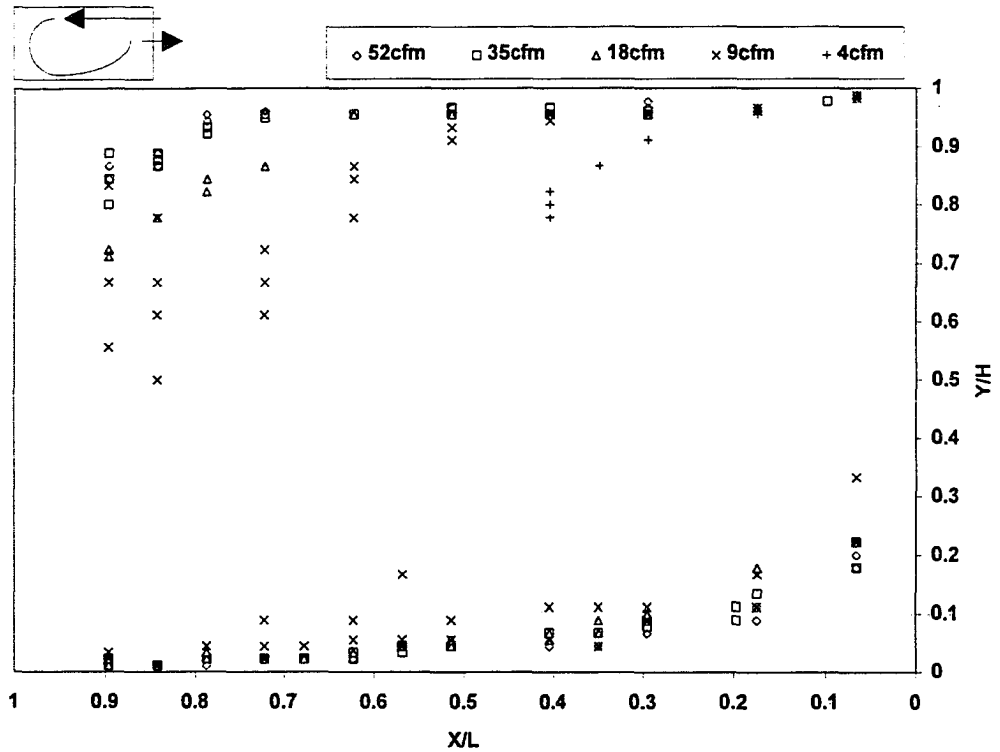

Figure 6.5 Peak airspeed trajectory of isothermal air-jet along scale-model's surface.

trajectories of peak airspeed were found in the prototype (Figure 6.4) at the top corner of the end wall due to secondary circulation flow. The results agreed with the conclusion that the airflow pattern was independent of airflow rate or any non-dimensional parameter as long as it was beyond the threshold value (Timmons, 1984).

Intermediate airflow zone. The ceiling trajectories diminished before the air-jet reached the end wall for both the scale-model and prototype with the intermediate airflow pattern (IP3, IM3). This is different than the situation described by Jin and Ogilvie (1990). Jin and Ogilvie (1990) described that near the ceiling (for intermediate airflow) the air-jet traveled to the end wall similar to the fully rotary airflow case, but than diminished rapidly during

reverse flow along the floor. The floor trajectory of the prototype (IP3) raised earlier than for fully rotary airflow. This phenomenon was not clear in the scale-model (IM3) and behaved similar to the fully rotary airflow zone cases.

Stagnant zone. The air-jet for unstable airflow (IP4, IP5, IM4, IM5) traveled a short distance along the ceiling and remained stagnant along the floor region with airspeeds less than 0.1 m/s. The trajectory was not clear in the prototype (IP4, IP5), and most peak airspeeds in the floor region were less than 0.1 m/s. The airflow pattern in the floor region for the scale-model (IM4, IM5) was similar to that for intermediate airflow except for a portion of the floor where airspeeds less than 0.1 m/s were measured.

The air-jet trajectory described the airflow pattern quantitatively. The airflow pattern categories were consistent with the classification of Jin and Ogilvie's (1990) results except at the floor region in the scale-model for the anticipated intermediate and stagnant airflow zone cases. The current results suggest that the transition from stagnant to intermediate airflow occurred at a slightly lower level than the I_o= 0.01 kg/m^2-s^2 as suggested by Kaul et al. (1975).

6.1.2.2. Airflow visualization

The air-jet trajectory was also observed using airflow visualization using a still camera and camcorder. The visualization pictures were compared with the air-jet trajectory results (Section 6.1.2.1) and are shown in Figure 6.6.

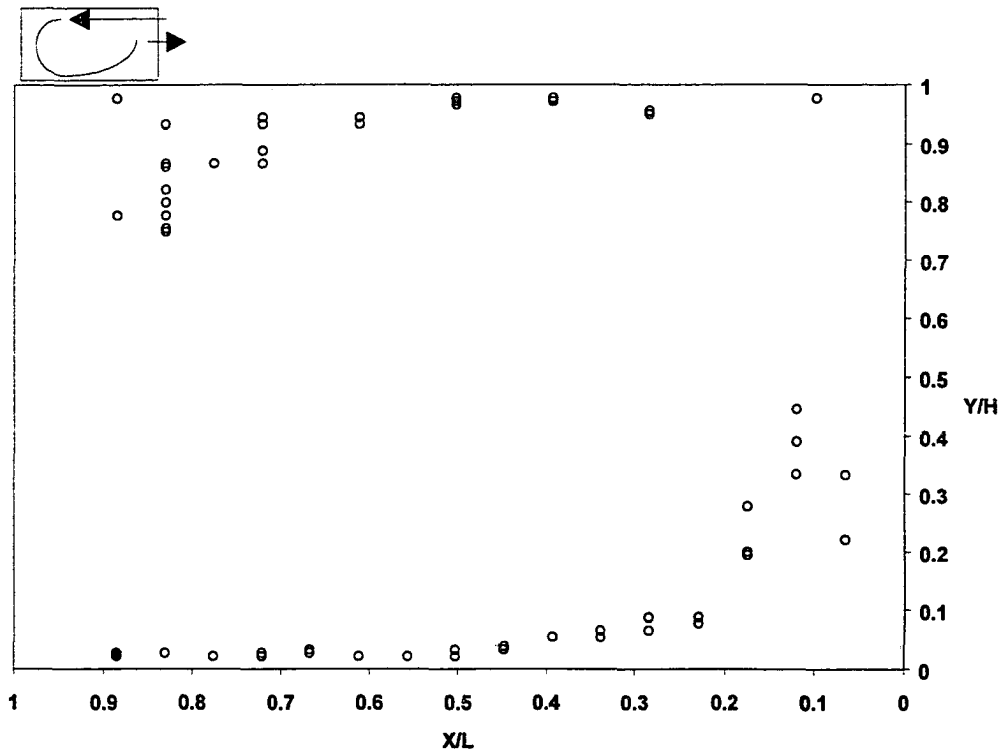

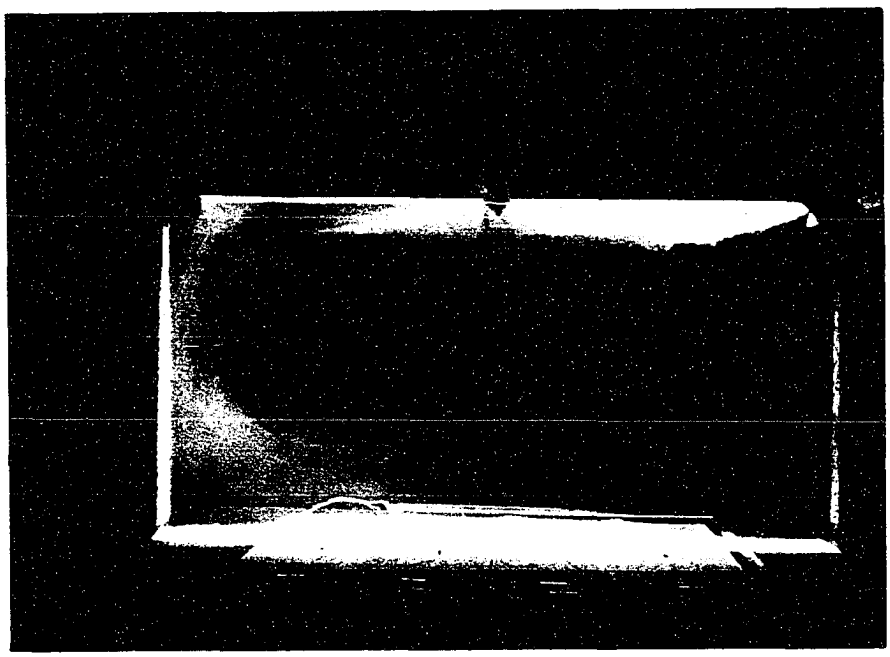

a. Scale: 1:3, Q_p=70cfm, $\Delta T=0^{\circ}$ C, Re_p=863, Rm_p=0.005.

Figure 6.6. Isothermal airflow pattern of trajectory measurement and smoke visualization. (°) denotes peak airspeed position across airflow direction (•) denotes peak airspeed less than 0.1 m/s

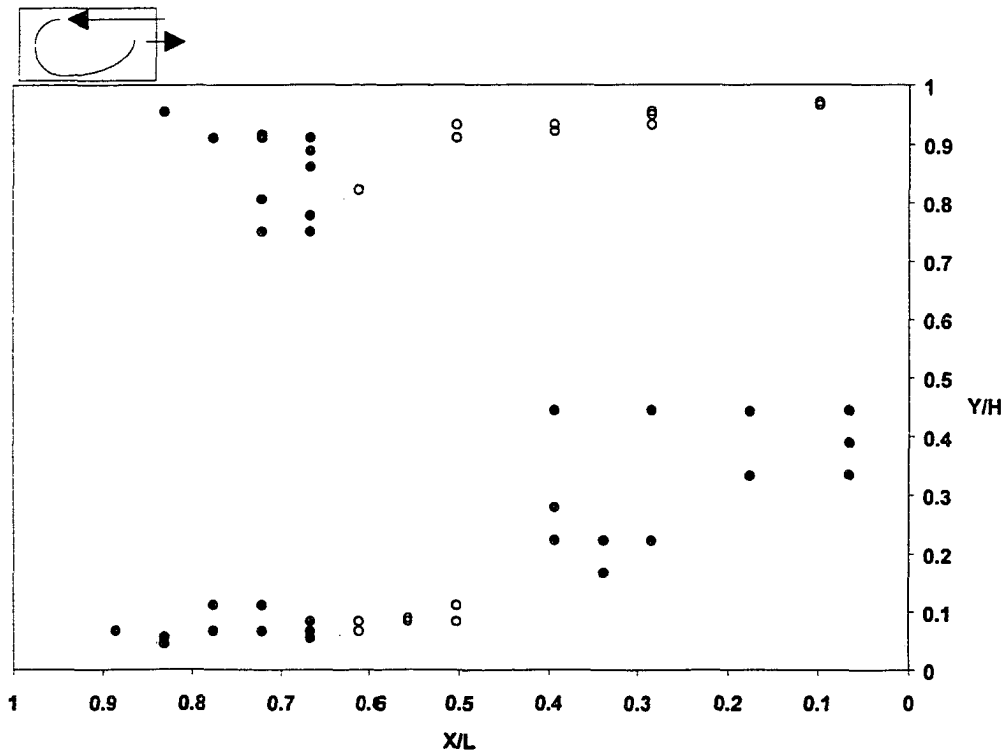

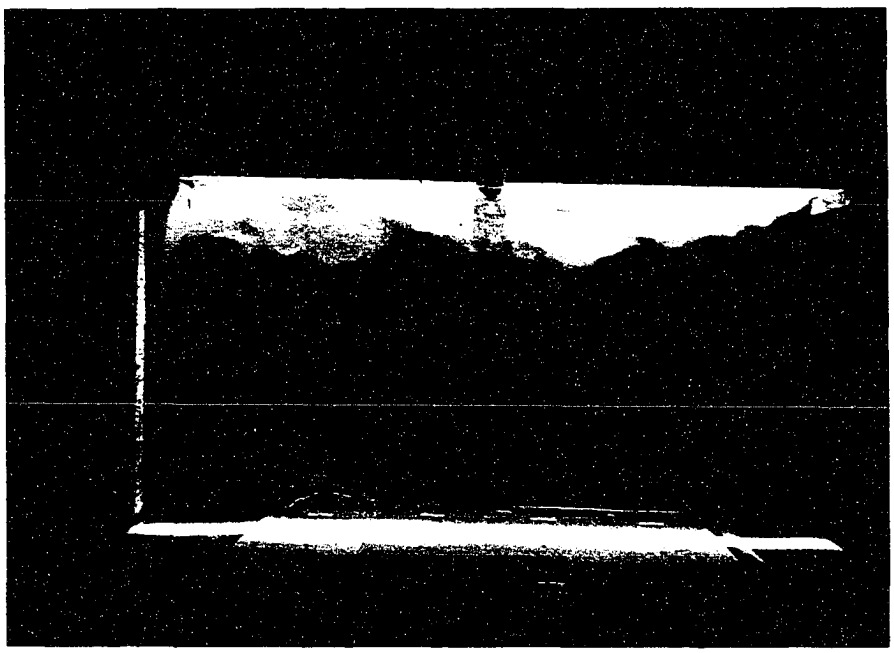

b. Scale: 1:3, Q_p=35cfm, ΔT=0° C, Re_p=435, Rm_p=0.001.

Figure 6.6. (continued)

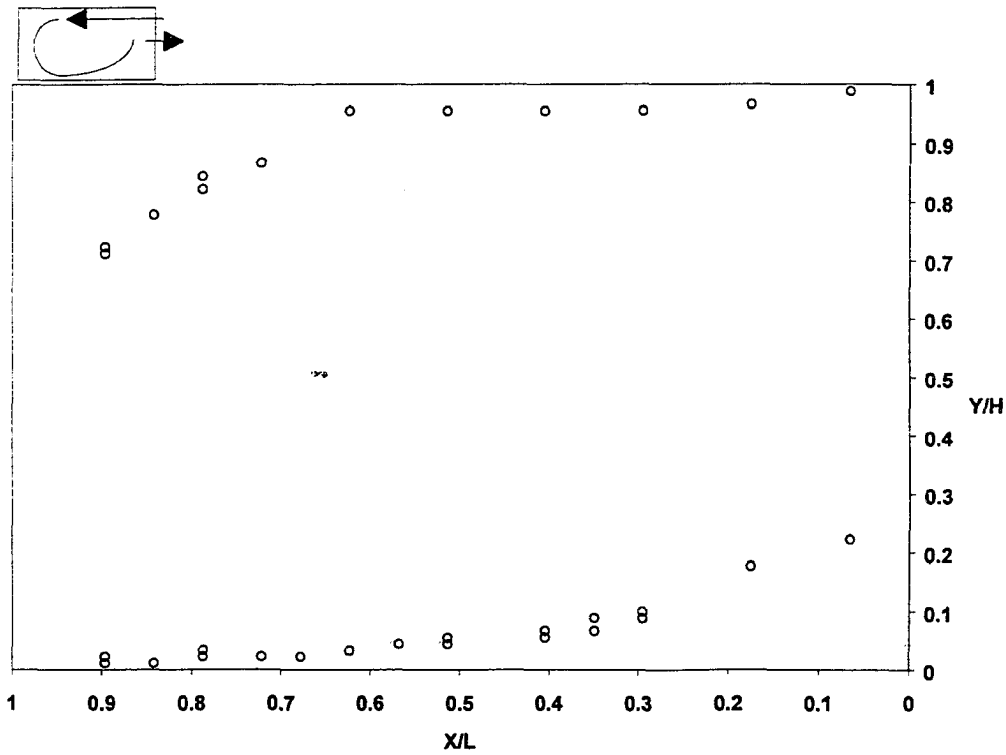

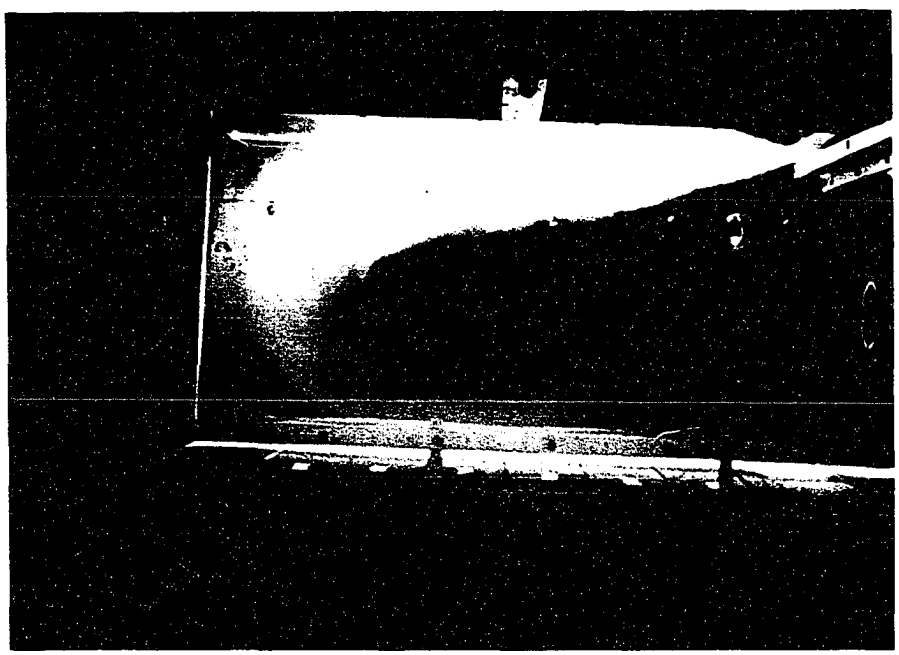

c. Scale: 1:6, Q_m=18cfm, ΔT=0° C, Re_m=454, Rm_m=0.006.

Figure 6.6. (continued)

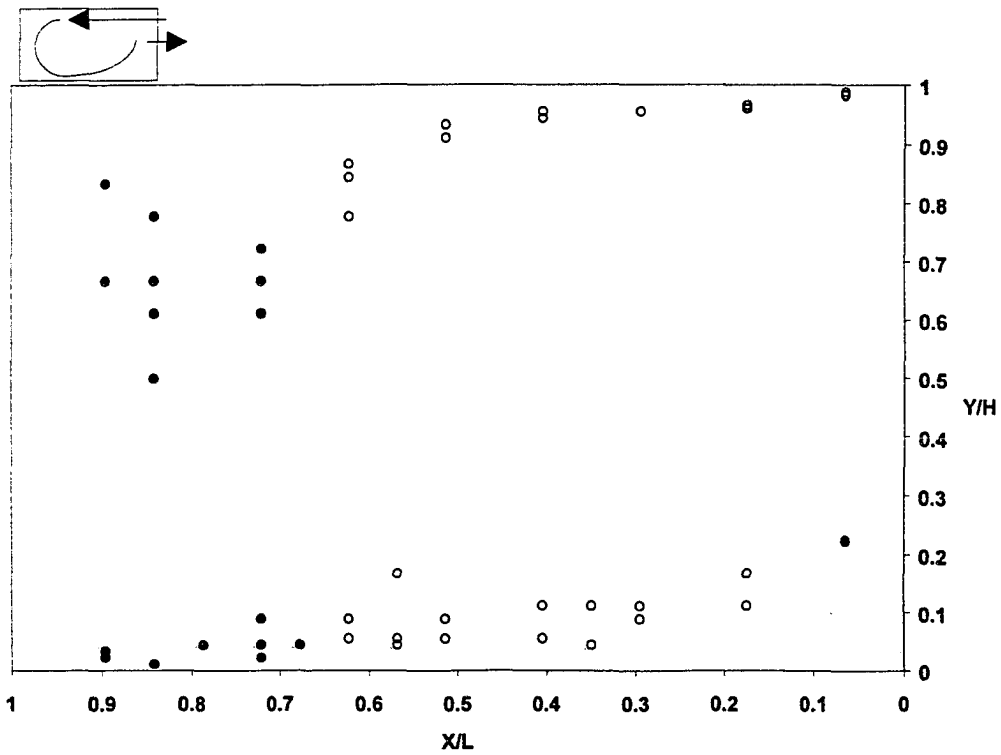

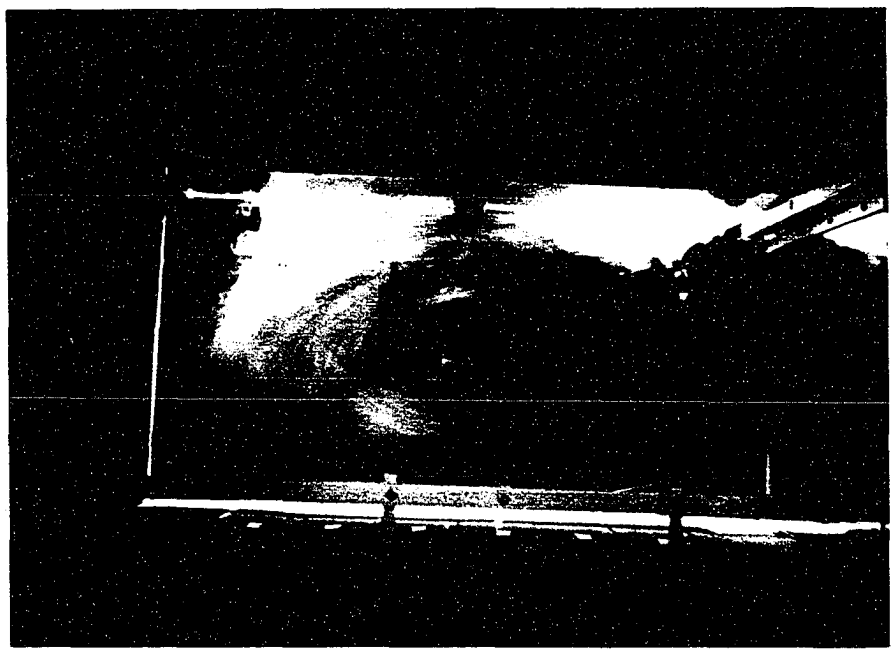

d. Scale: 1:6, Q_m=9cfm, $\Delta T=0^o$ C, Re_m=228, Rm_m=0.002.

Figure 6.6. (continued)

The air-jet separated from the ceiling and raised from the floor earlier for intermediate airflow (Figures 6.6 (a) and 6.6 (c)) than for the fully rotary condition. The airflow remained at the upper part of the prototype when the airflow rate fell to the stagnant zone as shown in Figure 6.6 (b). A rotary airflow pattern existed for the scale-model even when the airflow rate was classified in the stagnant airflow zone (Figure 6.6 (d)).

6.1.2.3. Air-jet trajectory comparison

The air-jet trajectory along the enclosure surfaces represents the maximum airspeed measured along the vertical airspeed profile across the air-jet in both the ceiling and floor regions. The airspeed profile was expected to increase after diffusing from the opening due to entrainment of ambient room air. The distance from the ceiling to the position of peak airspeed was also expected to increase as the airspeed profile increased. The near-floor airspeed profiles were expected to behave similarly as reported in Jin and Ogilvie (1990).

Figure 6.7 shows the air-jet trajectory for both the scale-model and prototype based on a similar Reynolds number. The airflow pattern for the scale-model was classified as fully rotary (IM2, Table 6.3) in Figure 6.7 (a), and classified as intermediate airflow for the prototype (IP3, Table 6.3). In Figure 6.7 (b) the airflow pattern for the prototype was classified in the stagnant airflow zone (IP4, Table 6.3) with the airflow pattern for the scale-model classified as intermediate airflow (IM3, Table 6.3). The comparison of peak airspeed trajectories between scale-model and prototype using the Reynolds number as the similitude criterion resulted in airflow pattern differences. This is specially evident with the results

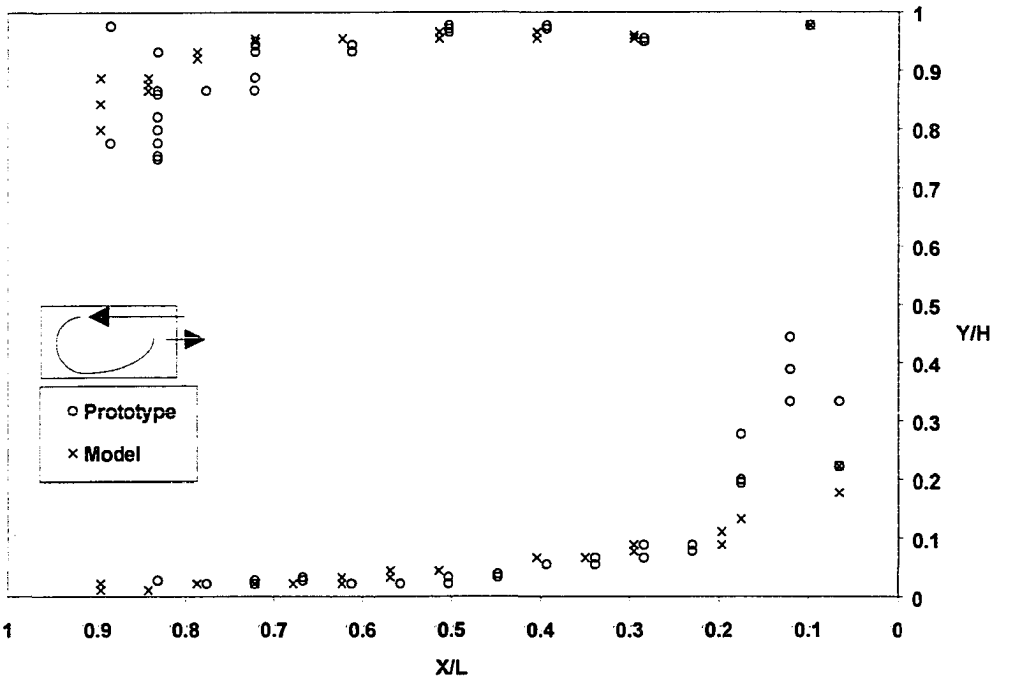

a. Q_p=70 cfm, Q_m=35 cfm, ΔT=0 °C, Re_p=863, Re_m=854.

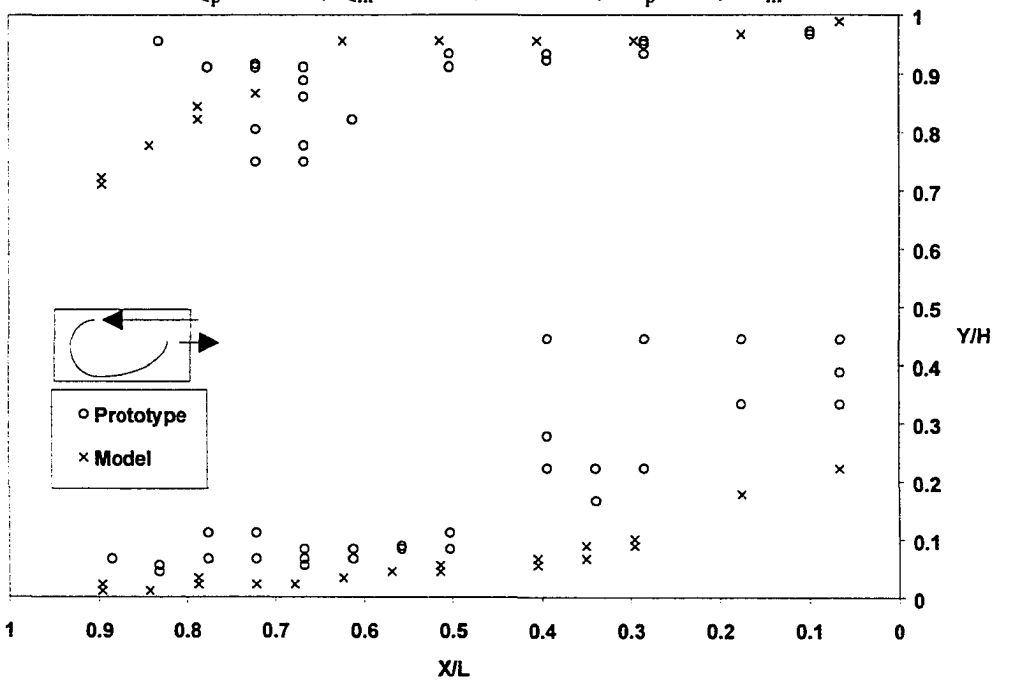

b. Q_p=35 cfm, Q_m=18 cfm, ΔT=0 °C, Re_p=435, Re_m=454.

Figure 6.7. The comparisons of peak airspeed trajectory for isothermal air-jet along enclosure surface based on similar Reynolds number (Re).

shown in Figure 6.7 (b) where the scale-model exhibits fully-rotary behavior and the prototype exhibits intermediate airflow behavior.

Figure 6.8 shows comparisons of peak airspeed trajectories along the ceiling and floor between the scale-model and prototype based on similar inlet jet momentum ratios (Rm). The results showed that similar airflow patterns were found for similar Rm. The trajectories near the floor in Figure 6.8 (d) suggest that the structure of the floor jet for the scale-model is stronger than that of the prototype.

It was concluded based on the results presented for airflow pattern similarity (Section 6.1.2) that similitude based on Rm for isothermal air-jet trajectories along the ceiling surface between scale-model and prototype was better than that based on Re. This conclusion agrees with the finding presented in Adre and Albright (1994).

6.1.3. The airspeed field

The similarity of airspeed field represents kinematic similitude between the scale-model and prototype. The longitudinal (x-direction) and vertical (y-direction) airspeed profiles were measured and compared to verify airspeed field similarity.

6.1.3.1. Longitudinal airspeed profiles along enclosure surfaces

The longitudinal air-jet profile along the ceiling and floor for both the scale-model and prototype are shown in Figures 6.9 and 6.10.

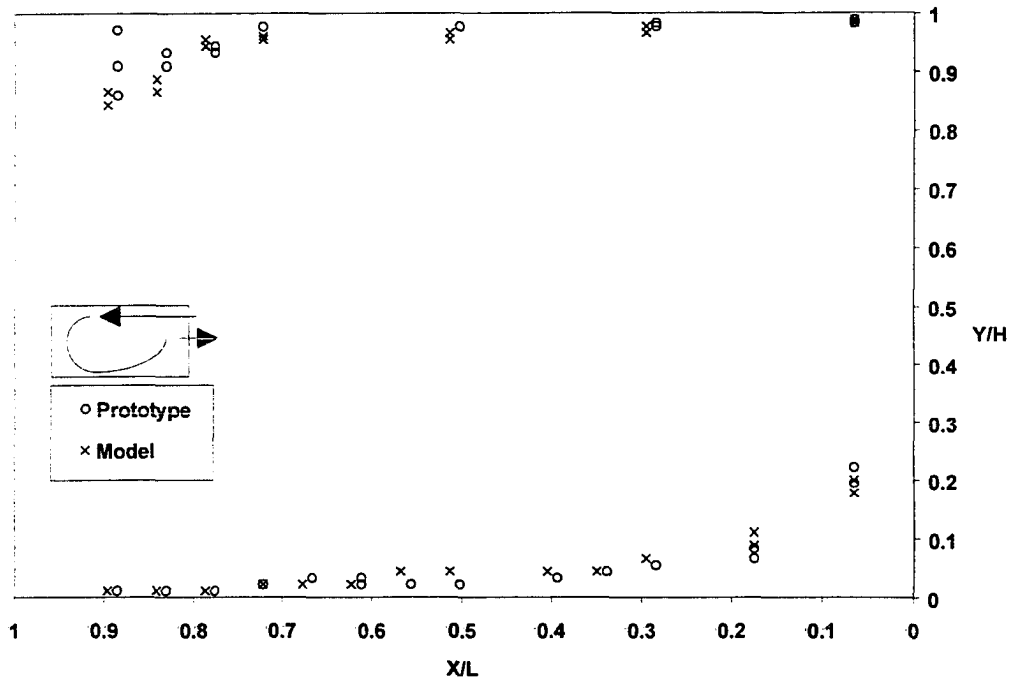

a. Q_p=205 cfm, Q_m=52 cfm, ΔT=0 °C, Rm_p=0.046, Rm_m=0.048.

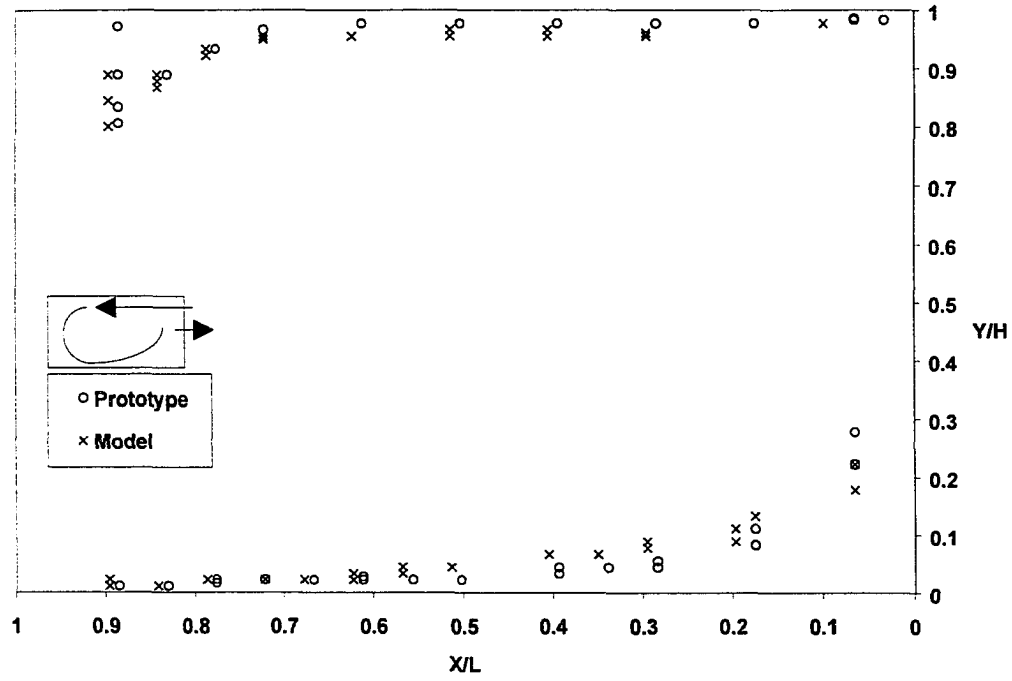

b. Q_p=140 cfm, Q_m=35 cfm, ΔT=0 °C, Rm_p=0.022, Rm_m=0.021.

Figure 6.8. The comparisons of peak airspeed trajectory for isothermal air-jet along enclosure surface based on similar inlet jet momentum ratio (Rm).

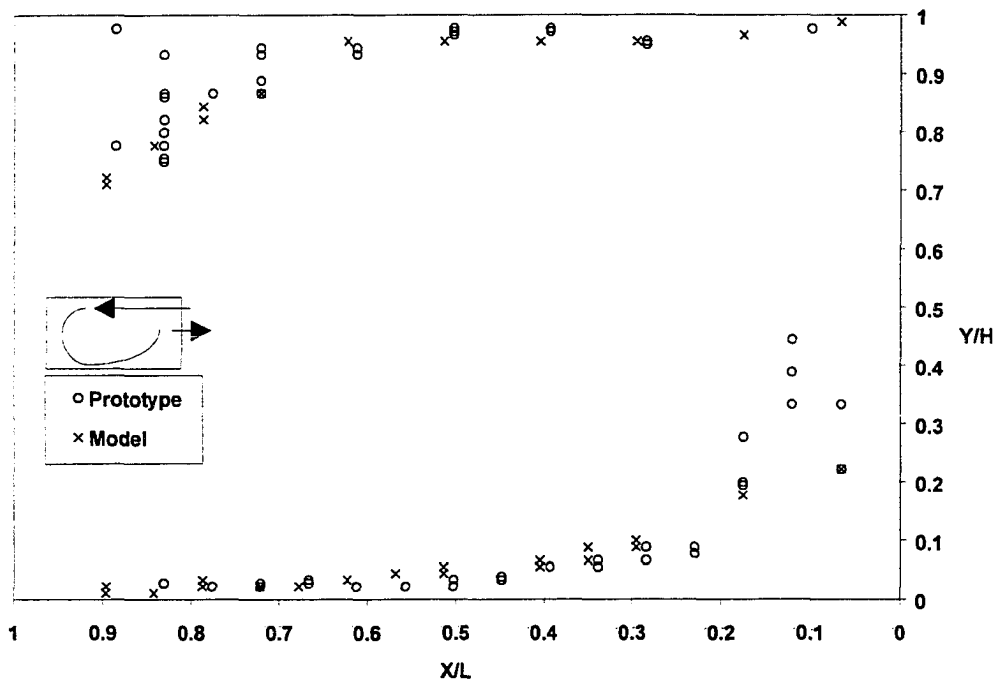

c. Q_p=70 cfm, Q_m=18 cfm, ΔT=0 °C, Rm_p=0.005, Rm_m=0.006

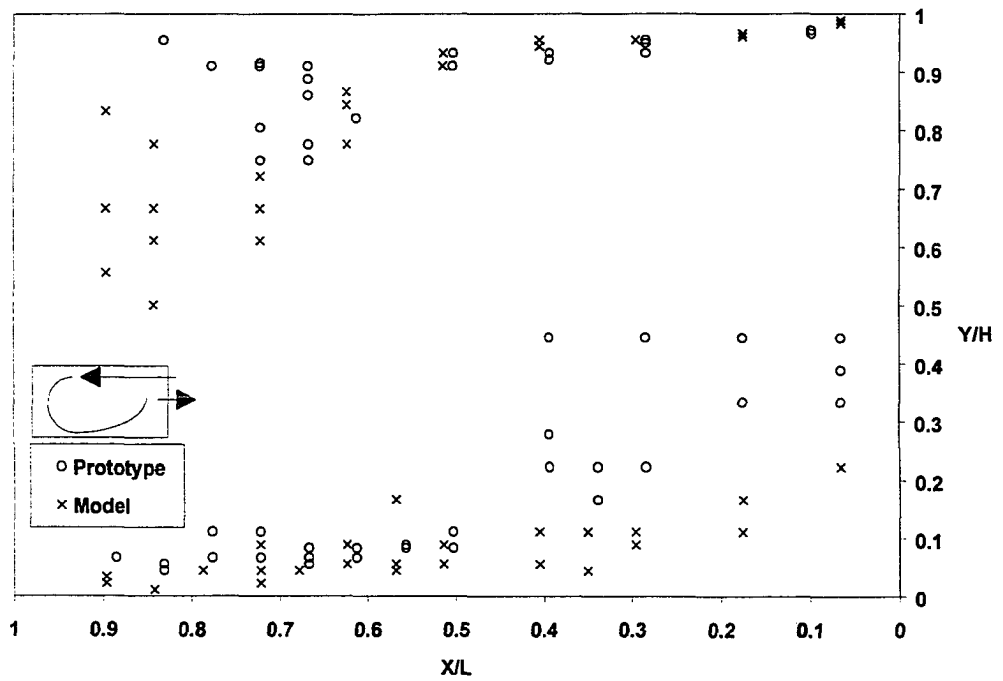

d. Q_p=35 cfm, Q_m=9 cfm, ΔT=0 °C, Rm_p=0.001, Rm_m=0.001.

Figure 6.8. (continued)

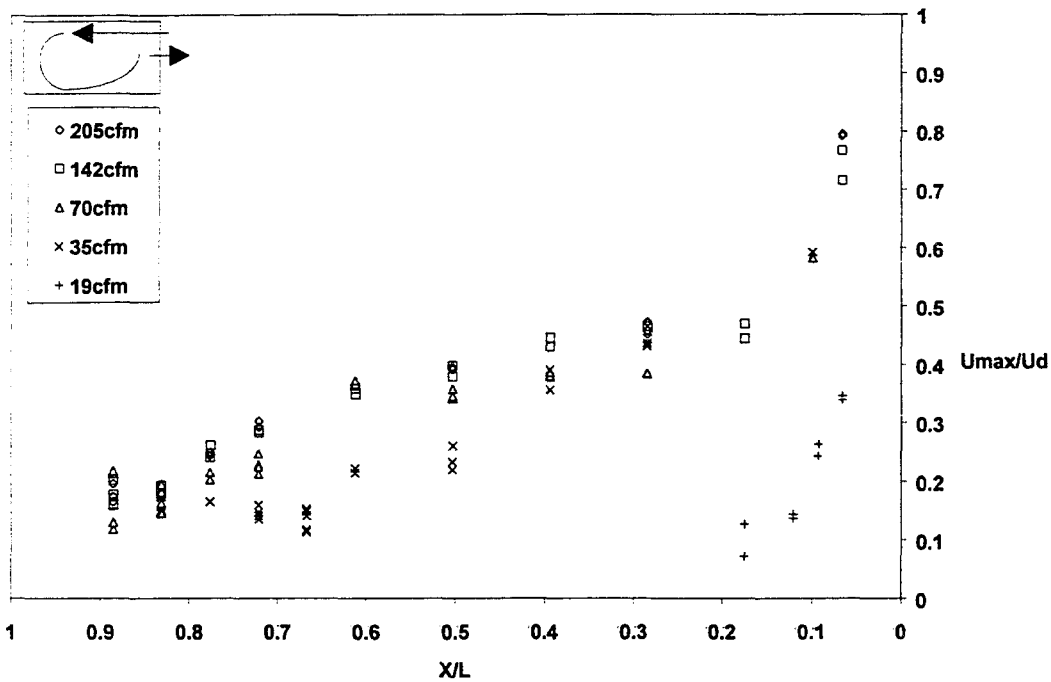

a. Ceiling region

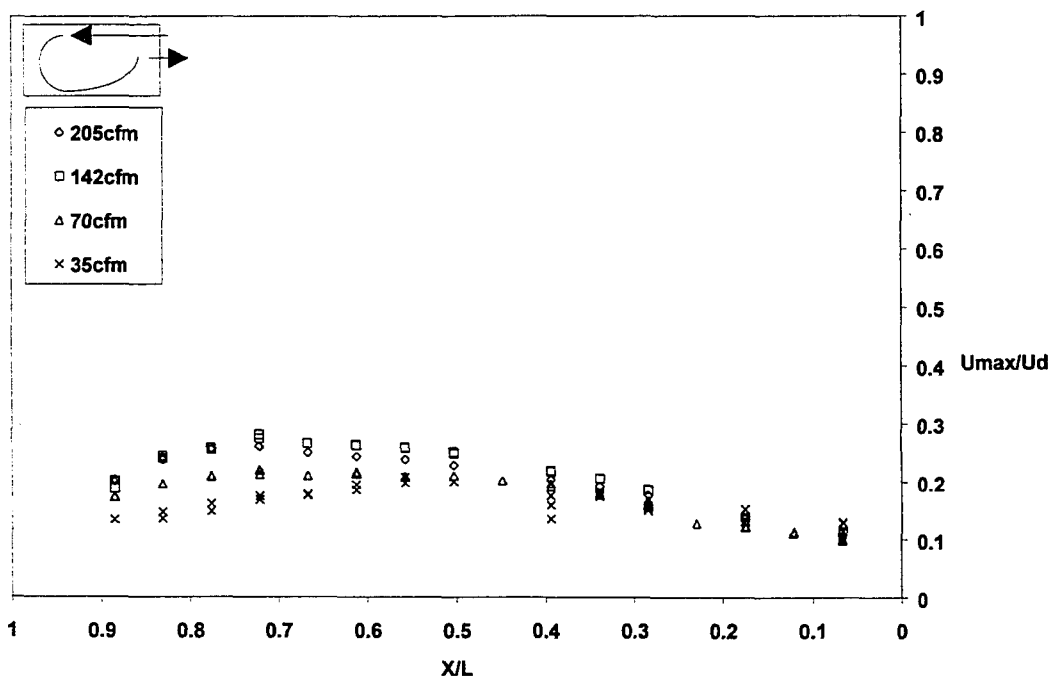

b. floor region

Figure 6.9. Non-dimensional peak airspeed of the isothermal air-jet along the ceiling slot-ventilated enclosure's (a) ceiling and (b) floor regions for the prototype (1:3).

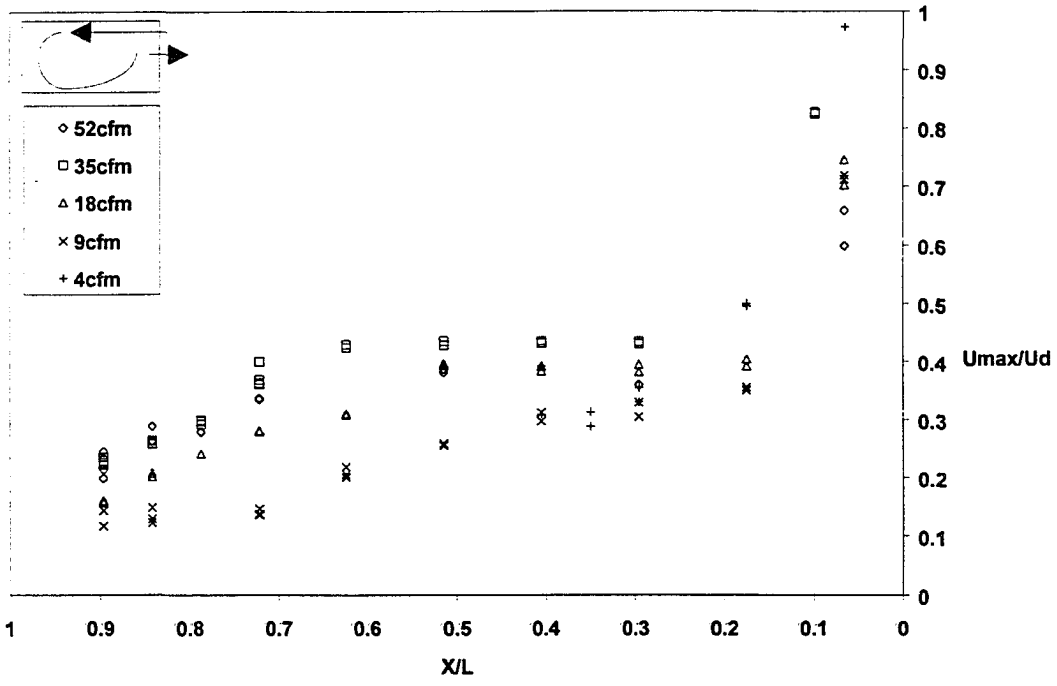

a. Ceiling region

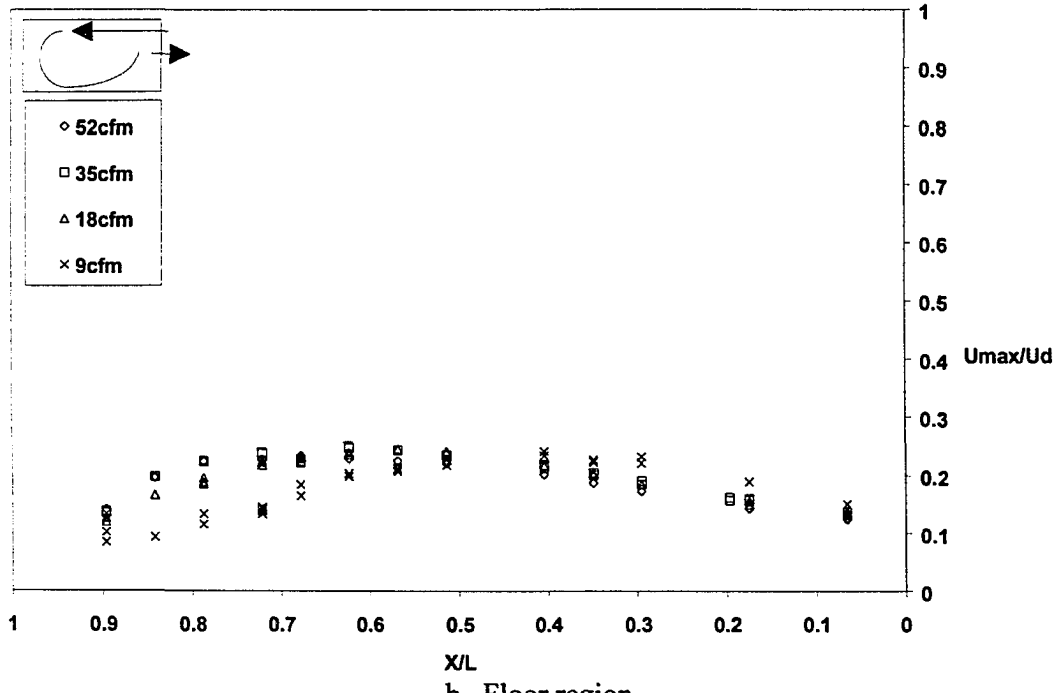

b. Floor region

Figure 6.10. Non-dimensional peak airspeed of the isothermal air-jet along the ceiling slot-ventilated enclosure's (a) ceiling and (b) floor regions for the scale-model (1:6).

Figure 6.9 (a) describes the prototype air-jet along the ceiling for cases IP1, IP2, IP3, IP4, and IP5 as shown in Table 6.3. The air-jet along the ceiling decayed gradually downstream and terminated rapidly when it reached a distance of about 100 h (0.7 L) from the supply opening for the fully rotary (IP1, IP2) and intermediate (IP3) airflow patterns. The airspeed profiles with the airflow rate beyond the stagnant airflow zone were similar. The distance where the air-jet terminated was less than 100h when the airflow pattern was within the stagnant (IP4, IP5) airflow region.

The non-dimensional prototype airspeed profiles along the floor were similar when the airflow pattern was fully rotary (IP1, IP2; Figure 6.9 (b)). The airspeed profile in the floor region indicates where the air-jet impinged and the variation of airspeed profiles was proportional to the airflow rate. The maximum non-dimensional airspeed was located in the region between 0.55 L to 0.75 L, which agreed with the 2/3 L distance reported by Nielsen (1988).

The airspeed profiles in both the ceiling and floor regions for the scale-model were similar to those of the prototype (Figure 6.10). The air-jet terminated at about 100 h from the inlet wall if the airflow rate was beyond the stagnant region (IM1, IM2, IM3; Figure 6.10 (a)). The airspeed in the ceiling region between 40 h (x/L=0.3) to 90 h (x/L=0.6) remained nearly constant for airflow rates beyond the threshold airflow rate (IM1, IM2, IM3). The air-jet terminated before 100 h for airflow patterns in the stagnant region.

The non-dimensional airspeeds in the floor region were similar to that found in the prototype where the maximum airspeed was located at about 2/3 L from the inlet wall (Figure

6.10 (b)). The non-dimensional floor airspeeds for stagnant airflow (IM4) were less than that found for the intermediate (IM3) and fully rotary (IM1, IM2) airflow cases.

The results showed that the non-dimensional longitudinal peak airspeed profiles along the ceiling were similar as long as the airflow rate was beyond the stagnant airflow pattern and before the air-jet terminated (x<100 h (0.7 L)) from the supply opening. The longitudinal airspeed profiles along the floor were similar as long as the airflow rate was beyond the fully rotary airflow pattern, with decreasing airspeeds as the airflow rate decreased. The maximum floor airspeed occurred at a distance of about 2/3 L from the inlet wall.

6.1.3.2. Comparison of longitudinal airspeed profiles

The airspeed profiles along the enclosure surfaces (ceiling and floor) were compared with the Reynolds number (Re) (Figure 6.11) and inlet jet momentum ratio (Rm) (Figure 6.12).

Air-jet peak airspeed profiles along the ceiling for the scale-model and prototype were not consistent based on Re (Figures 6.11 (a) and 6.11 (c)). The airflow rate of the scale-model (IM2, Figure 6.11 (a), (b); IM3, Figure 6.11 (c), (d)) and prototype (IP3, Figure 6.11 (a), (b); IP4, Figure 6.11 (c), (d)) belonged to different airflow pattern zones resulting in separate curves of airspeed in the ceiling region. However, the non-dimensional peak airspeed profiles for both the scale-model and prototype along the floor were similar as shown in Figures 6.11 (b) and 6.11 (d) with Re as the similitude criterion.

Figure 6.12 summarizes ceiling and floor peak airspeed profiles with Rm held similar between scale-model and prototype. Figures 6.12 (a), (c), and (e) show that the non-

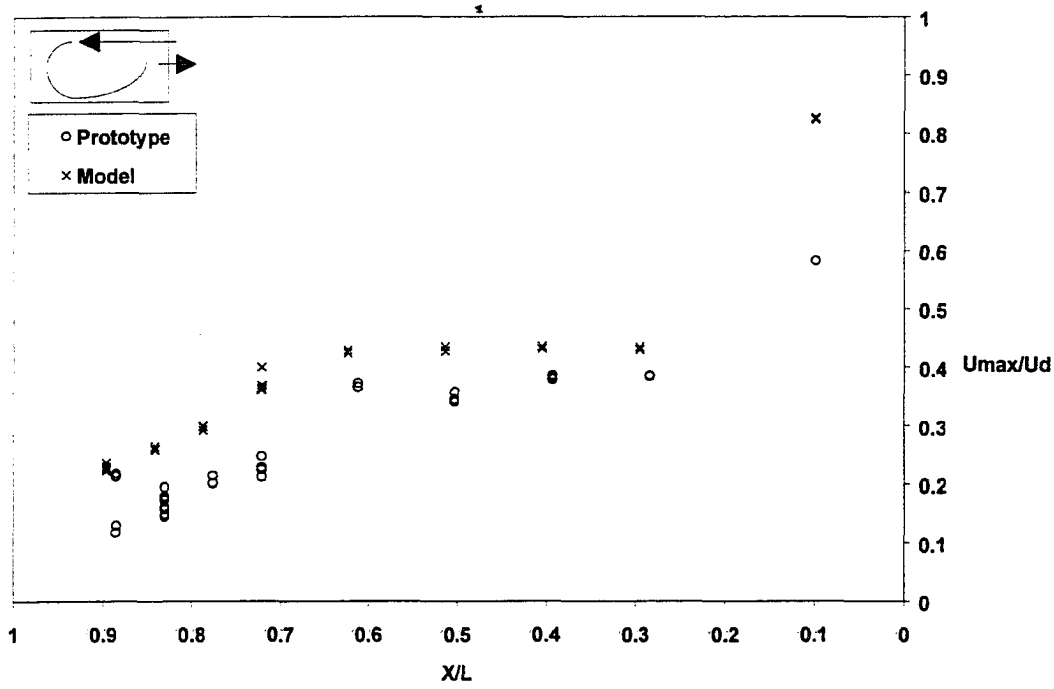

a. Ceiling region, Q_p=70 cfm, Q_m=35 cfm, ΔT=0 °C, Re_p=863, Re_m=854.

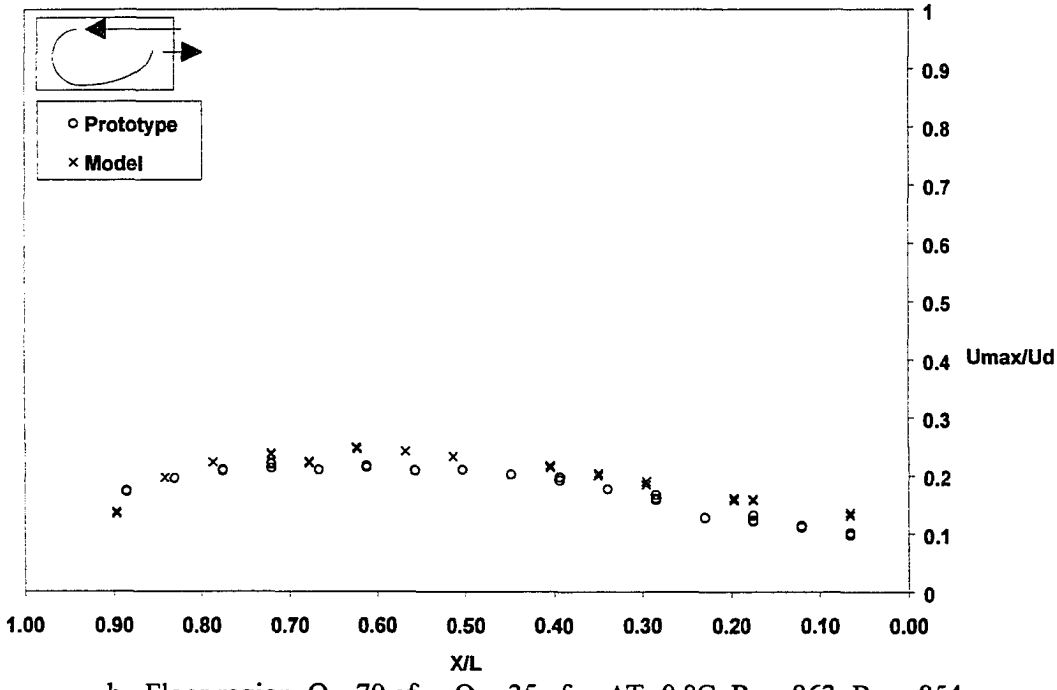

b. Floor region, Q_p=70 cfm, Q_m=35 cfm, ΔT=0 °C, Re_p=863, Re_m=854.

Figure 6.11. The comparisons of non-dimensional peak airspeed for isothermal air-jet along enclosure surface based on similar Reynolds number (Re)

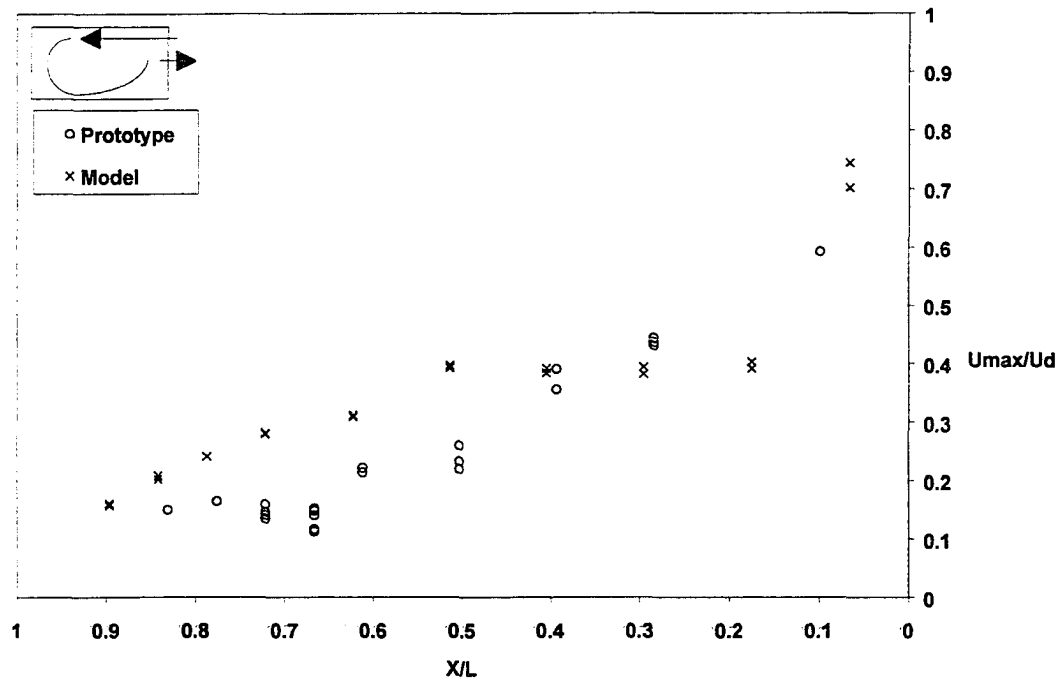

c. Ceiling region, Q_p=35 cfm, Q_m=18 cfm, ΔT=0 °C, Re_p=435, Re_m=454.

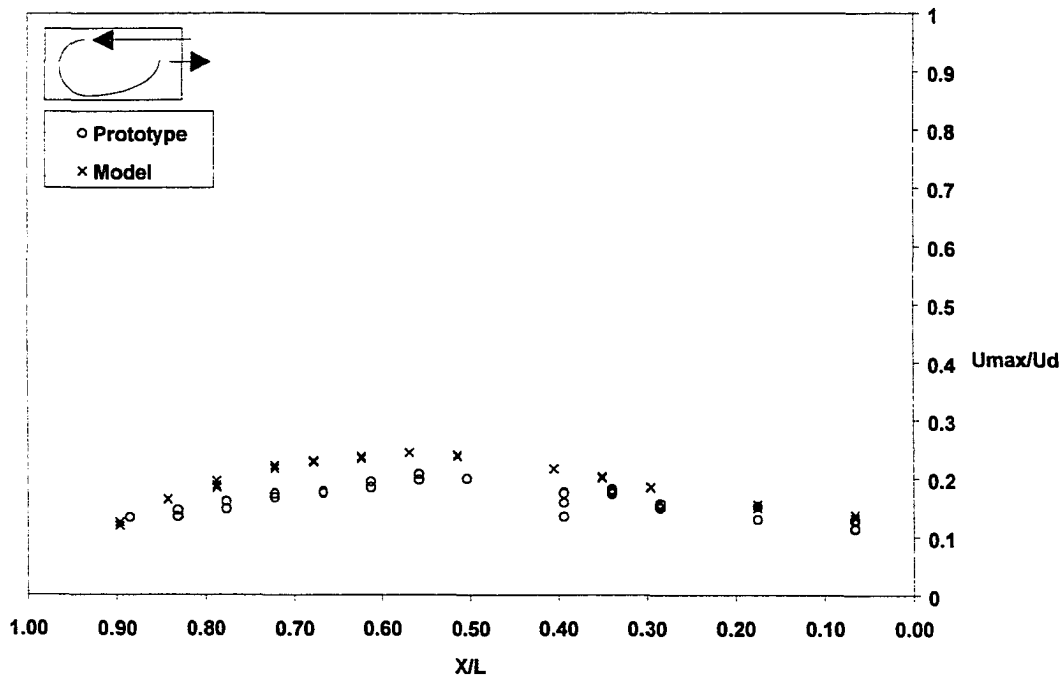

d. Floor region, Q_p=35 cfm, Q_m=18 cfm, ΔT=0 °C, Re_p=435, Re_m=454.

Figure 6.11. (continued)

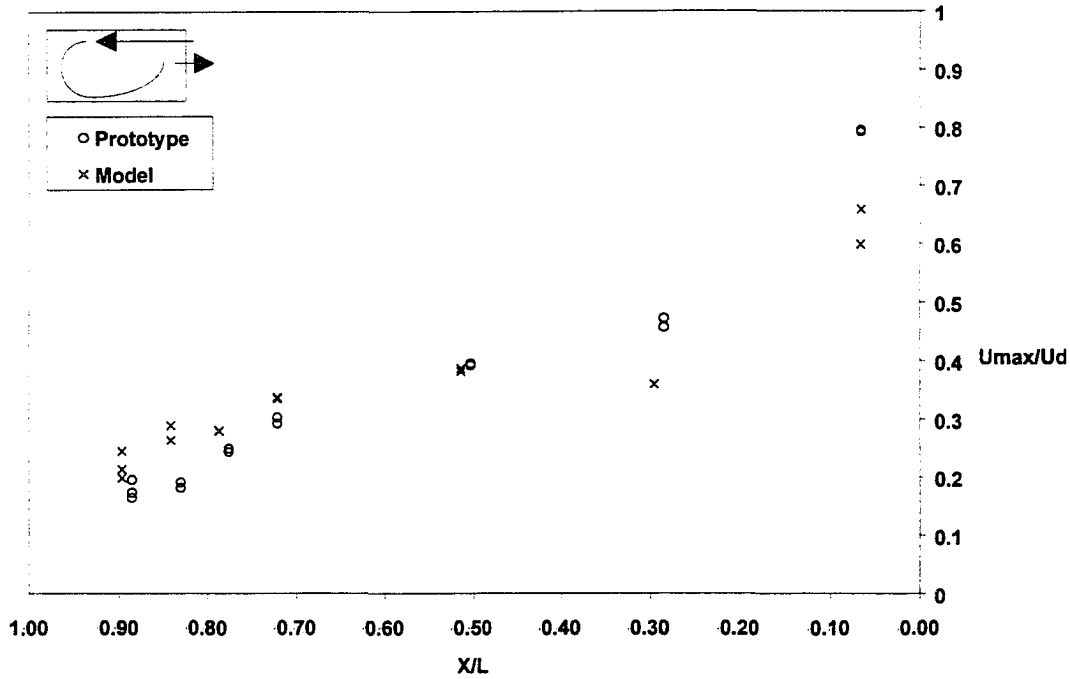

a. Ceiling region, Q_p=205 cfm, Q_m=52 cfm, ΔT=0 °C, Rm_p=0.046, Rm_m=0.048.

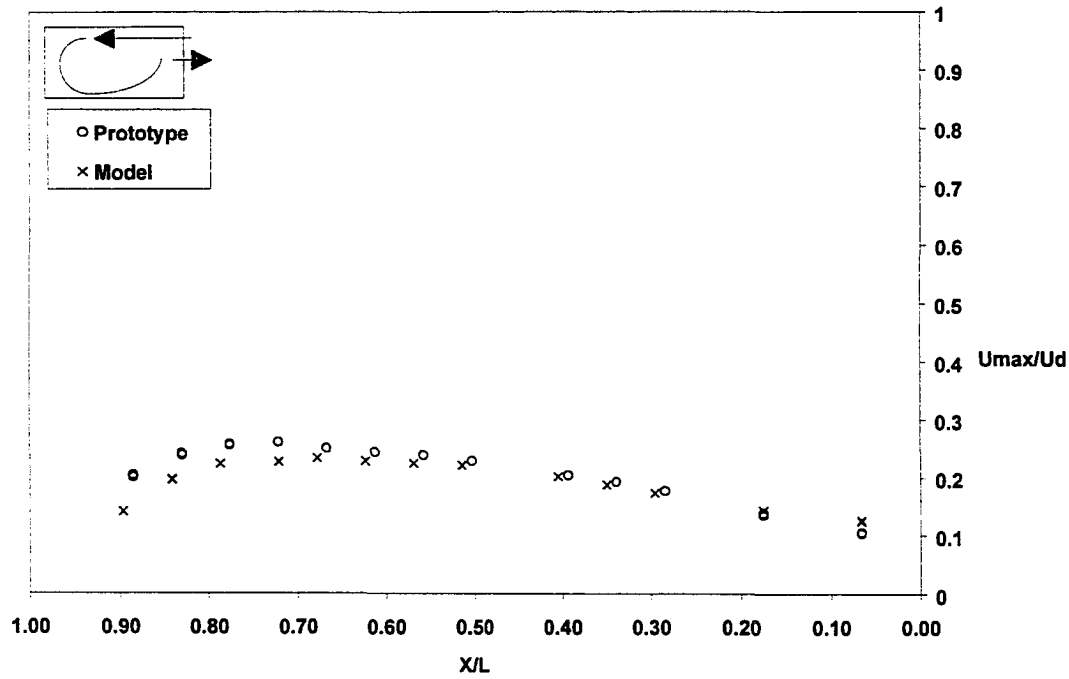

b. Floor region, Q_p=205 cfm, Q_m=52 cfm, ΔT=0 °C, Rm_p=0.046, Rm_m=0.048.

Figure 6.12. The comparisons of non-dimensional peak airspeed for isothermal air-jet along enclosure surface based on similar inlet momentum ratio (Rm).

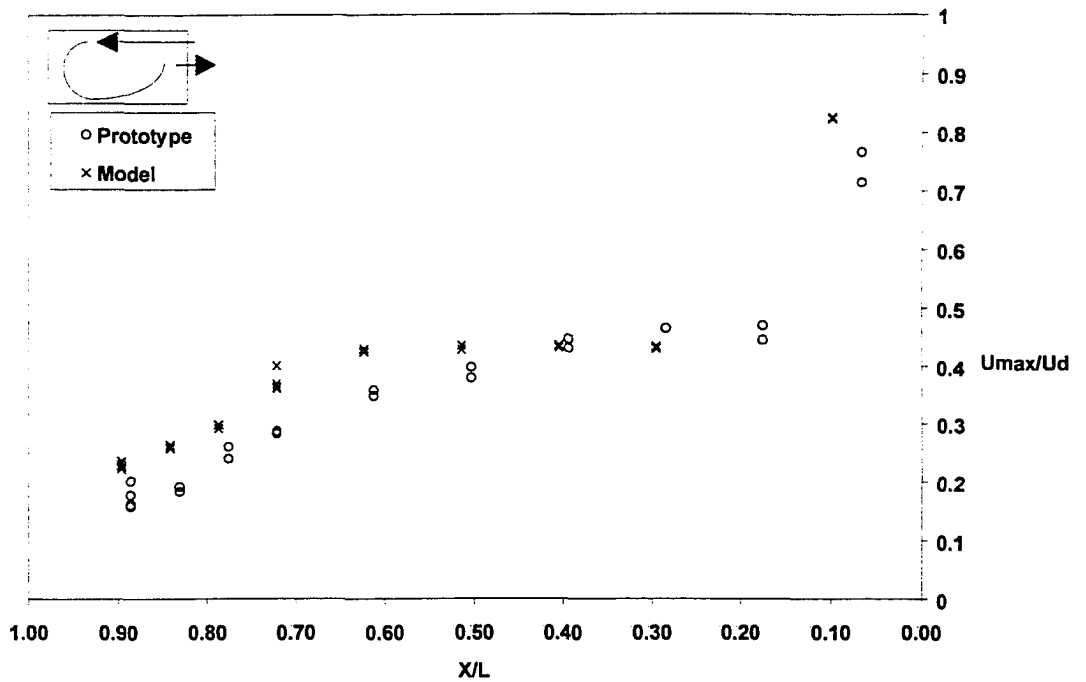

c. Ceiling region, Q_p=140 cfm, Q_m=35 cfm, ΔT=0 °C, Rm_p=0.022, Rm_m=0.021.

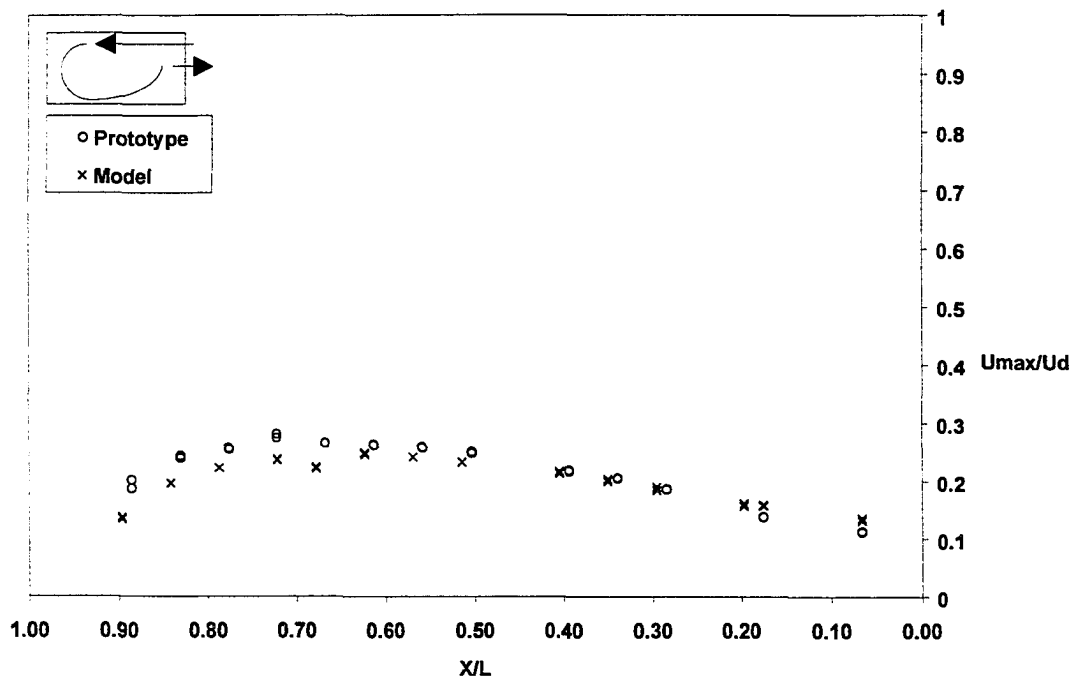

d. Floor region, Q_p=140 cfm, Q_m=35 cfm, ΔT=0 °C, Rm_p=0.022, Rm_m=0.021.

Figure 6.12. (continued)

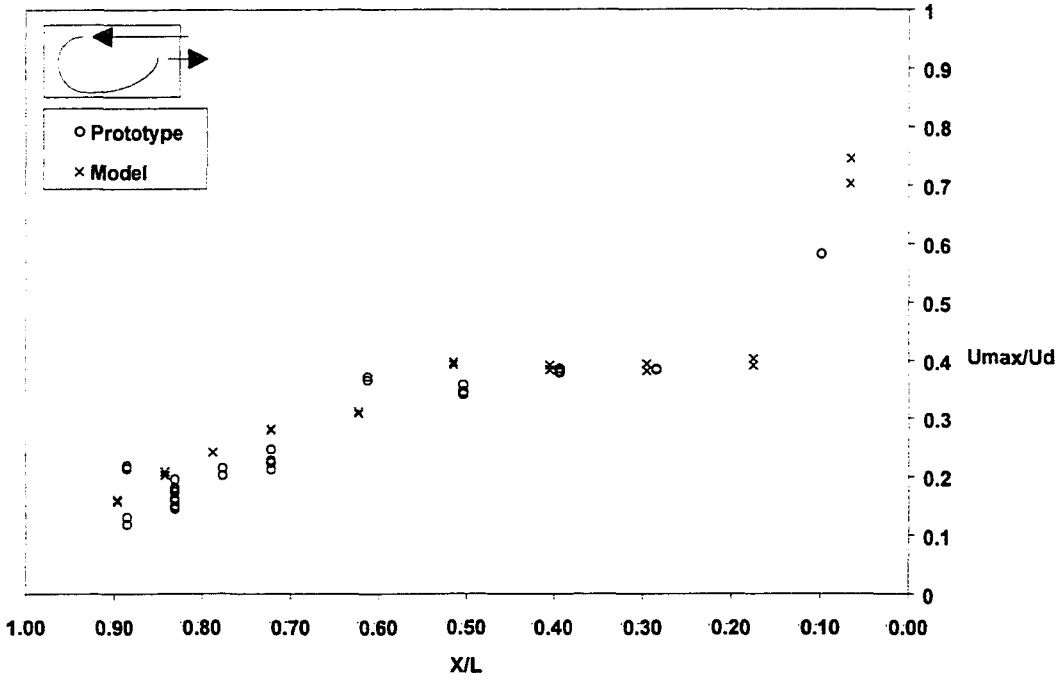

e. Ceiling region, Q_p=70 cfm, Q_m=18 cfm, ΔT=0 °C, Rm_p=0.005, Rm_m=0.006.

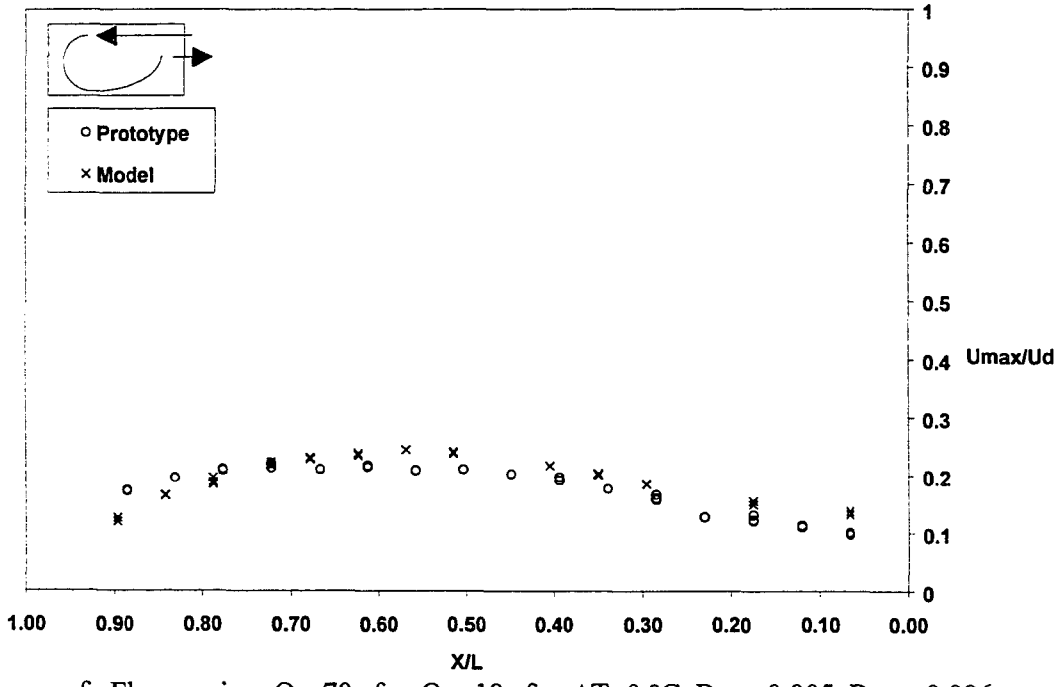

f. Floor region, Q_p=70 cfm, Q_m=18 cfm, ΔT=0 °C, Rm_p=0.005, Rm_m=0.006.

Figure 6.12. (continued)

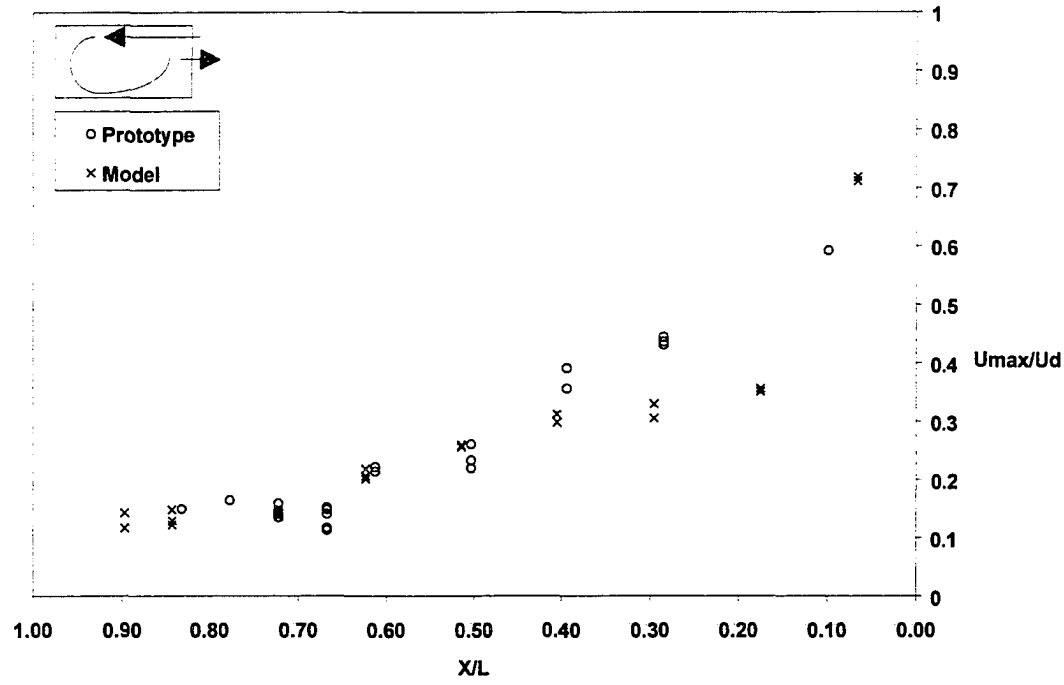

g. Ceiling region, Q_p=35 cfm, Q_m=9 cfm, ΔT=0 °C, Rm_p=0.001, Rm_m=0.002.

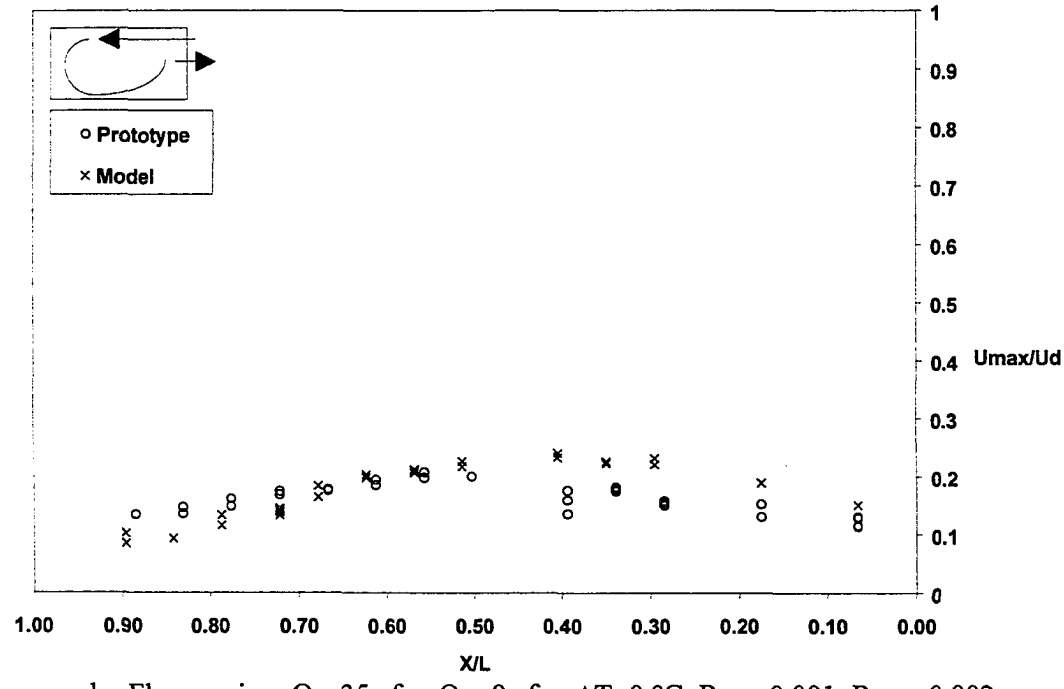

h. Floor region, Q_p=35 cfm, Q_m=9 cfm, ΔT=0 °C, Rm_p=0.001, Rm_m=0.002.

Figure 6.12. (continued)

dimensional peak airspeed profiles for the air-jet along the ceiling coincided between the scale-model and prototype before the air-jet terminated (i.e. before a distance of about 0.7 L from the opening) for airflow rates beyond the stagnant airflow zone. When the airflow patterns were stagnant, the profiles for both the scale-model and prototype were approximately similar as shown in Figure 6.12 (g).

All the profiles in the floor region (Figures 6.12 (b), (d), (f), and (h)) for both models were similar for similar Rm. It was concluded that Rm was better than the Re as the similitude parameter for isothermal airflow based on the evaluation of non-dimensional peak airspeed profiles along the ceiling for the scale-model and prototype. There was little effect on the profiles in the floor region regardless of whether Re or Rm was used as the similitude parameter.

6.1.3.3. Comparison of vertical airspeed profiles

The Re and Rm similitude parameters were further investigated at several additional airflow rates to assess vertical airspeed profiles. These additional conditions are summarized in Table 6.4. The airspeed profile along a vertical distance from the floor to the ceiling was measured in both the scale-model and prototype and these are shown in Figures 6.13 and 6.14.

The results showed little differences for normalized peak airspeed profiles based on Re (Figure 6.13) and Rm (Figure 6.14). The ceiling region removed from the opening and in the floor region close to the inlet wall exhibited the largest differences. These regions indicate a

Table 6.4. Test conditions of vertical airspeed measurement for isothermal airflow.

Test	Q,cfm[2]	U_d,m/s	ΔT,°C	Re	Rm	Anticipated airflow zone
IP6[1]	98	1.50	0	1202	0.011	Intermediate airflow
IP7	50	0.76	0	609	0.003	Stagnant zone
IM6	47	2.90	0	1159	0.039	Fully rotary
IM7	25	1.53	0	611	0.011	Intermediate airflow
IM8	13	0.79	0	315	0.003	Intermediate airflow

Note 1. I=isothermal, P=prototype, 6=test 6.
Note 2. The airflow rate (13 cfm) is close to the critical airflow rate stagnant zone of 12 cfm.

significant change in airflow pattern. The air-jet traveled along the ceiling with a terminated distance from the opening varying with the airflow rate. The peak airspeed decreased rapidly within this terminated zone. The position of the peak airspeed dropped significantly. Reverse flow was established after the air-jet impinged the floor. The air-jet traveled close to the inlet wall and raised back when it had sufficient air-jet momentum, otherwise the air-jet raised earlier and made a decreasing peak airspeed with a higher position.

These comparisons indicated that Rm was a little better than Re in describing non-dimensional vertical airspeed profiles, although both criteria appear to be acceptable.

6.1.3.4 Floor airspeed

Floor airspeed in an enclosure for isothermal airflow has been expressed as a function of Rm (Wang and Ogilvie, 1994b). The expression was derived based on equation (3.5) where:

$$U_{max} = C_w \sqrt{\frac{hU_d^2}{x}} \qquad (6.4)$$

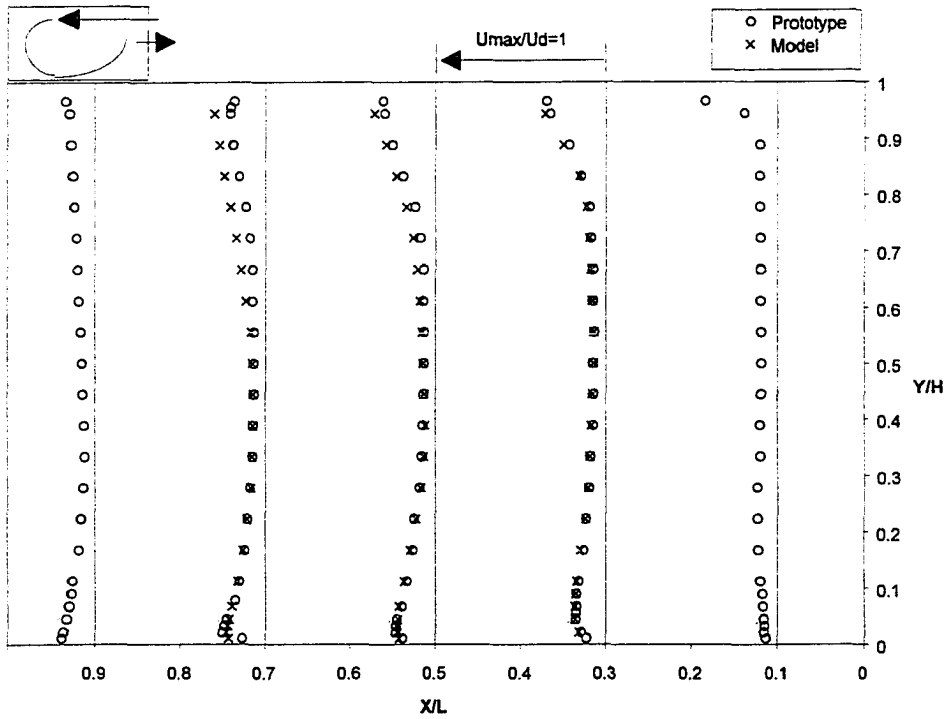

a. Q_p=98 cfm, Q_m=47 cfm, ΔT=0 °C, Re_p=1190, Re_m=1160, SD=3.3%.

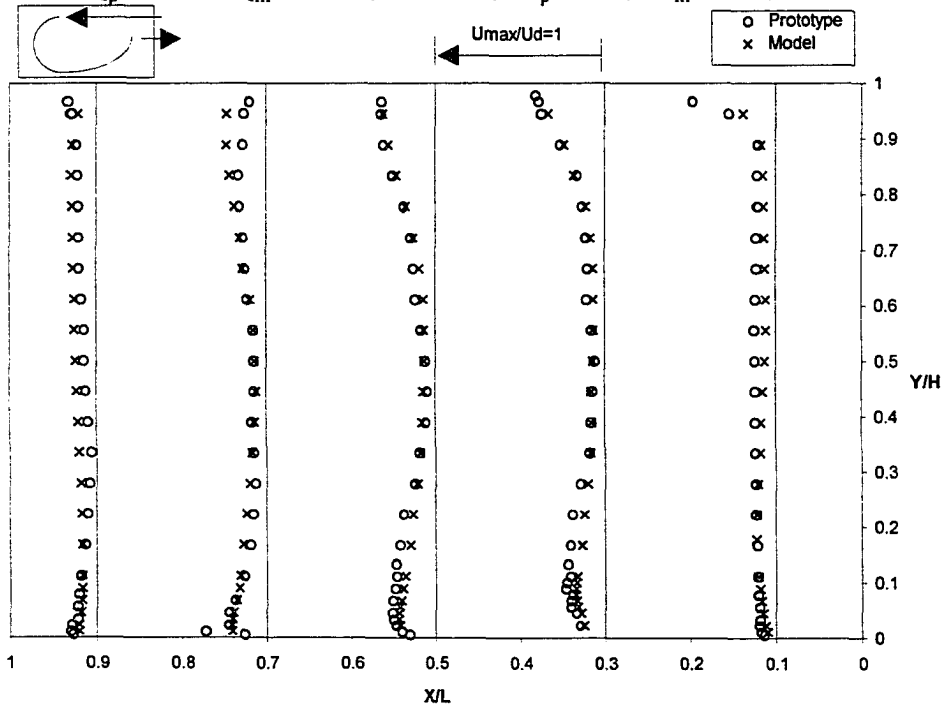

b. Q_p=50 cfm, Q_m=25 cfm, ΔT=0 °C, Re_p=610, Re_m=620, SD=4.2%.

Figure 6.13. The comparisons of vertical profiles of non-dimensional airspeed for isothermal air-jet based on similar Reynolds number (Re)

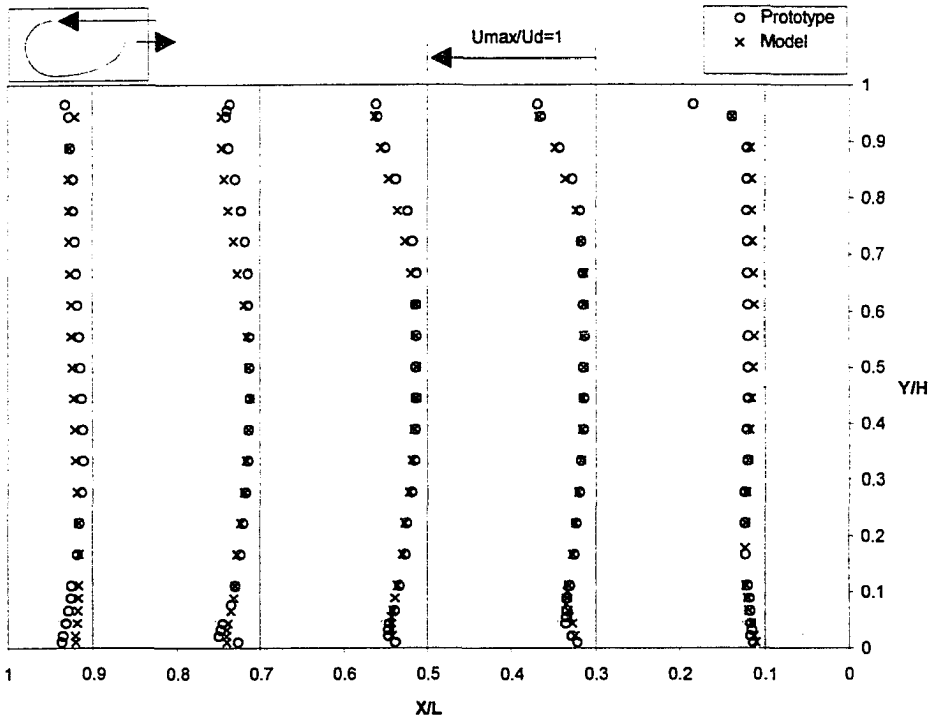

a. Q_p=98 cfm, Q_m=25 cfm, ΔT=0 °C, Rm_p=0.011, Rm_m=0.011, SD=2.8%.

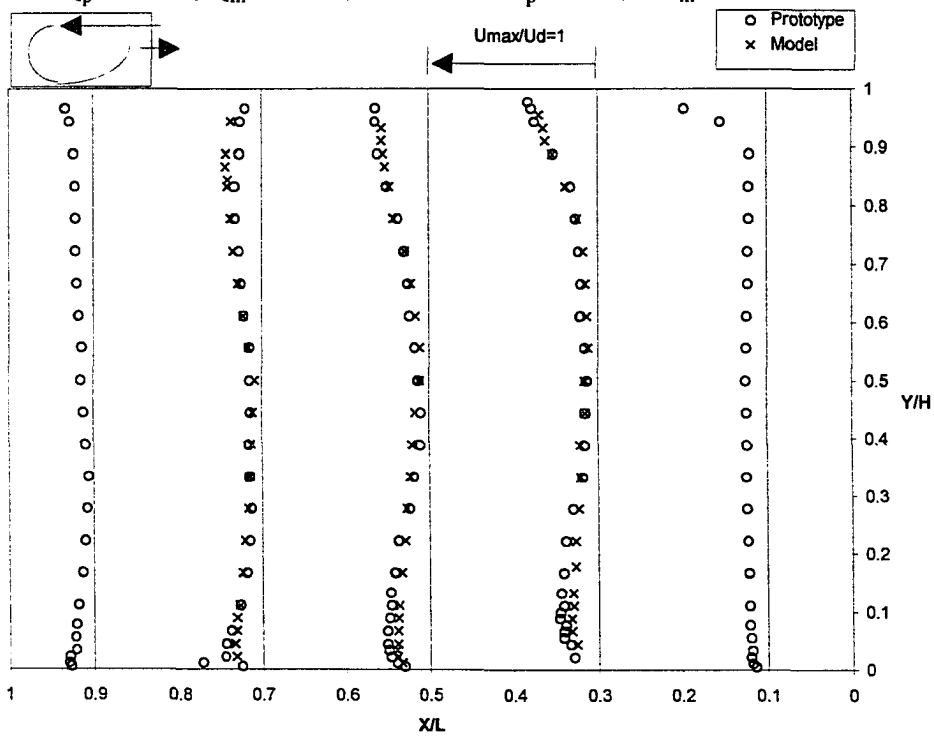

b. Q_p=50 cfm, Q_m=13 cfm, ΔT=0 °C, Rm_p=0.003, Rm_m=0.003, SD=3.7%.

Figure 6.14. The comparisons of vertical profiles of non-dimensional airspeed for isothermal air-jet based on similar inlet jet momentum ratio (Rm)

Wang and Ogilvie (1994b) replaced the air-jet travel distance x with the room perimeter (L+H) resulting in:

$$U_{max} = C_w \sqrt{\frac{hU_d^2}{(L+H)}} = C_w \sqrt{Rm} \qquad (6.5)$$

Using data collected from the above experiments, peak floor airspeeds at 0.3, 0.5, and 0.7L from the inlet wall for both scale-model and prototype were plotted as shown Figure 6.15. The scale-model and prototype data fell on the same curve at each unique position in the enclosure, and the higher peak floor airspeed was at position of x= 0.7L. The regression equations are given in Table 6.5.

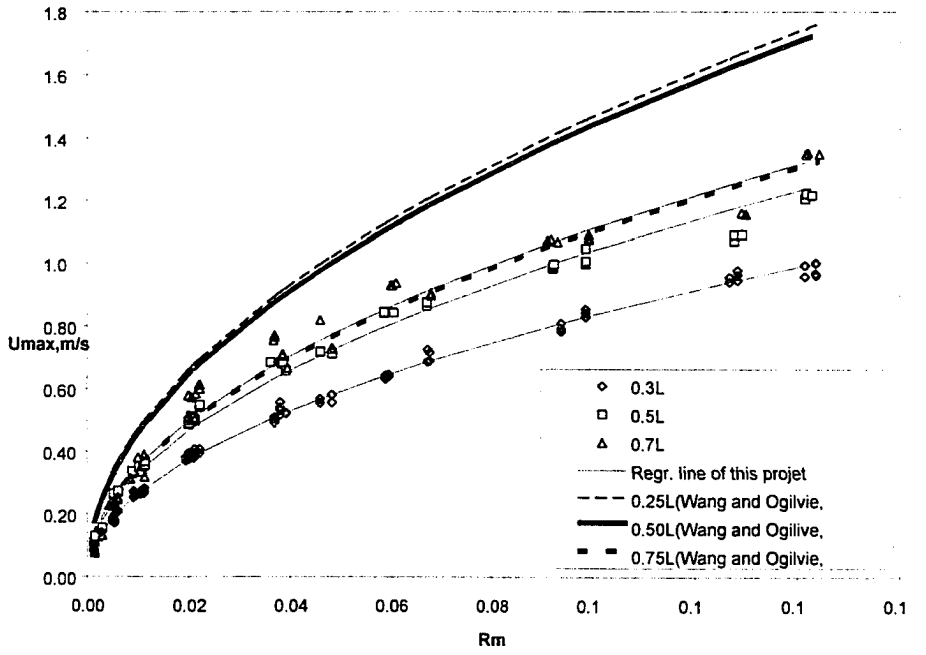

Figure 6.15. The peak floor airspeed as a function of position for both model and prototype versus inlet jet momentum ratio (Rm).

Table 6.5. The regression equations of peak floor airspeed at for both scale-model and prototype versus inlet jet momentum ratio (Rm).

Positions	Regression equations	Coefficient of determination, R^2
0.3L	$U_{rm}=2.65\sqrt{R_m}$	0.99
0.5L	$U_{rm}=3.29\sqrt{R_m}$	0.99
0.7L	$U_{rm}=3.52\sqrt{R_m}$	0.98

The expressions of peak floor airspeed were similar to those given by Wang and Ogilvie's (1994b) at a floor position of x close to 0.7L, but differed greatly at floor positions closer to the inlet wall. Part of this difference may be due to differences in geometric configuration of test room size where L/H= 2 for this test and L/H=1.71 for Wang and Ogilvie's (1994b) test. A more severe difference, however, is that Wang and Ogilive (1994b) predicted higher floor airspeeds closer to the inlet wall as opposed to the opposing end wall. This was in complete contrast to the findings reported with this research.

It was concluded that the peak floor airspeed was a function of the square root of the Rm for both the scale-model and prototype.

If peak floor airspeed is a function of Rm in both scale-model and prototype, then it can be said that:

$$U_{rm} \sim \sqrt{Rm} = \sqrt{\frac{hU_d^{\,2}}{L+H}} \tag{6.6}$$

implying further that the nondimensional peak floor airspeed is proportional to:

$$\frac{U_{rm}}{U_d} \sim \sqrt{\frac{h}{L+H}} \tag{6.7}$$

The prediction equation for similarity between scale-model and prototype can be expressed as:

$$(\frac{U_{rm}}{U_d})_p = (\frac{U_{rm}}{U_d})_m \tag{6.8}$$

implying that the similarity requirement between scale-model and prototype is:

$$(\sqrt{\frac{h}{L+H}})_p = (\sqrt{\frac{h}{L+H}})_m \tag{6.9}$$

Equation 6.7 implies that if geometric similarity is maintained, than kinematic similarity in the floor region is maintained. The analytical results agree with the experimental results presented in section 6.1.3.2.

6.2. Nonisothermal Airflow

The similitude criteria for nonisothermal airflow includes geometric similitude, dynamic similitude, kinematic similitude, thermal similitude, and similar boundary conditions. The evaluation items used for this research included the airflow pattern and airspeed fields as was the case for isothermal airflow with the temperature field added as an important evaluation term for nonisothermal airflow. The dominant similitude parameters for nonisothermal airflow include the Ar, Eu, and Re, where Eu is similar in concept to the Rm as a similarity requirement.

The experimental procedures for nonisothermal airflow were arranged to test air-jet penetration distance, airflow patterns, airspeed field, and temperature field using the methods

of airflow visualization, airspeed measurement, and temperature measurement within the scale-model and prototype enclosures.

6.2.1. Air-jet penetration distance

Two levels of heat load ($\Delta T = 10\ ^{\circ}C$ and $40\ ^{\circ}C$) were chosen to measure the air-jet penetration distance at various airflow rates. The test conditions are shown in Table 6.6. The results measured at $\Delta T = 10\ ^{\circ}C$ and $40\ ^{\circ}C$ were also compared with the results for isothermal airflow ($\Delta T = 0\ ^{\circ}C$).

Table 6.6. Test conditions of penetration distance for nonisothermal airflow

Test		Q, cfm	U_d, m/s	T_d,°C	T_f,°C	ΔT,°C	Re	Rm	Ar
Proto-type	Max.	389	5.98	65	25	40	4778	0.1662	0.0004
	Min.	28	0.44	65	25	40	349	0.0009	0.0811
	Max.	246	3.77	40	30	10	3014	0.0662	0.0003
	Min.	23	0.36	40	30	10	288	0.0006	0.0311
Scale-Model	Max.	88	5.40	65	25	40	2157	0.1355	0.0003
	Min.	6	0.34	65	25	40	135	0.0005	0.0454
	Max.	55	3.40	40	30	10	1357	0.0536	0.0002
	Min.	5	0.30	40	30	10	121	0.0004	0.0221

The air-jet penetration results for the scale-model and prototype are given as a function of Re (Figure 6.16), Rm (Figure 6.17), and Ar (Figure 6.18). The air-jet penetration distance increased with increasing Re and Rm and decreased with increasing Ar. The penetration distance remained constant when the airflow rate (i.e. increasing inlet airspeed) reached a threshold value at each specific temperature difference with Re or Rm. The airflow pattern became fully rotary when the penetration distance reached this maximum value. The threshold values for each similitude

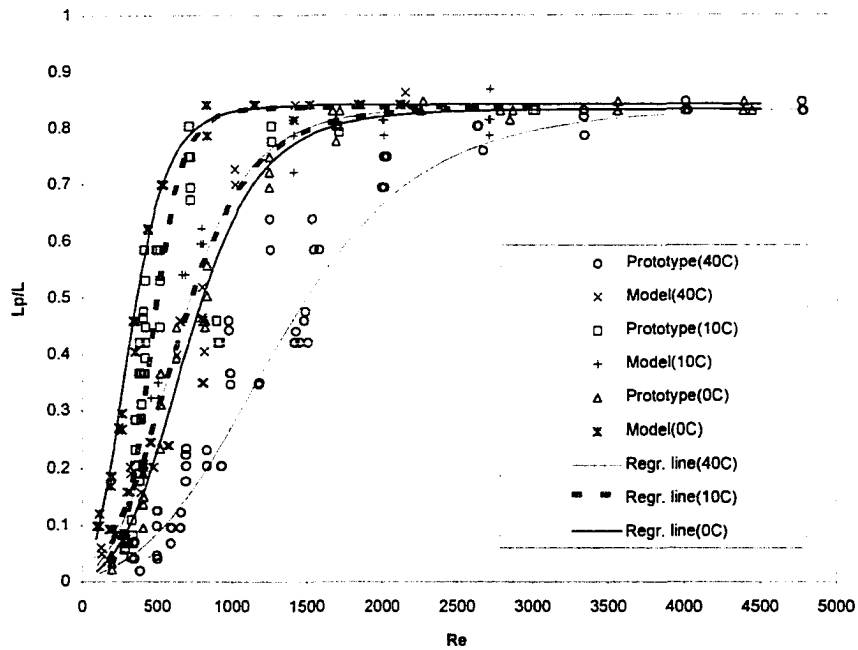

Figure 6.16. Normalized penetration distance as a function of Reynolds number (Re).

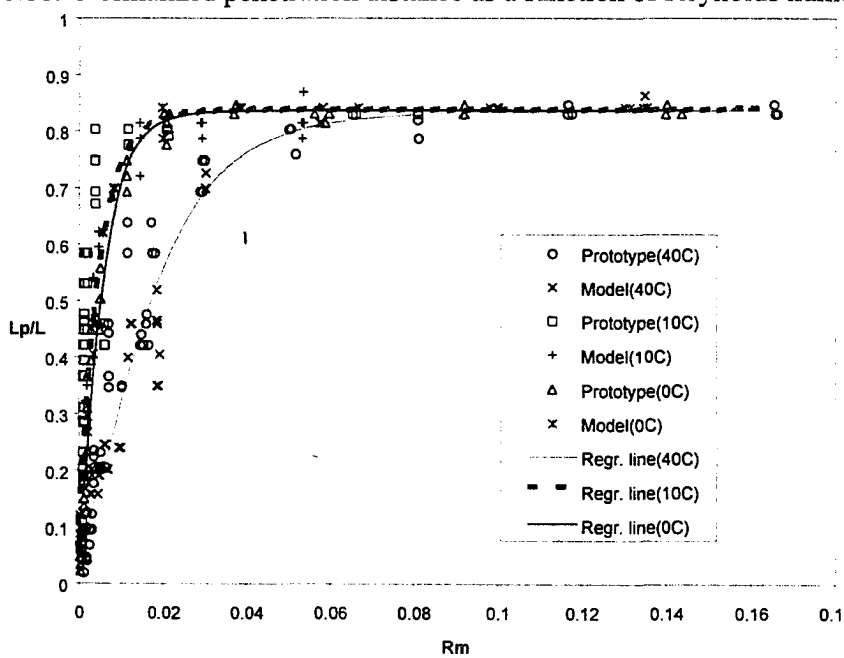

Figure 6.17. Normalized penetration distance as a function of inlet jet momentum ratio (Rm).

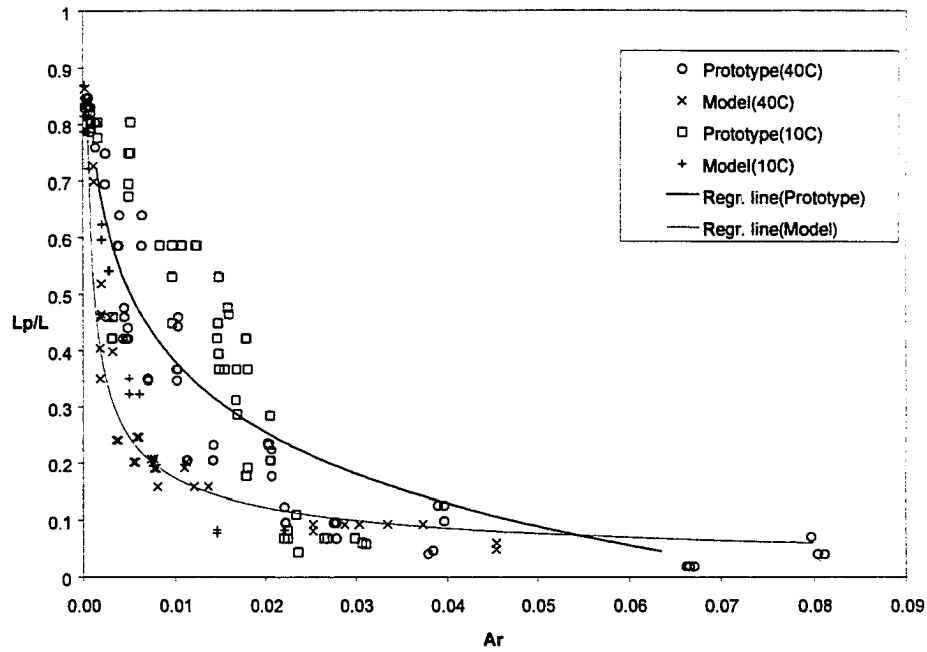

Figure 6.18. Normalized penetration distance as a function of Archimedes number (Ar).

parameter differed as the heat load changed, with a larger temperature difference resulting in a larger threshold value. The differences between $\Delta T = 10\ ^{\circ}C$ and $\Delta T = 0\ ^{\circ}C$ (i.e. isothermal airflow) were not significant however.

The plots of air-jet penetration distance against Re showed different curves for each enclosure even as the heat load remained unchanged. The air-jet penetration distance for the scale-model and prototype fell along the same curve as a function of Rm provided the heat load was similar. However, different curves existed when the heat load changed. All data showed very small differences between $\Delta T = 10\ ^{\circ}C$ and $\Delta T = 0\ ^{\circ}C$.

Figure 6.18 shows the air-jet penetration distance as a function of the Ar. Non-dimensional air-jet penetration distance within intermediate Ar ranges ($0.005 < Ar < 0.015$) showed a large difference between scale-model and prototype. This intermediate range was

close to the unstable range described by Randall and Battams (1979) ($30 < Ar_c < 75$) which corresponds to a range of $0.005 < Ar, 0.012$. All non-dimensional air-jet penetration distance data were similar between scale-model and prototype when the Ar was at either extreme (Ar> 0.015) or (Ar< 0.005).

It was concluded that the performance for a small heat load (small ΔT) for nonisothermal airflow (for example : $\Delta T = 10\ ^{\circ}C$) was similar to isothermal airflow. The maximum non-dimensional air-jet penetration distance for nonisothermal airflow was 0.85 L equaling that for isothermal airflow.

In conclusion, Re was an inappropriate similitude criterion for nonisothermal airflow. Rm can be used as a similarity requirement for nonisothermal airflow as long as a similar heat load (same ΔT) is maintained between the scale-model and prototype. Ar can be treated as the similitude criterion only at the regions of extreme Ar values of (i.e. Ar< 0.005 or Ar> 0.015). The threshold value of Re and Rm to reach 98% of threshold penetration distance for a heat load of $\Delta T = 0\ ^{\circ}C$, $10\ ^{\circ}C$,and $40\ ^{\circ}C$ for both the scale-model and prototype are shown in Table 6.7. The equation describing air-jet penetration distance as a function of Re and Rm are also shown in Table 6.7.

6.2.2. Airflow patterns

Airflow patterns were validated by air-jet trajectory measurements and airflow visualization. The air-jet trajectories between scale-model and prototype were compared for each similitude parameter.

Table 6.7. The expression equations and threshold values to reach threshold penetration distance.

Test room	ΔT, °C	Expression equations	R^2	Threshold value[1]
Both models	0	$\frac{L_p}{L} = \frac{0.84}{20.18e^{-47.29\sqrt{R_m}} + 1}$	0.92	Rm=0.02
Prototype	0	$\frac{L_p}{L} = \frac{0.84}{450e^{-0.23\sqrt{R_e}} + 1}$	0.96	Re=1900
Scale-model	0	$\frac{L_p}{L} = \frac{0.84}{205e^{-0.30\sqrt{R_e}} + 1}$	0.98	Re=950
Both models	10	$\frac{L_p}{L} = \frac{0.84}{13.91e^{-45.60\sqrt{R_m}} + 1}$	0.88	Rm=0.02
Prototype	10	$\frac{L_p}{L} = \frac{0.84}{20965e^{-0.46\sqrt{R_e}} + 1}$	0.79	Re=1800
Scale-model	10	$\frac{L_p}{L} = \frac{0.84}{256e^{-0.22\sqrt{R_e}} + 1}$	0.93	Re=900
Both models	40	$\frac{L_p}{L} = \frac{0.84}{26.14e^{-27.91\sqrt{R_m}} + 1}$	0.89	Rm=0.066
Prototype	40	$\frac{L_p}{L} = \frac{0.84}{306e^{-0.16\sqrt{R_e}} + 1}$	0.93	Re=3700
Scale-model	40	$\frac{L_p}{L} = \frac{0.84}{289e^{-0.23\sqrt{R_e}} + 1}$	0.95	Re=1800

Note 1. The threshold value was defined as the penetration distance required to reached 98% of the maximum penetration distance.

The dominant parameters that affect nonisothermal airflow were shown previously to be Ar, Eu, and Re. The air-jet penetration distance results showed that Re was an inappropriate similitude parameter for nonisothermal airflow (with similar heat load) and thus Re was not used as a similitude parameter for the following experiments. Eu was replaced by Rm for the same airspeed environment when it was used as the similitude parameter. Therefore, the Ar and Rm parameters were evaluated as the similarity criterion for nonisothermal airflow.

Randall and Battams (1979) found that the air-jet would remain horizontal when the Ar_c <30, would fall on entry when the Ar_c > 75, and would become unstable between these critical values (Figure 6.19 (a)). Mullejans (1966) suggested a critical Ar value using a similar definition as the Ar_c where:

$$Ar\frac{bh}{D} \leq 40 \qquad (6.10)$$

However, this criteria has been shown to vary with the geometric shape of the enclosure. Wang and Ogilvie (1994a) found similar results as Randall and Battams (1979) concluding that the airflow pattern would fall on entry under low inlet momentum conditions.

Randall and Battams (1979) concluded that if the air-jet was allowed to penetrate more than 0.5 L, than only one recirculation zone would form (Figure 6.19 (a)). If however the air-jet penetrated less than 0.5 L, two recirculation zones would form (Figure 6.19 (b)).

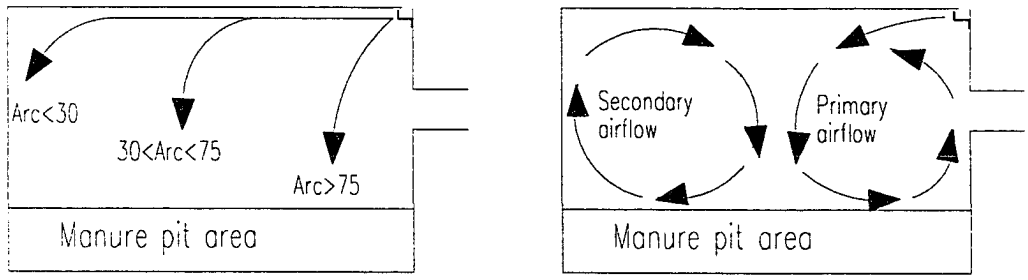

a. Nonisothermal airflow b. Two-circulation airflow

Figure 6.19. (a) Airflow patterns produced by a horizontally projected wall jet under nonisothermal conditions and (b) two-circulation zone airflow for intermediate Ar_c airflow.

The two recirculation zones consisted of a primary zone encompassing the air-jet itself and a secondary zone formed by shear stress from the falling air-jet (Figure 6.19 (b)). In addition, for low Ar values (Figure 6.19 (a)) and high Ar values a single stable recirculation zone was found. If the Ar was between these critical Ar limits, two recirculation zones would form, and these would be unstable implying that the airflow pattern could be easily changed.

The secondary zone (Figure 6.19 (b)) disappears when the air-jet penetrates a distance beyond the mid-point of the room (0.5 L). The critical airflow rates used to distinguish airflow patterns for $\Delta T = 40$ °C based on previous research and results from the air-jet penetration distance test (Section 6.2.1) are shown in Table 6.8.

6.2.2.1. Air-jet trajectory measurement

The air-jet trajectory was defined as the peak airspeed position along the ceiling or floor regions. The air-jet trajectory, as was shown in Section 6.1.2.1, describes airflow patterns within an enclosure very clearly. Several airflow rates around the critical ranges shown in Table 6.8 combined with two heating loads ($\Delta T = 40$°C, $\Delta T = 60$ °C) were chosen to measure the nonisothermal air-jet trajectory. The test conditions for quantifying air-jet trajectory are given in Table 6.9.

The air-jet trajectories for both the scale-model and prototype for a heat load of $\Delta T =$ 40°C are shown in Figures 6.20 and 6.21. The trajectories show that the airflow patterns

Table 6.8. The critical values of nonisothermal airflow patterns at $\Delta T = 40°C$ under otherwise noted.

Classification of airflow pattern	Airflow rate of prototype	Airflow rate of scale-model	Criteria	Reference
Fully rotary	212	53	$Rm \geq 0.066$ and $\Delta T = 40°C$ $Rm \geq 0.020$ and $\Delta T = 10°C$ $Ar_p \leq 0.0015$ $Ar_m \leq 0.00075$	Penetration distance test (section 6.2.1)
Air-jet remains horizontal	116	21	$Ar_c \leq 30$	Randall and Battams, 1979
Approximate isothermal airflow	125	22	$Ar\frac{bh}{D} \leq 40$	Mullejans, 1966
Air-jet behaves as Figure 6.19 (b)	131	33	$Ar_w = 40$	Wang and Ogilvie, 1994a
	74 to 116	13 to 21	$30 < Ar_c < 75$	Randall and Battams, 1979
Air-jet falls on entry	74	13	$Ar_c \geq 75$	Randall and Battams, 1979

were fully rotary (NP1, NP2, NM2) when the airflow rate was beyond the threshold critical value shown in Table 6.8 (prototype = 212 cfm, scale-model = 53 cfm).

For prototype airflow (Figure 6.20), full rotary airflow patterns were measured for cases (NP1, NP2) where the airflow was above the critical airflow (212 cfm) required for full rotary airflow (see Table 6.8). Randall and Battams (1979) predicted that the air-jet would remain horizontal if $Ar_c \leq 30$ (see Table 6.8) and for the prototype this corresponded to an airflow rate of 185 cfm (for $\Delta T = 40\,°C$). Figure 6.20 confirms this result with NP3 results. Randall and Battams further predicted that the air-jet would fall on entry if $Ar_c \geq 75$. For the prototype this corresponds to an airflow rate <100 cfm (for $\Delta T = 40\,°C$). The prototype results show that the air-jet fell on entry for airflow rates less than about 58 cfm (NP6, NP7). However at an airflow of 72 cfm (NP5), the air-jet fell intermediately forming a two-

Table 6.9. Test conditions of trajectory measurement for nonisothermal airflow.

Test	Q,cfm	U_d,m/s	T_d,°C	T_f,°C	ΔT,°C	Re	Rm	Ar	Ar_c
NP1[1]	324	4.97	61.5	21.5	40	3976	0.115	0.0006	4
NP2	221	3.39	61.5	21.5	40	2708	0.053	0.0014	8
NP3	150	2.30	57	17	40	1842	0.025	0.0030	18
NP4	105	1.61	57.5	17.5	40	1284	0.012	0.0062	37
NP5	72	1.10	54.5	14.5	40	882	0.006	0.0133	80
NP6	58	0.90	55.5	15.5	40	716	0.004	0.0201	121
NP7	53	0.81	62.77	22.77	40	649	0.003	0.0239	144
NP8	116	1.78	82.33	22.33	60	1424	0.015	0.0072	44
NP9	83	1.28	79.37	19.37	60	1025	0.008	0.0141	85
NP10	73	1.12	81.94	21.94	60	898	0.006	0.0182	110
NP11	59	0.90	79.56	19.56	60	723	0.004	0.0283	170
NM1	54	3.34	61	21	40	1334	0.052	0.0007	4
NM2	38	2.36	60	20	40	942	0.026	0.0014	9
NM3	26	1.60	60	20	40	641	0.012	0.0031	19
NM4	18	1.08	60	20	40	433	0.005	0.0068	41
NM5	14	0.84	62.8	22.8	40	334	0.003	0.0113	68
NM6	11	0.70	60	20	40	281	0.002	0.0161	97
NM7	9	0.54	58	18	40	217	0.001	0.0270	163
NM8	28	1.72	82.79	22.79	60	687	0.014	0.0039	23
NM9	21	1.28	79.83	19.83	60	513	0.008	0.0070	42
NM10	16	0.96	79.8	19.8	60	382	0.004	0.0127	76
NM11	14	0.83	81.71	21.71	60	333	0.003	0.0165	100
NM12	11	0.68	82.33	22.33	60	273	0.002	0.0246	148

Note 1. N= nonisothermal, P= prototype, M=scale-model, 1= test 1.

circulation airflow pattern as shown in Figure 6.19 (b).

For scale-model airflow (Figure 6.21), full rotary airflow patterns were meassured for cases (NM1, NM2, NM3) representing airflow rates of 54, 38, and 26 cfm, resepectively. The critical airflow shown in Table 6.8 for maintaining a horizontal air-jet in the scale-model was predicted to be > 28 cfm based on the criteria presented by Randall and Battams (1979). The measured results agree with Randall and Battams (1979). Based on Randall and Battams

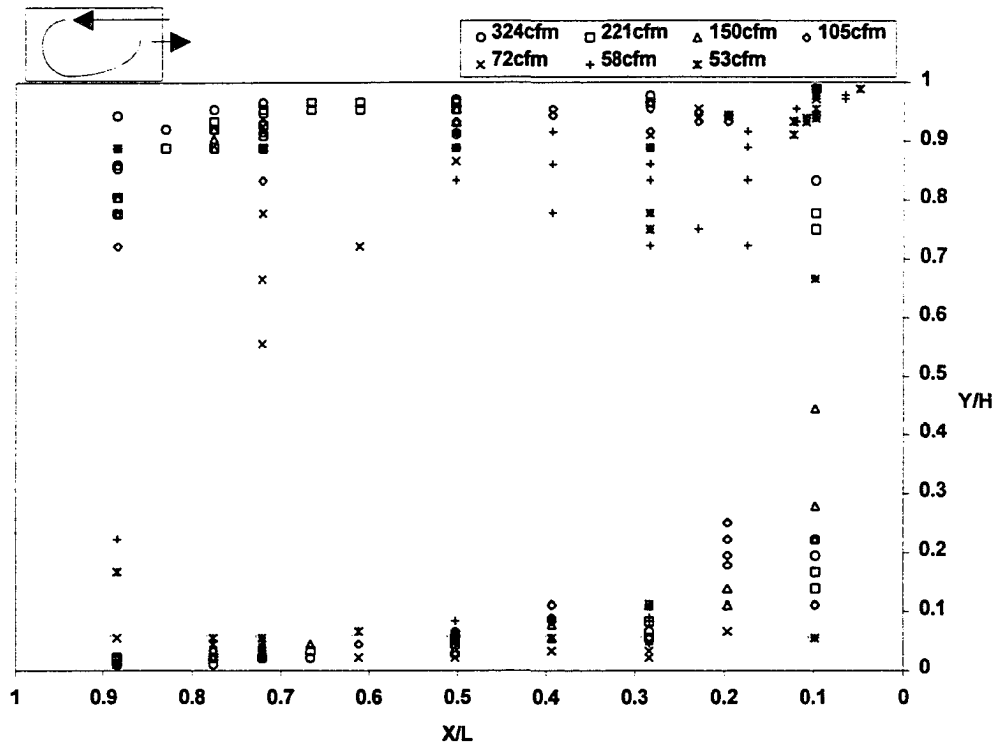

Figure 6.20. Peak airspeed trajectory of nonisothermal airflow for prototype at $\Delta T = 40$ °C.

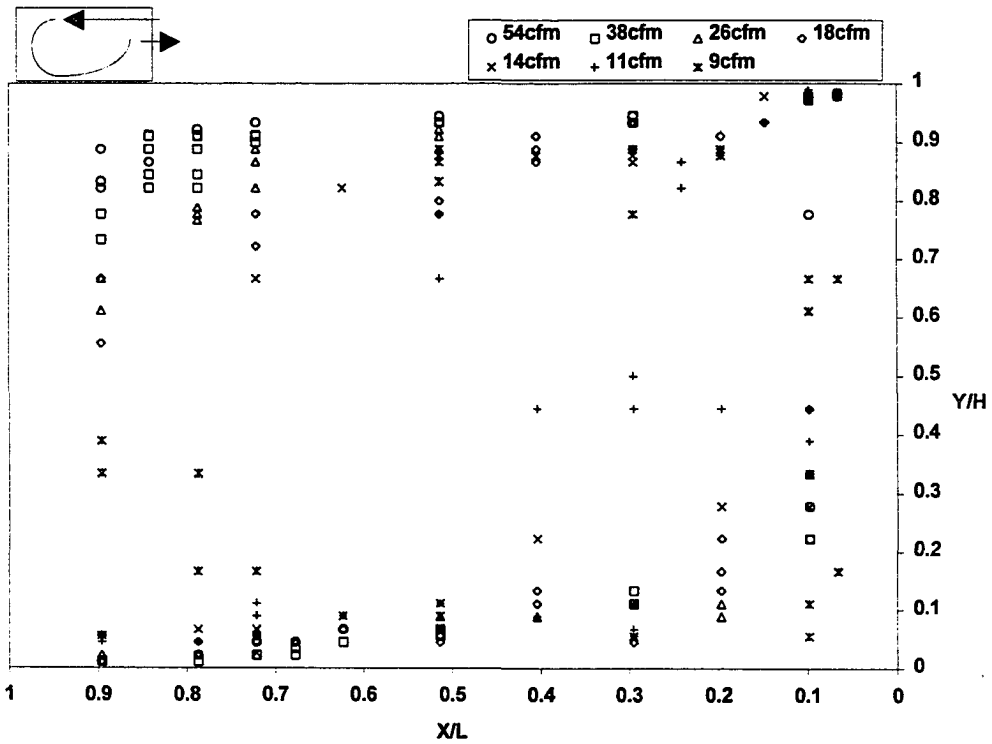

Figure 6.21 Peak airspeed trajectory of nonisothermal airflow for scale-model at $\Delta T = 40$ °C.

(1979) criteria ($Ar_c \geq 75$), the air-jet would be predicted to fall on entry for scale-model airflows < 18 cfm. The results shown in Figure 6.21 show this did happen but not until the airflow was reduced to ≤ 11 cfm (NM6, NM7).

The air-jet trajectory measurements confirmed the airflow patterns described in Table 6.8. However, the critical values of Ar_w proposed by Wang and Ogilvie (1994a) used to distinguish the existence of secondary airflow was not in agreement in this experiment. The secondary circulation airflow was removed at about 58 to 72 cfm for the prototype and 11 to 14 cfm for the scale-model.

6.2.2.2. Airflow visualization

Airflow patterns were observed using airflow visualization for various heat loads and these were compared with the air-jet trajectory measurements as shown in Figure 6.22. The critical value of Ar that described when the air-jet would fall on entry was observed by visualization to be equal to about Ar= 0.06 as shown in Figure 6.23.

The series of comparisons between the air-jet trajectory and airflow visualization confirm the correctness of using either method. The results provide a basis for evaluating various similitude parameters under different combinations of airflow rate and heat load. Section 6.2.2.3 provides this comparison.

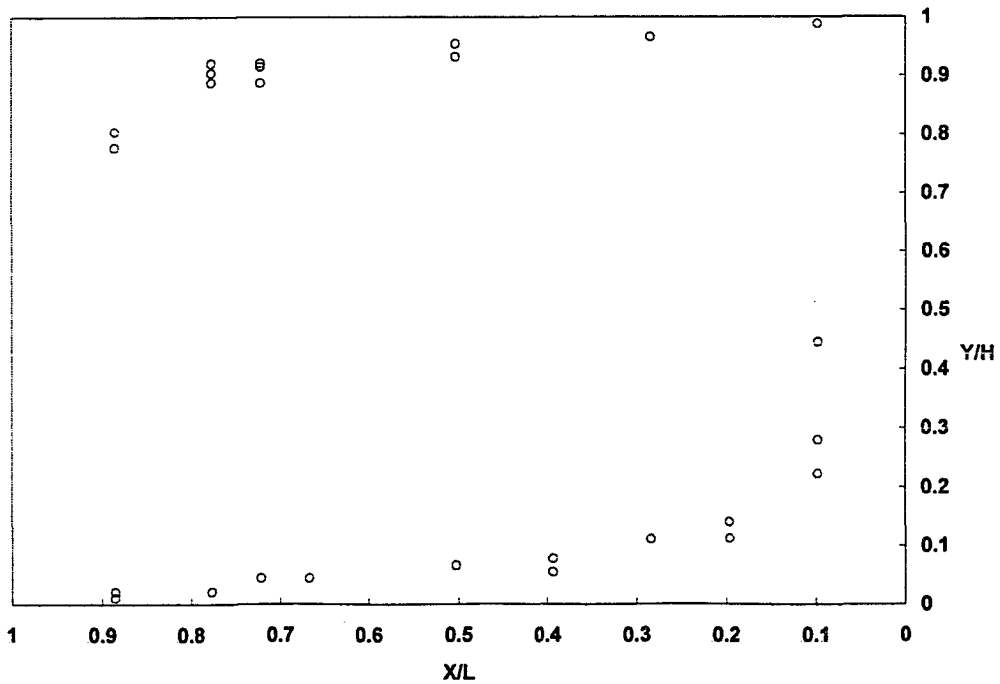

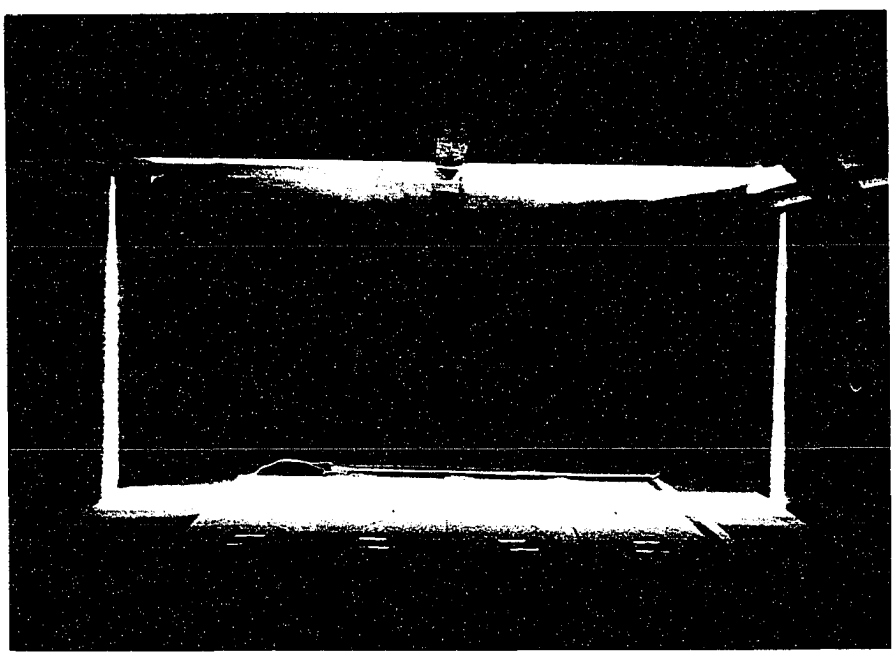

a. Scale: 1:3, Q_p=150cfm, ΔT=40° C, Ar_p=0.0030, Rm_p=0.025. (case NP3 of Table 6.8)

Figure 6.22. Nonisothermal airflow pattern of trajectory and smoke visualization. (°) denotes peak airspeed position across airflow, (•) denotes airspeed less than 0.1 m/s.

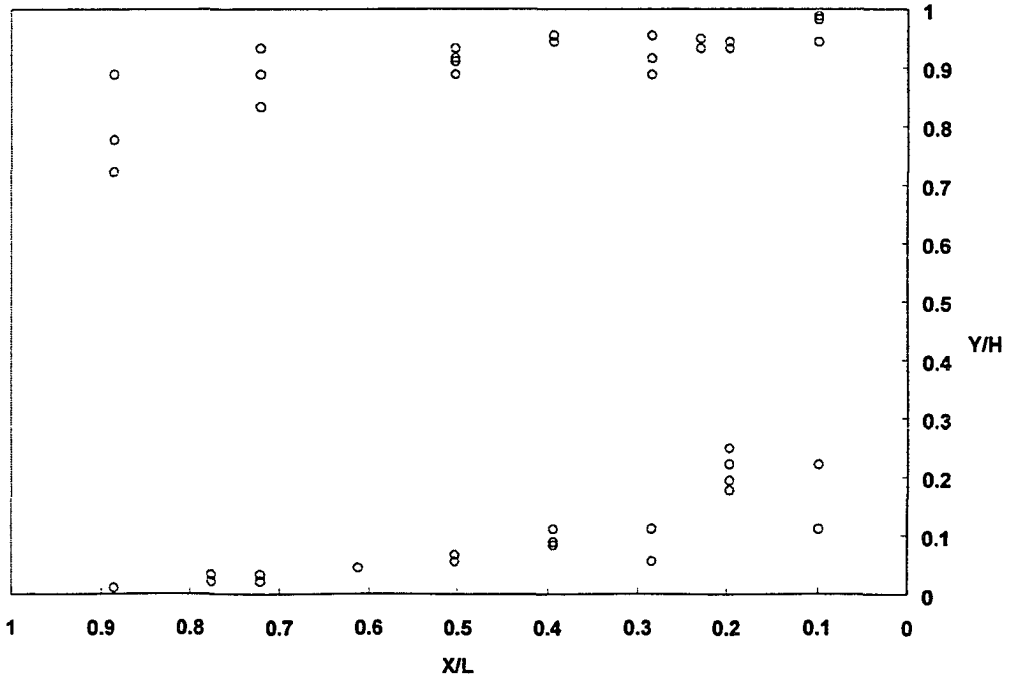

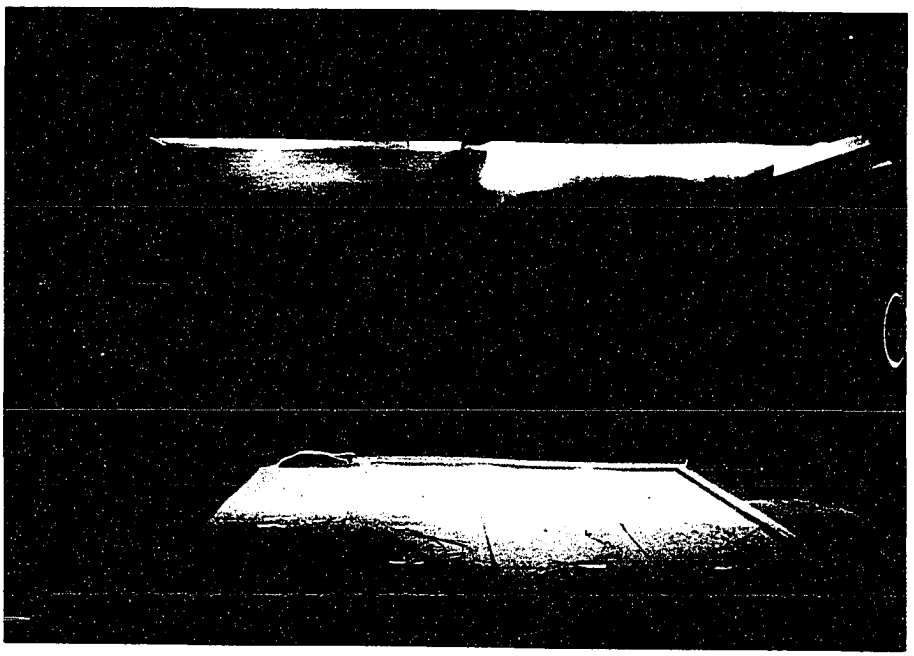

b. Scale: 1:3, Q_p=105cfm, ΔT=40° C, Ar_p=0.0062, Rm_p=0.012. (case NP4 of Table 6.8)

Figure 6.22. (continued)

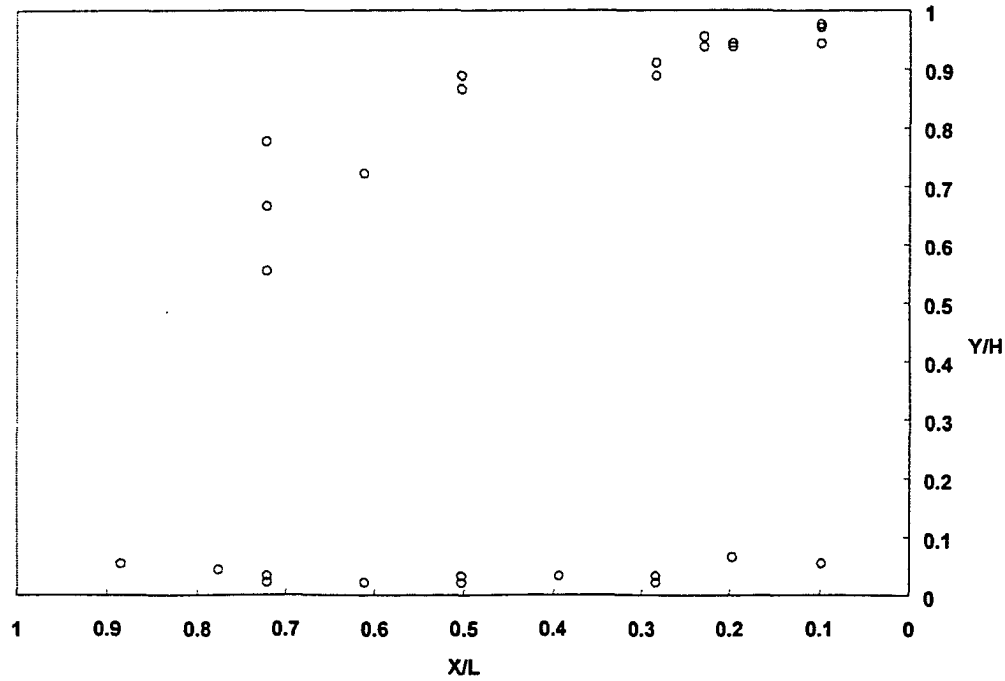

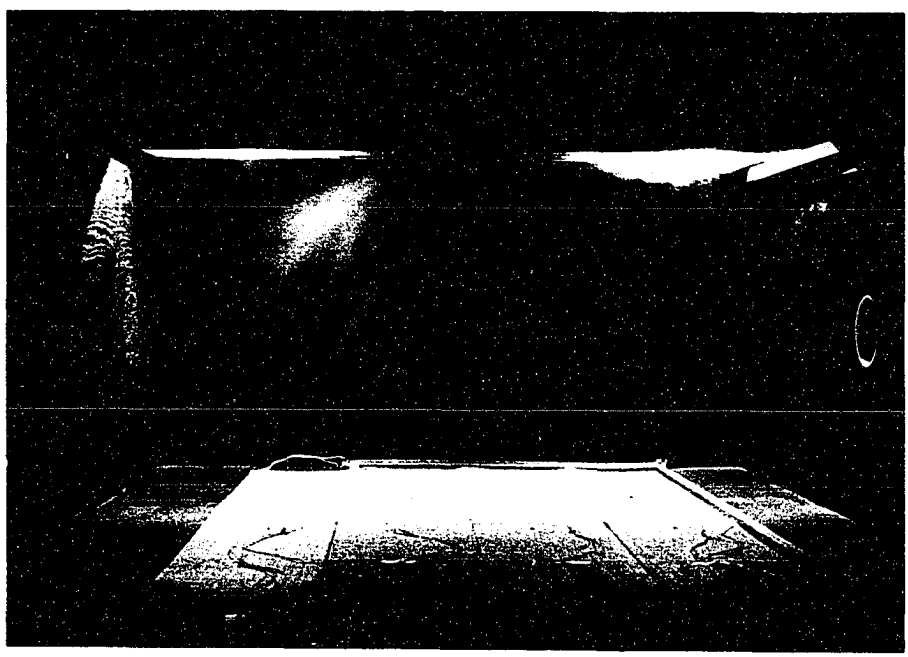

c. Scale: 1:3, Q_p=72cfm, ΔT=40° C, Ar_p=0.0130, Rm_p=0.006. (case NP5 of Table 6.8)

Figure 6.22. (continued)

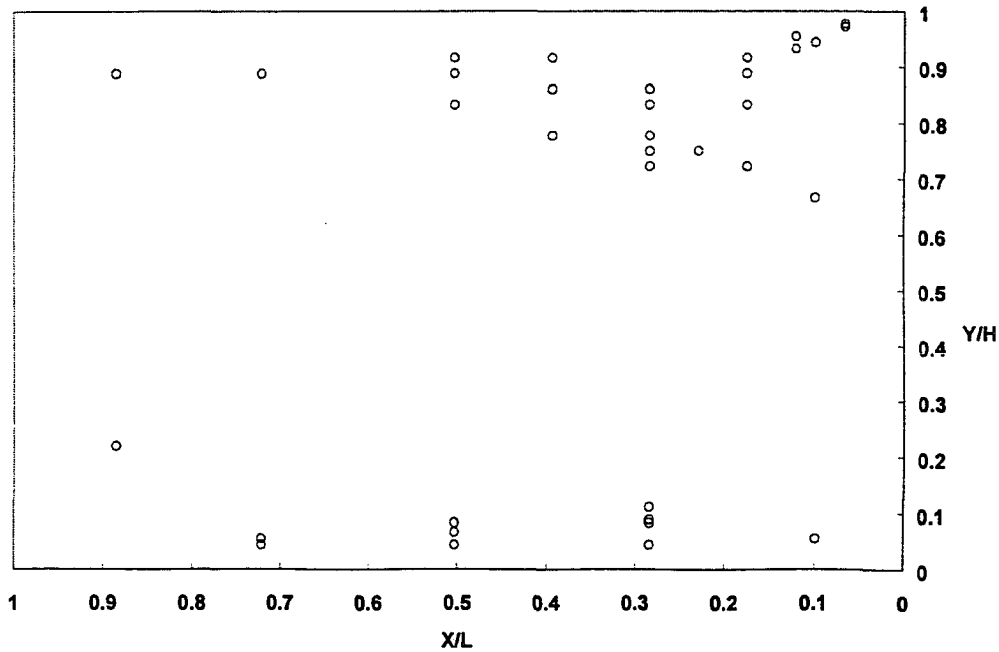

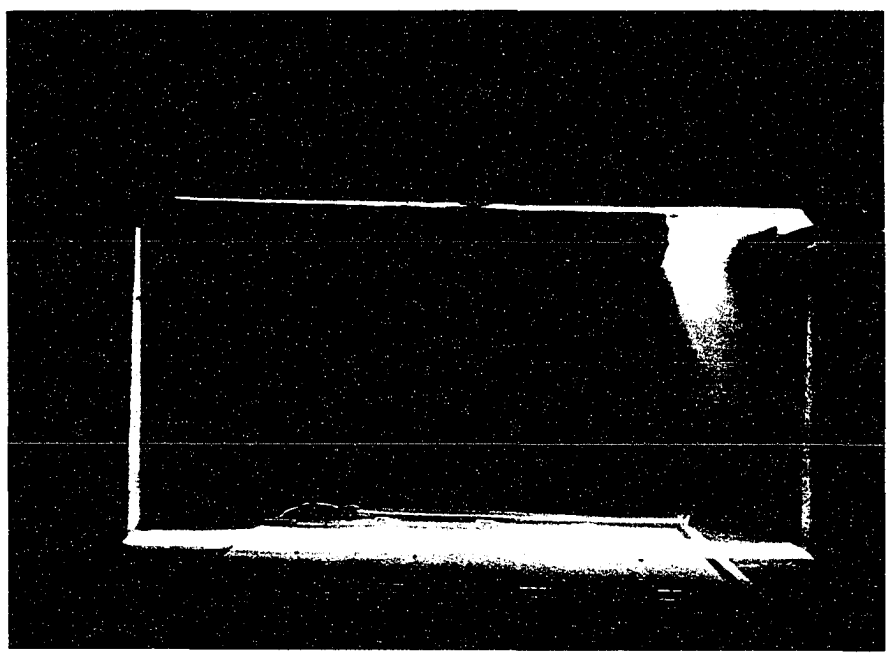

d. Scale: 1:3, Q_p=58cfm, ΔT=40° C, Ar_p=0.0200, Rm_p=0.004. (case NP6 of Table 6.8)

Figure 6.22. (continued)

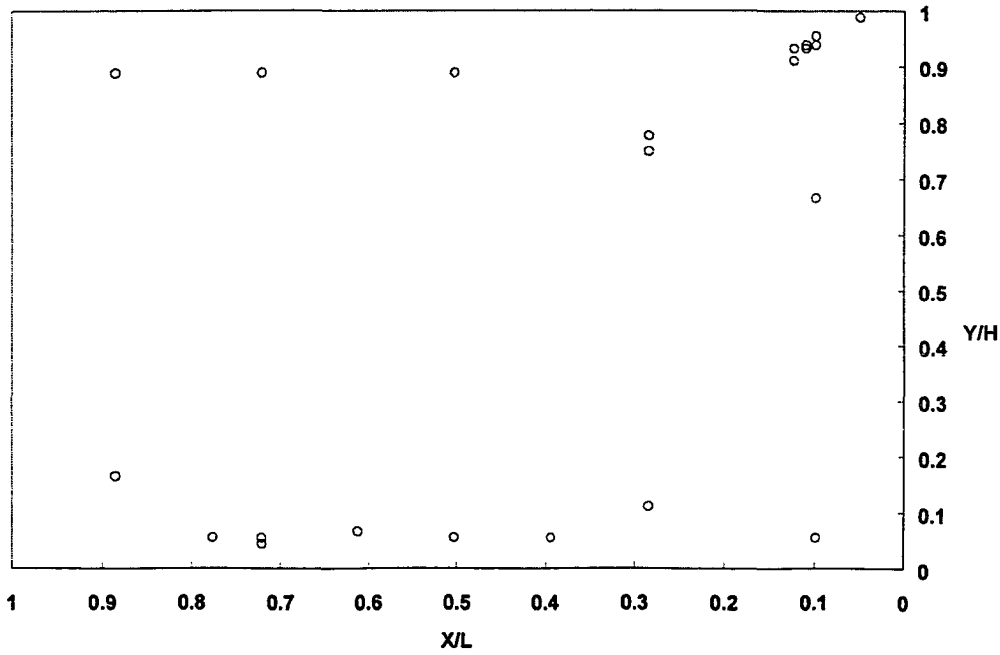

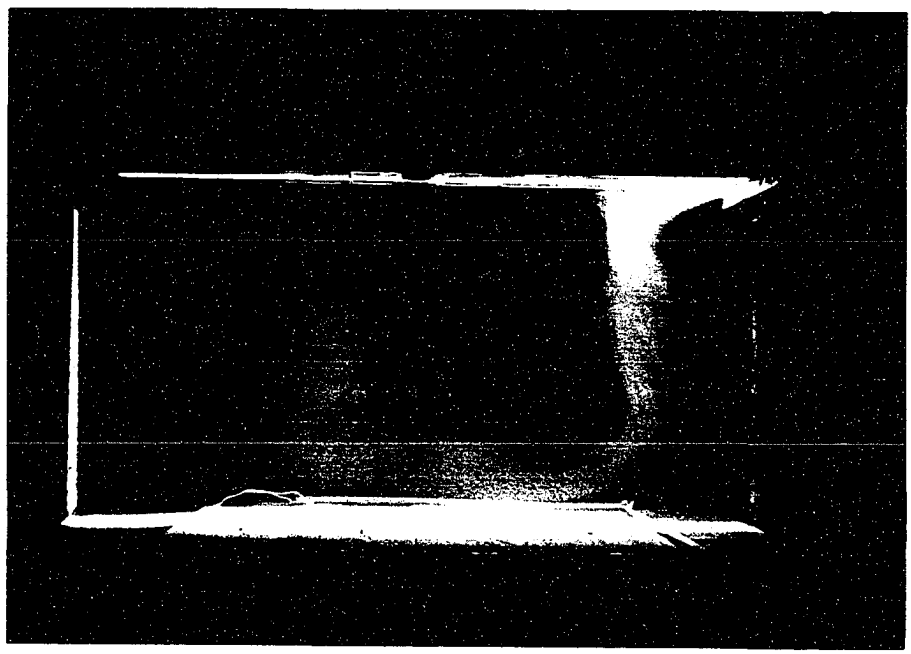

e. Scale: 1:3, Q_p=53cfm, ΔT=40° C, Ar_p=0.0239, Rm_p=0.003. (case NP7 of Table 6.8)

Figure 6.22. (continued)

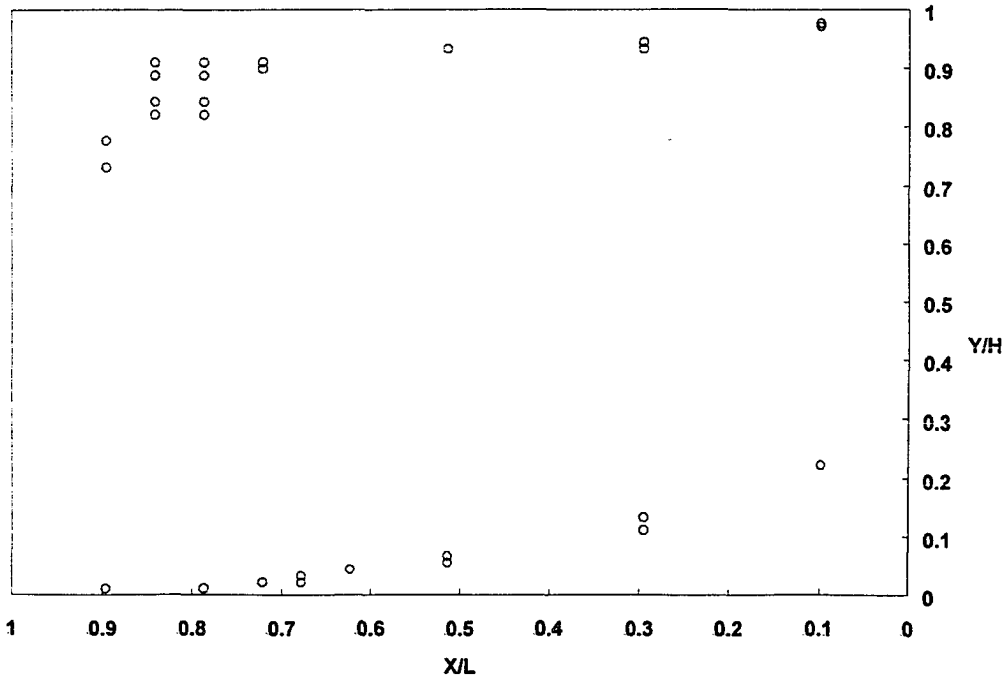

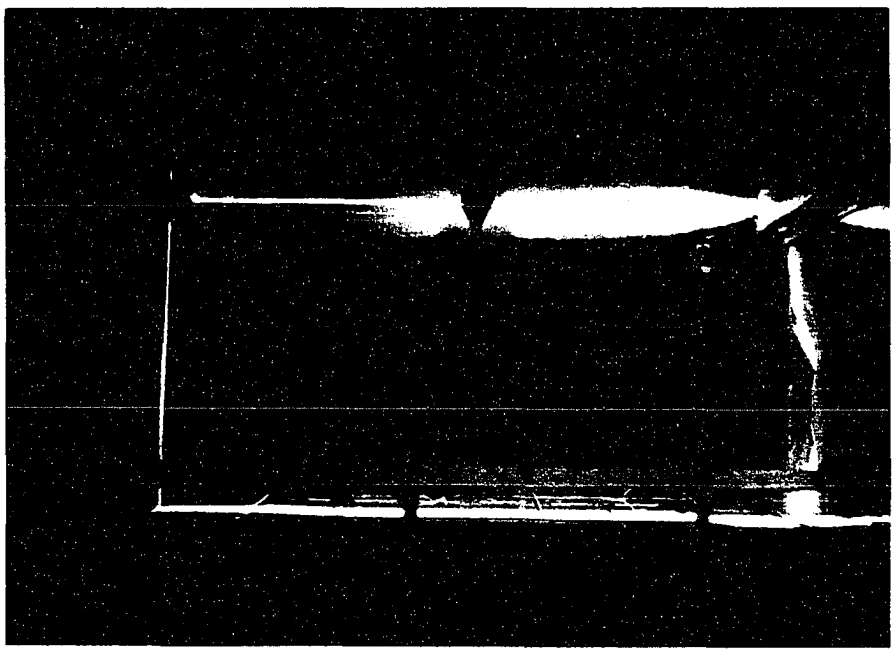

f. Scale: 1:6, Q_m=38cfm, ΔT=40° C, Ar_m=0.0014, Rm_m=0.026. (case NM2 of Table 6.8)

Figure 6.22. (continued)

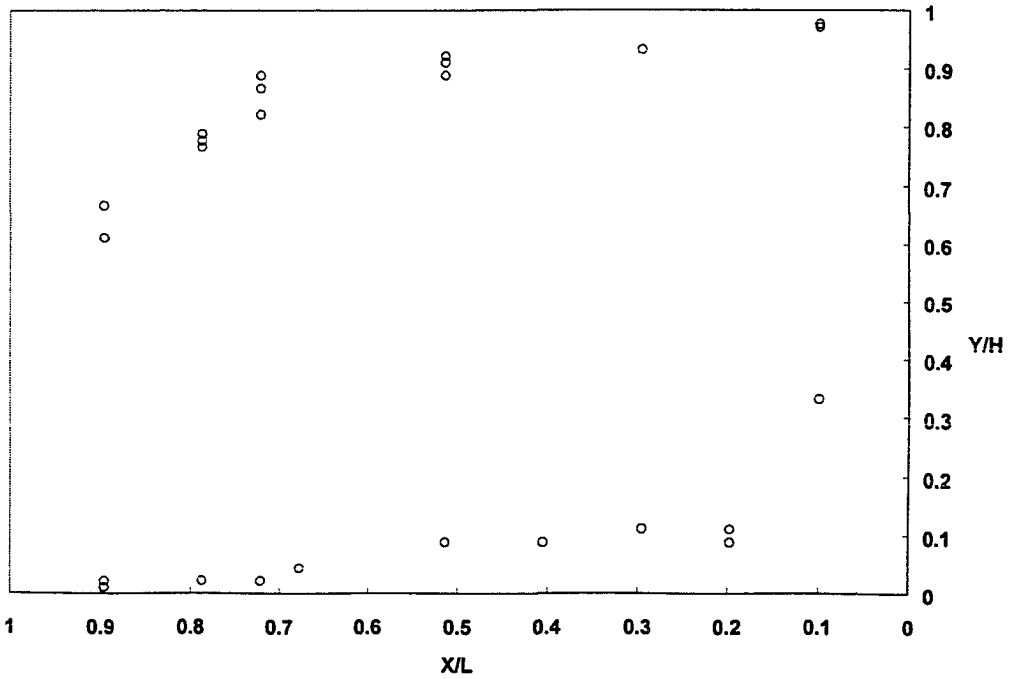

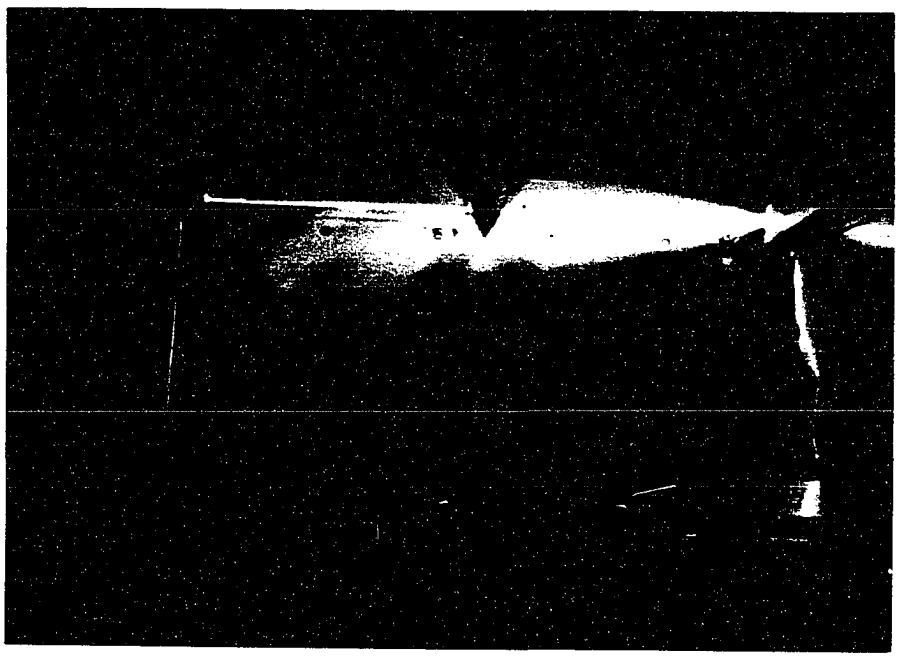

g. Scale: 1:6, Q_m=26cfm, ΔT=40° C, Ar_m=0.0031, Rm_m=0.012. (case NM3 of Table 6.8)

Figure 6.22. (continued)

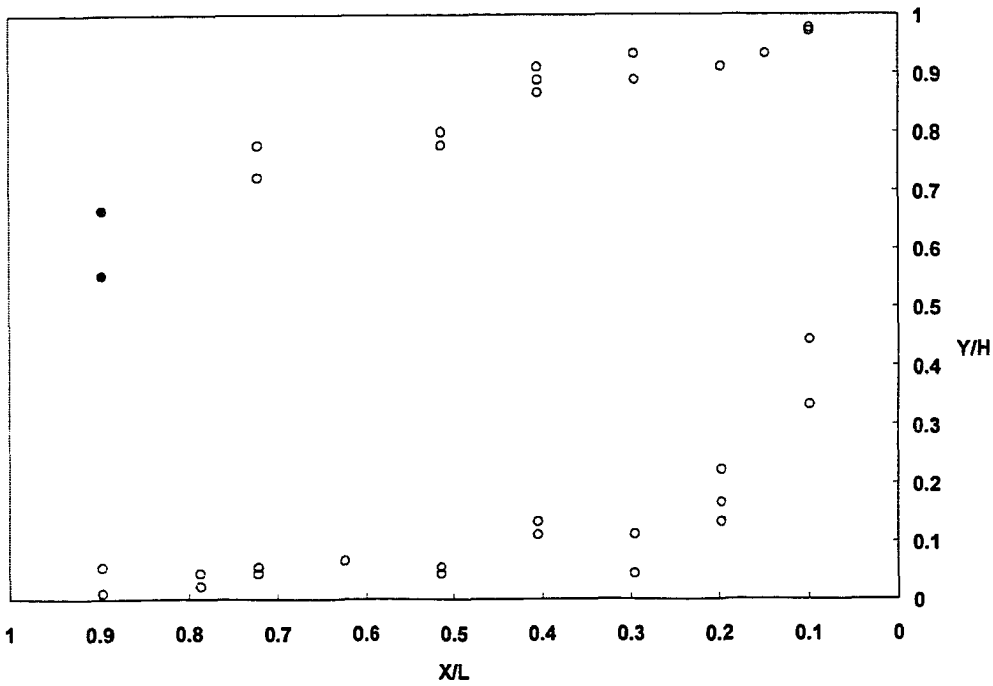

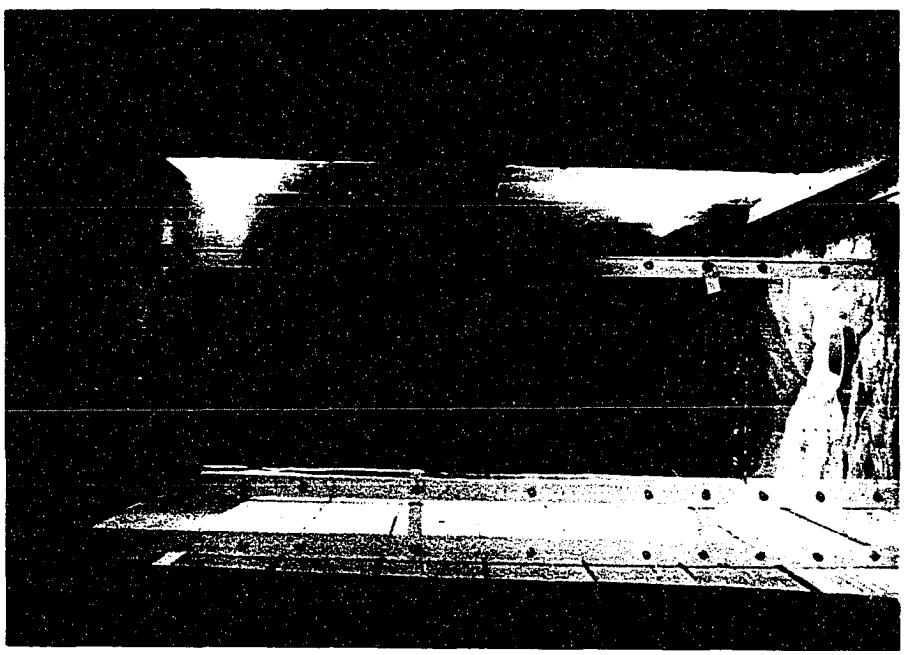

h. Scale: 1:6, Q_m=18cfm, ΔT=40° C, Ar_m=0.0068, Rm_m=0.005. (case NM4 of Table 6.8)

Figure 6.22. (continued)

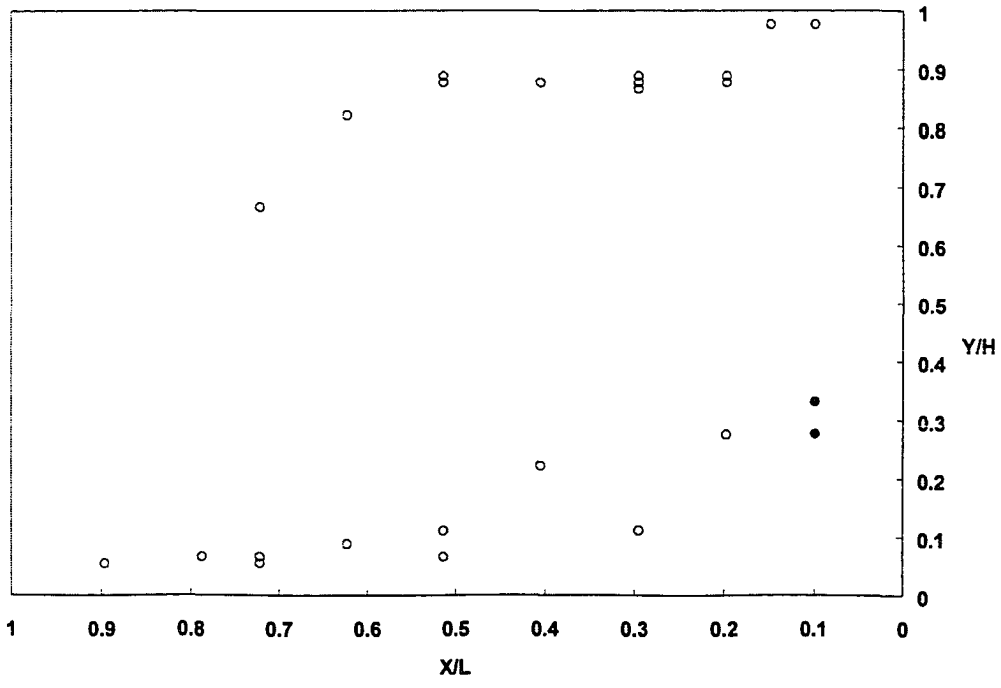

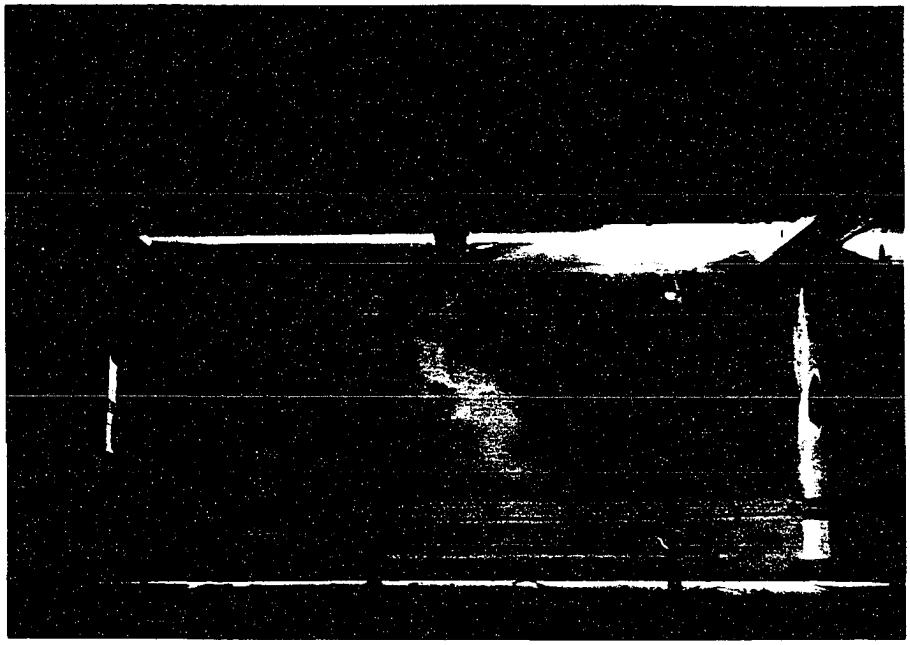

i. Scale: 1:6, Q_m=14cfm, ΔT=40° C, Ar_m=0.0113, Rm_m=0.003. (case NM5 of Table 6.8)

Figure 6.22. (continued)

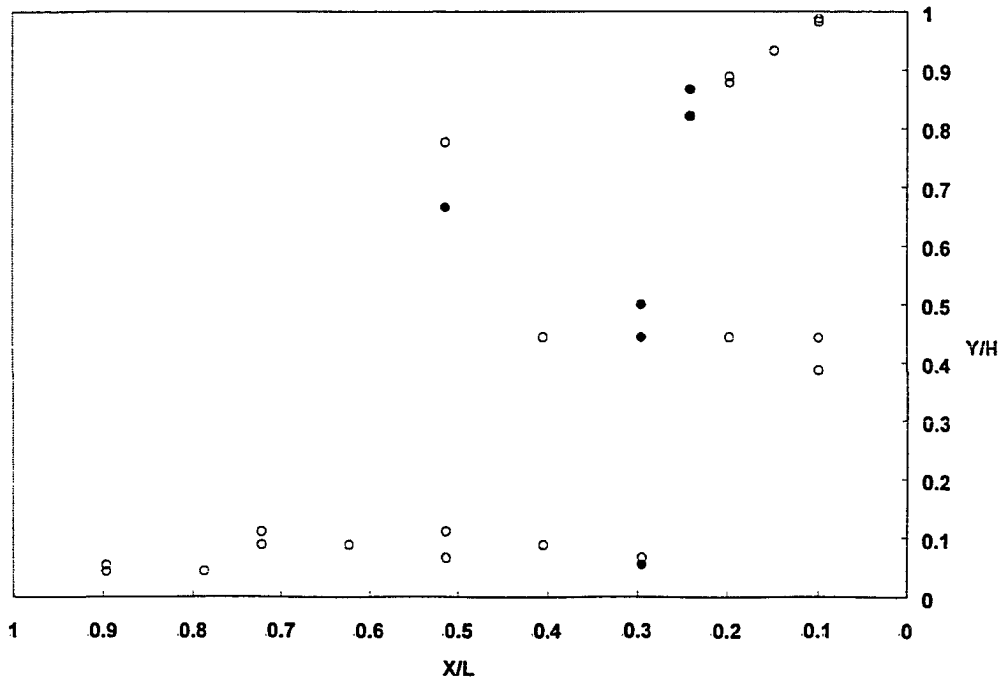

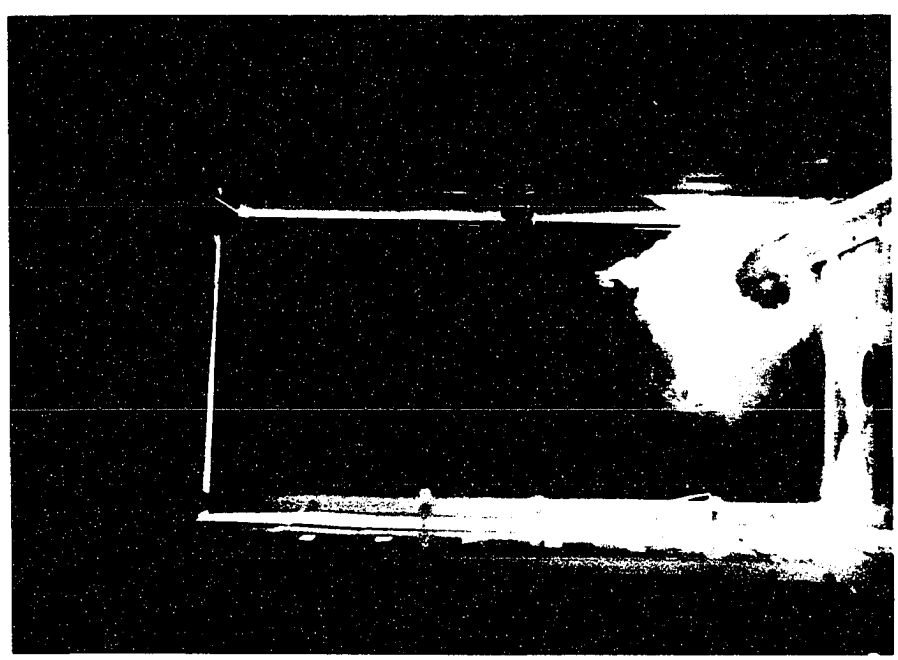

j. Scale: 1:6, Q_m=11cfm, ΔT=40° C, Ar_m=0.0161, Rm_m=0.002. (case NM6 of Table 6.8)

Figure 6.22. (continued)

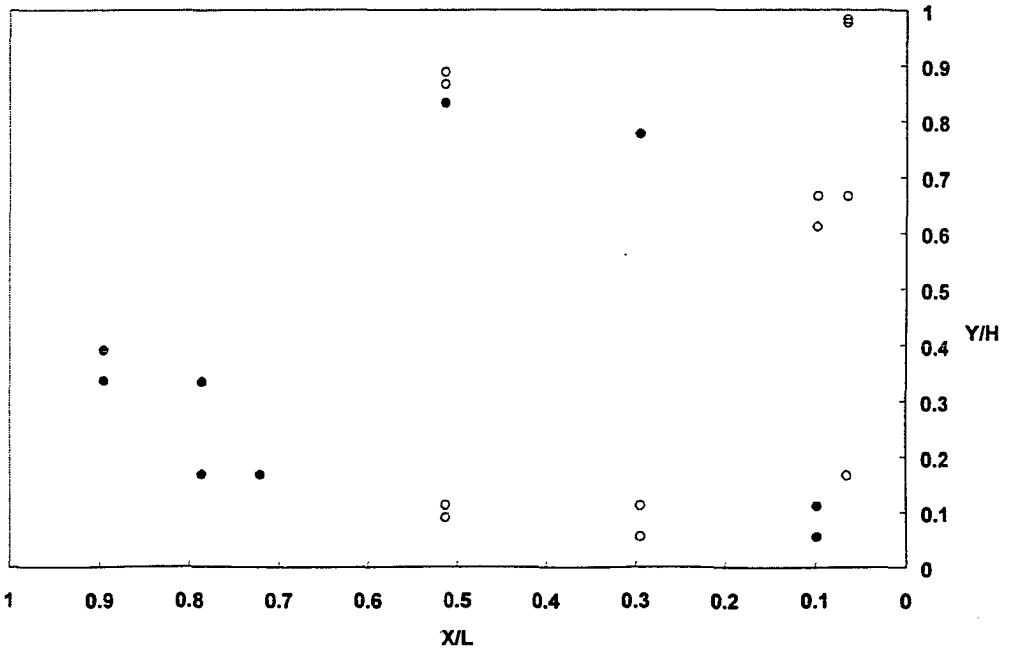

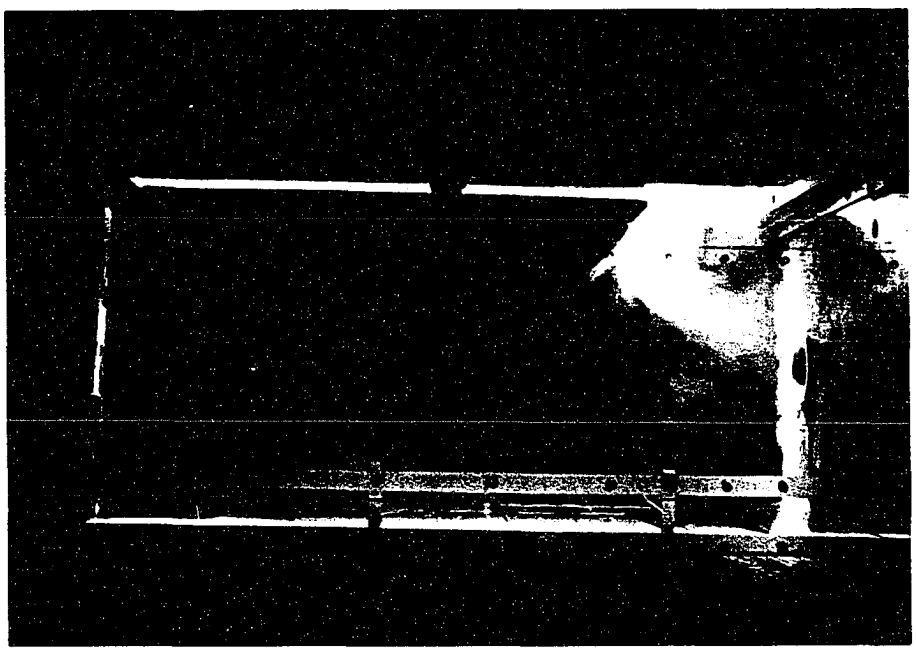

k. Scale: 1:6, Q_m=9cfm, ΔT=40° C, Ar_m=0.0270, Rm_m=0.001. (case NM7 of Table 6.8)

Figure 6.22. (continued)

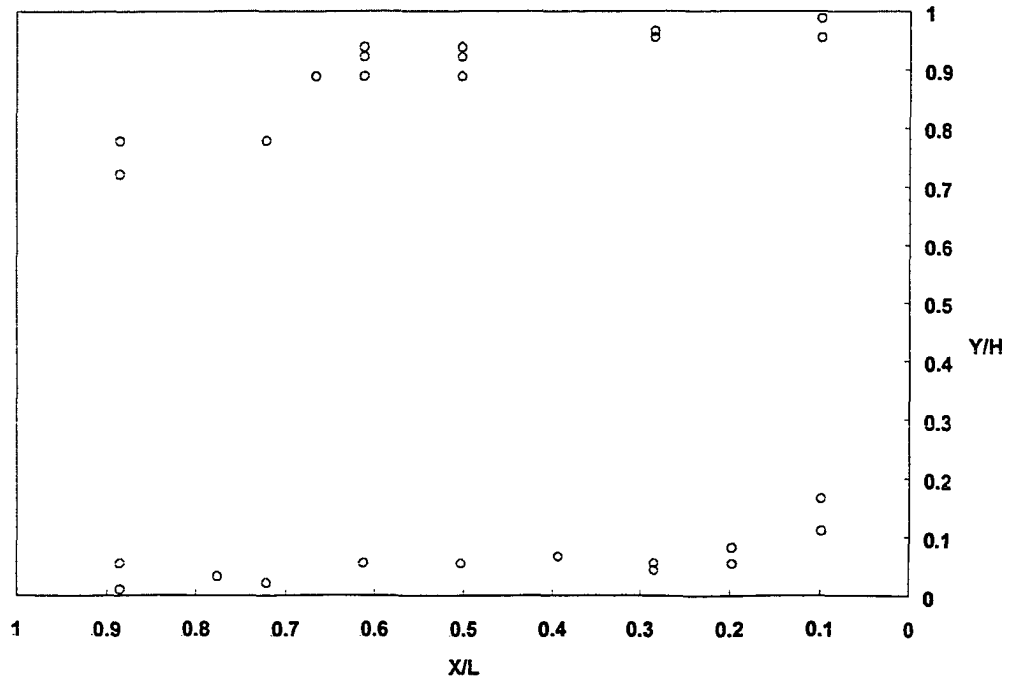

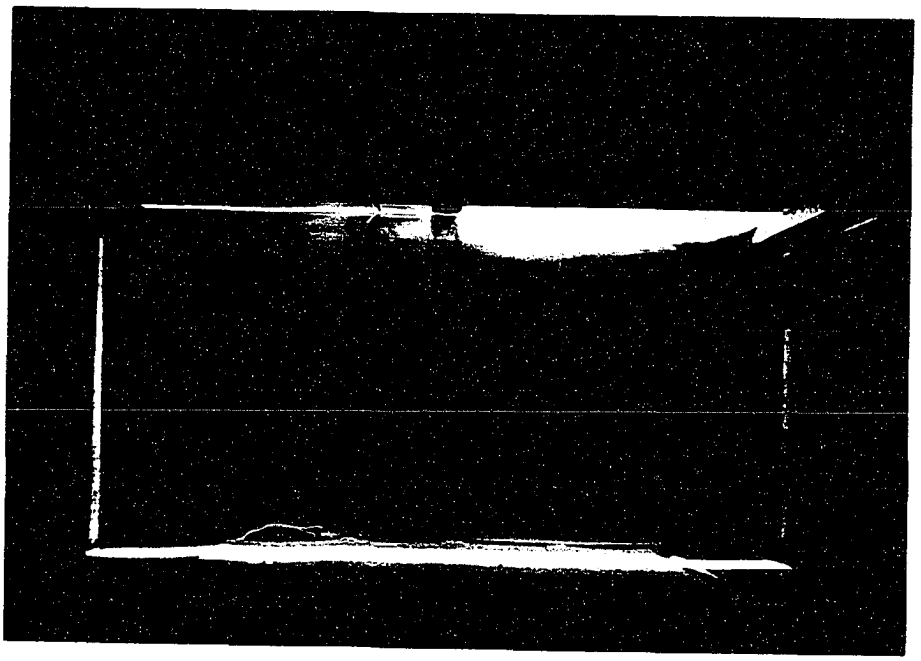

1. Scale: 1:3, Q_p=116cfm, ΔT=60° C, Ar_p=0.0072, Rm_p=0.015. (case NP8 of Table 6.8)

Figure 6.22. (continued)

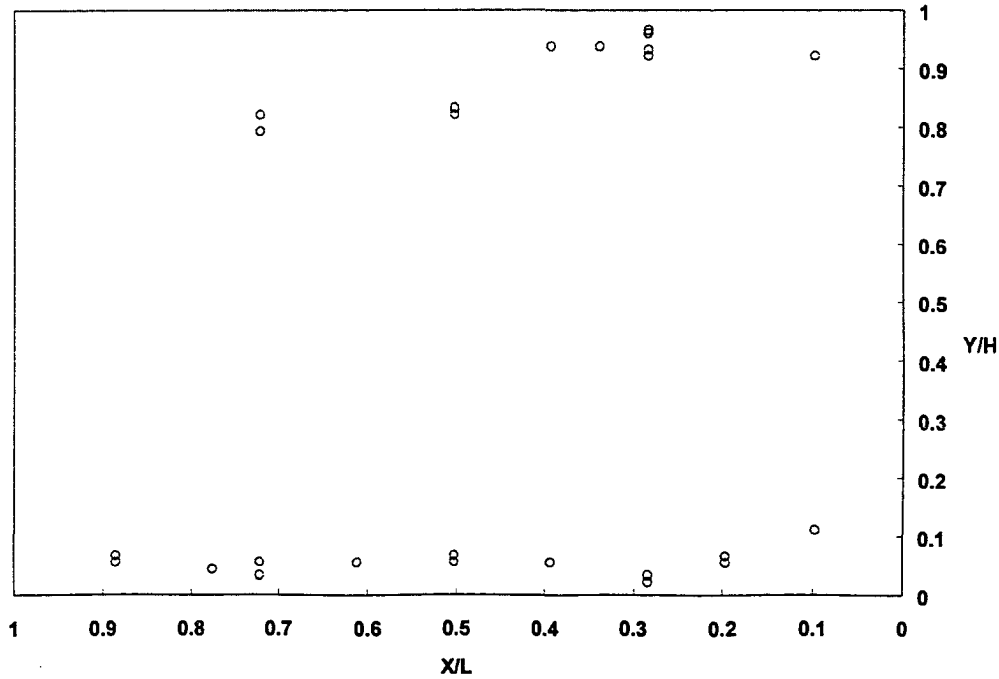

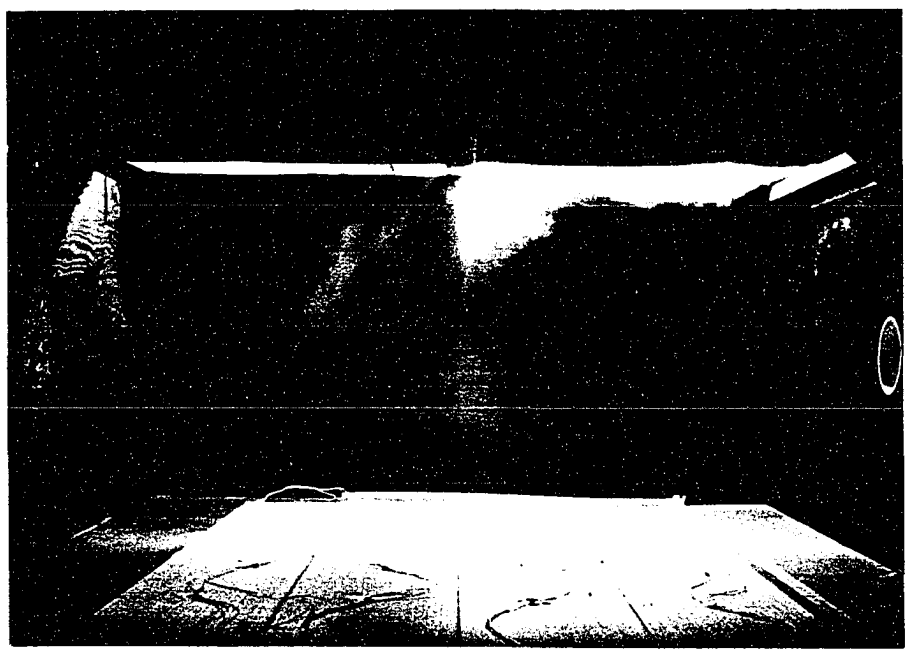

m. Scale: 1:3, Q_p=83cfm, ΔT=60° C, Ar_p=0.0141, Rm_p=0.008. (case NP9 of Table 6.8)

Figure 6.22. (continued)

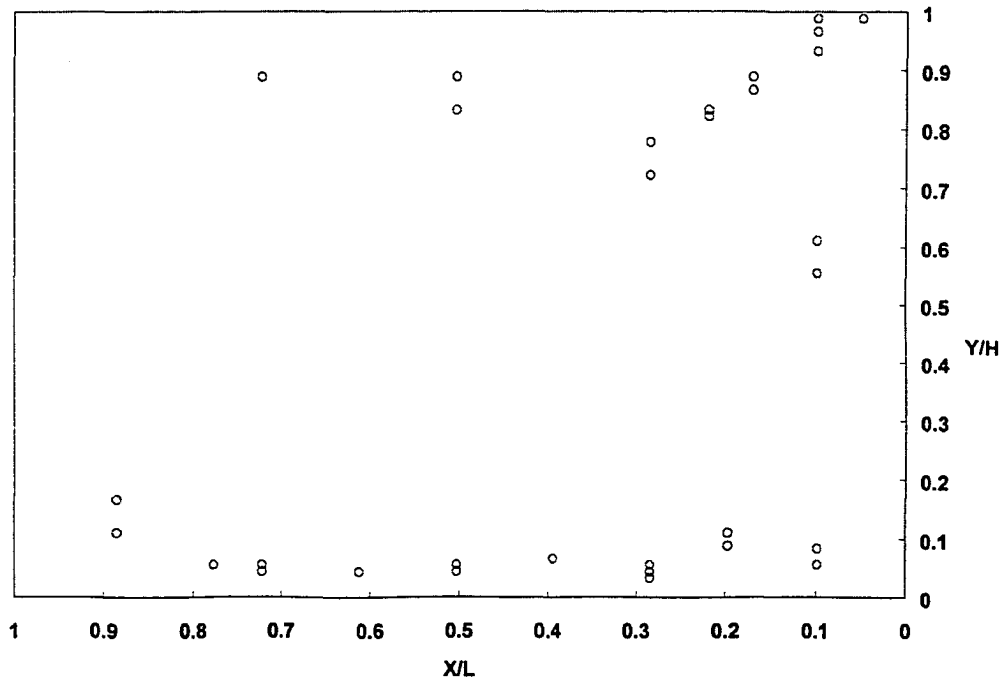

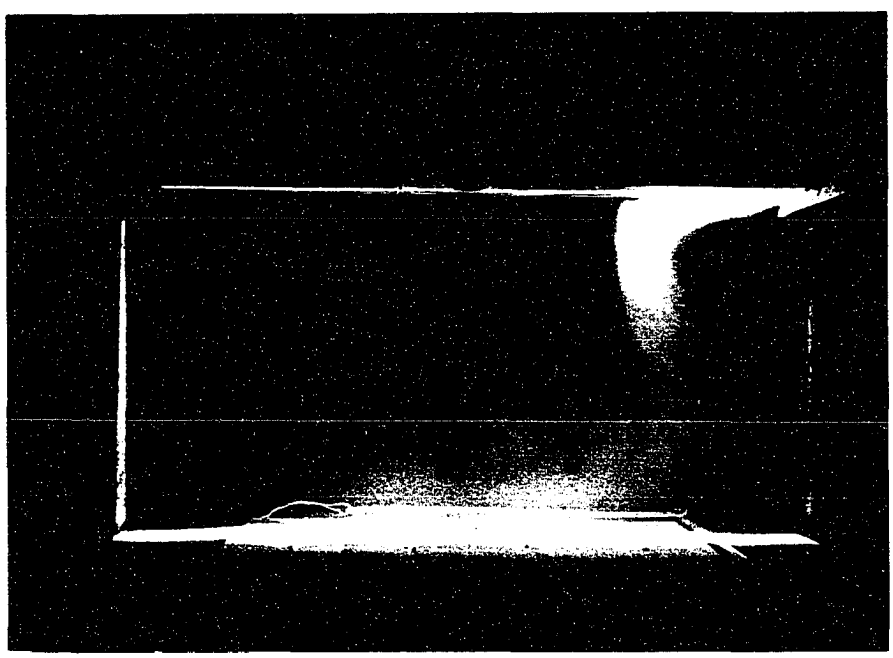

n. Scale: 1:3, Q_p=73cfm, ΔT=60° C, Ar_p=0.0182, Rm_p=0.006. (case NP10 of Table 6.8)

Figure 6.22. (continued)

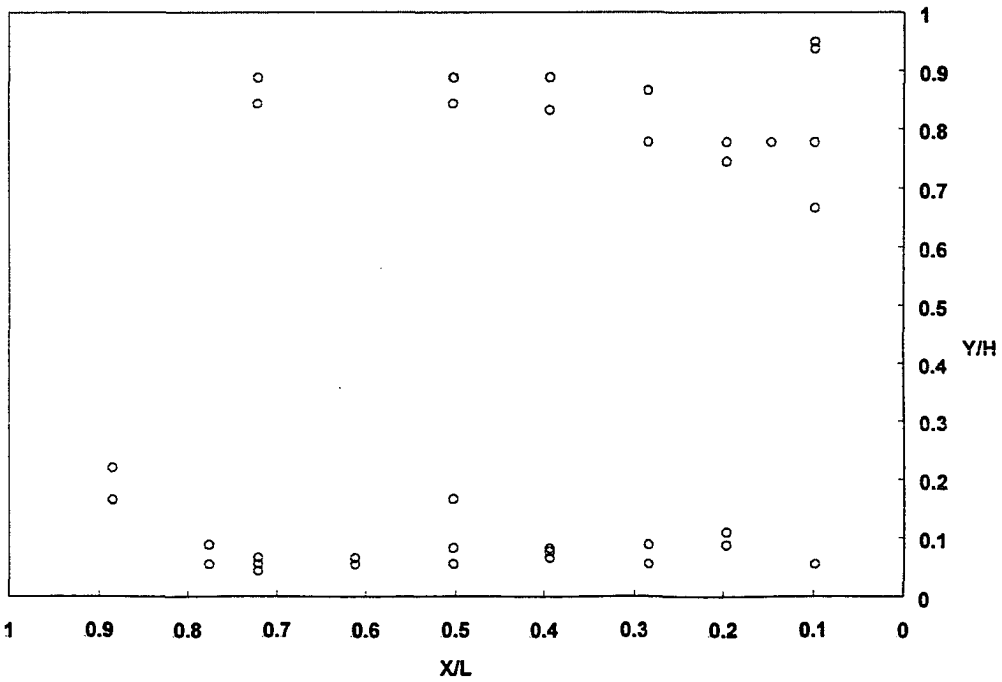

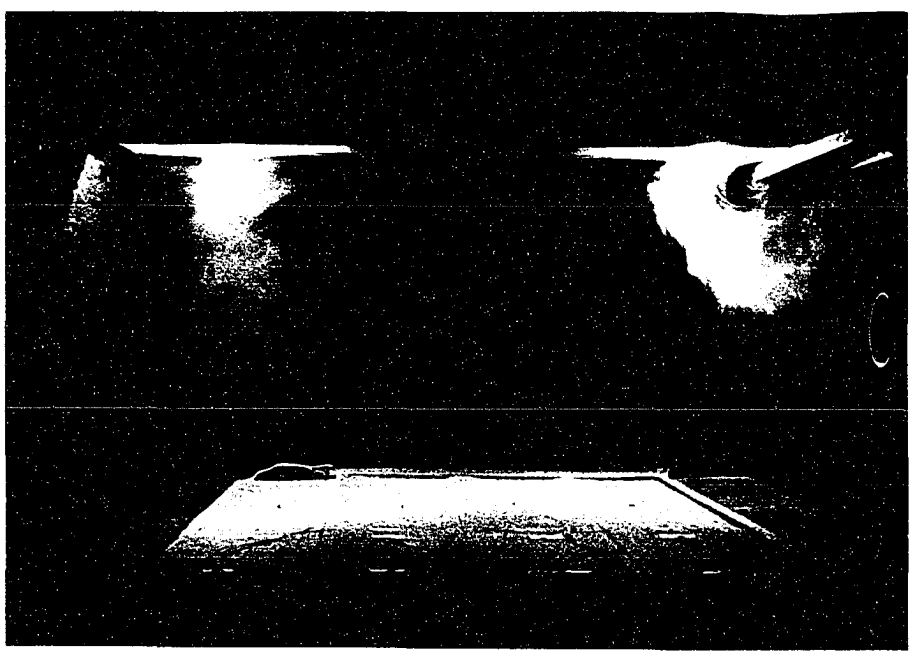

o. Scale: 1:3, Q_p=59cfm, ΔT=60° C, Ar_p=0.0283, Rm_p=0.004. (case NP11 of Table 6.8)

Figure 6.22. (continued)

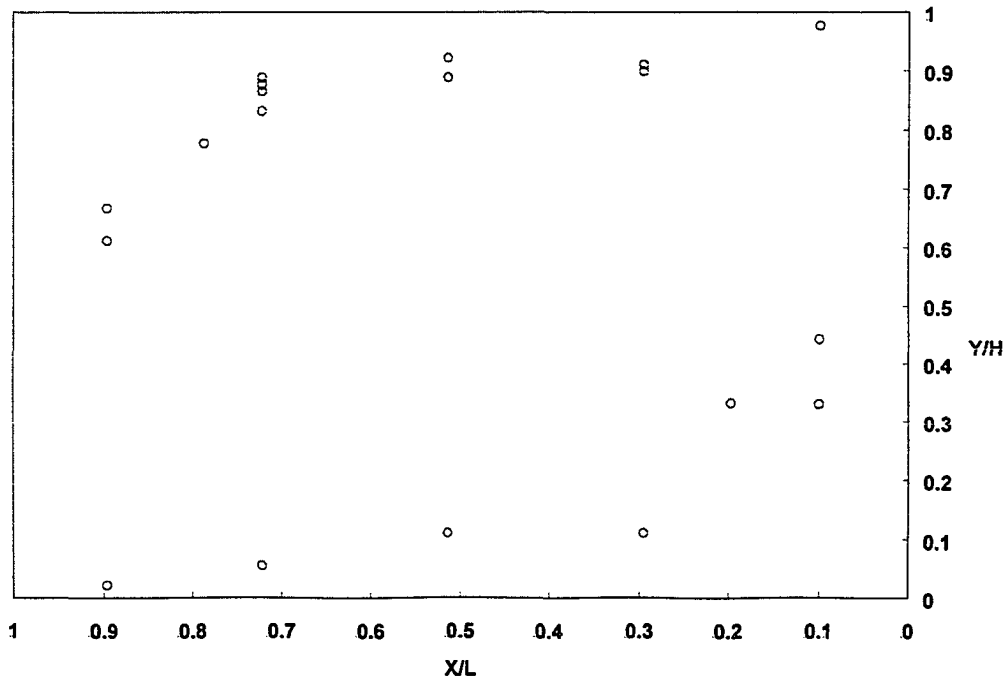

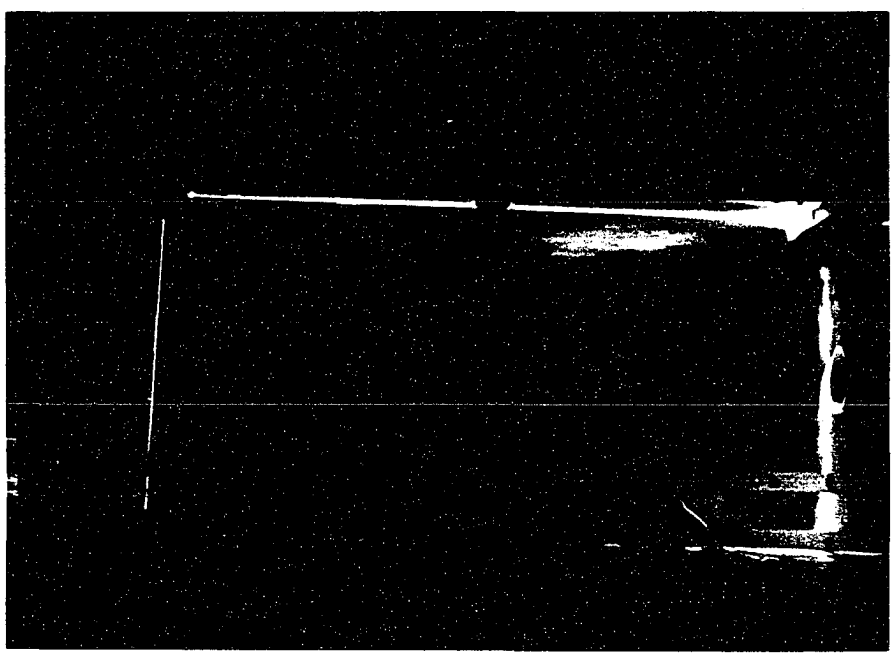

p. Scale: 1:6, Q_m=28cfm, ΔT=60° C, Ar_m=0.0039, Rm_m=0.014. (case NM8 of Table 6.8)

Figure 6.22. (continued)

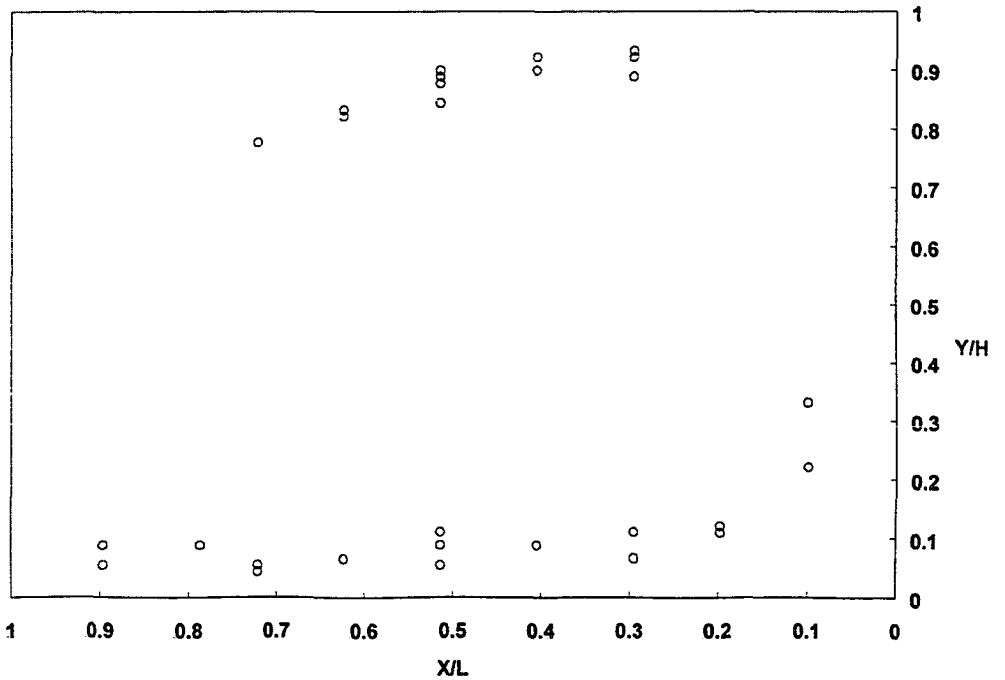

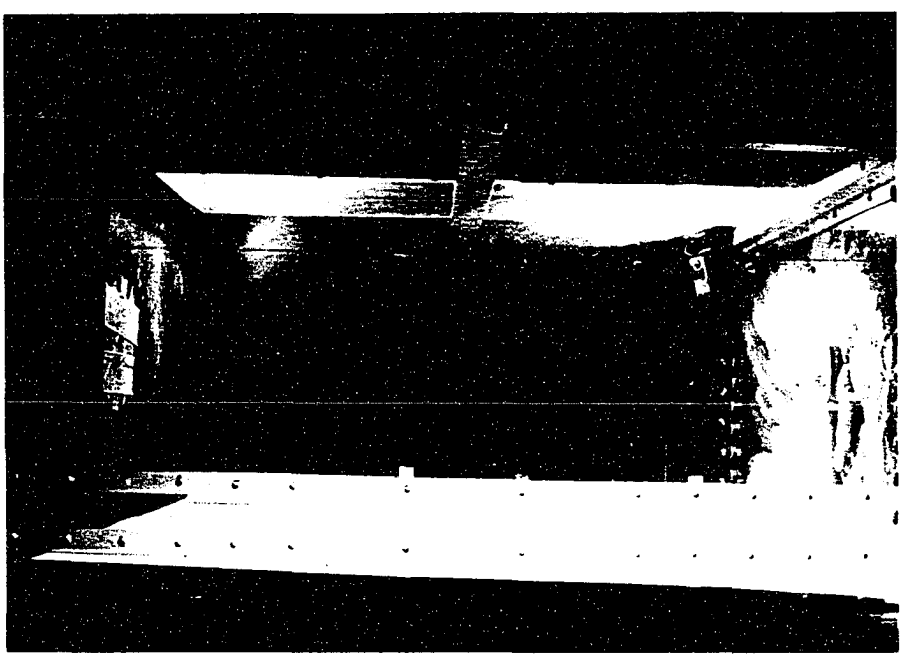

q. Scale: 1:6, Q_m=21cfm, ΔT=60° C, Ar_m=0.0070, Rm_m=0.008. (case NM9 of Table 6.8)

Figure 6.22. (continued)

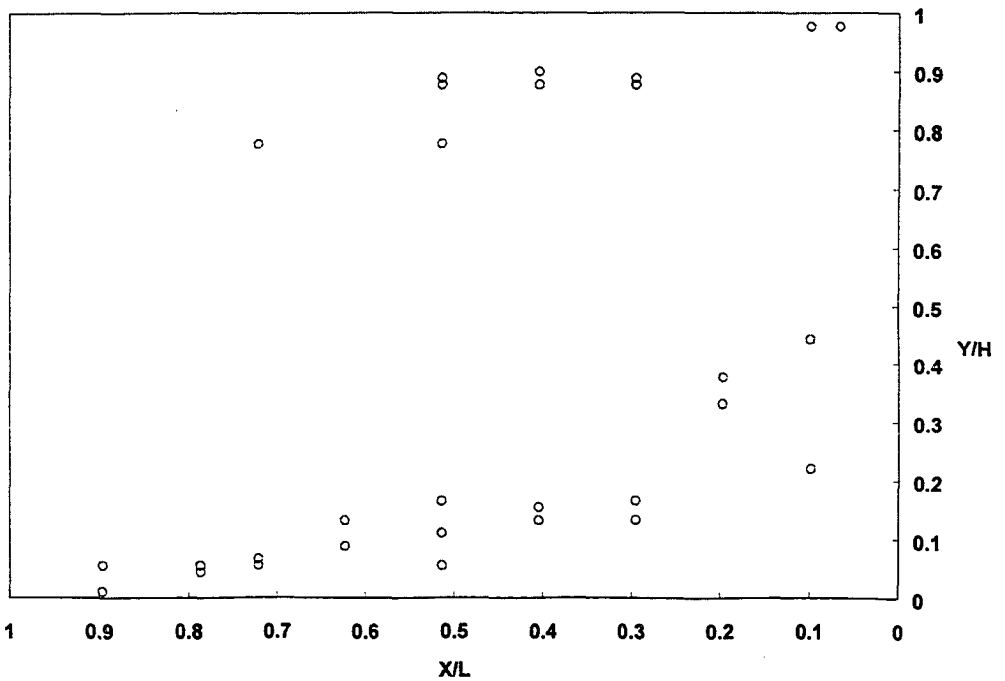

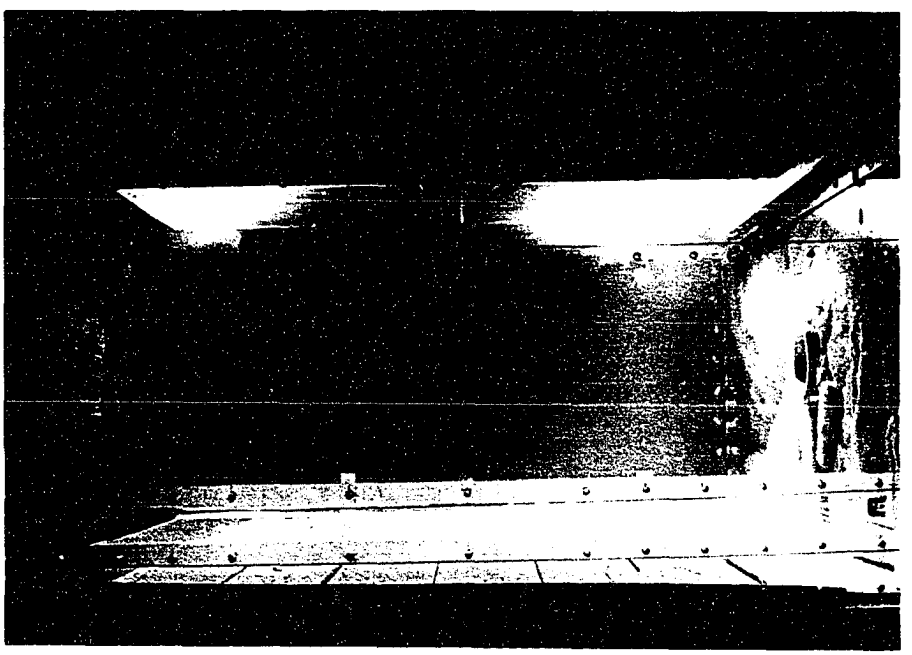

r. Scale: 1:6, Q_m=16cfm, ΔT=60° C, Ar_m=0.0127, Rm_m=0.004. (case NM10 of Table 6.8)

Figure 6.22. (continued)

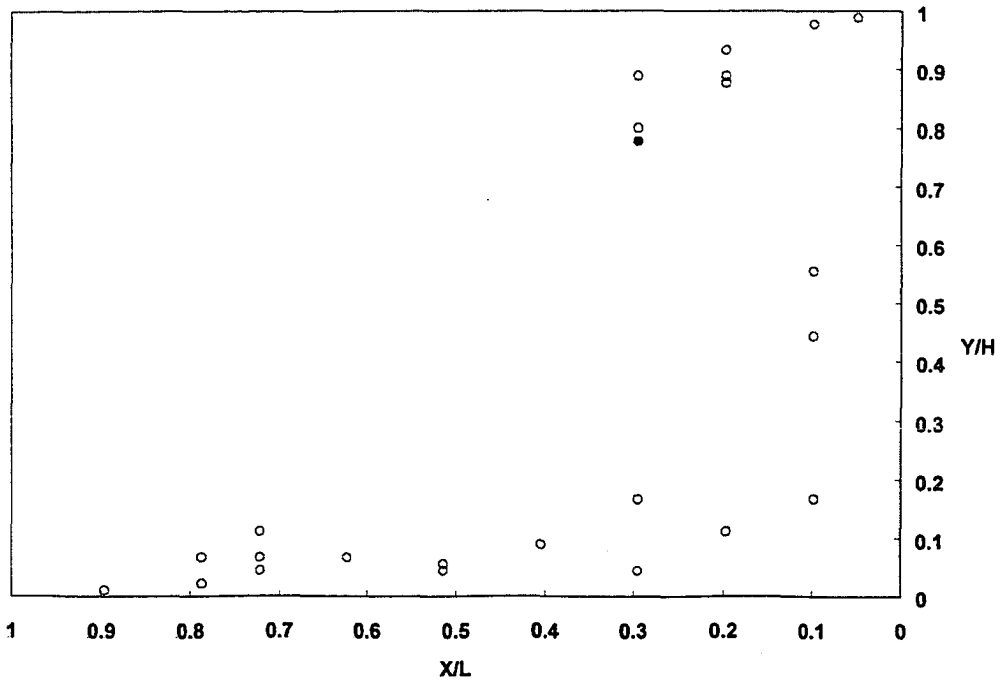

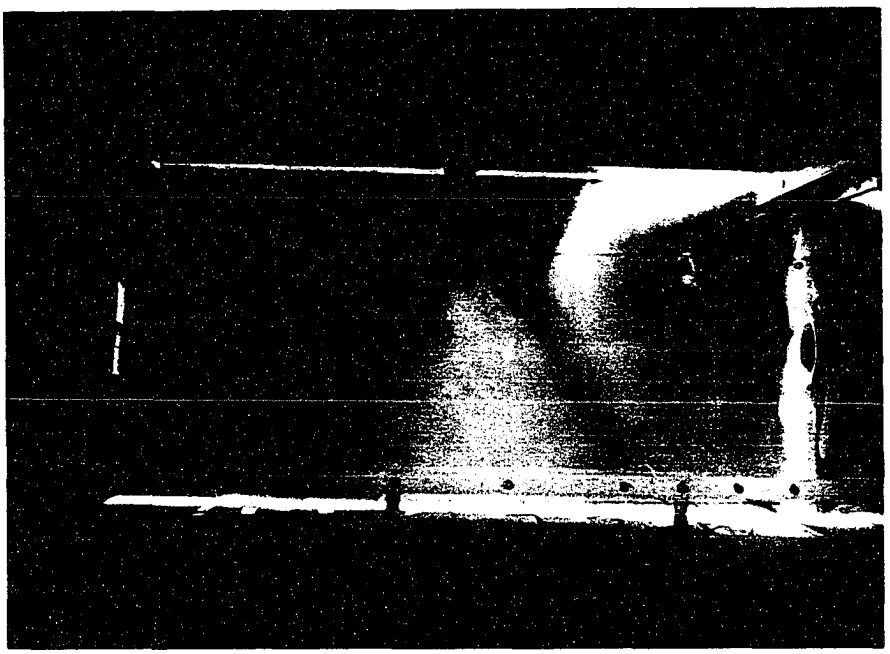

s. Scale: 1:6, Q_m=14cfm, ΔT=60° C, Ar_m=0.0165, Rm_m=0.003. (case NM11 of Table 6.8)

Figure 6.22. (continued)

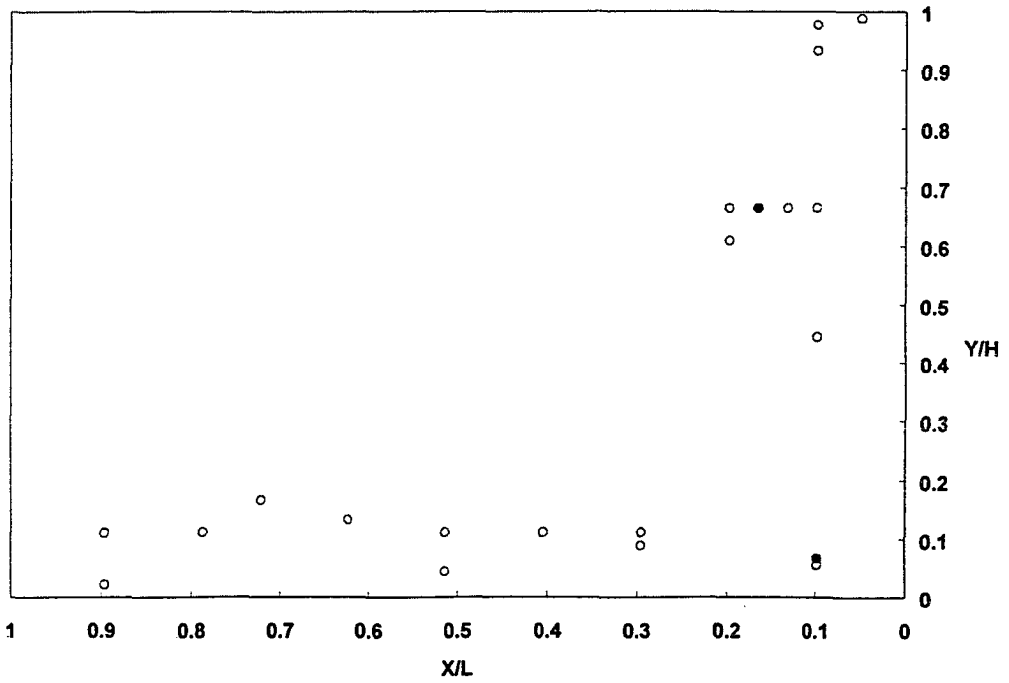

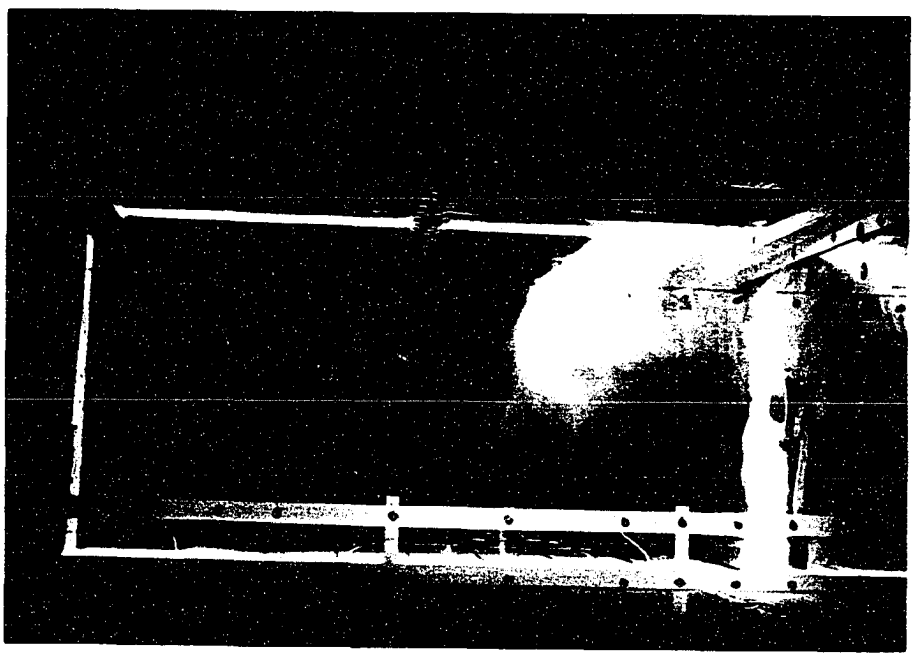

t. Scale: 1:6, Q_m=11cfm, ΔT=60° C, Ar_m=0.0246, Rm_m=0.002. (case NM12 of Table 6.8)

Figure 6.22. (continued)

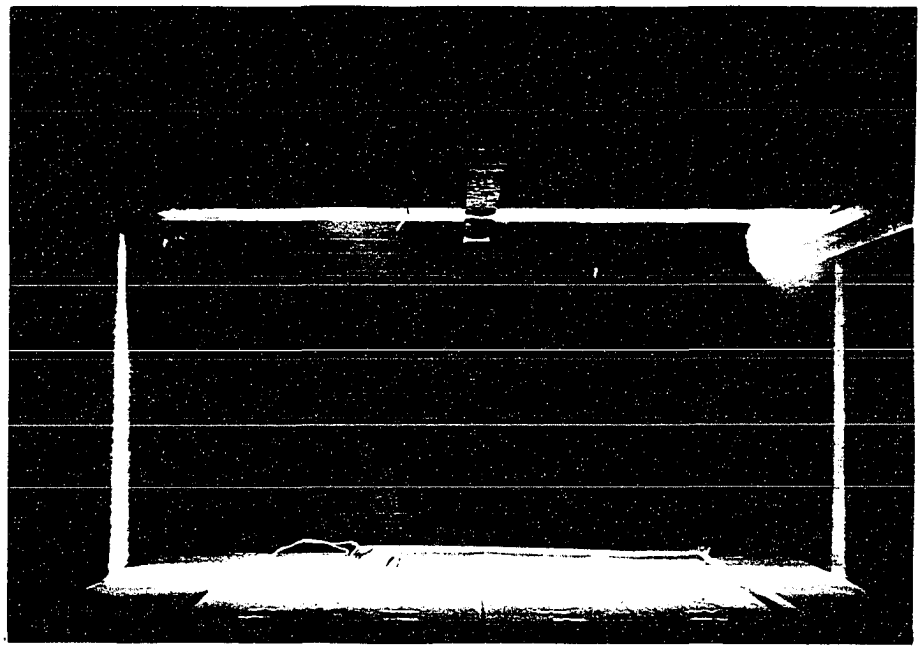

a. Scale: 1:3, Q_p=42cfm, ΔT=60° C, Ar_p=0.055, Rm_p=0.002.

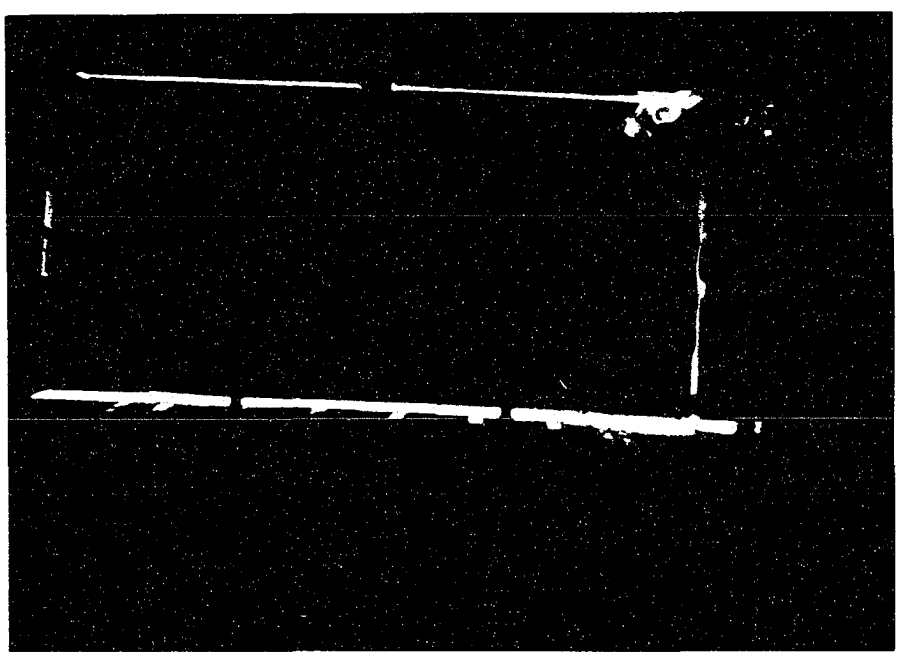

b. Scale: 1:6, Q_m=7cfm, ΔT=60° C, Ar_m=0.055, Rm_m=0.001.

Figure 6.23. Nonisothermal airflow pattern fall on entry visualized by smoke .

6.2.2.3. Air-jet trajectory comparison

Air-jet trajectory comparisons were used to quantitatively verify airflow patterns between scale-model and prototype under nonisothermal conditions. The comparisons are presented based on Ar and Rm for $\Delta T = 40\,^{\circ}C$ or $\Delta T = 60\,^{\circ}C$ (Figure 6.24).

Air-jet trajectories were compared and the similitude parameter that showed the better consistency between measured data from the scale-model and prototype was chosen as the appropriate similitude parameter. Based on the results shown in Figure 6.24, it was concluded that using Ar as the similitude criterion gave better consistency between data with a similar heat load when the airflow pattern within the enclosure consisted of two circulation airflow zones as a result of the air-jet penetration not exceeding 0.5 L (the situation shown in Figure 6.19 (b)). These cases are shown in Figures 6.24 (a), 6.24 (c), and 6.24 (e). When the airflow rate increased to produce a single recirculation airflow zone, using Rm with a similar heat load gave better consistency of the measured data as shown in Figures 6.24 (g), 6.24 (i), 6.24 (k), 6.24 (m), and 6.24 (o). When the airflow rate was beyond the critical condition where the air-jet remained horizontal, there was no significant difference between the air-jet trajectories for either Ar or Rm (see Figures 6.24 (q), and 6.24 (r)). This is probably due to the fact that the airflow pattern is independent of the airflow rate when it is beyond the threshold value.

The air-jet trajectory results showed that the Ar may be used as the similitude criterion as long as the buoyancy force dominates the airflow pattern for low inlet jet momentum conditions (i.e. low inlet velocity). When the airflow rate increases, the air-jet behaves like

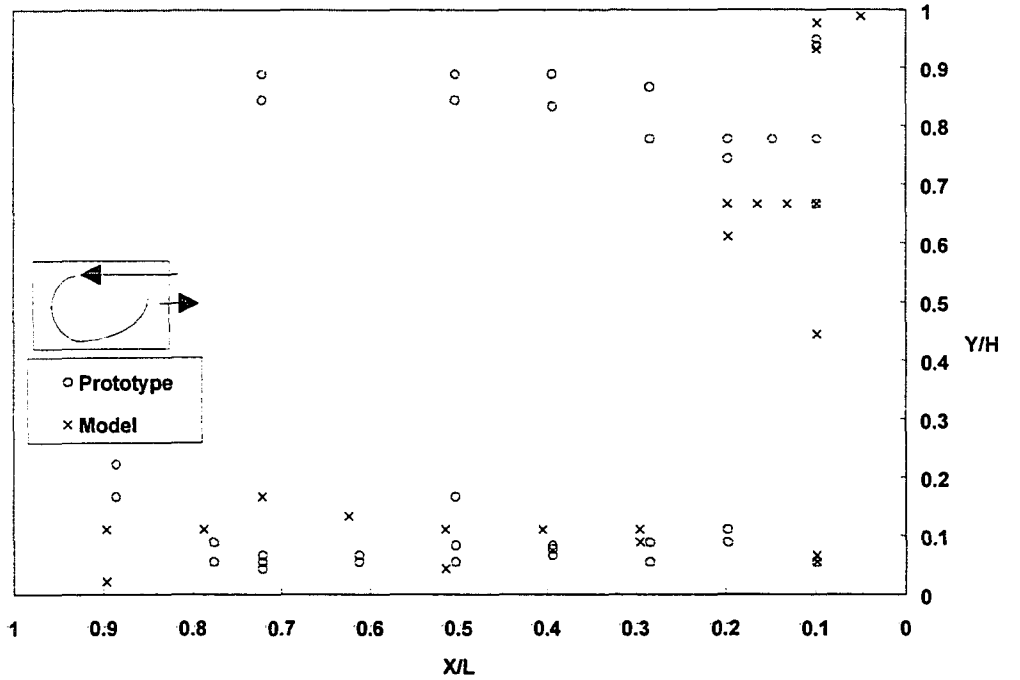

a. Q_p=59 cfm, ΔT=60 °C, Ar_p=0.0283, Rm_p=0.004
Q_m=11 cfm, ΔT=60 °C, Ar_m=0.0246, Rm_m=0.002

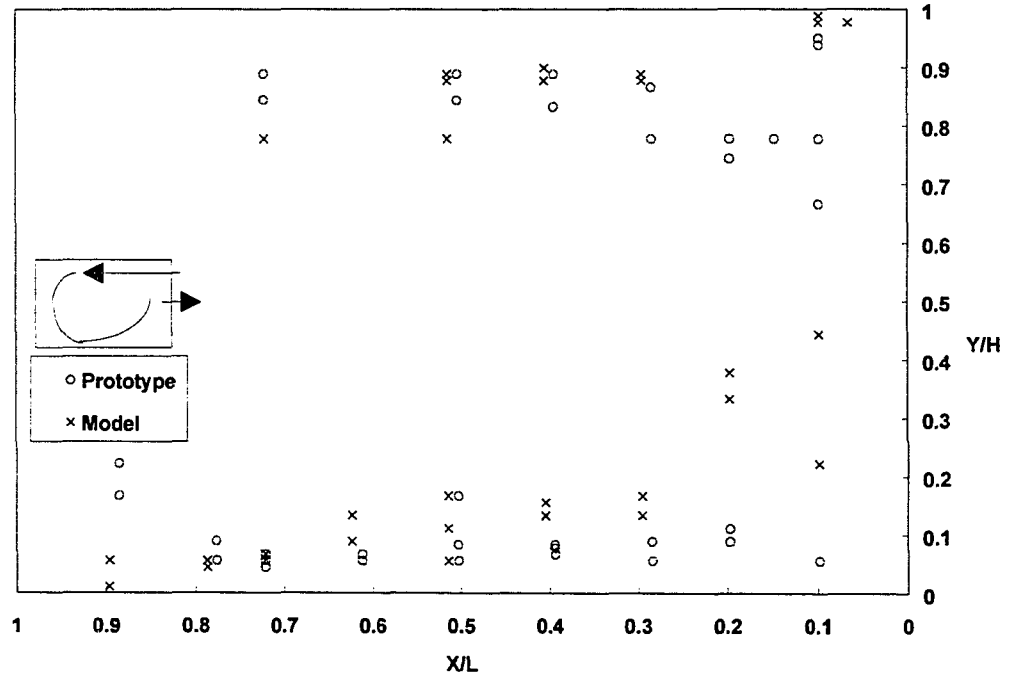

b. Q_p=59 cfm, ΔT=60 °C, Ar_p=0.0283, Rm_p=0.004
Q_m=16 cfm, ΔT=60 °C, Ar_m=0.0127, Rm_m=0.004

Figure 6.24. The comparisons of peak airspeed trajectory for the nonisothermal air-jet along the ceiling and floor based on either the Ar or Rm as the similitude criteria.

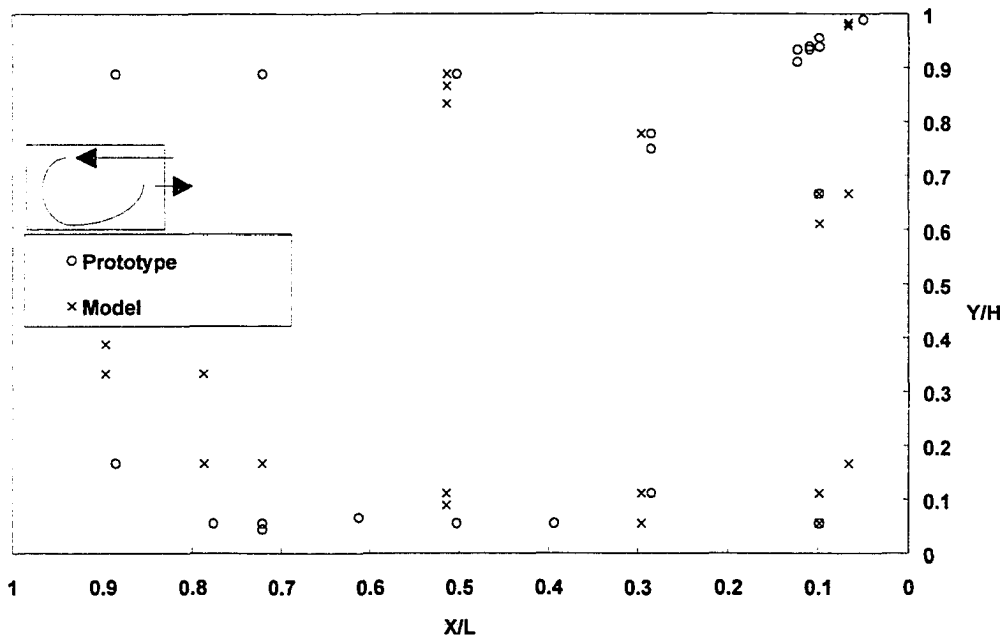

c. Q_p=53 cfm, ΔT=40 °C, Ar_p=0.0239, Rm_p=0.003
Q_m=9 cfm, ΔT=40 °C, Ar_m=0.0270, Rm_m=0.001

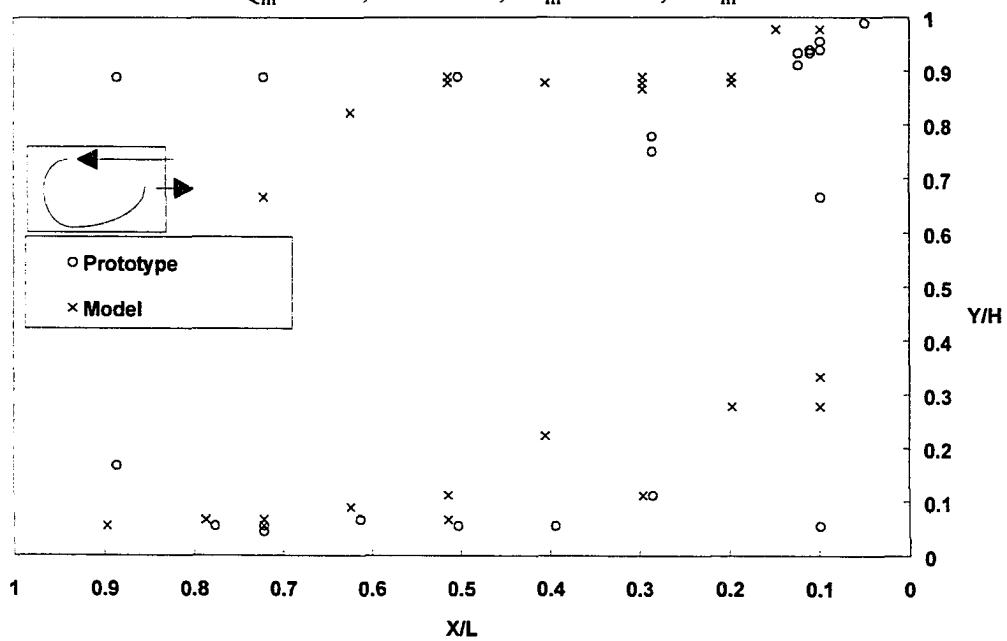

d. Q_p=53 cfm, ΔT=40 °C, Ar_p=0.0239, Rm_p=0.003
Q_m=14 cfm, ΔT=40 °C, Ar_m=0.0113, Rm_m=0.003

Figure 6.24. (continued)

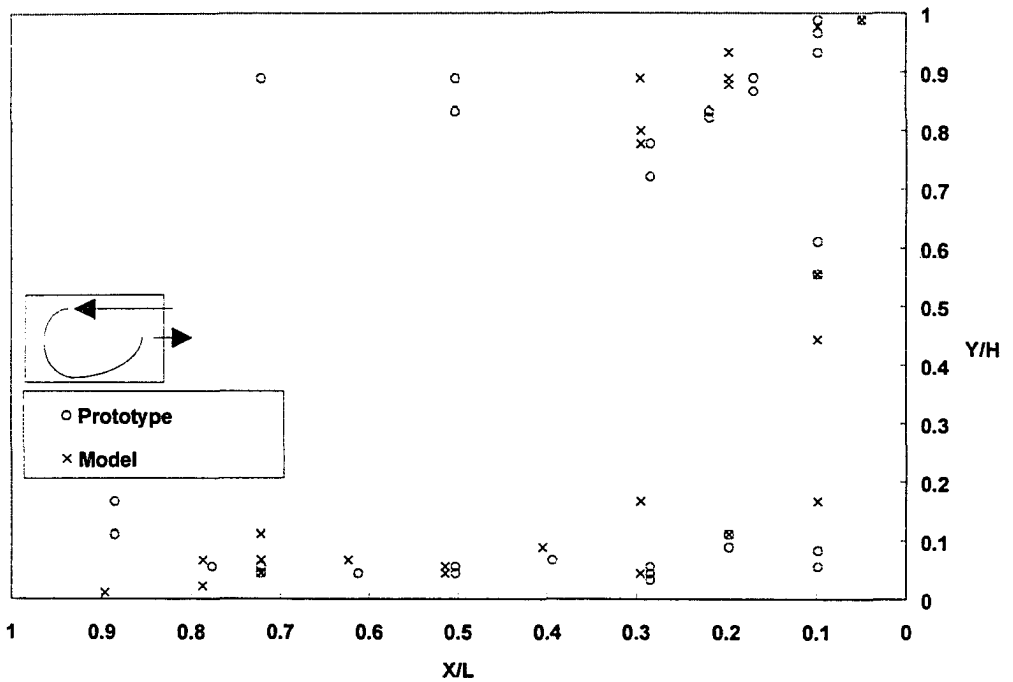

e. Q_p=73 cfm, ΔT=60 °C, Ar_p=0.0182, Rm_p=0.006
Q_m=14 cfm, ΔT=60 °C, Ar_m=0.0165, Rm_m=0.003

Figure 6.24. (continued)

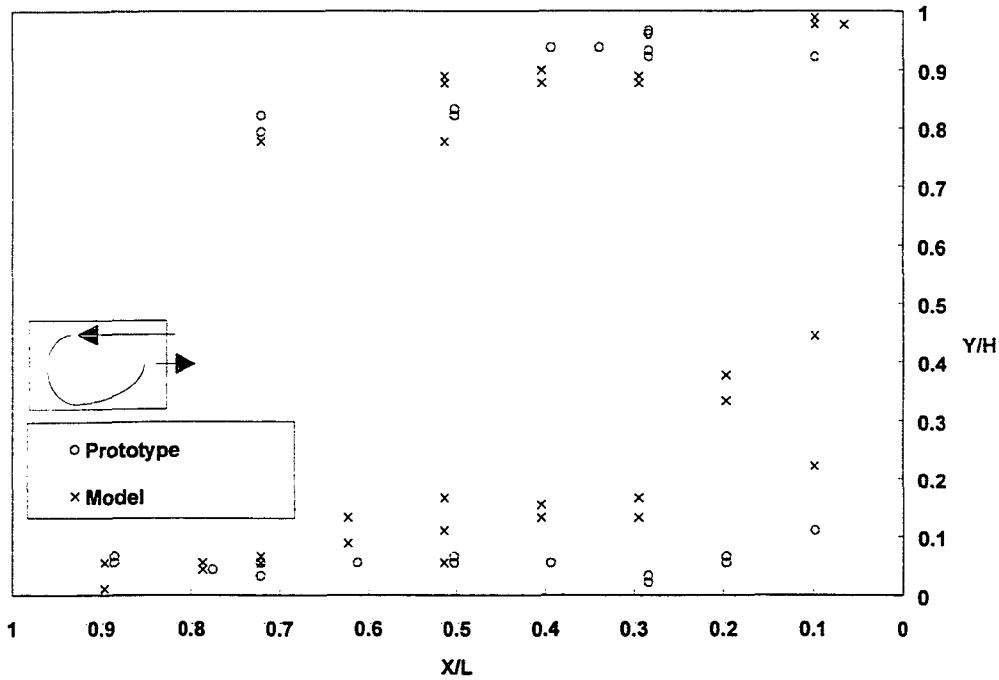

f. Q_p=83 cfm, ΔT=60 °C, Ar_p=0.0141, Rm_p=0.008
Q_m=16 cfm, ΔT=60 °C, Ar_m=0.0127, Rm_m=0.004

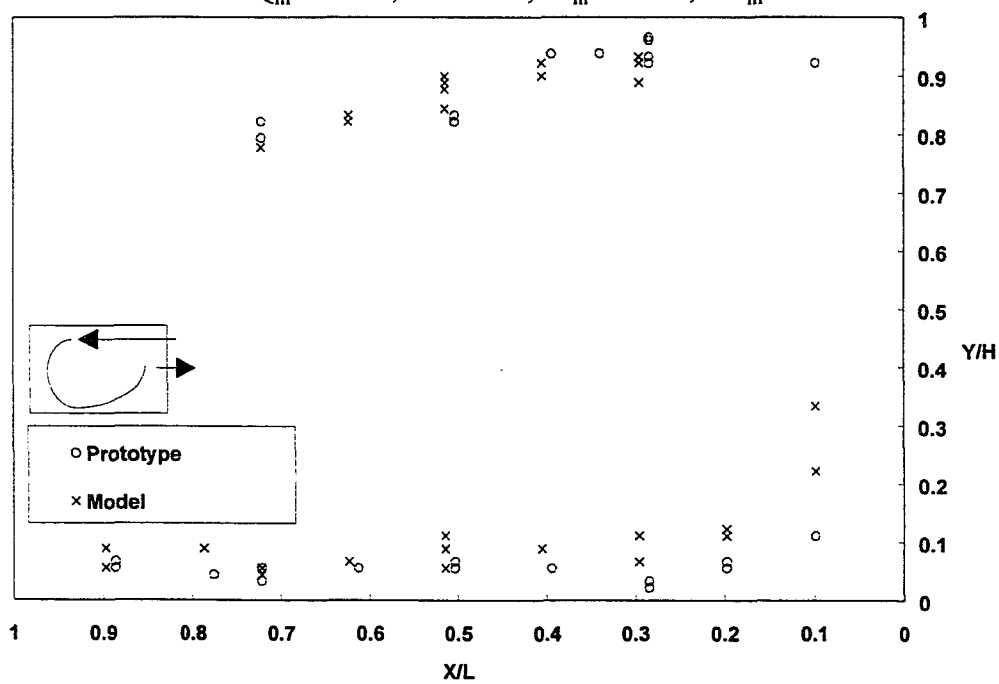

g. Q_p=83 cfm, ΔT=60 °C, Ar_p=0.0141, Rm_p=0.008
Q_m=21 cfm, ΔT=60 °C, Ar_m=0.0070, Rm_m=0.008

Figure 6.24. (continued)

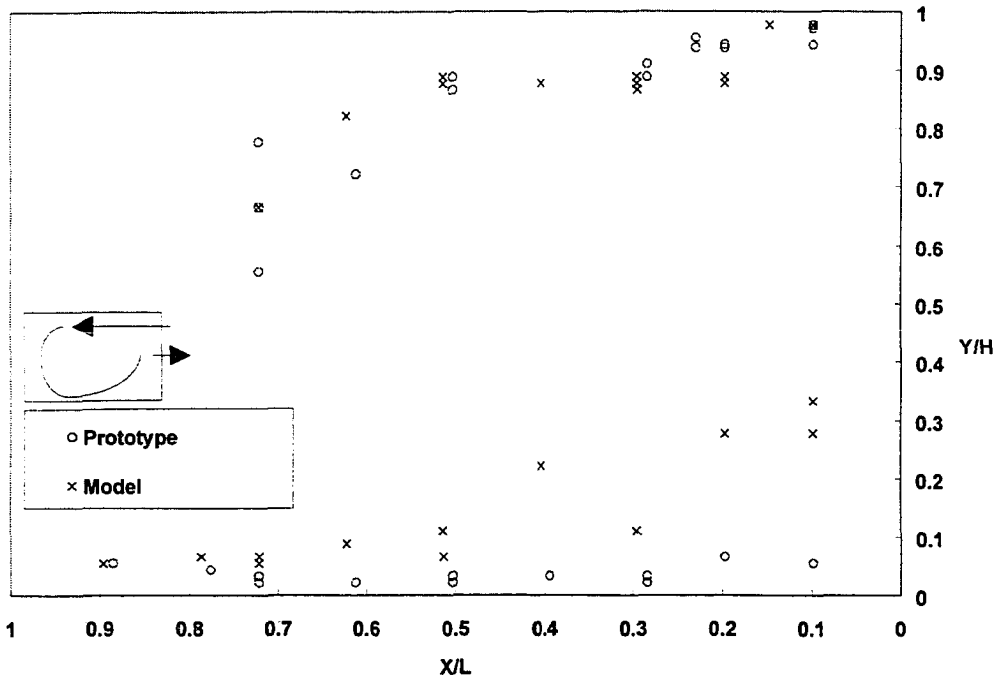

h. Q_p=72 cfm, ΔT=40 °C, Ar_p=0.0130, Rm_p=0.006
Q_m=14 cfm, ΔT=40 °C, Ar_m=0.0113, Rm_m=0.003

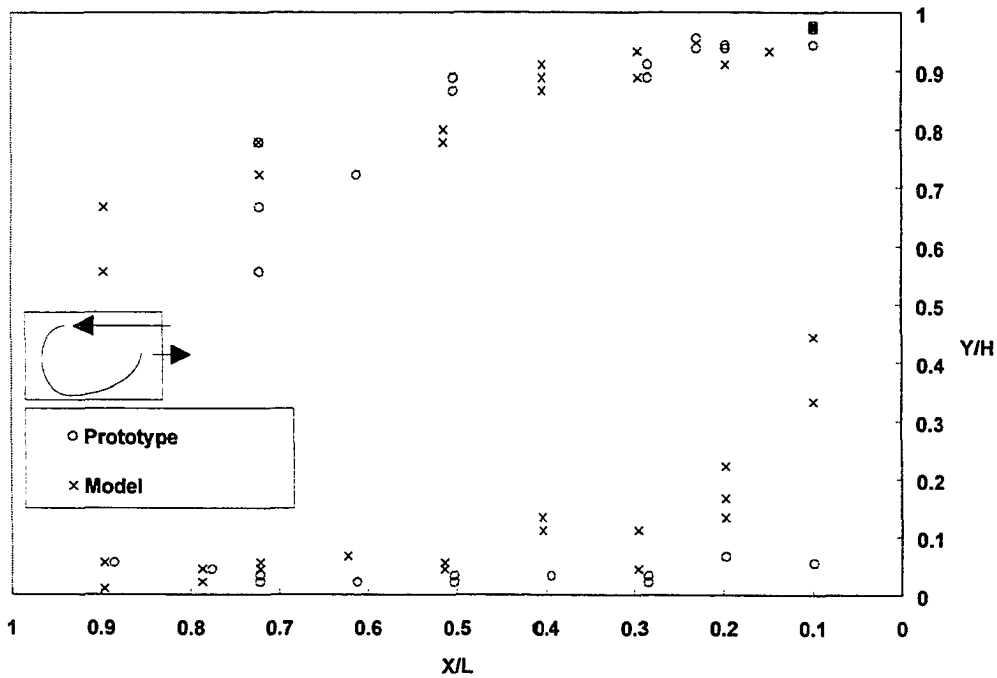

i. Q_p=72 cfm, ΔT=40 °C, Ar_p=0.0130, Rm_p=0.006
Q_m=18 cfm, ΔT=40 °C, Ar_m=0.0068, Rm_m=0.005

Figure 6.24. (continued)

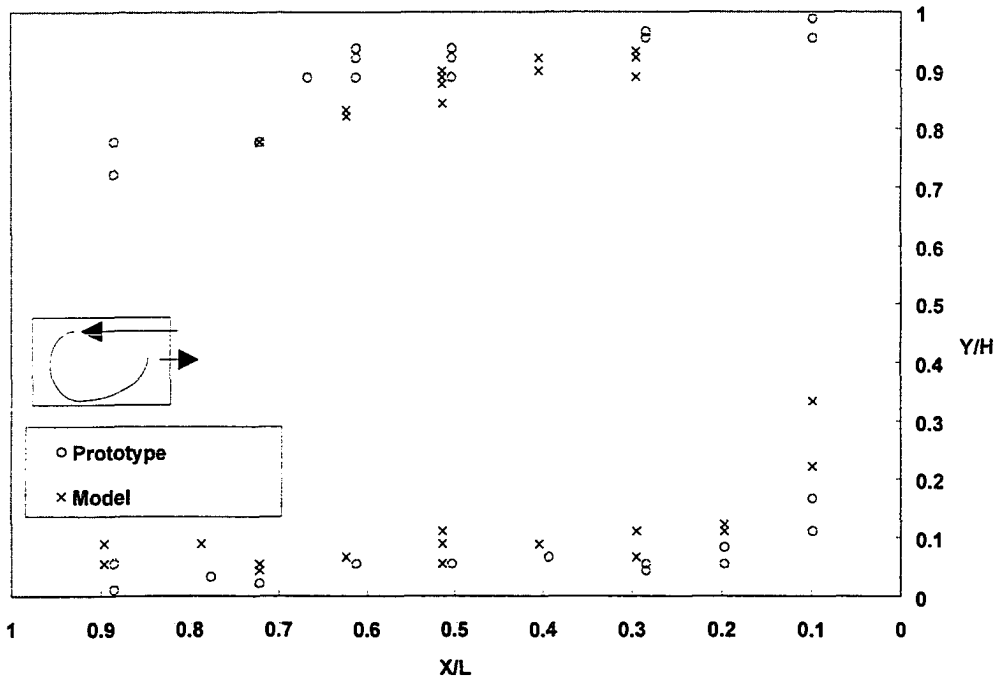

j. Q_p=116 cfm, ΔT=60 °C, Ar_p=0.0072, Rm_p=0.015
Q_m=21 cfm, ΔT=60 °C, Ar_m=0.0070, Rm_m=0.008

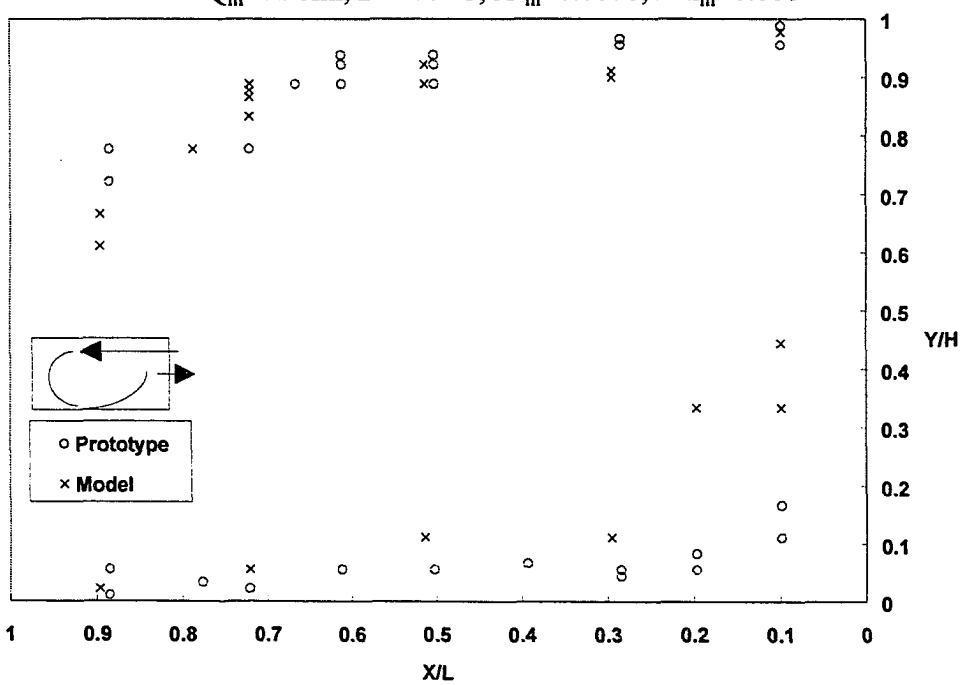

k. Q_p=116 cfm, ΔT=60 °C, Ar_p=0.0072, Rm_p=0.015
Q_m=28 cfm, ΔT=60 °C, Ar_m=0.0039, Rm_m=0.014

Figure 6.24. (continued)

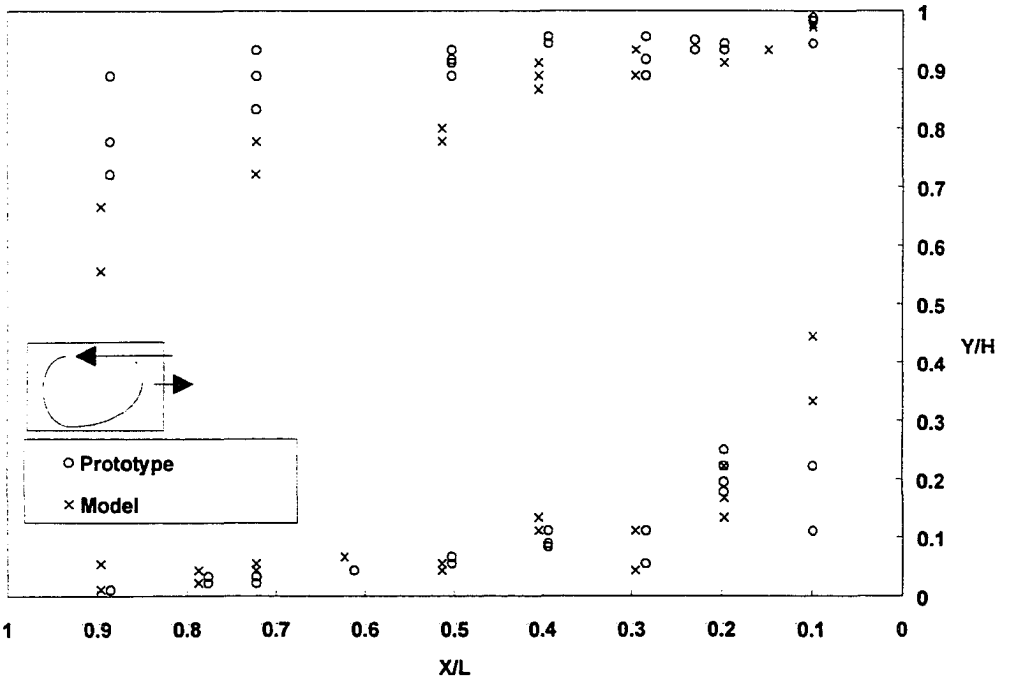

l. Q_p=105 cfm, ΔT=40 °C, Ar_p=0.0062, Rm_p=0.012
Q_m=18 cfm, ΔT=40 °C, Ar_m=0.0068, Rm_m=0.005

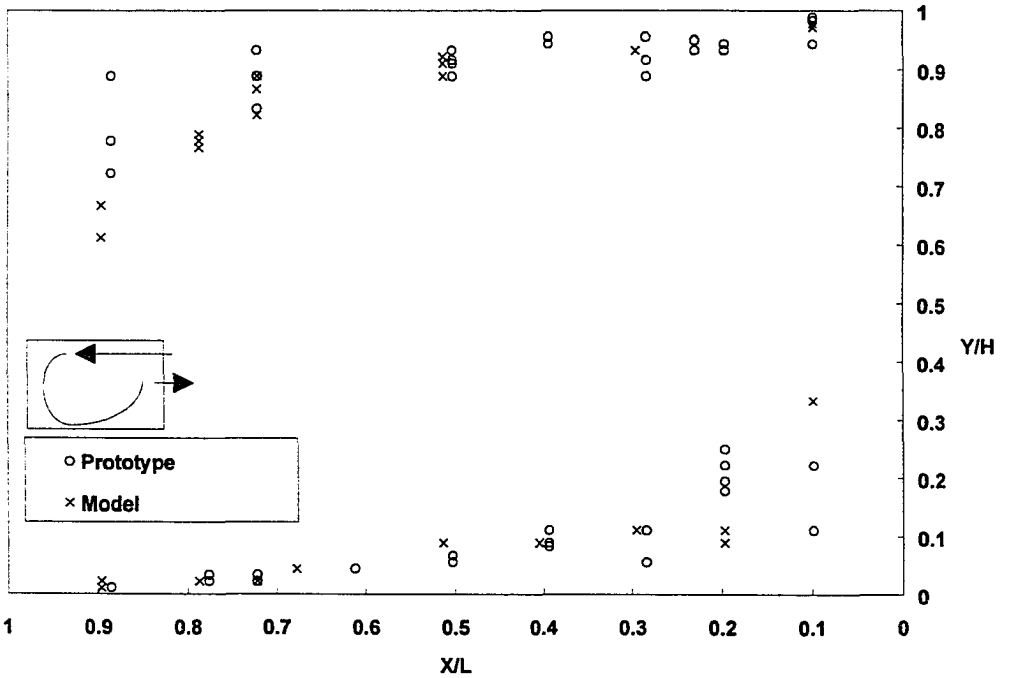

m. Q_p=105 cfm, ΔT=40 °C, Ar_p=0.0062, Rm_p=0.012
Q_m=26 cfm, ΔT=40 °C, Ar_m=0.0031, Rm_m=0.012

Figure 6.24. (continued)

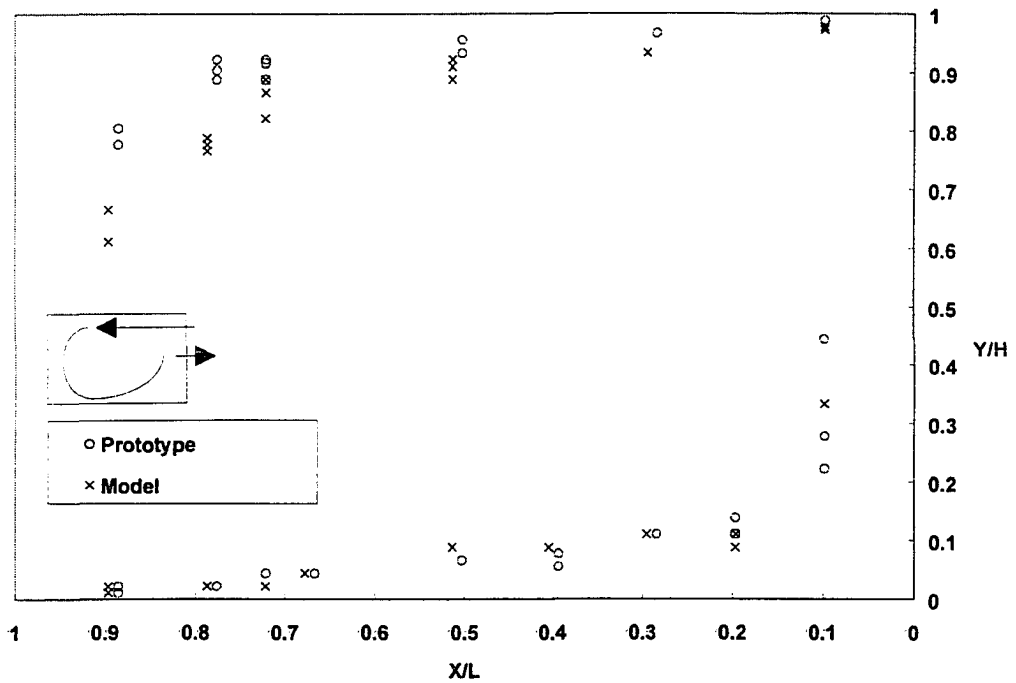

n. Q_p=150 cfm, ΔT=40 °C, Ar_p=0.0030, Rm_p=0.025
Q_m=26 cfm, ΔT=40 °C, Ar_m=0.0031, Rm_m=0.012

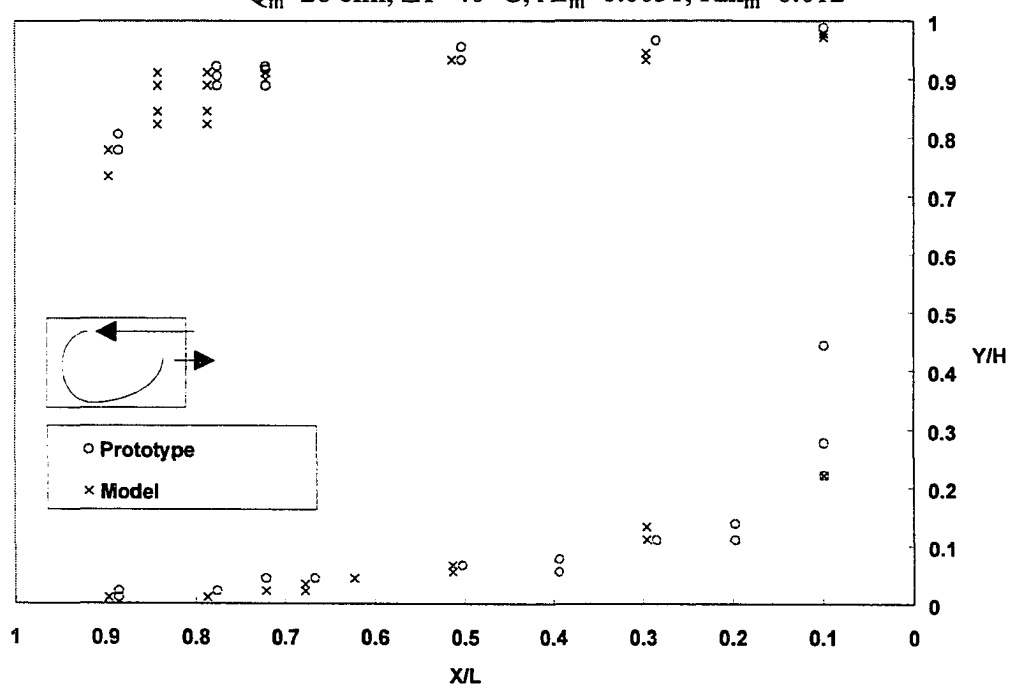

o. Q_p=150 cfm, ΔT=40 °C, Ar_p=0.0030, Rm_p=0.025
Q_m=38 cfm, ΔT=40 °C, Ar_m=0.0014, Rm_m=0.026

Figure 6.24. (continued)

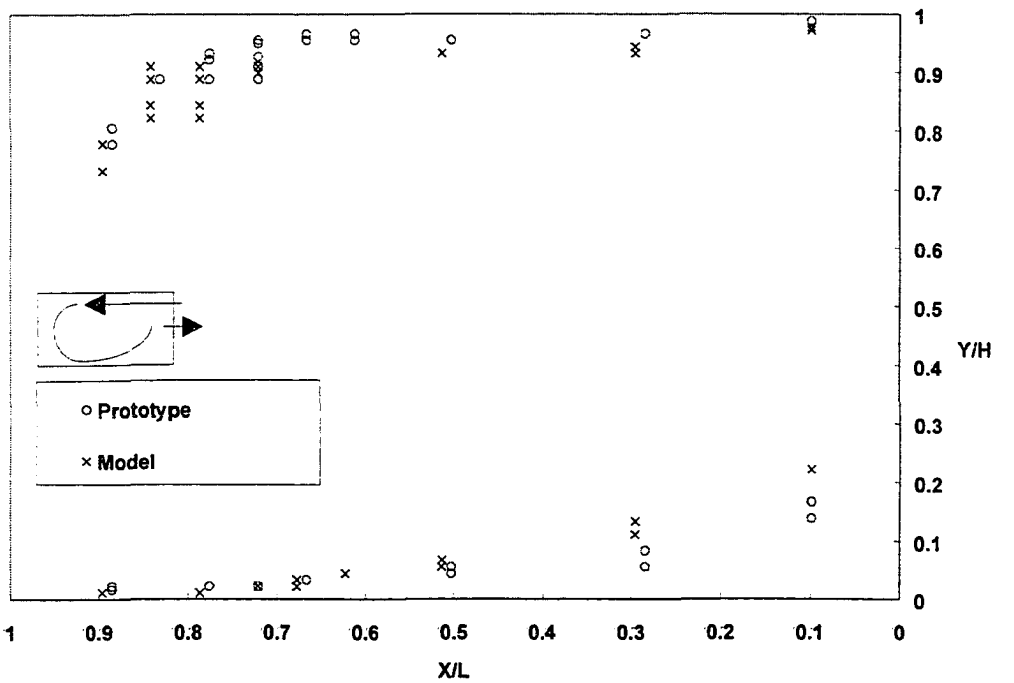

p. Q_p=221 cfm, ΔT=40 °C, Ar_p=0.0014, Rm_p=0.053
Q_m=38 cfm, ΔT=40 °C, Ar_m=0.0014, Rm_m=0.026

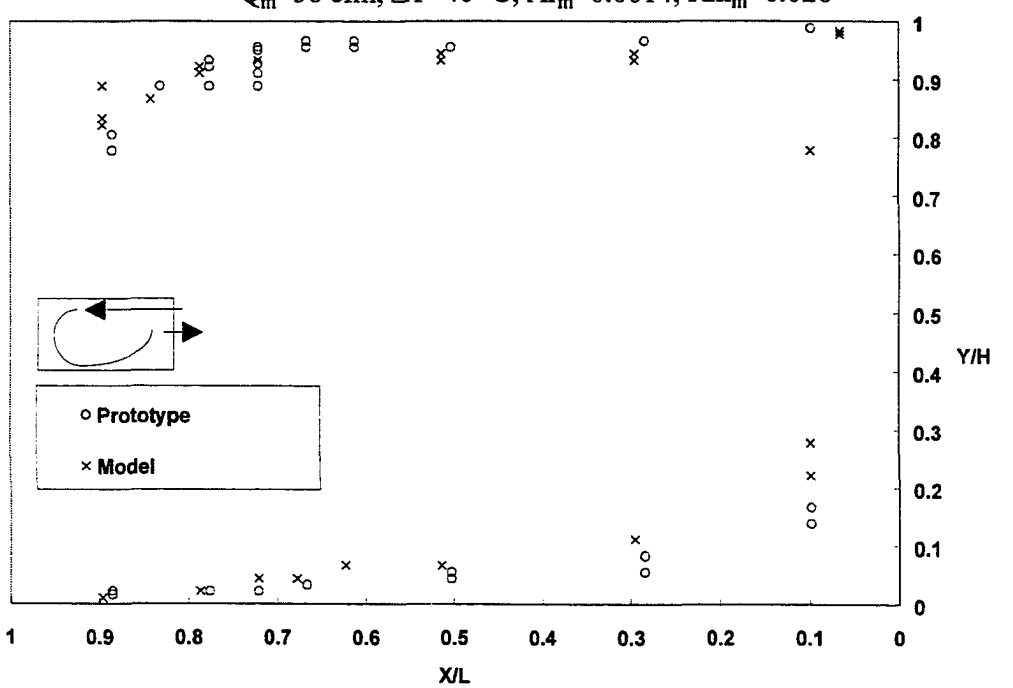

q. Q_p=221 cfm, ΔT=40 °C, Ar_p=0.0014, Rm_p=0.053
Q_m=54 cfm, ΔT=40 °C, Ar_m=0.0007, Rm_m=0.052

Figure 6.24. (continued)

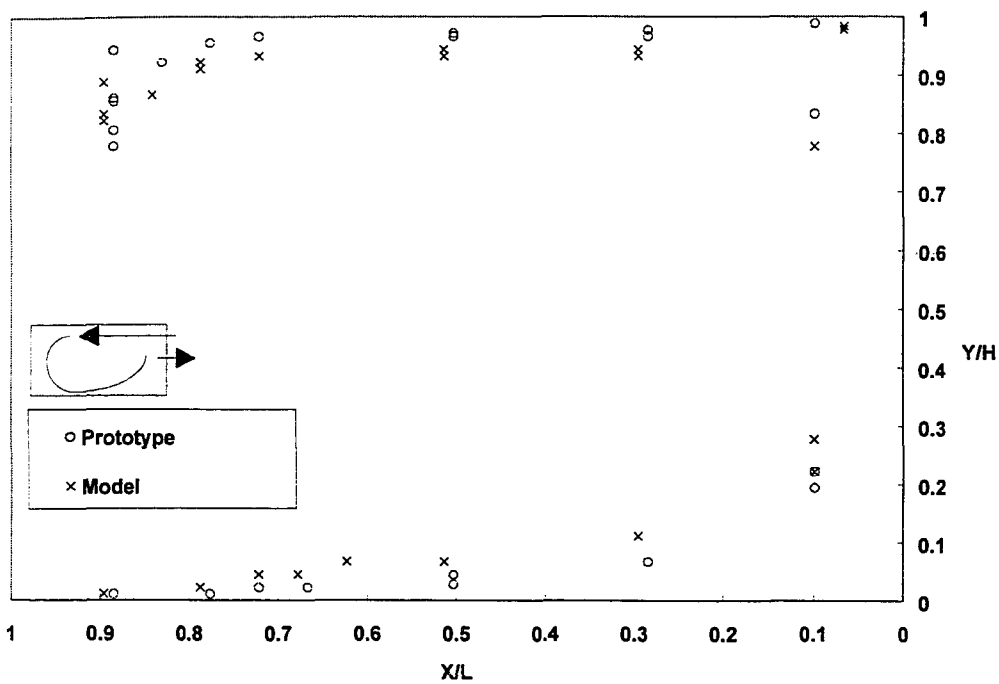

r. Q_p=324 cfm, ΔT=40 °C, Ar_p=0.0006, Rm_p=0.115
Q_m=54 cfm, ΔT=40 °C, Ar_m=0.0007, Rm_m=0.052

Figure 6.24. (continued)

isothermal airflow and the similitude criteria changes to the Rm assuming similar heat loads between the scale-model and prototype.

The critical values measured and used to distinguish the behavior of nonisothermal air-jets are summarized in Figure 6.25 and Table 6.10. Figure 6.25 was generated based on observed (airflow visualization) and measured (Section 6.2.2) airflow patterns. At critical Ar< 0.005 a single-circulation airflow pattern exists and the airflow pattern is governed by isothermal behavior, where either Ar or Rm may be used as the similitude parameter. At critical Ar> 0.015, buoyancy forces dominate and Ar should be used as the similitude parameter. For intermediate ranges (0.005< Ar < 0.015), the better similitude parameter for duplicating airflow pattern is Rm with the same heating load.

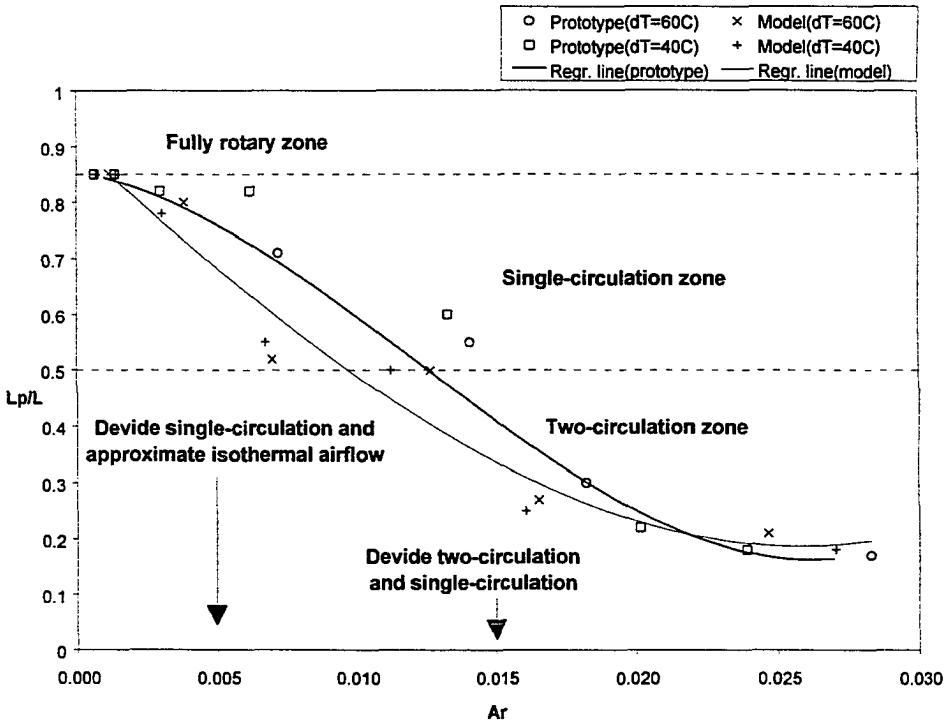

Figure 6.25. Critical values to distinguish nonisothermal airflow patterns based on normalized air-jet penetration distance versus Archimedes number.

Table 6.10. The critical values of nonisothermal airflow patterns determined using air-jet trajectories.

Classification of airflow pattern	Critical values measured	Similitude criteria
Air-jet falls on entry or two-circulation airflow	$Ar>0.015$ $Ar_c \geq 90$	Archimedes number
Single-circulation airflow, air-jet falls between inlet and end wall	$0.005<Ar<0.015$ $30<Ar_c<90$	Rm with same heat load between model and prototype
Air-jet remains horizontal, and behaves as isothermal airflow	$Ar \leq 0.005$ $Ar_c \leq 30$	Either Ar or Rm may be used

6.2.3. The airspeed field

The experimental procedure for measuring the airspeed field for nonisothermal airflow was similar to the procedure used for isothermal airflow. Both longitudinal (x-direction) peak airspeed profiles and vertical (y-direction) airspeed profiles were measured and compared to verify similitude between the scale-model and prototype.

6.2.3.1. Longitudinal peak airspeed profiles along enclosure surface

The longitudinal peak airspeed profiles along the ceiling and floor in both the scale-model and prototype (with $\Delta T = 40°C$) are shown in Figures 6.26 and 6.27. The results show that the nonisothermal peak airspeed profiles behave similarly to the isothermal cases when the airflow patterns were beyond a specific critical value. Figure 6.26.(a) describes the peak airspeed profiles along the ceiling for the prototype. The peak airspeed decays were similar beyond the critical value of ≥105 cfm, and terminated rapidly after a distance of 100h (0.7L).

The peak airspeed profiles along the floor for the prototype (Figure 6.26 (b)) showed that the maximum floor airspeed occurred at about a distance of 2/3 L from the inlet wall for high

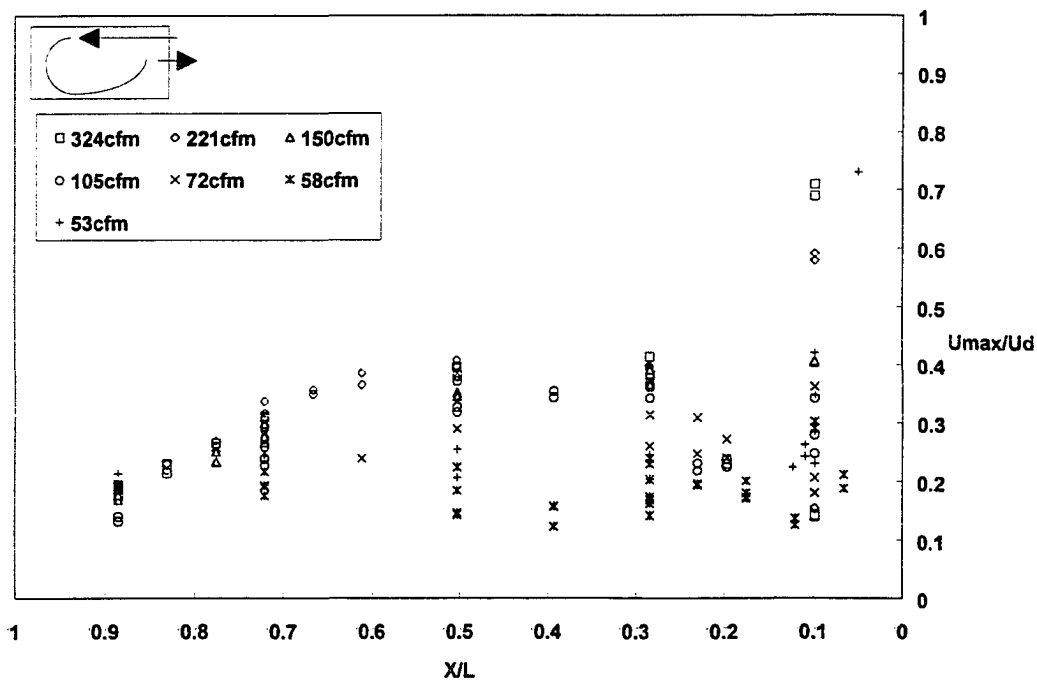

a. ceiling region

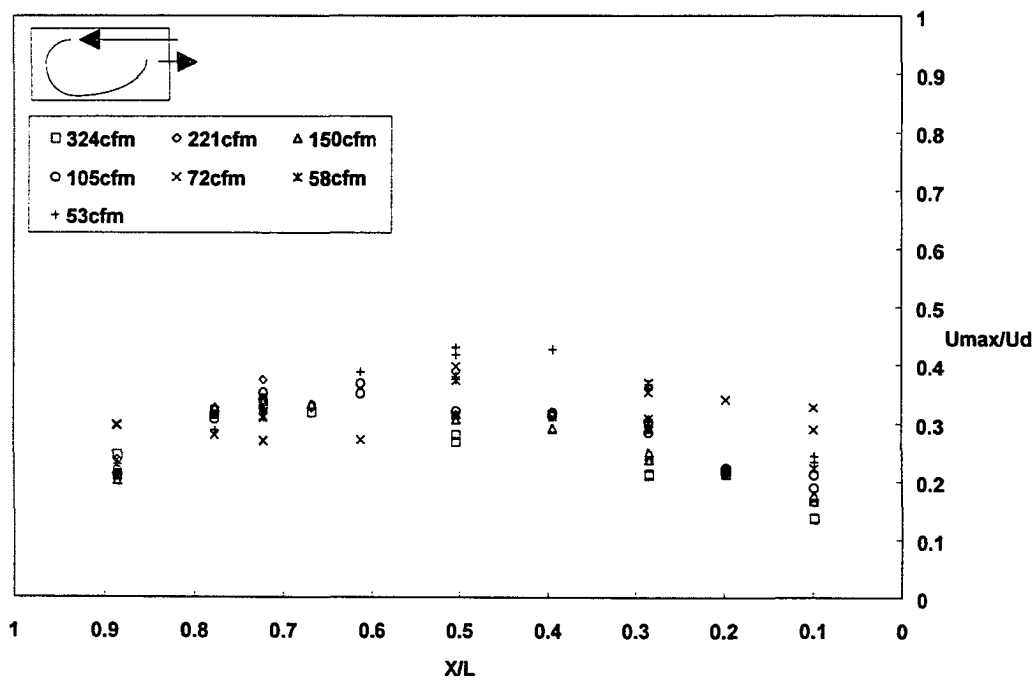

b. floor region

Figure 6.26. Non-dimensional peak airspeed of nonisothermal air-jet along ceiling slot-ventilated enclosure's surface for prototype.

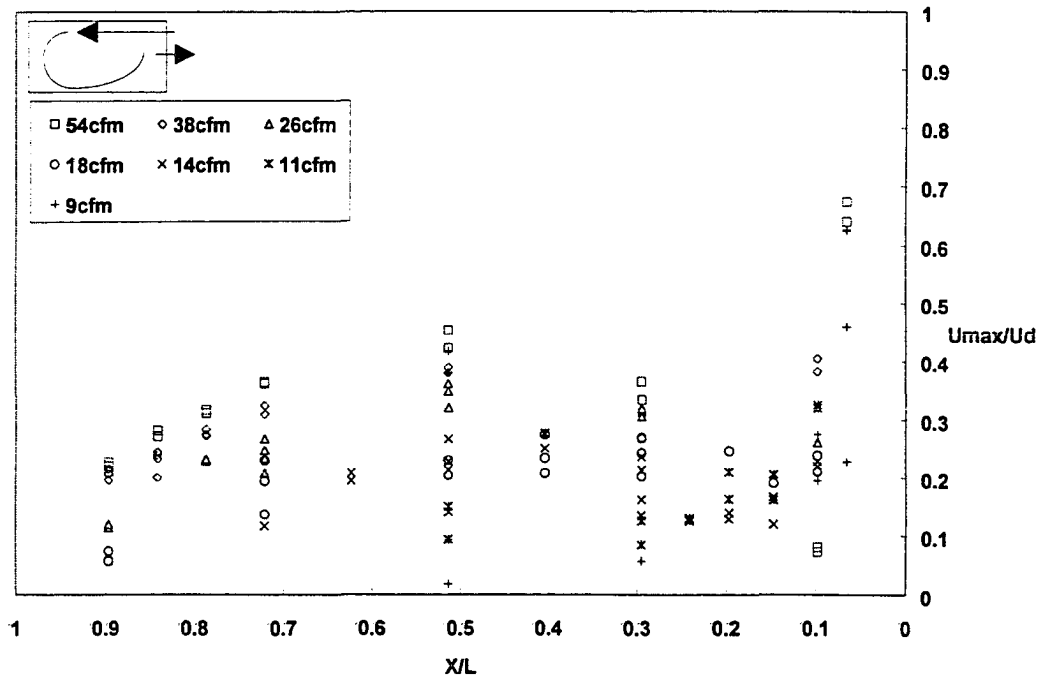

a. ceiling region

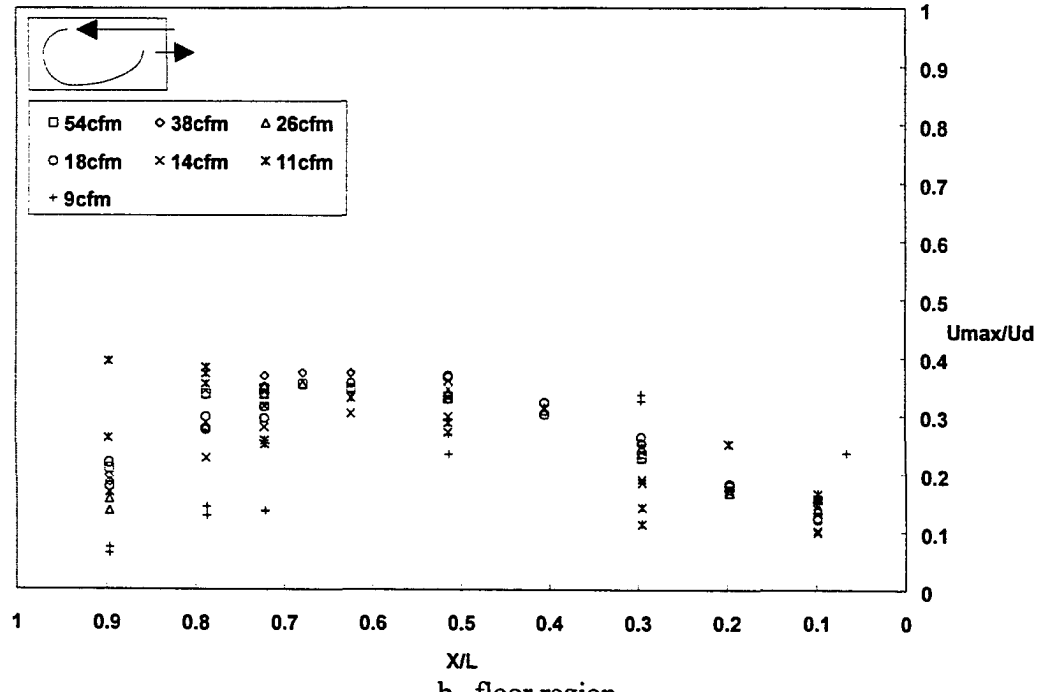

b. floor region

Figure 6.27. Non-dimensional peak airspeed of nonisothermal air-jet along ceiling slot-ventilated enclosure's surface for scale-model.

airflow rates (≥105 cfm). The maximum floor airspeed position moves toward the inlet wall with decreased airflow rate consistent with the characteristics of two circulation zone airflow (see Figure 6.19 (b)).

The peak airspeed profiles along the ceiling and floor in the scale-model showed similar characteristics as in the prototype and these are shown in Figure 6.27. Similar peak airspeed profiles along the floor for the scale-model were measured as long as the airflow rate was ≥26 cfm.

In summary, the ceiling airspeed profiles were similar when the airflow rate was beyond a critical value (i.e. $Ar_c < 40$) and the air-jet terminated at a distance of about 100h (0.7L) from the inlet opening. The floor airspeed profiles were similar when the airflow rate was beyond a critical value of about $Ar_c < 40$ and the maximum floor airspeed occurred at a distance of about 2/3 L from inlet wall.

6.2.3.2. Comparison of longitudinal peak airspace profiles

The longitudinal peak airspeed profile along the ceiling and floor were compared with the Archimedes number (Ar) and inlet jet momentum ratio (Rm) with heat loads of $\Delta T = 40\ ^{\circ}C$ or $\Delta T = 60\ ^{\circ}C$ for two-circulation zone airflow patterns (Figures 6.28 and 6.29), single-circulation zone airflow patterns (Figures 6.30 and 6.31), and approximate isothermal airflow (Figures 6.32 and 6.33).

The consistency of peak airspeed profiles between scale-model and prototype generally depend on the consistency of air-jet trajectories as was shown in Figure 6.24. If the air-jet

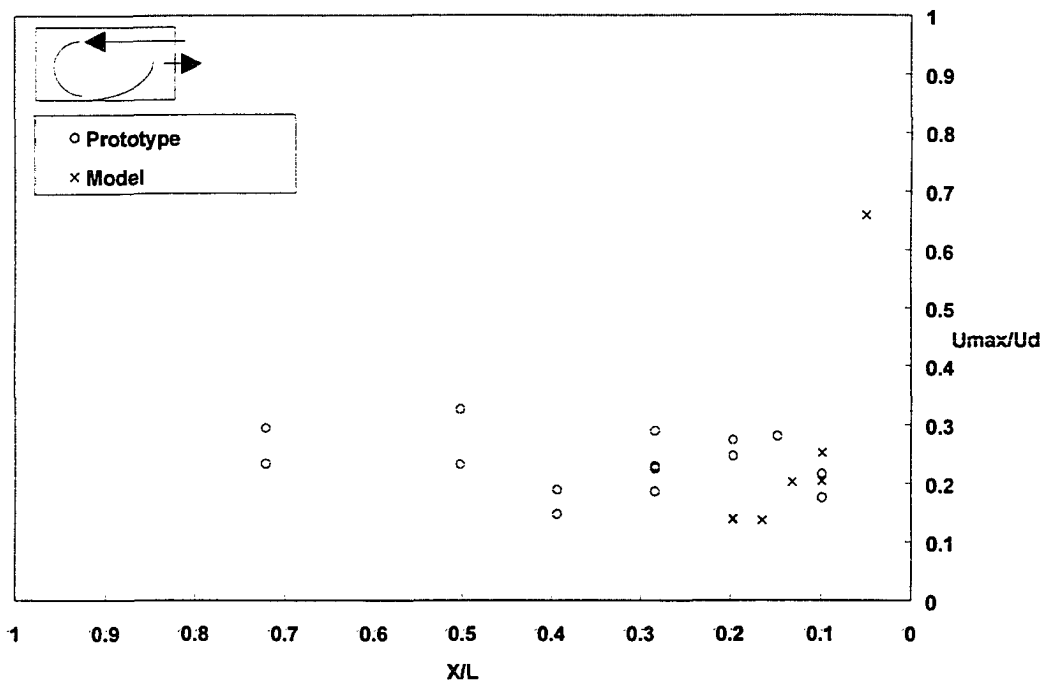

a. Ceiling region

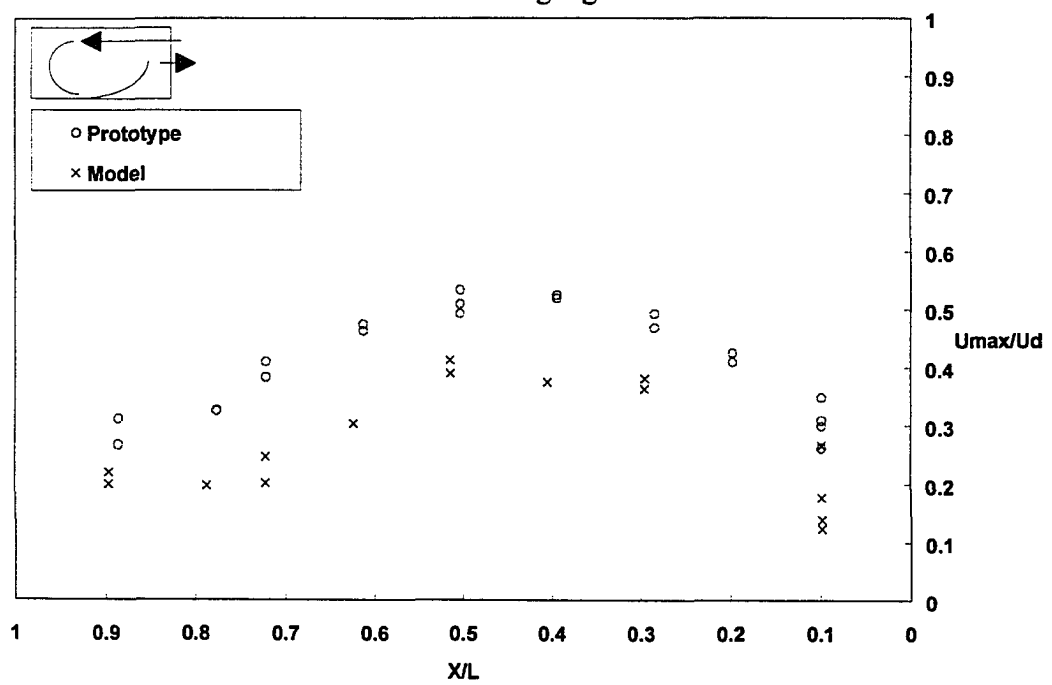

b. Floor region.

Figure 6.28. Comparisons of nondimensional peak airspeed for nonisothermal air-jet based on Ar within two-circulation airflow, Q_p=59cfm, Q_m=11cfm, ΔT_p=60°C, ΔT_m=60°C, Ar_p=0.0283, Ar_m=0.0246, Rm_p=0.004, Rm_m=0.002.

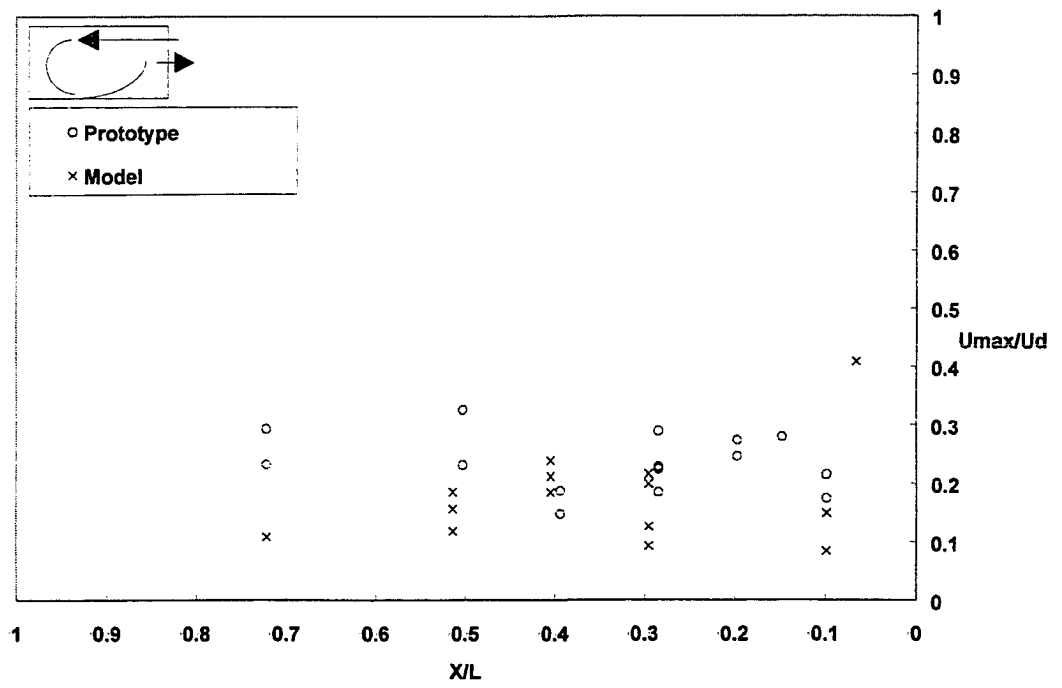

a. Ceiling region

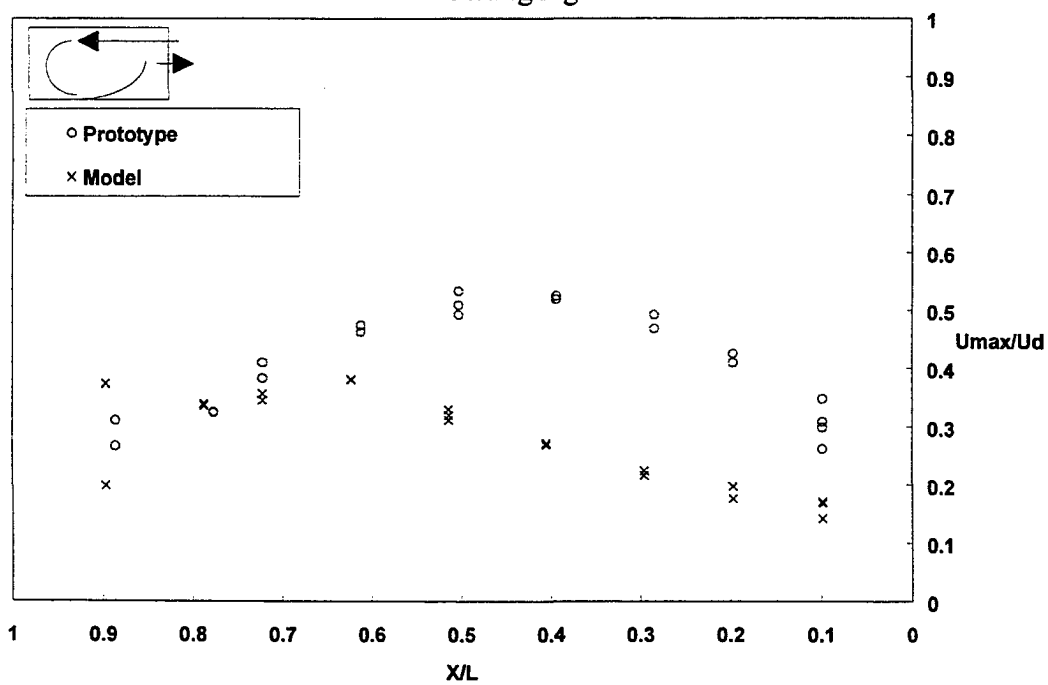

b. Floor region.

Figure 6.29. Comparisons of nondimensional peak airspeed for nonisothermal air-jet based on Rm and same heat load within two-circulation airflow, Q_p=59cfm, Q_m=16cfm, ΔT_p=60°C, ΔT_m=60°C, Ar_p=0.0283, Ar_m=0.0127, Rm_p=0.004, Rm_m=0.004.

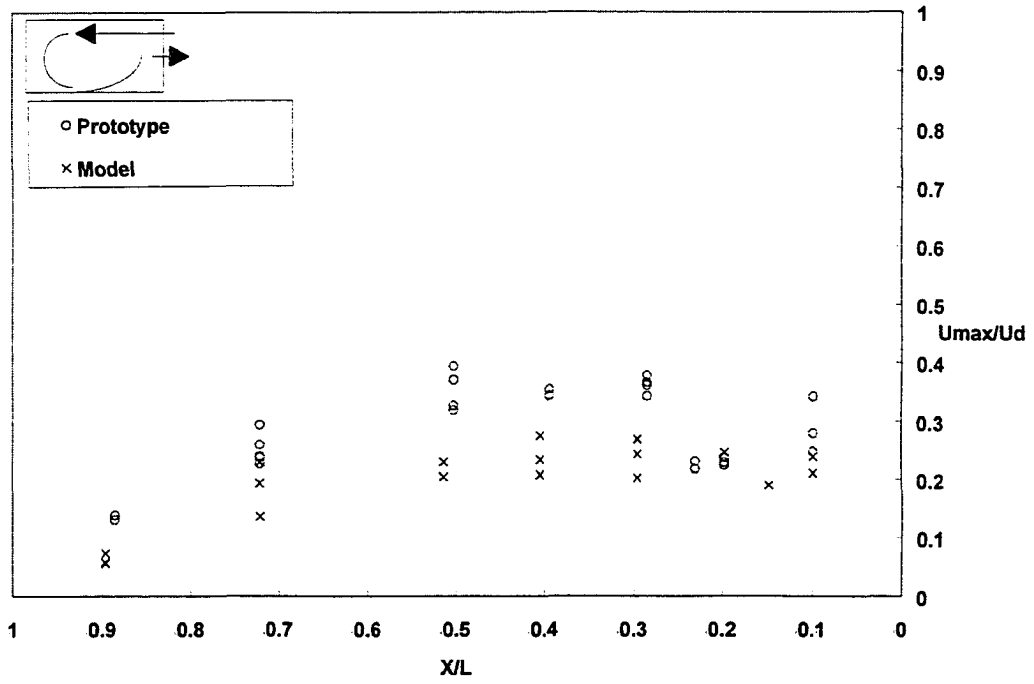

a. Ceiling region

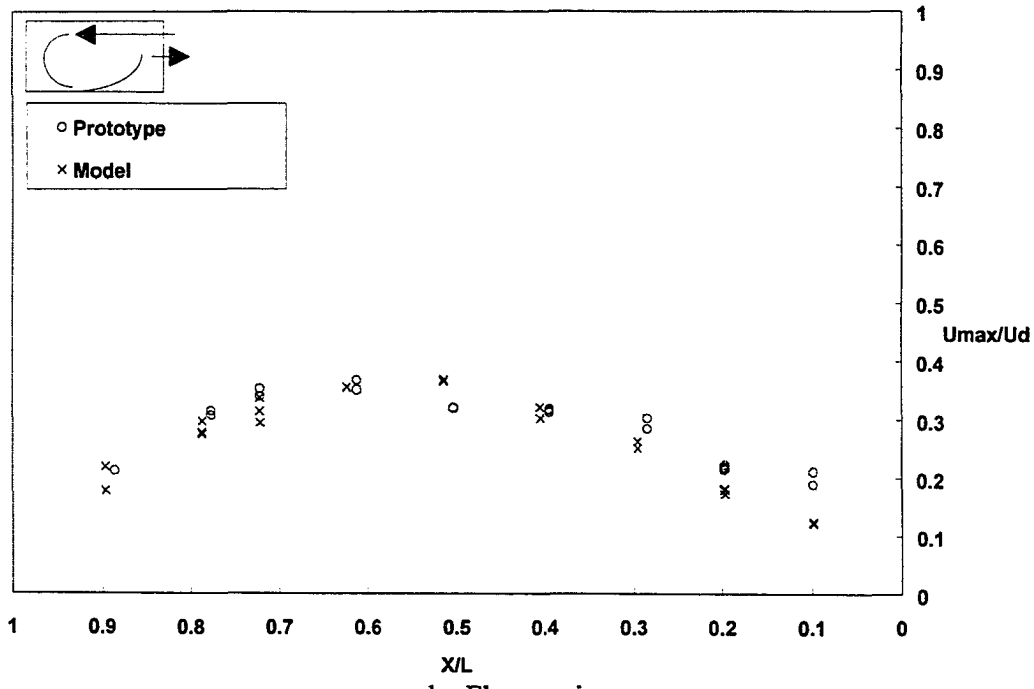

b. Floor region.

Figure 6.30. Comparisons of nondimensional peak airspeed for nonisothermal air-jet based on Ar within single-circulation airflow, Q_p=105cfm, Q_m=18cfm, ΔT_p=40°C, ΔT_m=40°C, Ar_p=0.0062, Ar_m=0.0068, Rm_p=0.012, Rm_m=0.005.

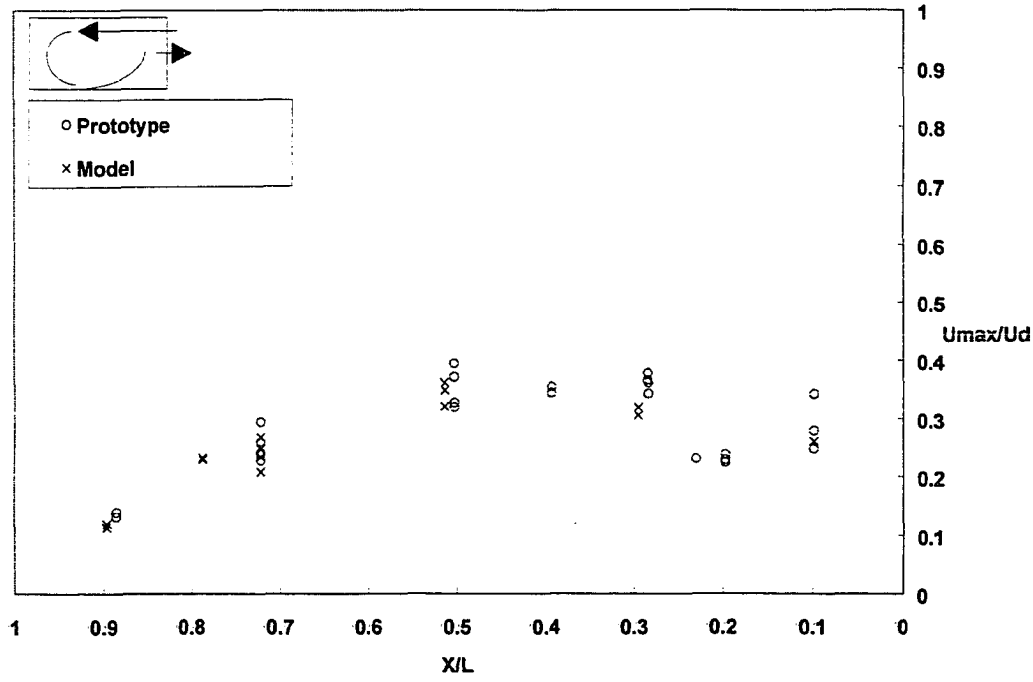

a. Ceiling region

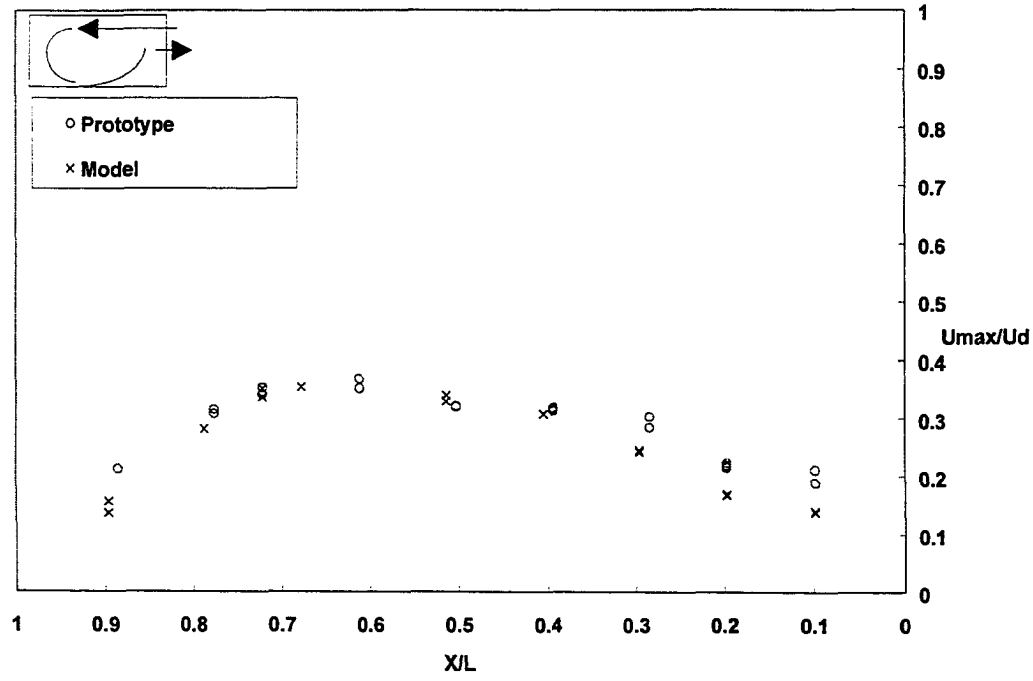

b. Floor region.

Figure 6.31. Comparisons of nondimensional peak airspeed for nonisothermal air-jet based on Rm and same heat load within single-circulation airflow, Q_p=105cfm, Q_m=26cfm, ΔT_p=40°C, ΔT_m=40°C, Ar_p=0.0062, Ar_m=0.0031, Rm_p=0.012, Rm_m=0.012.

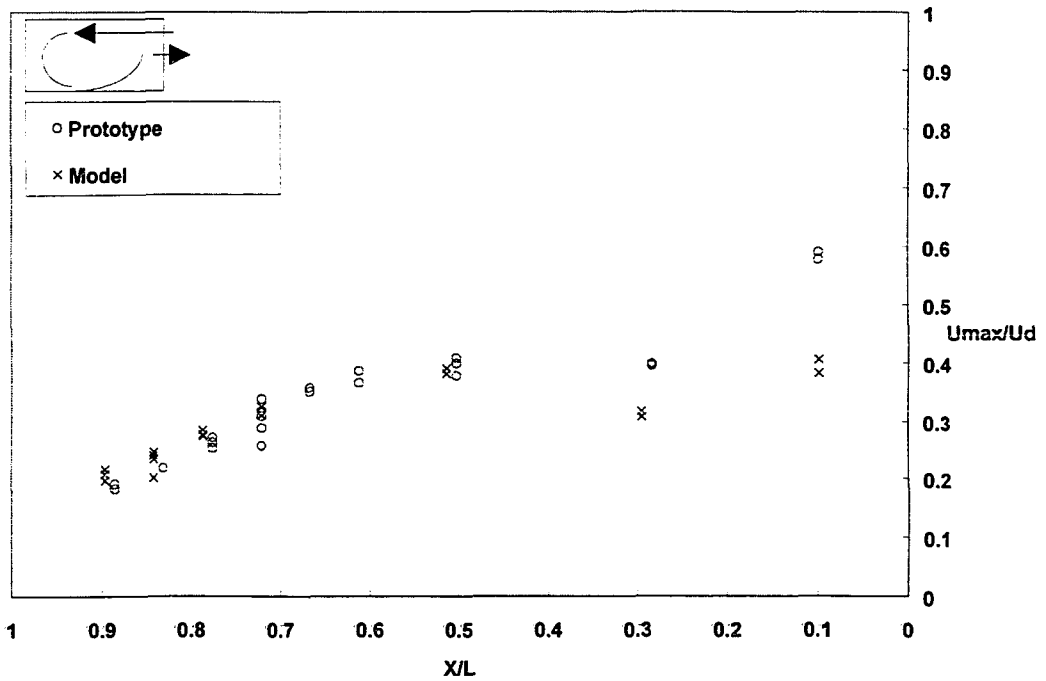

a. Ceiling region

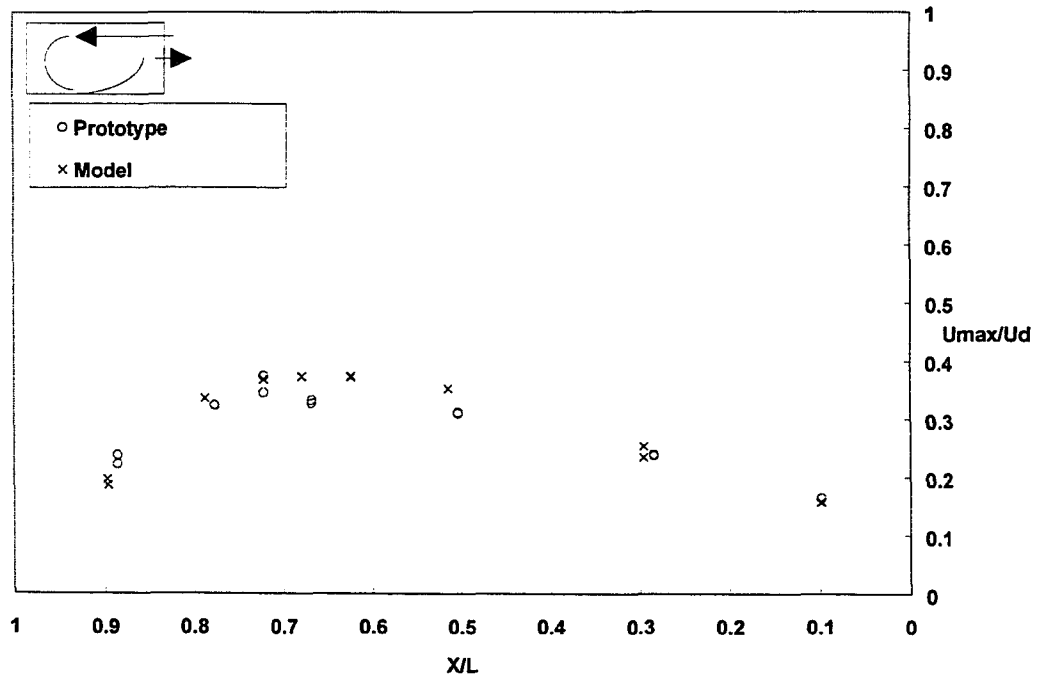

b. Floor region.

Figure 6.32. Comparisons of nondimensional peak airspeed for nonisothermal air-jet based on Ar within approximate isothermal airflow, Q_p=221cfm, Q_m=38cfm, ΔT_p=40°C, ΔT_m=40°C, Ar_p=0.0014, Ar_m=0.0014, Rm_p=0.053, Rm_m=0.026.

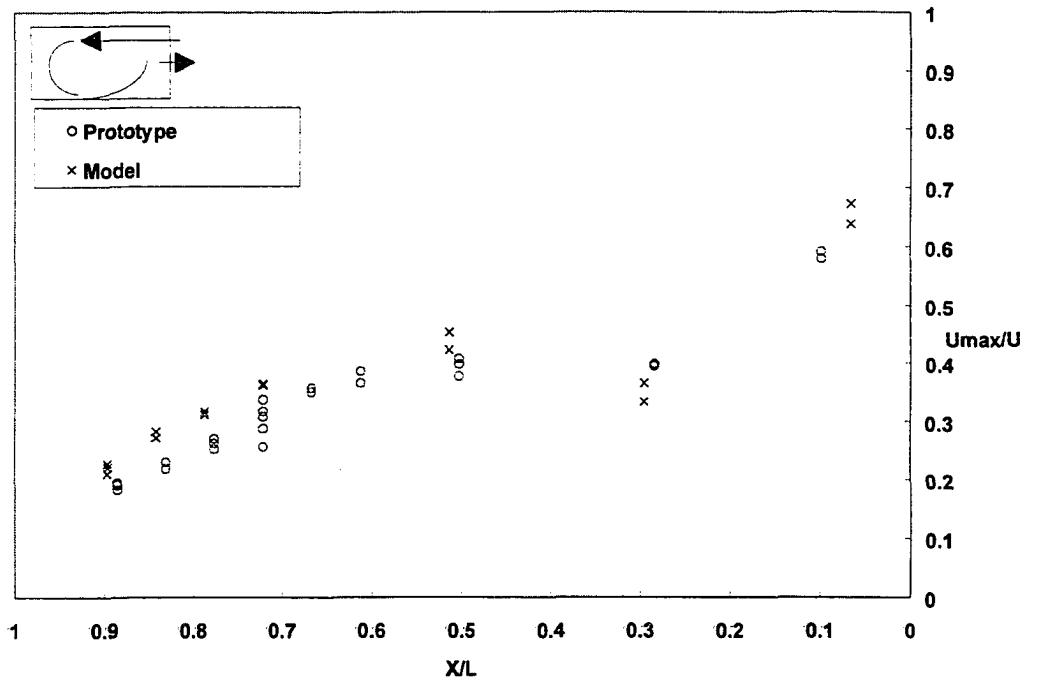

a. Ceiling region

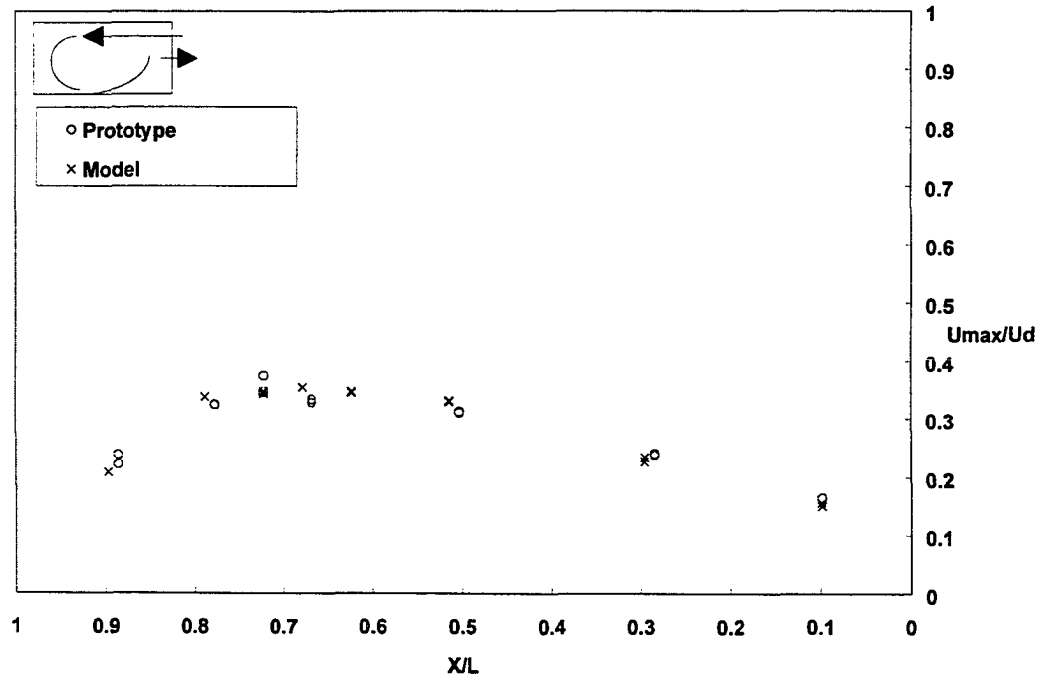

b. Floor region.

Figure 6.33. Comparisons of nondimensional peak airspeed for nonisothermal air-jet based on Rm and same heat load within approximate isothermal airflow, Q_p=221cfm, Q_m=54cfm, ΔT_p=40°C, ΔT_m=40°C, Ar_p=0.0014, Ar_m=0.007, Rm_p=0.053, Rm_m=0.052.

trajectories between the scale-model and prototype were similar, than the peak airspeed profiles were similar as well. However, when two-circulation zone airflow is present in the enclosure (see Figure 6.19 (b)), the peak airspeed profiles did not agree even when the air-jet trajectories were consistent (Figures 6.28 and 6.29). In these cases, the airflow rate usually was very small and only the peak airspeeds close to the entry were large enough to make a measurable air-jet. As a consequence of this, only the portion of peak airspeed profiles close to the entry were similar.

It was concluded that the longitudinal peak airspeed profiles along the ceiling and floor were similar as those found for the air-jet trajectory results between the scale-model and prototype. Ar is an appropriate similitude parameter when the Ar is beyond the critical value required to move from a two-circulation zone airflow pattern to a single-circulation zone airflow pattern. Rm is an appropriate similitude parameter below the above described critical Ar when both the scale-model and prototype have similar heat load. All the profiles were similar when the airflow patterns reached the fully rotary state as $Ar < 0.005$ (Figures 6.32 and 6.33).

6.2.3.3. Comparison of vertical airspeed profiles

The similitude requirements based on Ar and Rm with similar heat loads maintained between the scale-model and prototype were evaluated by comparing the vertical normalized airspeed profiles. The normalized airspeed profiles within each enclosure were compared based on the Archimedes number (Ar) and inlet jet momentum ratio (Rm) with heat loads of

$\Delta T = 40$ °C or $\Delta T = 60$ °C for two-circulation zone airflow (Figure 6.34), single-circulation zone airflow (Figure 6.35), and approximate isothermal airflow (Figure 6.36). The plots present the dimensionless airspeed magnitudes without indication of airflow direction.

The comparisons between both the scale-model and prototype profiles showed similar trends as was found for the air-jet trajectory experiments. When the airflow pattern was two-circulation zone airflow, the profiles were similar based on Ar as the similitude criterion (Figure 6.34). Figure 6.35 describes the vertical airspeed comparison when a single-circulation zone airflow pattern exists. The profiles showed better similarity based on Rm assuming the same heat load compared to using Ar. When the airflow pattern was close to the fully rotary airflow rate ($Ar < 0.005$), comparisons of vertical airspeed profiles were similar irregardness of whether Rm or Ar was used (Figure 6.36).

It was concluded that the comparisons of vertical airspeed profiles had similar results as those found with the air-jet trajectory results. Ar is an acceptable similitude criterion for nonisothermal airflow as long as the airflow pattern is beyond the critical Ar of 0.0161 to 0.0182 based on the vertical airspeed profile evaluation. When the airflow pattern was similar to isothermal airflow, Rm and a similar heat load become the better similarity criteria.

6.2.3.4. Floor airspeed

The behavior of floor airspeed for nonisothermal airflow was similar for the isothermal condition described in section 6.1.3.4. The maximum floor airspeed can also be expressed as equation (6.3) within a specific temperature difference. The peak floor airspeeds at 0.3, 0.5,

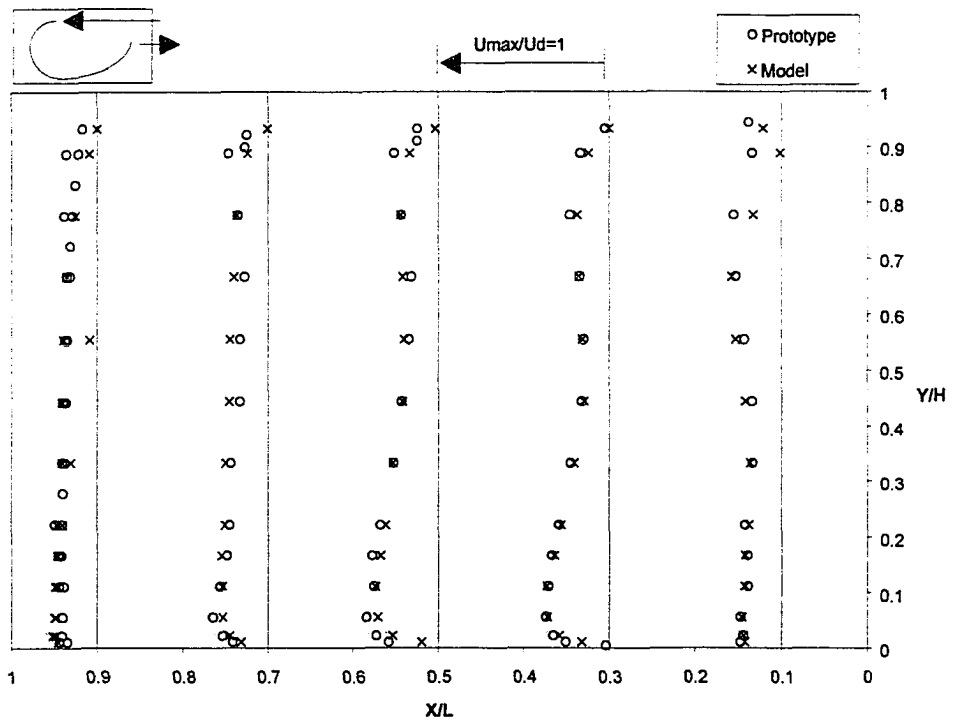

a.Q_p=59cfm,Q_m=11cfm,Ar_p=.0283,Ar_m=.0246,Rm_p=0.004,Rm_m=0.002,ΔT=60°C,SD=9.2%

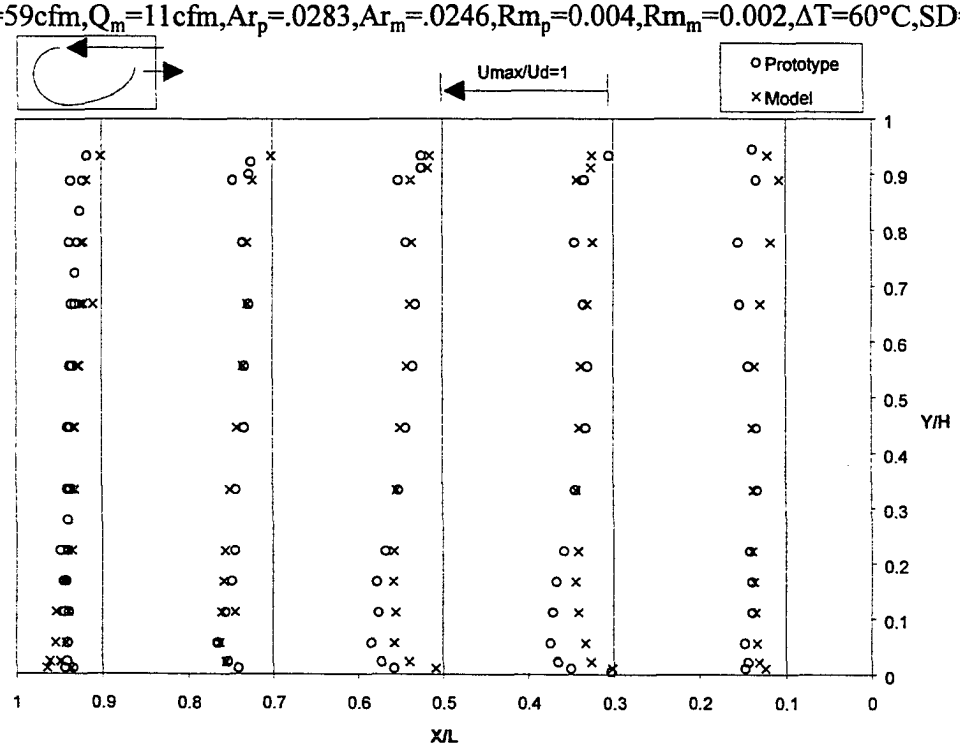

b.Q_p=59cfm,Q_m=16cfm,Ar_p=.0283,Ar_m=.0127,Rm_p=0.004,Rm_m=0.004,ΔT=60°C,SD=11.6%

Figure 6.34. Comparisons of vertical nondimensional peak airspeed for nonisothermal air-jet within two-circulation airflow.

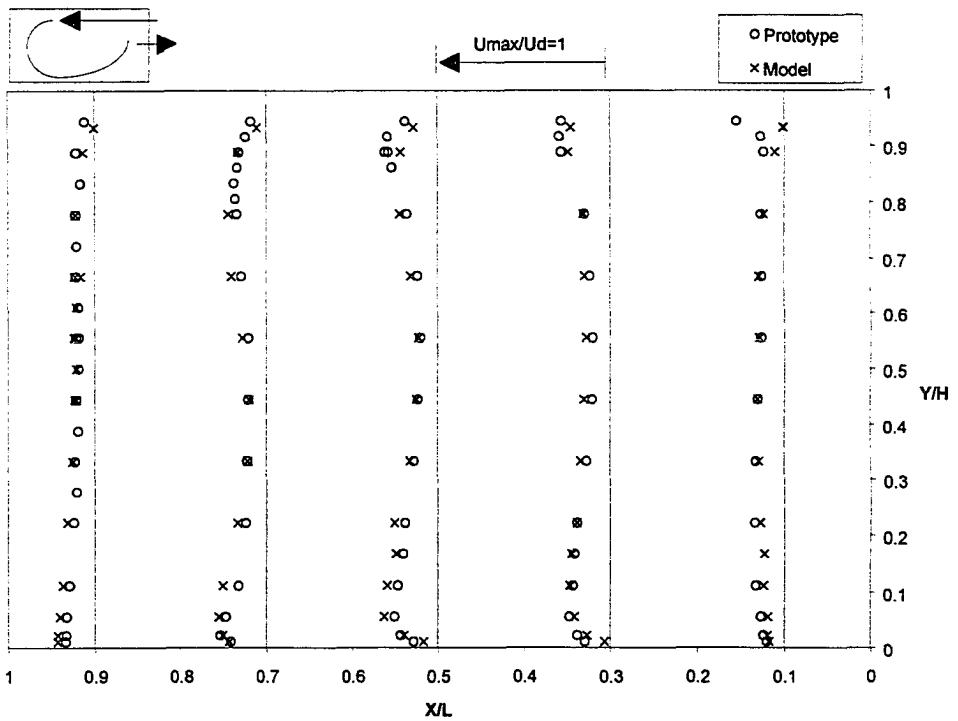

a.Q_p=105cfm,Q_m=18cfm,Ar_p=.0062,Ar_m=.0068,Rm_p=0.012,Rm_m=0.005,ΔT=40°C,SD=7.9%

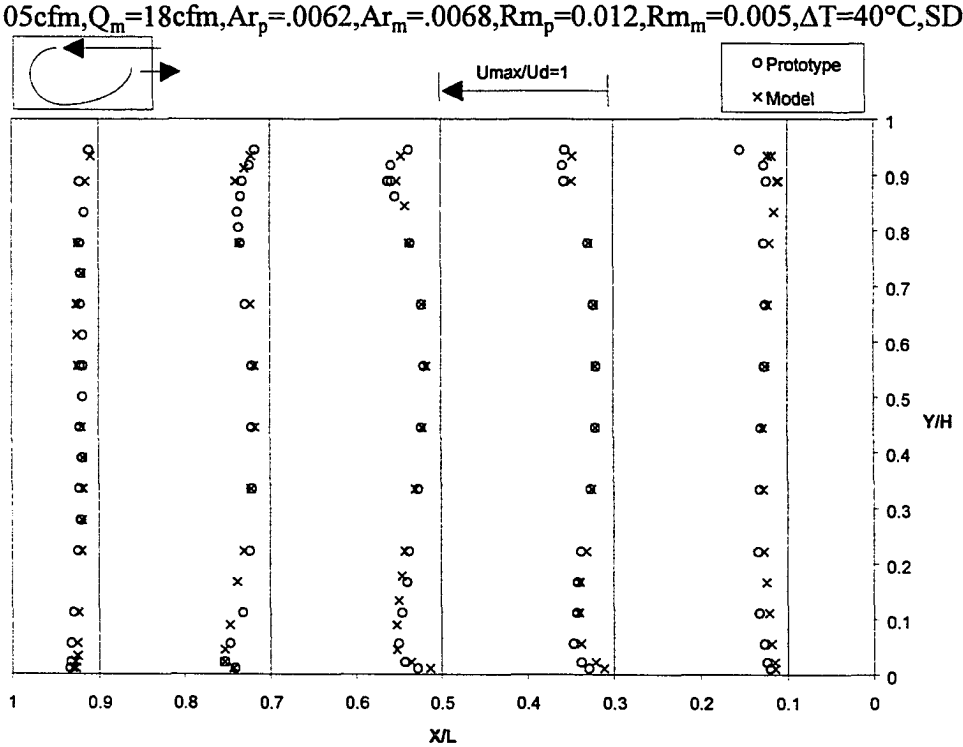

b.Q_p=105cfm,Q_m=26cfm,Ar_p=.0062,Ar_m=.0031,Rm_p=0.012,Rm_m=0.012,ΔT=40°C,SD=5.6%

Figure 6.35. Comparisons of vertical nondimensional peak airspeed for nonisothermal air-jet within single-circulation airflow.

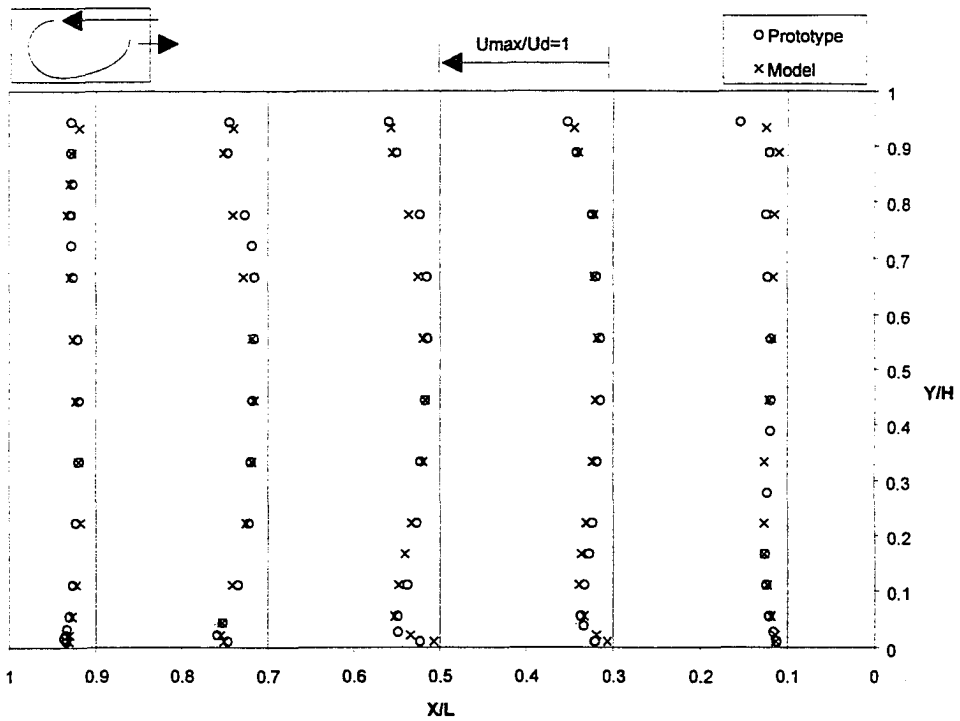

a.Q_p=221cfm,Q_m=38cfm,Ar_p=.0014,Ar_m=.0014,Rm_p=0.053,Rm_m=0.026,ΔT=40°C,SD=5.6%

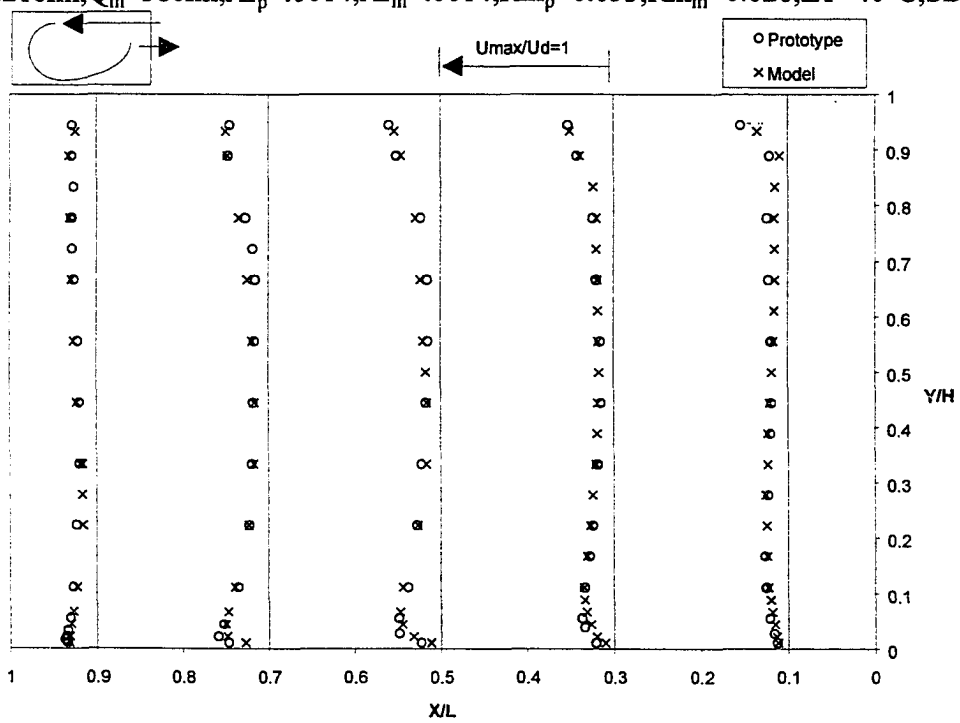

b.Q_p=221cfm,Q_m=54cfm,Ar_p=0.0014,Ar_m=0.007Rm_p=0.053,Rm_m=0.052,ΔT=40°C,SD=4.4%

Figure 6.36. Comparisons of vertical nondimensional peak airspeed for nonisothermal air-jet within approximate isothermal airflow.

and 0.7 L from the inlet wall with a heat load of ΔT=40 °C are shown in Figure 6.37. The regression equations are presented in Table 6.11.

The plots show that thermal buoyancy near the floor resulted in dynamic air movement that increased the peak floor airspeed compared to the isothermal condition. This is in agreement with the results from Wang and Ogilvie (1994b). Thus, higher buoyant forces resulted in an increased peak floor airspeed. When the inlet jet momentum increased, the difference in peak floor airspeed between the isothermal and nonisothermal conditions decreased.

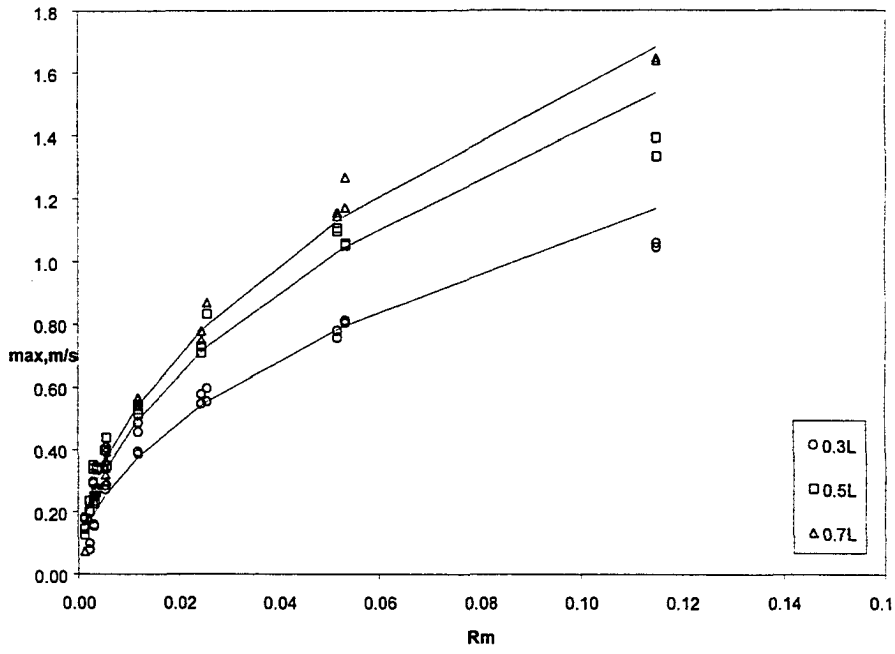

Figure 6.37. The peak floor airspeed at different position with ΔT=40 °C of both scale-model and prototype versus inlet jet momentum ratio (Rm).

Table 6.11. The regression equations of peak airspeed at different positions with ΔT=40 °C of both model and prototype versus inlet jet momentum ratio (Rm).

Positions	Regression equations	Coefficient of determination, R^2
0.3L	$U_{rm}=3.44\sqrt{R_m}$	0.93
0.5L	$U_{rm}=4.53\sqrt{R_m}$	0.96
0.7L	$U_{rm}=4.96\sqrt{R_m}$	0.99

6.2.4. The temperature field

The study of the temperature field is an important evaluation tool for similitude between a scale-model and prototype for nonisothermal airflow. This is so because the temperature field is established based on the combined influences of the airspeed field and heat transfer mechanisms.

6.2.4.1. Comparison of longitudinal temperature profiles along enclosure surfaces

The horizontal normalized temperature at each peak airspeed position was compared between the scale-model and prototype. The normalized temperature profiles compared with Ar and Rm with $\Delta T = 40$ °C or $\Delta T = 60$ °C are given for two-circulation zone airflow (Figures 6.38 and 6.39), single-circulation zone airflow (Figures 6.40 and 6.41), and approximate isothermal airflow (Figures 6.42 and 6.43).

The comparison of longitudinal temperature profiles for two-circulation zone airflow are shown in Figures 6.38 and 6.39. Only a small region close to the inlet wall were similar with Ar as the similitude criterion (Figure 6.38). The temperature profiles were similar with Rm (Figure 6.39), but the airflow patterns were completely different. The similar temperature

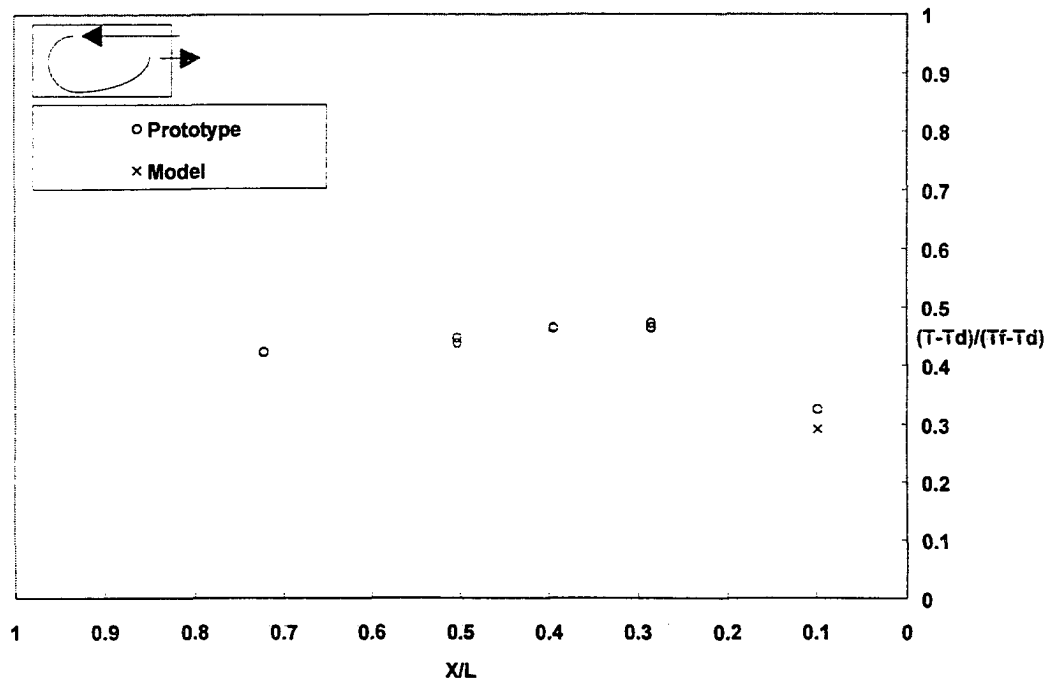

a. Ceiling region

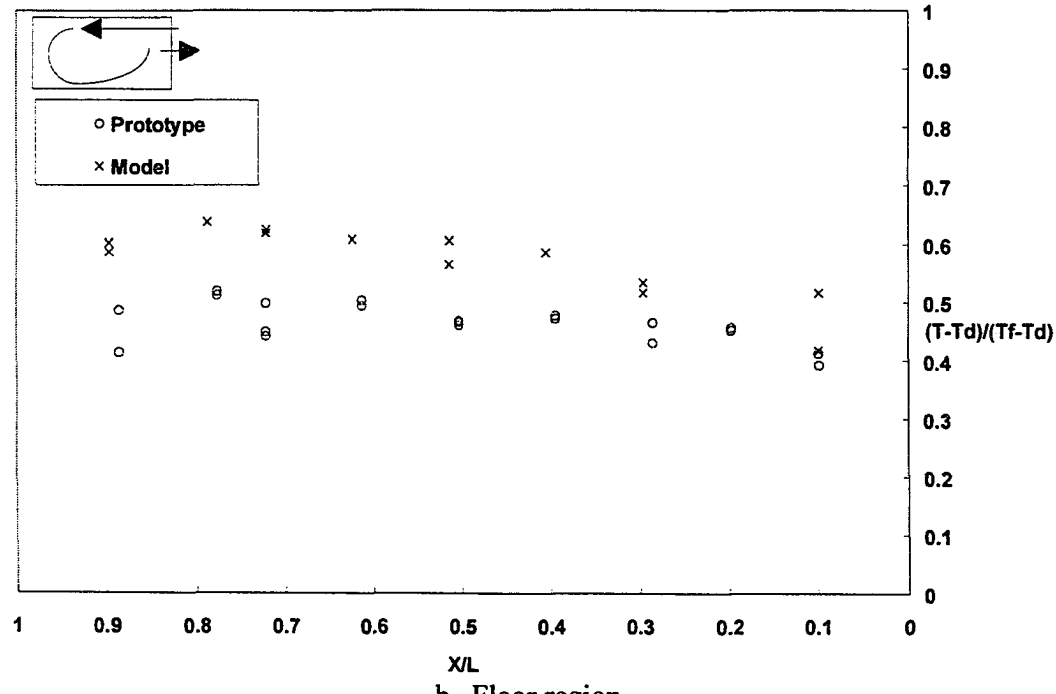

b. Floor region.

Figure 6.38. Comparisons of longitudinal normalized peak temperature for nonisothermal air-jet based on Ar within two-circulation airflow, Q_p=59cfm, Q_m=11cfm, ΔT_p=60°C, ΔT_m=60°C, Ar_p=0.0283, Ar_m=0.0246, Rm_p=0.004, Rm_m=0.002.

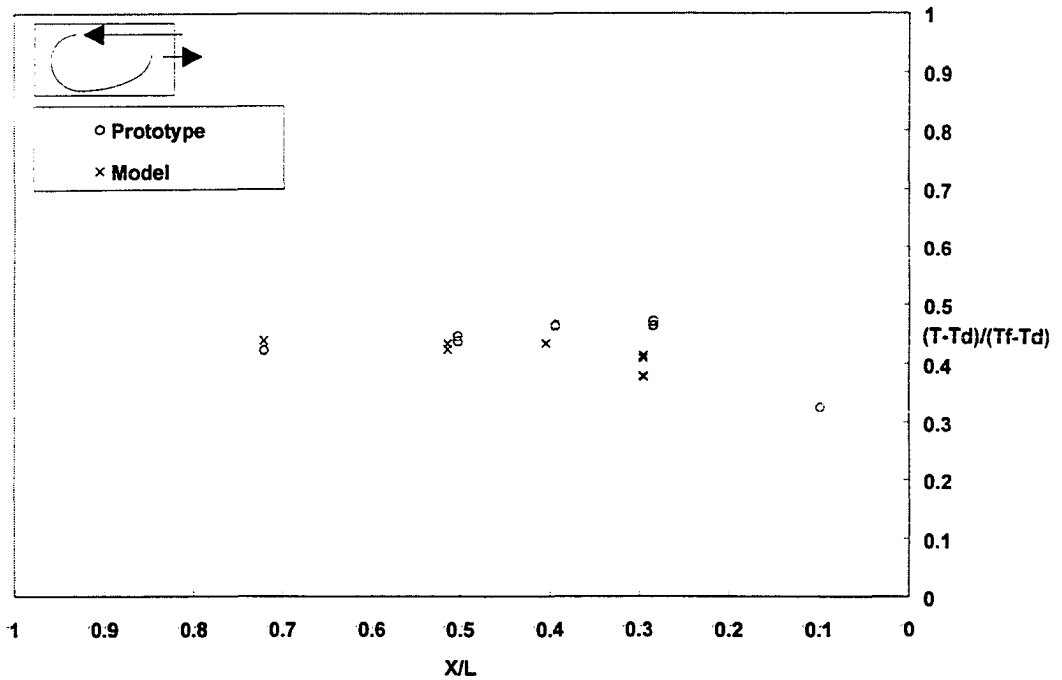

a. Ceiling region

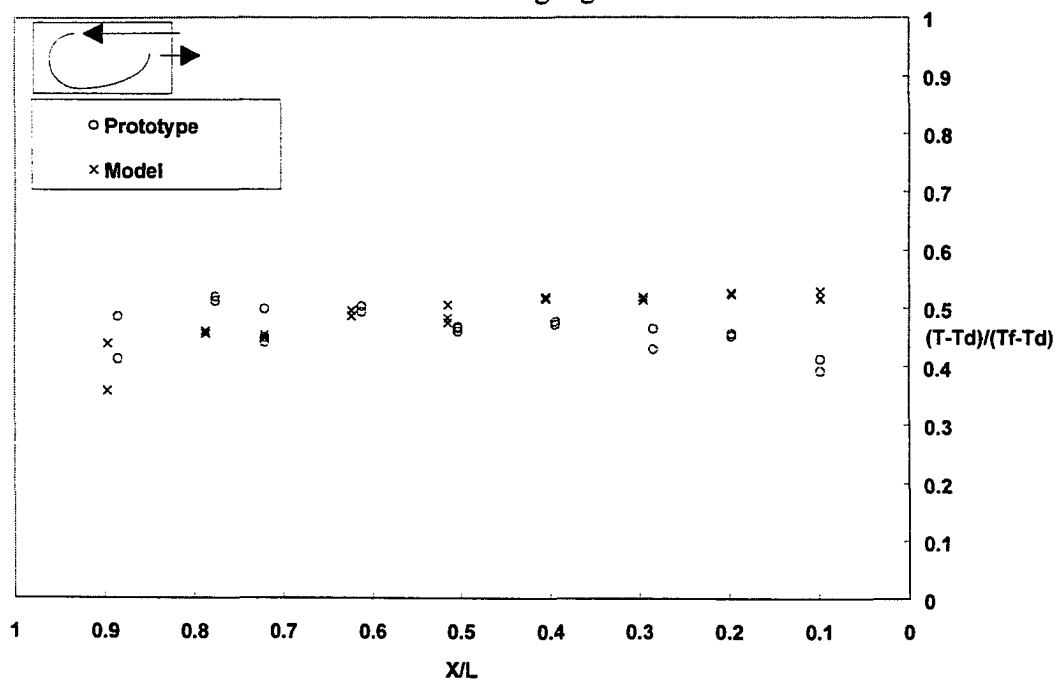

b. Floor region.

Figure 6.39. Comparisons of longitudinal normalized peak temperature for nonisothermal air-jet based on Rm and same heat load within two-circulation airflow, Q_p=59cfm, Q_m=16cfm, ΔT_p=60°C, ΔT_m=60°C, Ar_p=0.0283, Ar_m=0.0127, Rm_p=0.004, Rm_m=0.004.

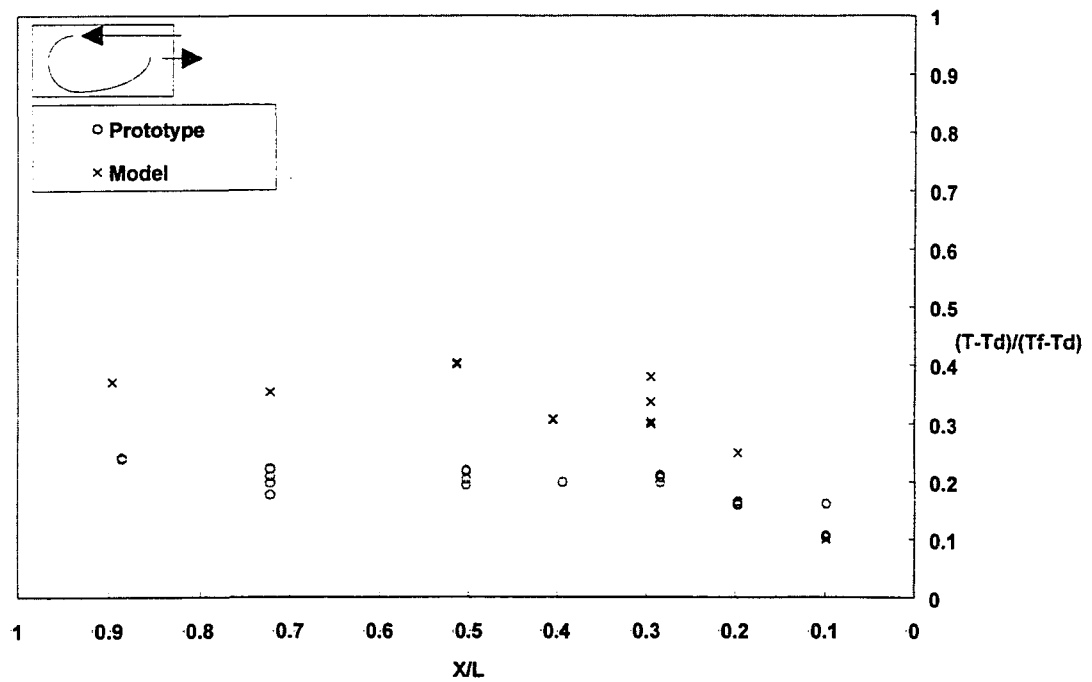

a. Ceiling region

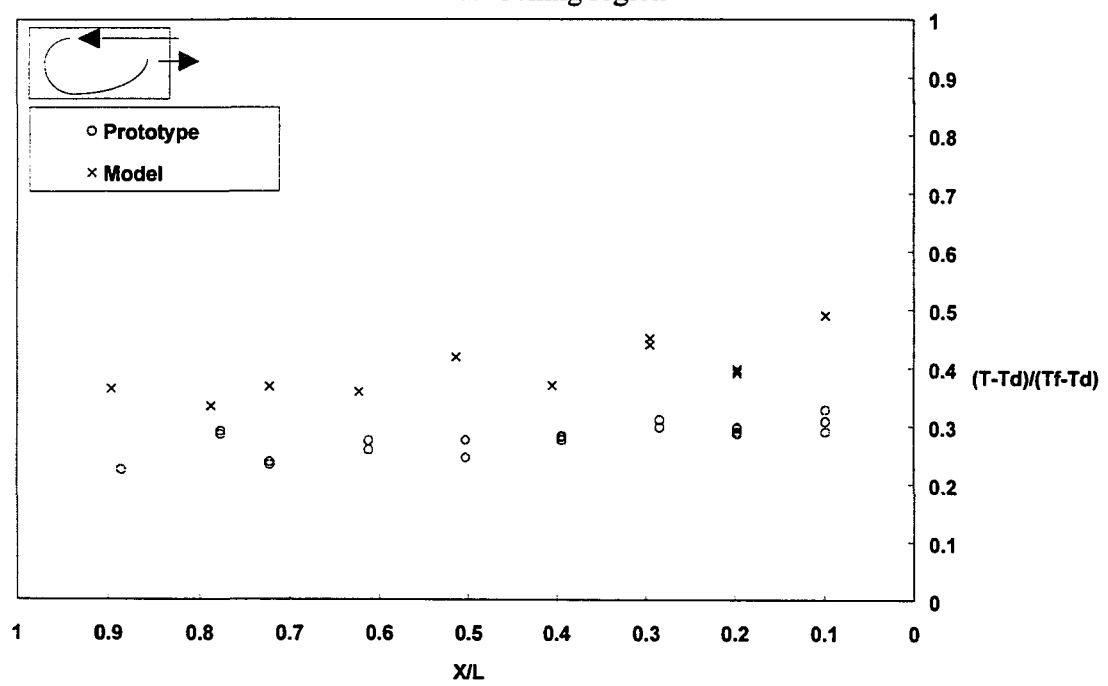

b. Floor region.

Figure 6.40. Comparisons of longitudinal normalized peak temperature for nonisothermal air-jet based on Ar within single-circulation airflow, Q_p=105cfm, Q_m=18cfm, ΔT_p=40°C, ΔT_m=40°C, Ar_p=0.0062, Ar_m=0.0068, Rm_p=0.012, Rm_m=0.005.

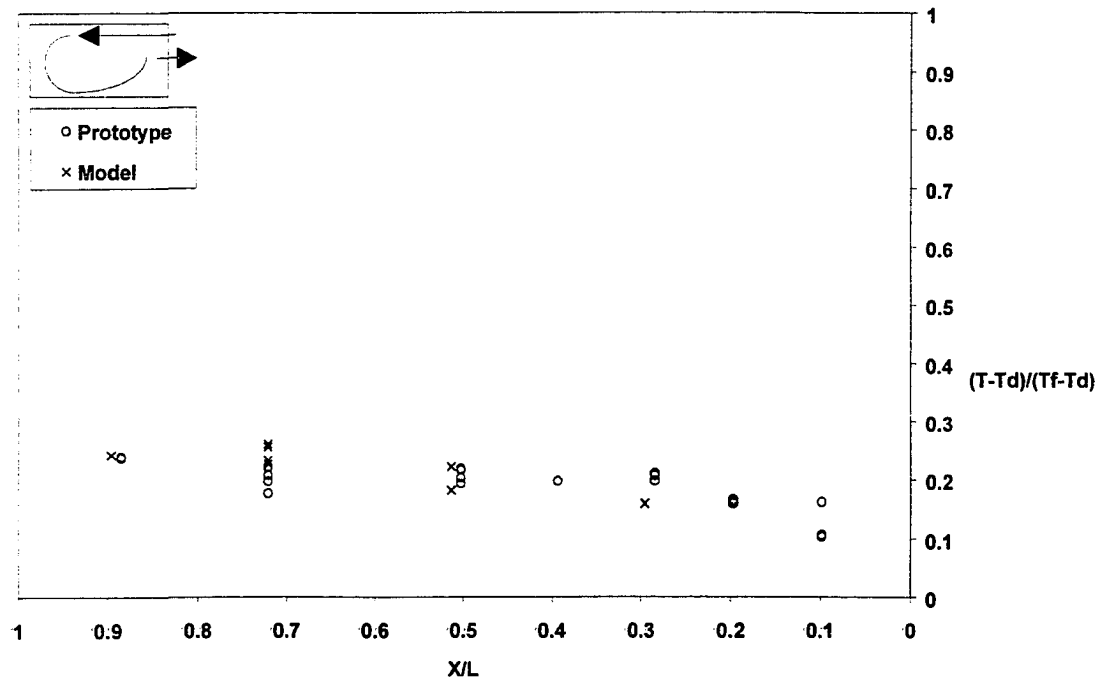

a. Ceiling region

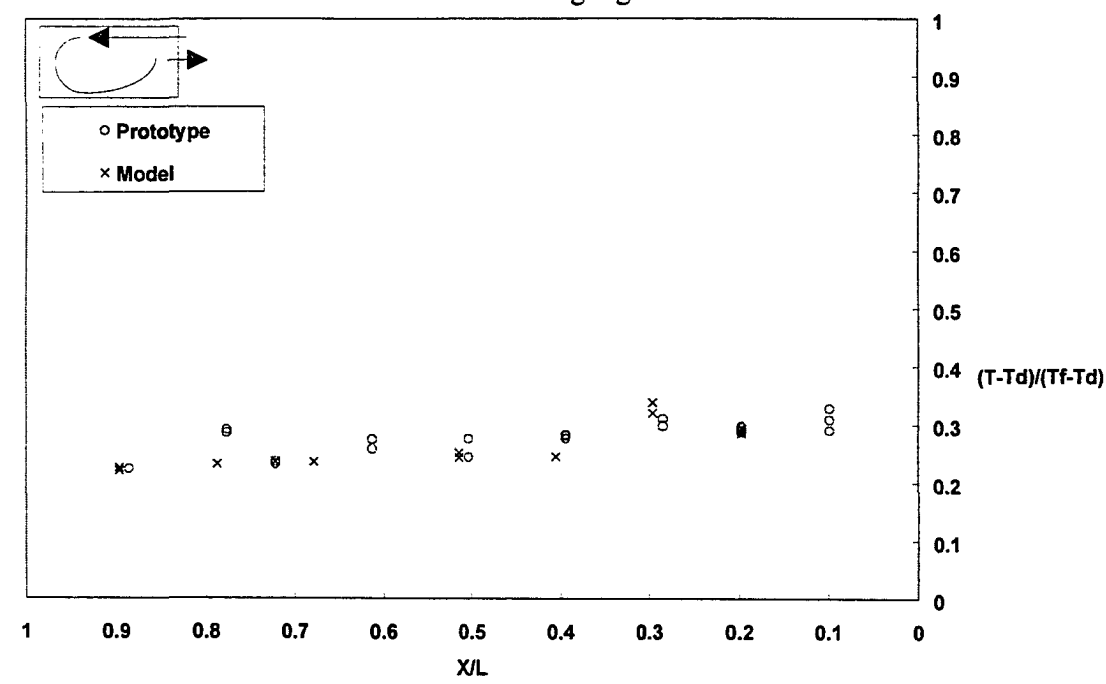

b. Floor region.

Figure 6.41. Comparisons of longitudinal normalized peak temperature for nonisothermal air-jet based on Rm and same heat load within single-circulation airflow, Q_p=105cfm, Q_m=26cfm, ΔT_p=40°C, ΔT_m=40°C, Ar_p=0.0062, Ar_m=0.0031, Rm_p=0.012, Rm_m=0.012.

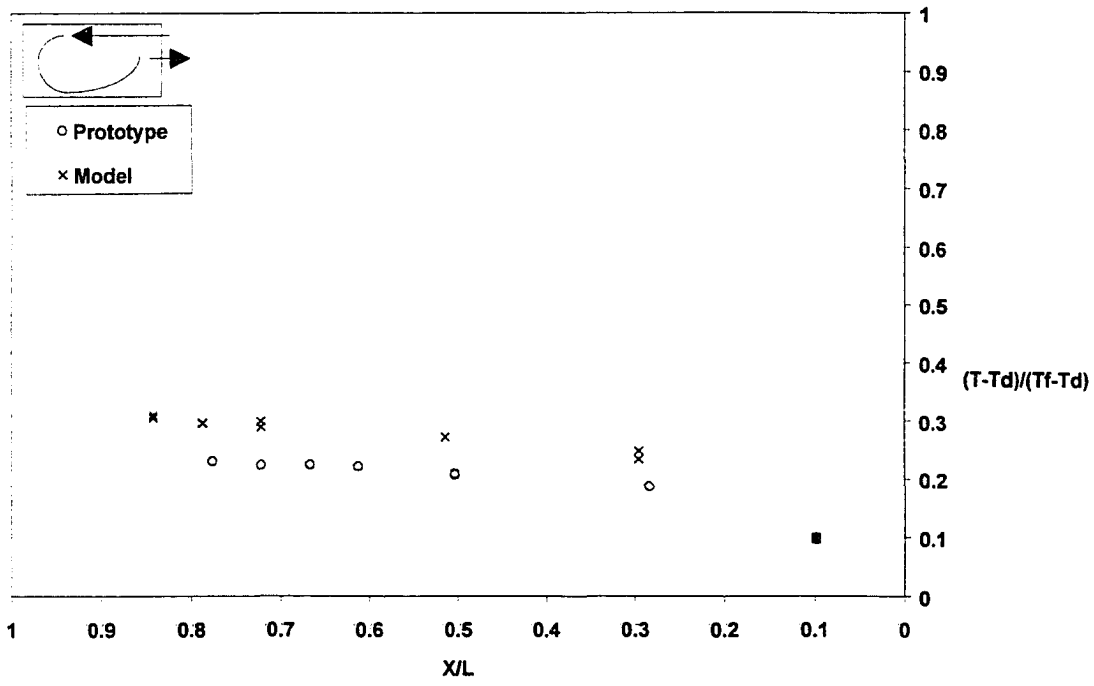

a. Ceiling region

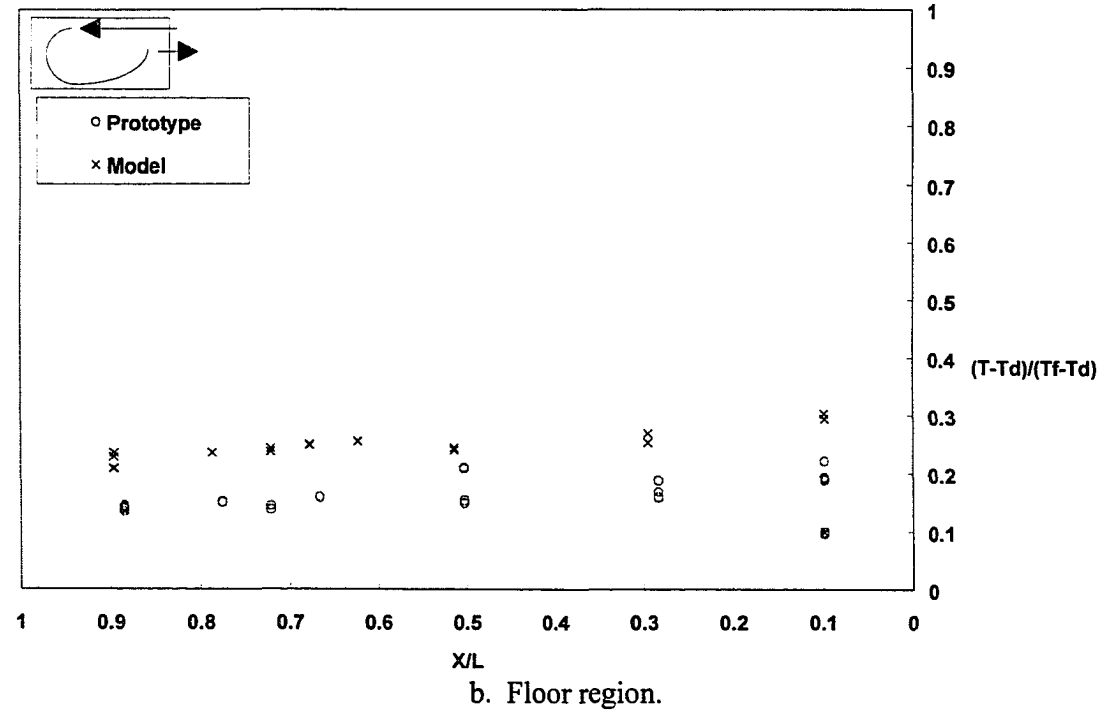

b. Floor region.

Figure 6.42. Comparisons of longitudinal normalized peak temperature for nonisothermal air-jet based on Ar within approximate isothermal airflow, Q_p=221cfm, Q_m=38cfm, ΔT_p=40°C, ΔT_m=40°C, Ar_p=0.0014, Ar_m=0.0014, Rm_p=0.053, Rm_m=0.026.

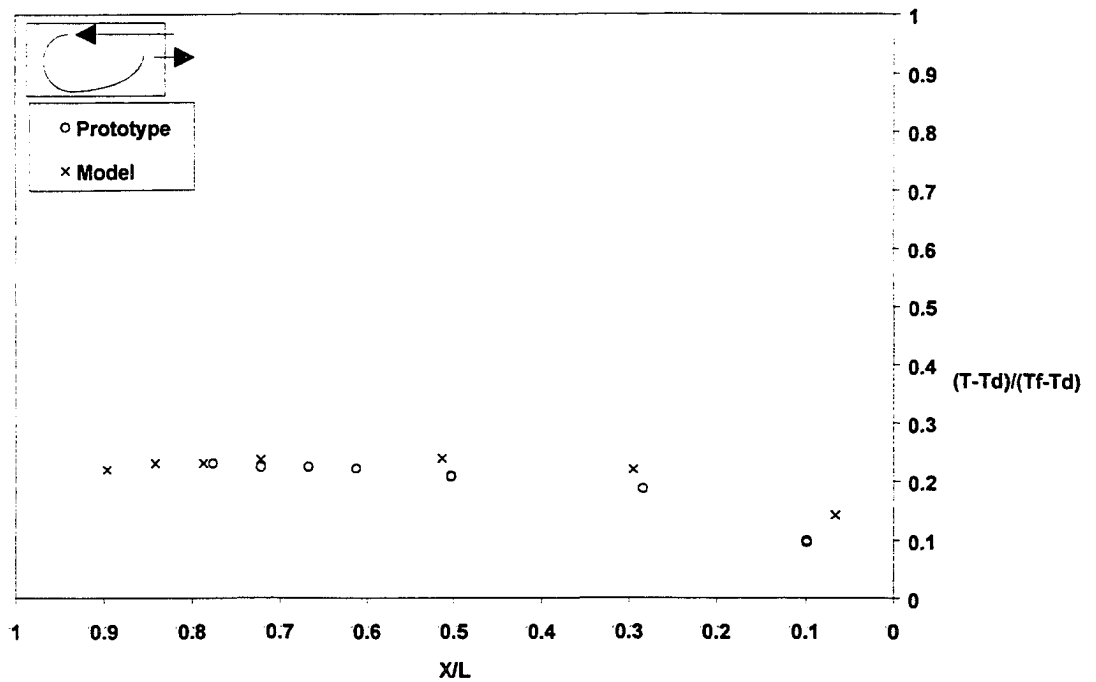

a. Ceiling region

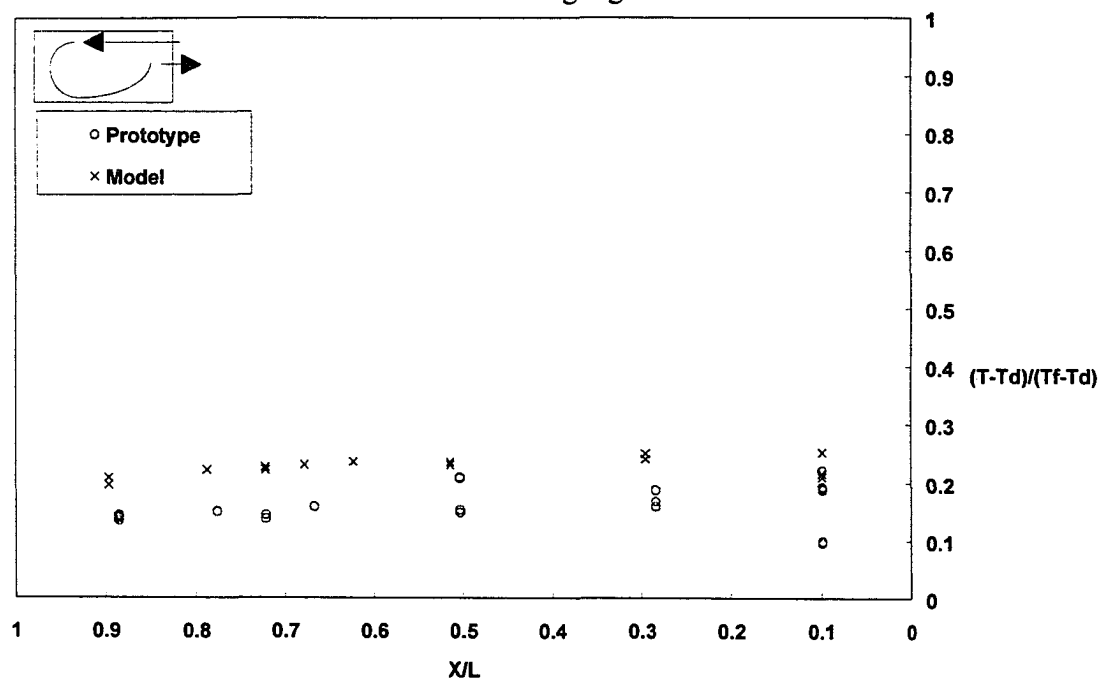

b. Floor region.

Figure 6.43. Comparisons of longitudinal normalized peak temperature for nonisothermal air-jet based on Rm and same heat load within approximate isothermal airflow, Q_p=221cfm, Q_m=54cfm, ΔT_p=40°C, ΔT_m=40°C, Ar_p=0.0014, Ar_m=0.007, Rm_p=0.053, Rm_m=0.052.

profiles may have resulted in the small airflow rate where insignificant convective heat transfer effects were occurring on the temperature field.

When the airflow rate increased to produce a single-circulation zone airflow pattern, the temperature profiles showed a better fit using Rm and a similar heat load (Figures 6.40 versus 6.41). Figures 6.42 and 6.43 show that when the airflow pattern is approximately similar to isothermal airflow, the horizontal normalized temperature profiles between the scale-model and prototype based on Rm were consistently better than those based on Ar. The airflow pattern unchanged when the airflow rate reached the threshold value, but the temperature field was influenced by the magnitude of the airspeed. Lower airspeed caused higher temperatures, thus the temperature profile based on Ar (lower inlet airspeed) (Figure 6.42) was higher than that based on Rm (higher inlet airspeed) as shown in Figure 6.43.

It was concluded that the longitudinal temperature profiles between the scale-model and prototype for two-circulation zone airflows were equally described using either the Ar or Rm with the same heat load. When the airflow pattern reached a single-circulation zone airflow, Rm and the same heat load became the appropriate similitude criteria. The temperature field was not independent of the similarity parameter even when the airflow pattern was fully rotary and unchanged with increasing airflow rate. For these cases, Rm with the same heat load is still the more appropriate similitude criteria.

6.2.4.2. Comparison of vertical temperature profiles

Similar test results using vertical temperature profiles were found as the previous section and these are shown in Figures 6.44 to 6.46. The comparisons for two-circulation zone airflow (Figure 6.44) showed that the Ar gave better agreement in the region close to the inlet wall. The remaining room zone had a similar temperature profile using Rm and the same heat load. As the airflow pattern reached the single-circulation zone airflow, Rm was found to be the appropriate similitude criterion (Figure 6.45). When the airflow was approximately isothermal, using Rm as the similitude criteria gave better agreement than Ar (Figure 6.46). It was concluded that the temperature profiles were generally similar as the results of airflow pattern and airspeed field except in the low airflow rate region. When convection heat transfer did not control the thermal environment within the enclosure, the temperature field in the region close to the inlet wall was similar based on Ar. The temperature field in the remaining regions of the scale-model needed a higher ventilation rate (i.e. higher inlet airspeed) to compensate for the higher room temperature due to the reduced volume of the scale-model. When the airflow pattern became a single-circulation zone airflow, the Rm became the appropriate similitude criteria. The temperature field was not independent of the airflow rate when the airflow rate was beyond the threshold value. For this case, the Rm with the same heat load is the better similarity criteria between scale-model and prototype.

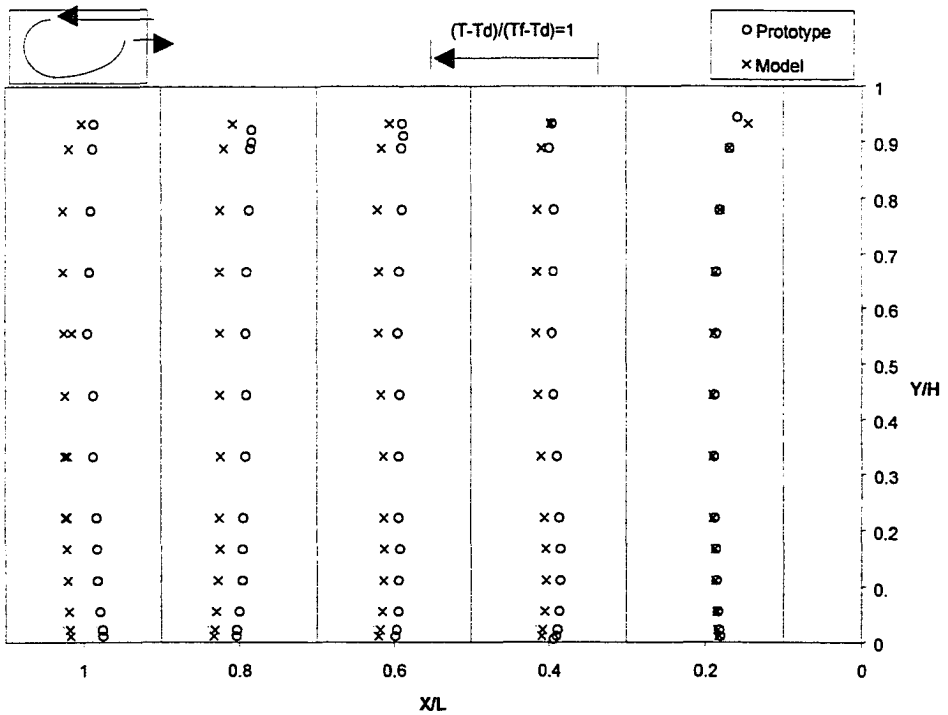

a.Q_p=59cfm,Q_m=11cfm,Ar_p=.0283,Ar_m=.0246,Rm_p=0.004,Rm_m=0.002,ΔT=60°C,SD=12.8%

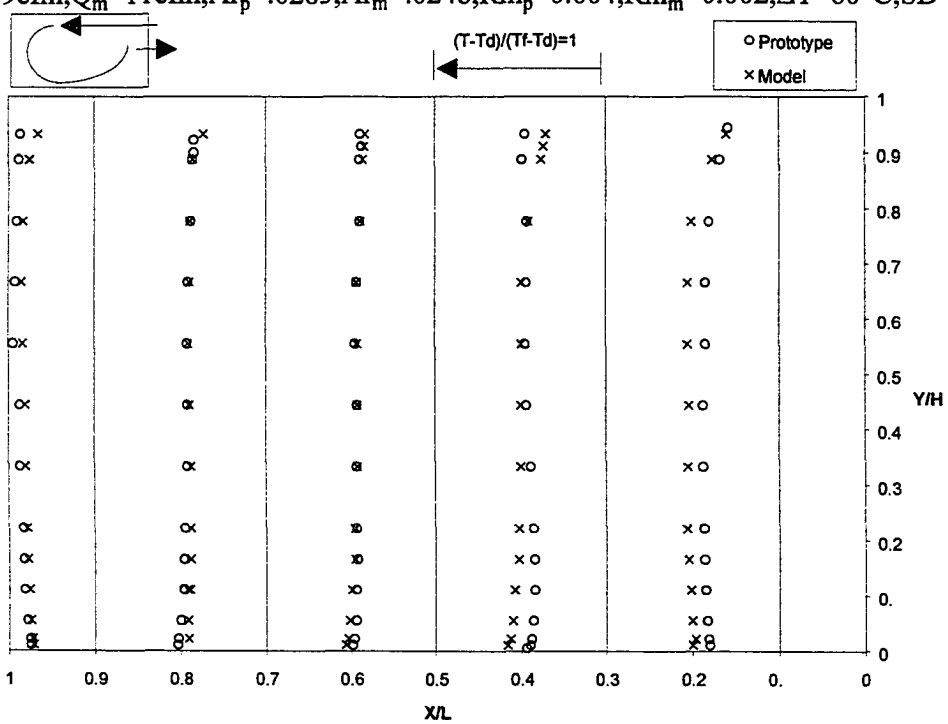

b.Q_p=59cfm,Q_m=16cfm,Ar_p=0.0283,Ar_m=.0127,Rm_p=0.004,Rm_m=0.004,ΔT=60°C,SD=6.2%

Figure 6.44. Comparisons of vertical nondimensional peak temperature for nonisothermal air-jet within two-circulation airflow.

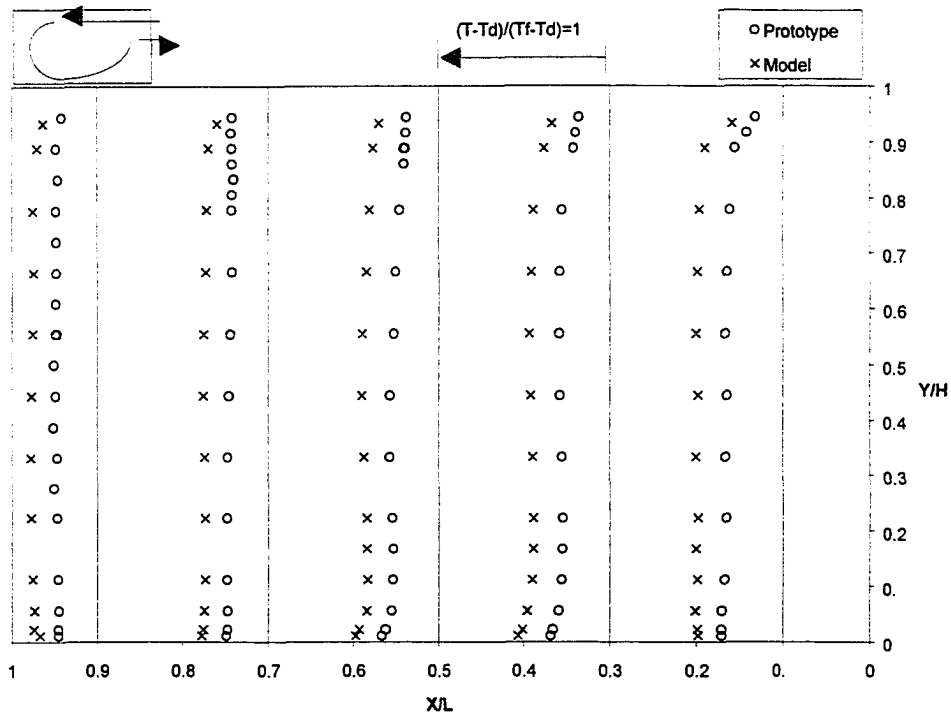

a.Q_p=105cfm,Q_m=18cfm,Ar_p=.0062,Ar_m=.0068,Rm_p=.012,Rm_m=0.005,ΔT=40°C,SD=23.4%

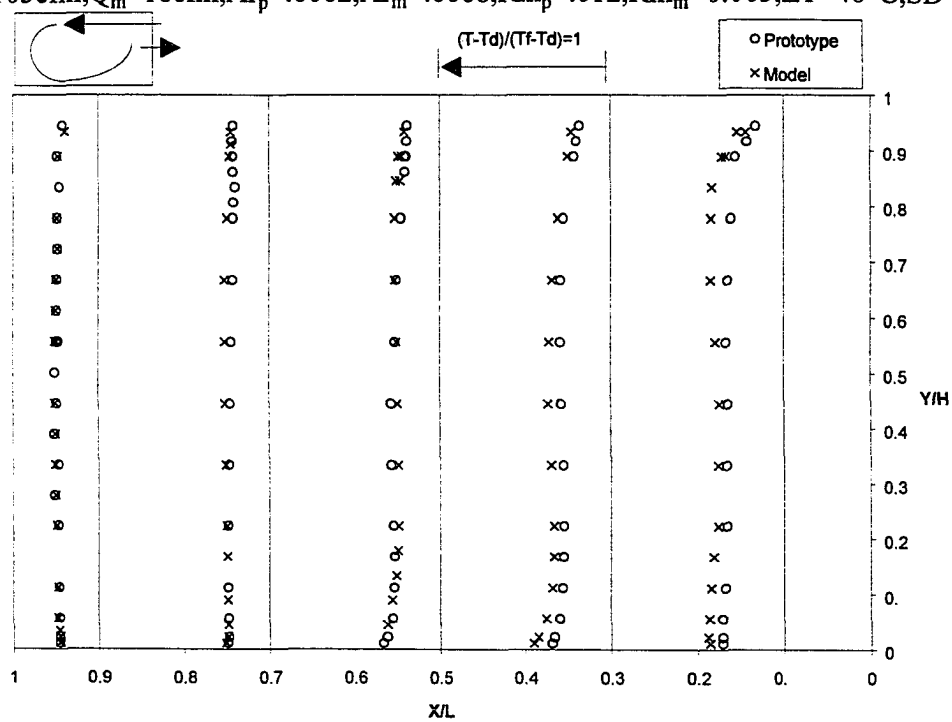

b.Q_p=105cfm,Q_m=26cfm,Ar_p=.0062,Ar_m=.0031,Rm_p=.012,Rm_m=0.012,ΔT=40°C,SD=11.8%

Figure 6.45. Comparisons of vertical nondimensional peak temperature for nonisothermal air-jet within single-circulation airflow.

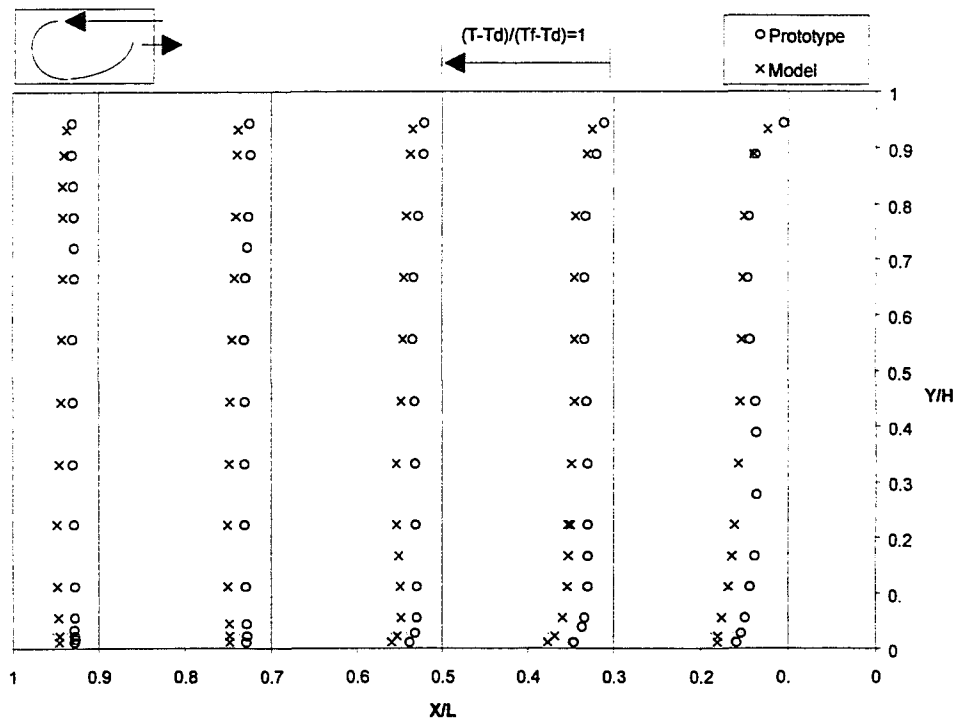

a.Q_p=221cfm,Q_m=38cfm,Ar_p=.0014,Ar_m=.0014,Rm_p=.053,Rm_m=0.026,ΔT=40°C,SD=13.6%

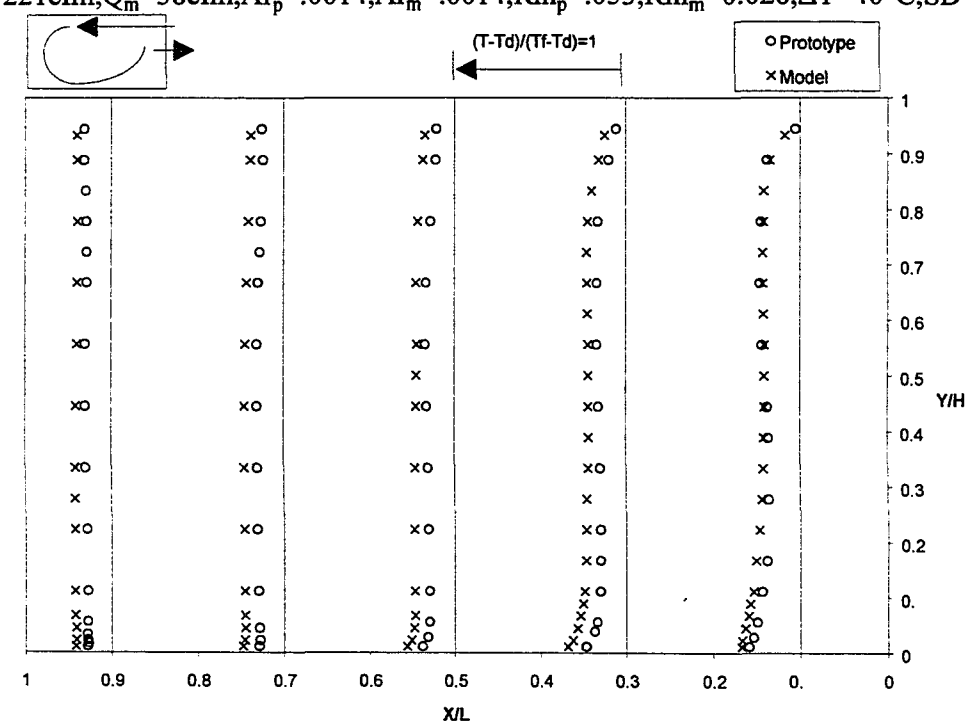

b.Q_p=221cfm,Q_m=54cfm,Ar_p=.0014,Ar_m=.007,Rm_p=0.053,Rm_m=0.052,ΔT=40°C,SD=11.1%

Figure 6.46. Comparisons of vertical nondimensional peak temperature for nonisothermal air-jet within approximate isothermal airflow.

CHAPTER 7. PRACTICAL USE OF THE RESULTS

This chapter summarizes the experimental results by giving guidelines for practical use for future studies using scale-model ceiling slot-ventilated agricultural enclosures. Figures, graphs, and tables required are presented using an example problem.

7.1. Example Problem

A prototype pig house in Ames, Iowa described in Table 7.1 and Figure 7.1 represents the building to study. The room aspect ratio (L/H) has been set to 2 when applying the results from this research.

Table 7.1. The description of a practical problem.

Items	Description
Building	Swine barn
Location	Ames, Iowa
Size L×W×H	6×20×3m
Inlet	Ceiling slot on one wall, h= 0.05m
Outlet	Circular duct on the same wall for exhaust fan, Dia.= 0.45m
Room aspect ratio	L/H=2

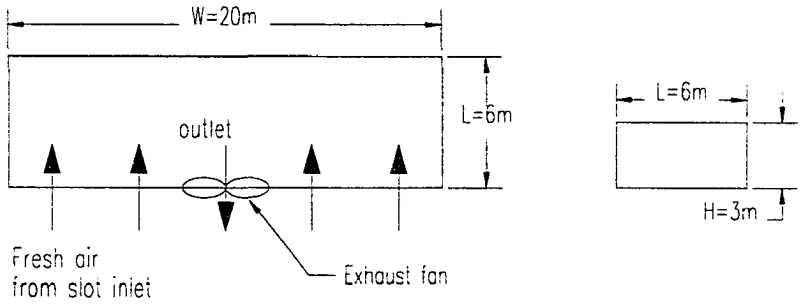

a. Top view b. End view

Figure 7.1. Configuration of the building.

7.2. Scale-Model Settings

The similitude requirements and scale-model design procedures are described in Table 7.2.

7.3. Governing Similitude Parameters for the Scale-Model

Inlet jet momentum ratio (Rm)

The Rm is defined as:

$$Rm = \frac{hU_d^{\,2}}{(L+H)} \tag{7.1}$$

where

h = slot-inlet width (= 0.05 m for this case)

U_d = inlet airspeed, m/s ($= \frac{Q}{Wh}$)

L = room length (= 6 m for this case)

H = room height (= 3 m for this case)

Table 7.2. The similitude requirements and scale-model design procedures.

Similitude requirement	Scale-model design procedure
Geometric similitude	Scaling significant dimensions and angles
Kinematic similitude	Control airflow rate based on Rm or Ar
Dynamic similitude	Control airflow rate based on Rm or Ar
Thermal similitude	Maintain similar ΔT to provide heat flux as $\frac{q_p}{q_n} = n^2$
Boundary conditions	Use similar working fluid (air), construction materials, heating source, ventilating method, and inlet design

Archimedes number (Ar)

The Ar is defined as:

$$Ar = \frac{g\beta\Delta Th}{U_d^{\ 2}} \tag{7.2}$$

where

g = gravitational acceleration rate (m/s^2)

β = thermal expansion coefficient defined as $\frac{1}{(T_f + T_d)/2}$, (1/K)

$\Delta T = T_f - T_d$ (°C) (= 10 °C at summer, and = 40 °C at winter)

h = slot-inlet width (= 0.05 m)

U_d = inlet airspeed, m/s

7.4. Airflow Pattern Similarity

The airflow pattern similarity requirements differ depending on the airflow pattern expected. The criteria based on expected airflow patterns are shown in Table 7.3. The controlling airflow rates for each airflow pattern are shown in Figure 7.2.

Table 7.3. Airflow patterns and distinguishing criteria.

Airflow patterns		Critical values	Similitude criteria	Critical summer airflow rate ΔT=10 °C		Critical winter airflow rate ΔT=40 °C	
				Q_p, cfm	Q_m, cfm	Q_p, cfm	Q_m, cfm
Two-circulation	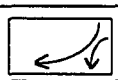	Ar>0.015	Ar	2183	$2183n^{-2.5}$	4477	$4477\ n^{-2.5}$
single-circulation	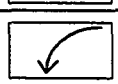	0.015>Ar >0.005	Rm, ΔT[1]	2183 to 3782	$2183\ n^{-2}$ to $3782\ n^{-2}$	4477 to 7754	$4477\ n^{-2}$ to $7754\ n^{-2}$
Fully rotary	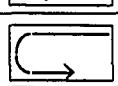	Ar<0.005	Rm, ΔT	3782	$3782\ n^{-2}$	7754	$7754\ n^{-2}$

Note 1. Similar Rm with the same heat load.

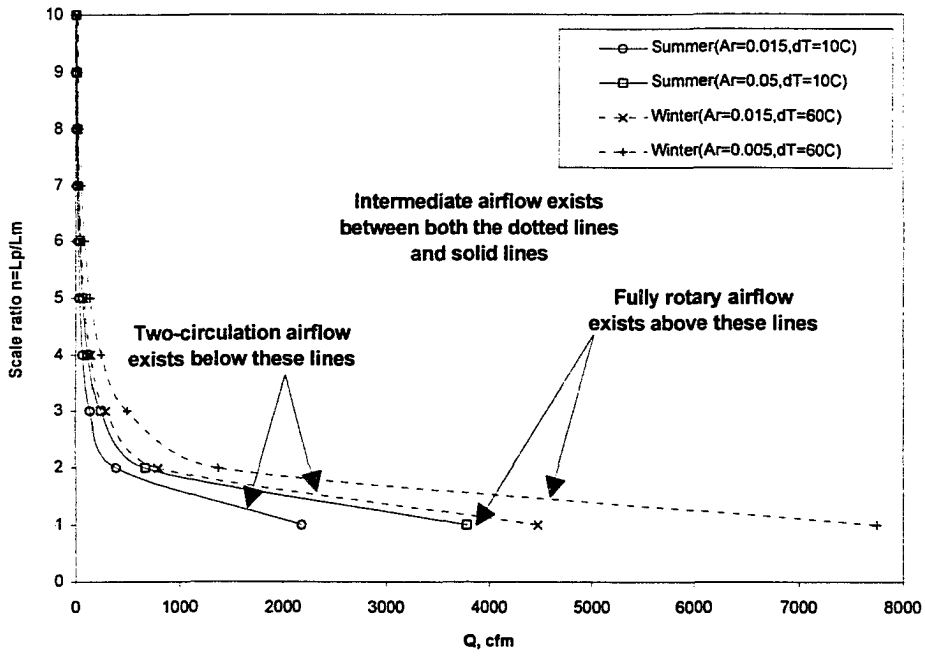

Figure 7.2. Controlled airflow rates for different airflow patterns.

7.5. Air-Jet Penetration Distance

The expression for air-jet penetration distance varies with the similitude criteria which is related to the expected airflow pattern. The design regression curves and equations are shown in Figures 7.3 and 7.4 and Table 7.4.

7.6. Floor Airspeed Distribution

The peak floor airspeed as a function of axial location and Rm with a similar ΔT and Ar are shown in Figure 7.5 and 7.6 and Table 7.5.

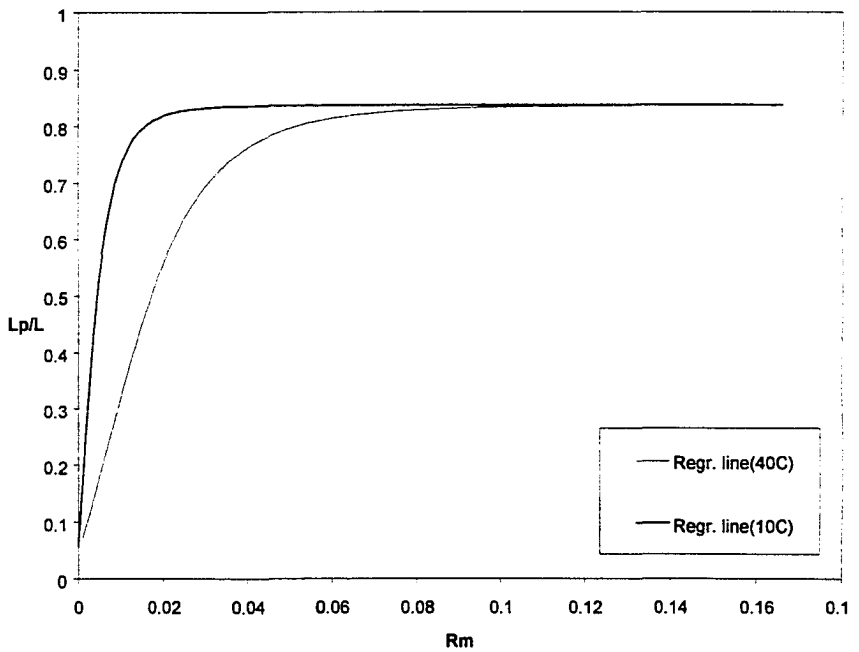

Figure 7.3. Regression curves of normalized penetration distance with Rm for single-circulation and fully rotary airflow.

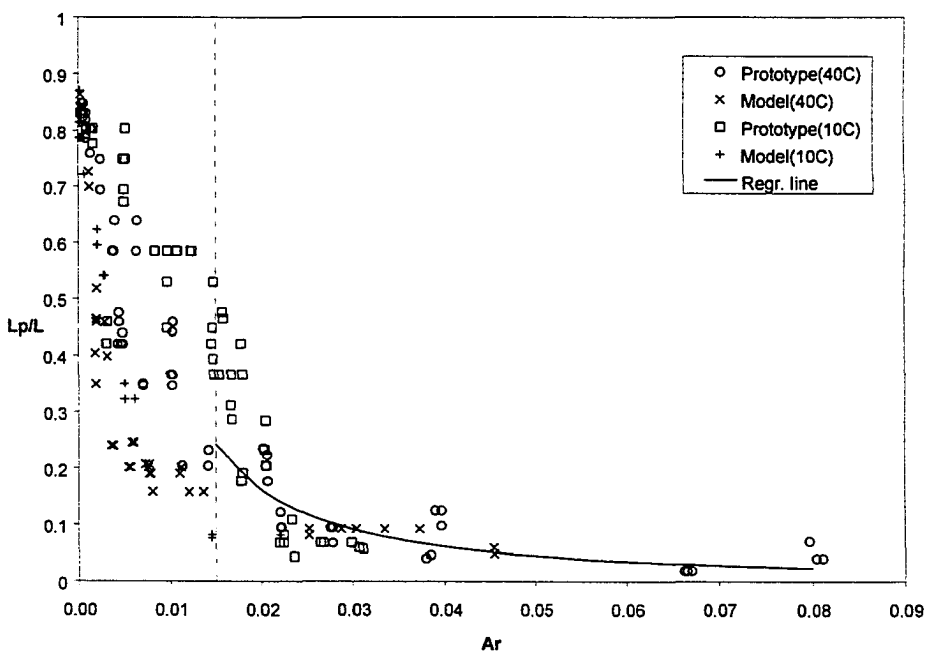

Figure 7.4. Regression curve of normalized penetration distance with Ar for two-circulation airflow.

Table 7.4. Regression equations of normalized penetration distance.

Classified regions	Similitude criteria	Equation	R^2
Isothermal airflow	Rm	$\frac{L_p}{L} = \frac{0.85}{20.18e^{-47.29\sqrt{R_m}} + 1}$	0.92
Ar<0.015	Rm and ΔT=10 °C	$\frac{L_p}{L} = \frac{0.85}{13.91e^{-45.60\sqrt{R_m}} + 1}$	0.88
	Rm and ΔT=40 °C	$\frac{L_p}{L} = \frac{0.85}{26.14e^{-27.91\sqrt{R_m}} + 1}$	0.89
Ar>0.015	Ar	$\frac{L_p}{L} = 0.0007Ar^{-1.3931}$	0.64

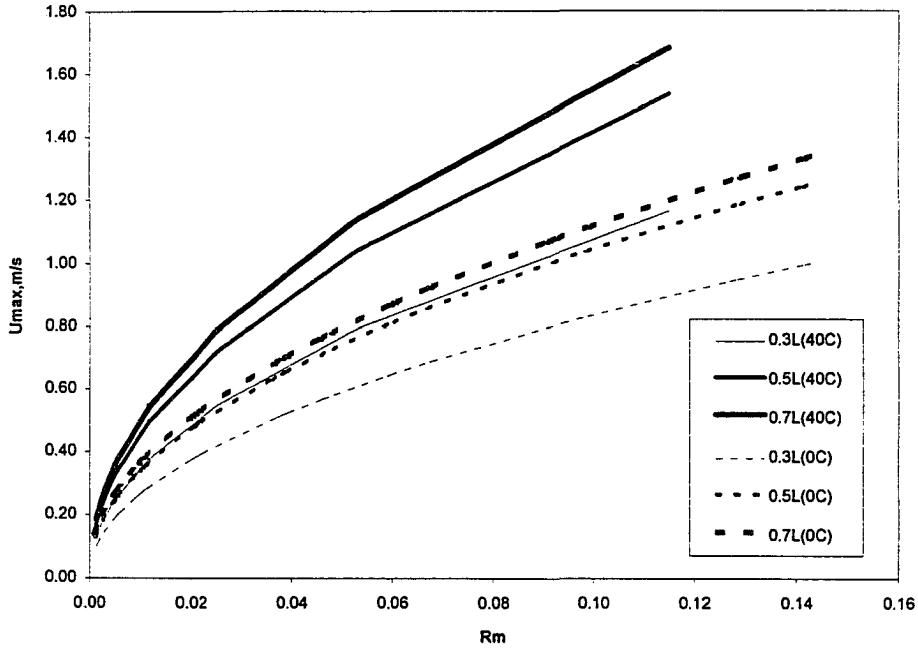

Figure 7.5. The peak floor airspeed at different position of both scale-model and prototype versus inlet jet momentum ratio (Rm).

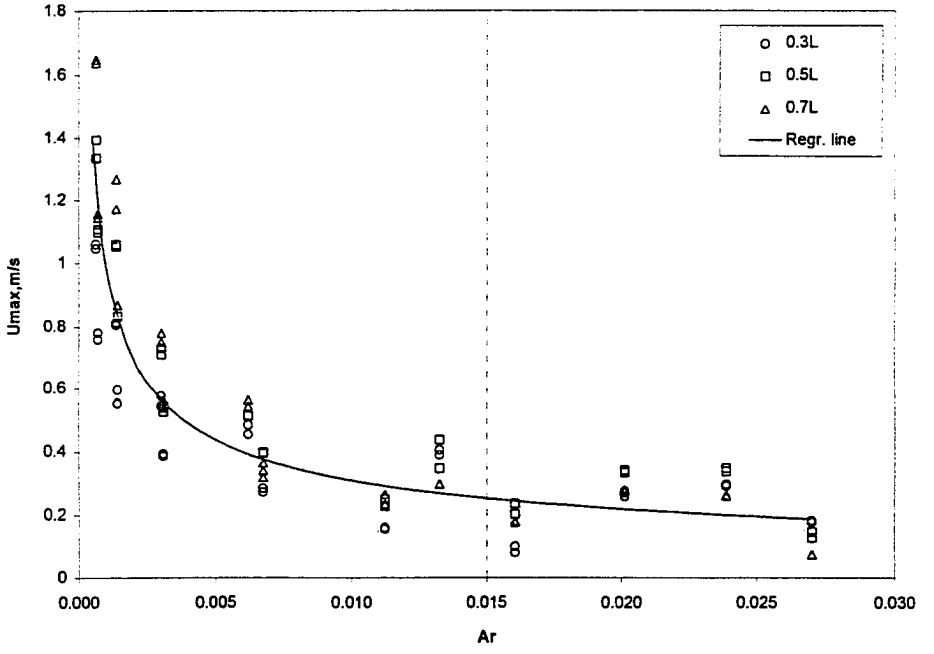

Figure 7.6. The peak floor airspeed at different positions of both scale-model and prototype versus Archimedes number (Ar) for two-circulation airflow (Ar>0.015).

Table 7.5. The regression equations of peak floor airspeed at different positions of both scale-model and prototype versus Rm or Ar.

Conditions		Positions	Regression equations	R^2
Winter time $\Delta T=40\ ^{\circ}C$	Ar<0.015	0.3L	$U_{rm}=3.44\sqrt{Rm}$	0.93
		0.5L	$U_{rm}=4.53\sqrt{Rm}$	0.96
		0.7L	$U_{rm}=4.96\sqrt{Rm}$	0.99
	Ar>0.015	0.3L to 0.7L	$U_{rm}=0.03/\sqrt{Ar}$	0.77
Summer time $\Delta T=0\ ^{\circ}C$		0.3L	$U_{rm}=2.65\sqrt{Rm}$	0.99
		0.5L	$U_{rm}=3.29\sqrt{Rm}$	0.99
		0.7L	$U_{rm}=3.52\sqrt{Rm}$	0.98

7.7. Floor Temperature Distribution

The floor temperature at the peak floor airspeed position as a function of distance from the inlet correlated to Rm as shown in Figures 7.7 and 7.8 and is expressed in Table 7.6.

7.8. The Scale-Model Design

Scale-model settings

As an example scale-model design procedure, scale-factor of n = 5 was chosen. The resulting similitude requirements are given in Table 7.7.

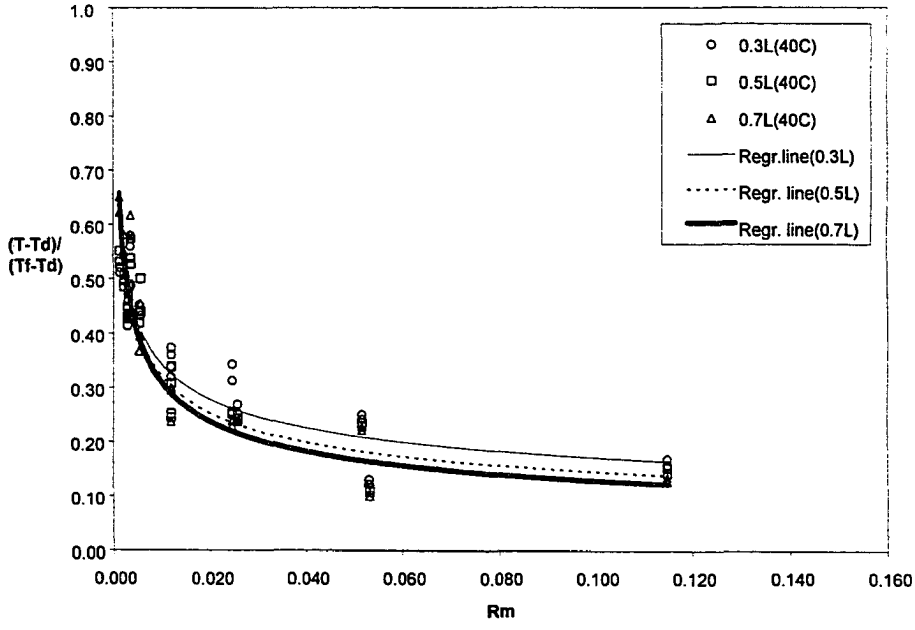

Figure 7.7. Regression curves of temperature located at peak floor airspeed at different position for both scale-model and prototype with ΔT=40 °C (winter time) versus inlet jet momentum ratio (Rm) for single-circulation and fully rotary airflow (Ar < 0.015).

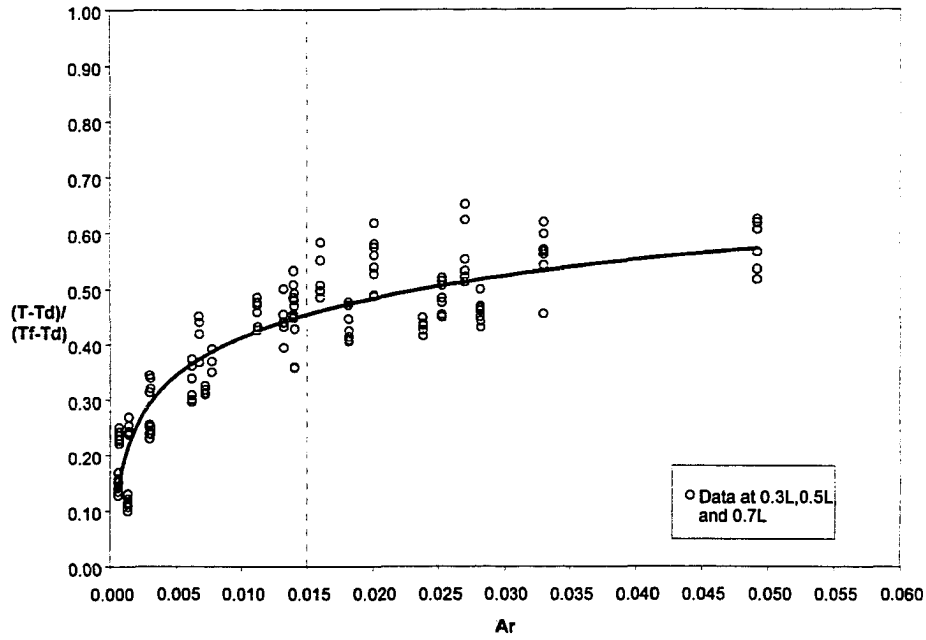

Figure 7.8. Regression curves of temperature located at peak floor airspeed at different position for both scale-model and prototype versus inlet jet momentum ratio (Rm) for two-circulation airflow (Ar > 0.015).

Table 7.6. The regression equations of temperature located at the peak floor airspeed for both scale-model and prototype.

Conditions		Positions	Regression equations	R^2
Winter time $\Delta T=40\ ^{\circ}C$	Ar < 0.015	0.3L	$\frac{T_{max}-T_d}{T_f-T_d}=0.086Rm^{-0.30}$	0.83
		0.5L	$\frac{T_{max}-T_d}{T_f-T_d}=0.066Rm^{-0.35}$	0.86
		0.7L	$\frac{T_{max}-T_d}{T_f-T_d}=0.054Rm^{-0.38}$	0.88
	Ar > 0.015	0.3L to 0.7L	$\frac{T_{max}-T_d}{T_f-T_d}=0.1\ Ln(Ar)+0.87$	0.82
Summer time $\Delta T=0\ ^{\circ}C$ [1]			$T_{max}=T_d$	

Note 1: Treat $\Delta T=0\ ^{\circ}C$ as $\Delta T=10\ ^{\circ}C$ in summer time, and the temperature environment is similar as the isothermal condition.

Table 7.7. The similitude requirements and scale-model design procedures for scale-model based on Table 7.1.

Similitude requirement	Scale-model design procedure
Geometric similitude	Scale ratio n=5 L×W×H=1.2×4×0.6 h=0.01m L/H=2
Kinematic similitude and dynamic similitude	Summer time with 60 ACH,Q_p =12713 cfm Winter time with 5 ACH, Q_p =1059 cfm Spring time with 15 ACH, Q_p= 3178 cfm Q_m is determined based on Table 7.2.
Thermal similitude	$T_{f,m} = T_{f,p} = 33°C$[1] $T_{d,m} = T_{d,p} = T_o$ (= 33°C at summer, and = -7°C at winter, and = 23°C at spring) $\Delta T_m = \Delta T_p$
Boundary conditions	Use air as working fluid, same construction materials, heating source, ventilating method, and inlet design

Note 1. The average pig skin temperature assumed 33°C.

Airflow pattern similarity

One of the objectives with the scale-model (n = 5) is to simulate expected summer and winter ventilation airflow patterns. Table 7.8 describes the similitude requirements and expected airflow patterns in the prototype. For summer conditions, the Ar_p= 0.0005 which is less than 0.005 implying that the proper similarity parameter is the Rm. as indicated in Table 7.8. The expectations are that fully rotary airflow will occur. This airflow pattern condition will be simulated if the scale-model is tested at Q_m= 509 cfm. In contrast to this, winter performance of the prototype results in an AP_R 0.275 which is > 0.015 therefore requiring Ar similarity. The expectations are that two-circulation zone airflow patterns will exist. To simulate this behavior, a scale-model airflow of Q_m= 19 cfm will be required.

Table 7.8. Airflow patterns and distinguishing criteria for scale-model based on Table 7.3.

Conditions	Q_p, cfm	Ar_p	Rm_p	Similitude criteria	Airflow patterns		Q_m ,cfm
Summer ΔT= 0°C	12713	0	0.2	Rm	Fully rotary	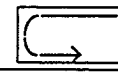	509
Winter ΔT= 40°C	1059	0.274	0.0014	Ar	Two-circulation	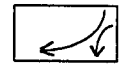	19
Spring ΔT= 10°C	3178	0.007	0.0125	Rm, ΔT	Single-circulation	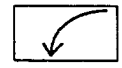	127

Air-jet penetration distance

Table 7.9 outlines the expected air-jet penetration distance in the scale-model (last column) based on the regression equations outline in Table 7.4.

Floor airspeed distribution

Table 7.10 summarizes the expected peak floor airspeeds for both the scale-model and prototype. These results were based on the regression equations shown in Table 7.5.

Table 7.9. The normalized air-jet penetration distance expected based on Table 7.4.

Conditions	Ar_p	Rm_p	Equation	L_p, m	
				Scale-model	Proto-type
Summer ΔT= 0°C	0	0.2	$\frac{L_p}{L} = \frac{0.85}{20.18e^{-47.29\sqrt{R_m}} + 1} = 0.85$	1.02	5.10
Winter ΔT= 40°C	0.274	0.0014	$\frac{L_p}{L} = 0.0007Ar^{-1.3931} = 0.0042$	0.005	0.025
Spring ΔT= 10°C	0.007	0.00125	$\frac{L_p}{L} = \frac{0.85}{13.91e^{-45.60\sqrt{R_m}} + 1} = 0.78$	0.94	4.7

Table 7.10. The peak floor airspeed at different positions based on Table 7.5.

Conditions	Positions	Regression equations	U_{rm}, m/s	
			Scale-model	Proto-type
Summer time $\Delta T = 0^{\circ}C$	0.3L	$U_{rm} = 2.65\sqrt{Rm}$	1.19	1.19
	0.5L	$U_{rm} = 3.29\sqrt{Rm}$	1.47	1.47
	0.7L	$U_{rm} = 3.52\sqrt{Rm}$	1.57	1.57
Winter time $\Delta T = 40^{\circ}C$	0.3L to 0.7L	$U_{rm} = 0.03/\sqrt{Ar}$	0.06	0.06
Spring time $\Delta T = 10^{\circ}C$[1]	0.3L	$U_{rm} = 2.65\sqrt{Rm}$	0.30	0.30
	0.5L	$U_{rm} = 3.29\sqrt{Rm}$	0.37	0.37
	0.7L	$U_{rm} = 3.52\sqrt{Rm}$	0.39	0.39

Note 1: Treat $\Delta T = 10^{\circ}C$ as $\Delta T = 0^{\circ}C$ in spring time to estimate peak floor airspeed.

Floor temperature distribution

Table 7.11 summarizes the expected floor temperature at the peak floor airspeed position for the scale-model and the prototype. Regression equations used to generate these results were given in Table 7.6.

Table 7.11. The temperature located at peak floor airspeed at different positions based on Table 7.6.

Conditions	Positions	Regression equations	T_{max}, °C	
			Scale-model	Proto-type
Summer time $\Delta T = 0^{\circ}C$	All floor region	$T_{max} = T_d$	33.0	33.0
Winter time $\Delta T = 40^{\circ}C$	0.3L to 0.7L	$\frac{T_{max} - T_d}{T_f - T_d} = 0.1\mathrm{Ln}(Ar) + 0.87 = 0.74$	22.6	22.6
Spring time $\Delta T = 10^{\circ}C$	All floor region	$T_{max} = T_d$	23.0	23.0

Note 1: Treat $\Delta T = 10^{\circ}C$ as $\Delta T = 0^{\circ}C$ in spring time, and the temperature environment is similar as the isothermal condition.

Table 7.7 to 7.11 identified the expected airflow behavior in the scale-model and prototype for summer and winter ventilation performance. At intermediate airflow, the scale-model results can be used to predict the air-jet behavior in the prototype.

CHAPTER 8. CONCLUSIONS

Scale-model studies of the ventilation characteristics inside enclosures is a reliable method to simulate airflow patterns, the velocity field, and the temperature field in a prototype, provided that an acceptable similitude scaling parameter can be found. The results conducted from both the isothermal and nonisothermal experiments are summarized below.

8.1. Isothermal Airflow

A comparison of airflow patterns and the airspeed field between a scale-model and prototype using either inlet jet momentum ratio (Rm) and Reynolds number (Re) as the similarity criteria indicated that for isothermal airflow in a ceiling slot-ventilated enclosure, Rm was better than Re for use as the similarity criterion. The comparisons of airspeed field along ceilings showed that Rm is better than Re as the similitude parameter. However, the comparisons of Rm and Re had insignificant difference in the floor region.

The evaluation of using either the Rm or Re as the similitude parameter was conducted using measurements of air-jet penetration distance, airflow pattern, and airspeed field. From these results, the following conclusions are made:

1. The threshold air-jet penetration distance was 0.84 L and the threshold Rm was 0.02 for both the scale-model and prototype.
2. The normalized air-jet penetration distance in both scale-model and prototype can be described using equation 6.3, where:

$$\frac{L_p}{L} = \frac{0.84}{20.18e^{-47.29\sqrt{Rm}} + 1} \tag{8.1}$$

3. The airflow patterns for isothermal airflow were approximately similar to those described by Jin and Ogilvie (1990).

4. Fully rotary airflow resulted in self-similar flow between the scale-model and prototype and was independent of further increases in either the Re or Rm.

5. Rm was found to be the appropriate similitude criterion for ceiling slot-ventilated enclosures for intermediate airflow. Intermediate airflow was defined as the airflow pattern between the stagnant and fully rotary zones.

The peak airspeed decay follows equation (3.5) before the air-jet terminated. The jet throw can be determined by this property, and the airflow pattern is also affected by this characteristic. The throw constant (C_w) related to the variation of momentum flux. Thus, similar momentum flux variation resulted in a similar airspeed field between scale-model and prototype (Launder and Rodi, 1981).

Pressure variation along the air-jet due to friction loss reflected the momentum flux variation. The pressure forces appear to dominate the air-jet performance within an enclosure, which has been stated by previous researchers (Timmons, 1979; Roussea and Albright, 1996). The Euler number (Eu) (related to Rm) is justified to be the similarity criterion for isothermal airflow in a ceiling slot-ventilated enclosure.

It is concluded that similarity criteria are dependent only on geometric similitude and similar boundary conditions when the airflow rate was beyond the fully rotary airflow pattern. The pressure forces dominate airflow within an enclosure and Rm (related to Eu) is

the similarity requirement within intermediate airflow and stagnant zone. Re is expected to be the similarity requirement when viscous forces dominate the airflow at low values of Re.

8.2. Nonisothermal Airflow

Similitude for nonisothermal airflow was determined by the magnitude of governing forces. The main forces affecting airflow motion for nonisothermal airflow within a room are inertial forces, buoyant forces, pressure forces, and viscous forces accounted for in the parameters Ar, Re, and Eu. Ar and Rm (related to Eu) were studied in this research project.

The comparison of using Ar and Rm with the same heat load between the scale-model and prototype for nonisothermal airflow was conducted using measurements of air-jet penetration distance, airflow pattern, airspeed field, and temperature field. From these results the following conclusions were made:

1. The threshold penetration distance was 0.84 L, where the threshold Rm was 0.066 for $\Delta T = 40\ ^{\circ}C$ and 0.02 for $\Delta T = 10\ ^{\circ}C$ for both the scale-model and prototype.
2. The penetration distance was found to be a function of the Rm and is described in Table 6.7.
3. The nonisothermal airflow patterns were classified as shown in Table 6.10, with ranges similar to the results shown by previous research (Mullejans, 1966; Randall and Battams, 1979).

4. Fully rotary airflow patterns were self-similar, and since the thermal environment was affected by the airspeed field, it was shown that similitude could be reached with a similar Rm and heat load.

5. Nonisothermal airflow will be similar to isothermal airflow when the Ar is below 0.005 (Ar_c=30) which agrees with Randall and Battams (1979).

6. Ar is the appropriate similitude criterion between scale-model and prototype when the airflow pattern is a two-circulation zone airflow.

When the Ar is below 0.005 (A_c< 30), the behavior of nonisothermal airflow is similar to isothermal airflow using Rm (related to Eu) and the same heat load as the appropriate similarity criteria. Fully rotary airflow was reached with an increased airflow rate or decreased heat load and Rm with the same heat load between scale-model and prototype was still the appropriate similarity criteria because the thermal environment is effected by the airspeed field and the temperature field is not independent of the airflow rate. When the nonisothermal airflow condition becomes two-circulation zone airflow (Ar>0.015), buoyant forces and inertial forces dominate the airflow behavior resulting in the Ar being the appropriate similarity criterion. The airflow pattern between two-circulation zone airflow and approximate isothermal airflow is single-circulation airflow using Rm and same heat load as similitude criteria.

CHAPTER 9. RECOMMENDATIONS

The critical values for various airflow patterns such as the threshold values that divide single-circulation and two-circulation airflow, and unstable versus stable airflow patterns are important evaluations for similitude between a scale-model and prototype. The threshold Reynolds number (Re) for isothermal airflow patterns is proportional to model scale (Timmons, 1984), but the same threshold inlet jet momentum ratio (Rm) was found between different scale-models by Adre and Albright (1994) and this research-project.

The threshold Rm was different between the above experiments due to differences in scale-model configuration. Further investigations to determine an identity threshold value for a similarity parameter between different scale-models with similar configurations are required to validate the appropriate similarity parameters for isothermal airflow. In the same manner, using the jet momentum function (I_o= 0.01 kg/m^2-s^2) as a critical value of airflow rate to distinguish stable and unstable airflow patterns needs further investigation since the results of stable airflow pattern existed in the scale-model when defined as unstable airflow according to the jet momentum function.

It is believed that Re should dominate the airflow pattern behavior within the room for specific conditions but the critical value is still unknown.

On the other hand, a more critical evaluation of the air-jet parameters should be measured to confirm the similarity between scale-model and prototype. For example, the separation point of the air-jet may be measured from the static pressure variation at the ceiling. The

performance of air-jets inside an enclosure may be influenced by the static pressure, turbulence intensity, turbulent kinetic energy, and momentum flux. Understanding these characteristics of confined airflow are helpful to verify similitude between scale-model and prototype.

Most of the realistic airflow patterns expected ranged between unstable airflow and fully rotary airflow. Future research should extend the range of intermediate airflow to provide more observations to validate the airflow between scale-model and prototype in this region. One possible method is to extend the enclosure length such that more measurements can be made in varied intermediate airflow.

Different scale dimensions and configuration of scale-models affect airflow behavior inside an enclosure. Investigations among various layouts between different room sizes are recommended to validate the change of similarity criteria in different buildings.

Further experiments can be improved by maintaining a similar thermal environment. One available method is to reduce radiation heat transfer by shielding walls with aluminum foil. Better control of the surrounding environment is required to assure the required inlet air properties and boundary conditions. Advanced techniques of instrumentation should be used in this experiment including image processing and laser anemometry.

Most research regarding the air-jet has been focused on the unconfined air-jet. The characteristics of confined airflow should be investigated to provide more information for practical problems such as of building environmental control.

The validation of similitude between scale-model and prototype were accomplished experimentally. It would be interesting to find the results from computational simulation and compare these results with the results from this project.

To find a universal similitude criterion for both isothermal and nonisothermal airflow in all conditions between scale-model and prototype in a ceiling slot-ventilated enclosure may be impossible but the pursuit of this is the final goal of this research.

APPENDIX A. CALIBRATION OF EXPERIMENTAL MEASUREMENTS

A.1. Orifices

The airflow rate experiments were measured by using orifices with diameters of 2 1/2 and 4 in. Airflow rate data was acquired from the pressure difference between the upstream and downstream locations of the orifice as was shown in Figure 5.4. Calibration of the 2 1/2 in orifices were made using a venturi flow meter (Model 2017L-V; TSI, Inc.). The results are shown in Figures A.1 and A.2. Calibration of the 4 in orifice was achieved using the calibrated fan-chamber in the Air Quality Laboratory of the Agricultural and Biosystems Engineering Department at Iowa State University. The venturi flow meter was also used to calibrate the 4 in orifice as a further calibration check. The results are shown in Figure A.3.

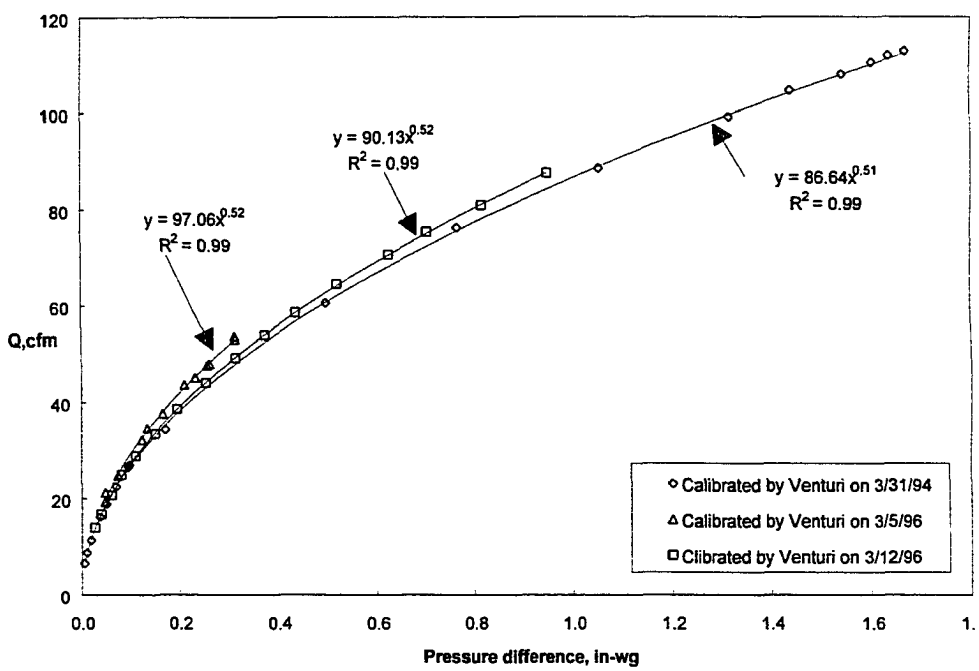

Figure A.1. Calibration of No.3 2.5 in orifice.

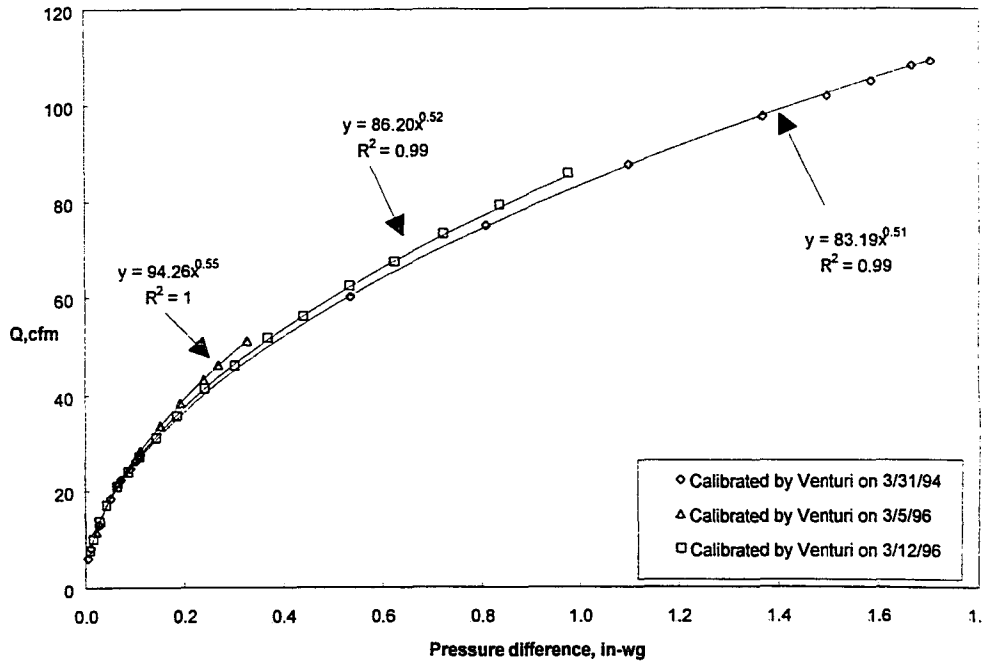

Figure A.2. Calibration of No.4 2.5 in orifice.

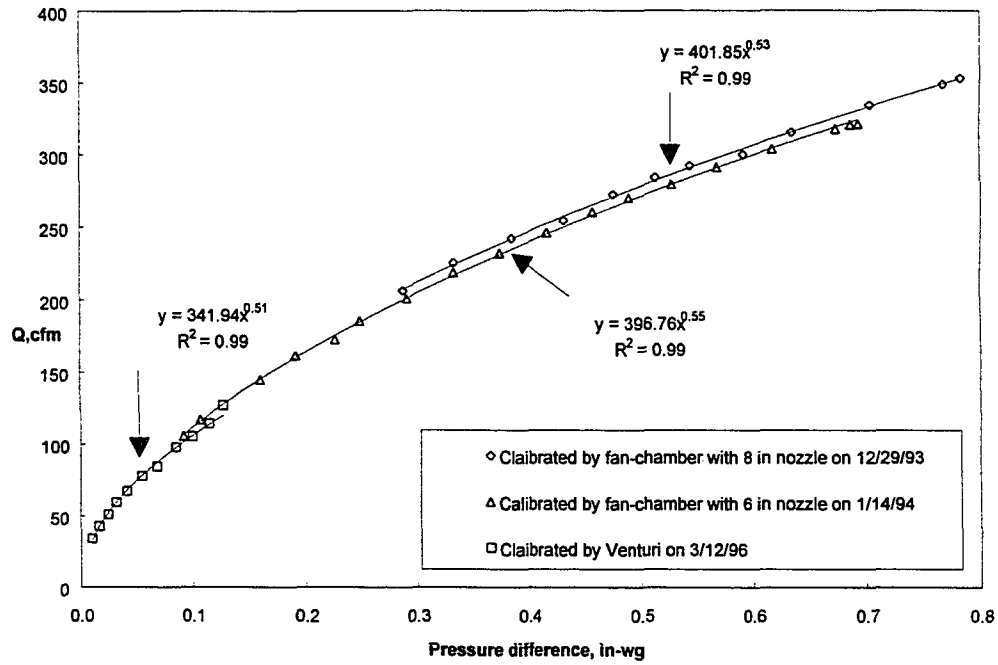

Figure A.3. Calibration of No.3 4 in orifice.

All calibration plots show similar results with each method used. The regression equations are shown in Table A.1. The 95% confidence interval for each coefficient are also listed Table A.1.

A.2. Hot-Film Anemometers

Calibration of each hot-film anemometer was made with intervals of three months. One such calibration was made on March 13, 1996 and this is shown in Figure A.4. The calibration airspeed was derived from the venturi flow meter. The maximum velocity (U_{max}) in a turbulent Hagen-Poiseuille flow (i.e. circular pipe flow) has been experimentally expressed as (Fox and McDonald, 1973):

$$\frac{U_{max}}{U_{avg}} = \frac{(n+1)(2n+1)}{2n^2} \qquad (A.1)$$

where

U_{avg} = average velocity of pipe defined as Q/A (m/s);

n = a value that varies with the Reynolds number as shown in Table A.2

Table A.1. The calibration characteristics of orifices.

Orifice number	Diameter, in	Constants for regression equation $Q = \alpha(PD)^{\beta}$			R^2
		Q	α	β.	
3	2.5	$86.64(PD)^{0.51}$±1.03	86.64±1.01	0.51±0.0035	0.99
4	2.5	$83.19(PD)^{0.51}$±1.03	86.64±1.01	0.51±0.0045	0.99
3	4	$396.76(PD)^{0.55}$±1.02	396.76±1.01	0.55±0.0065	0.99

Note 1: Q = airflow rate (cfm), PD = pressure difference across orifice (in-wg).

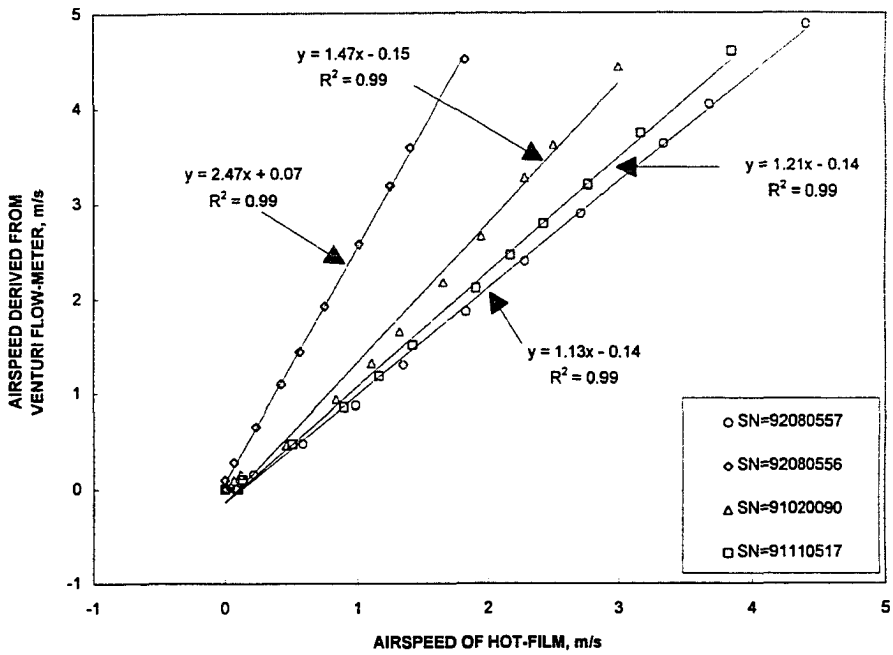

Figure A.4. Calibration curves for each hot film anemometer used. SN stands for the Serial Number of the probe.

The calibrated anemometer probe was placed at the center of the tube to measure the peak airspeed. Four hot-film anemometers with different Serial numbers (SN) showed different curves related to the airspeed derived from the venturi flow meter. The regression equations and 95% confidence levels are shown in Table A.3.

Table A.2. Values of n in equation (A.1).

Re	n
4.0×10^{3}	6
1.1×10^{5}	7
3.2×10^{6}	10

Table A.3. The calibration characteristics for each hot-film anemometer.

Serial number	Constants of regression equation $y=\alpha x+\beta^1$			R^2
	y	α	β	
91020090	1.47x-0.15±0.31	1.47±0.091	-0.15±0.146	0.99
91110517	1.21x-0.14±0.17	1.21±0.039	-0.14±0.077	0.99
92080556	2.47x+0.07±0.09	2.47±0.044	0.07±0.039	0.99
92080557	1.13x-0.14±0.15	1.13±0.031	-0.14±0.071	0.99

Note 1: y = standard airspeed derived from Venturi flow meter (m/s),
x = airspeed measured by hot-film anemometer (m/s).

A.3. Thermocouple Wires

The temperature was measured using T-type thermocouple wires. The calibration was conducted with intervals of three months. The calibration was compared with the temperature measured by a mercury thermometer by placing both the thermocouple and thermometer in clean water with different temperatures. The results of calibration on April 3, 1995 are shown in Figure A.5. The regression equation and 95% confidence uncertainly were shown in Table A.4.

Table A.4. The calibration characteristics of thermocouple wires.

Sensor	Constants of regression equation $y=\alpha x+\beta^1$			R^2
	y	α	β	
1	1.03x-0.76±0.50	1.03±0.0175	-0.76±0.686	0.99
2	x-0.37±0.76	1±0.0258	-0.37±1.031	0.99
3	1.02x-1.68±1.36	1.02±0.0470	-1.68±1.913	0.99

Note 1: y = temperature of thermometer (°C),
x = temperature of thermocouple wires (°C).

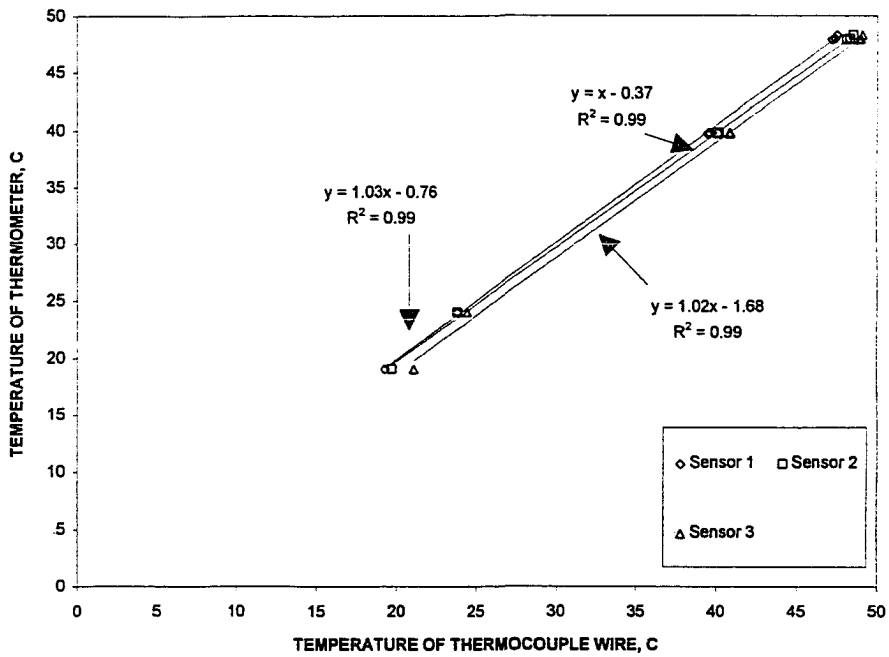

Figure A.5. Calibration of thermocouple wires.

REFERENCES

Abramovich, G. N. 1963. *The theory of turbulent jets*. MIT Press. Cambridge, MA.

Adre, N. And L. D. Albright. 1991. Establishment of desired air flow patterns in slotted-inlet ventilated enclosures. ASAE Paper No. 91-4022. St. Joseph, MI.

Adre, N. And L. D. Albright. 1994. Criterion for establishing similar air flow patterns (isothermal) in slotted-inlet ventilated enclosures. *Transactions of the ASAE* 37(1):235-250.

Adre N., L. D. Albright and M. L. Hellickson. 1995. Control of nonisothermal airflow patterns in livestock confinement facilities equipped with slotted-inlet ventilation systems(sives). ASAE Paper No. 95-4643. St. Joseph, MI.

Albertson, M. L., Y. B. Dai, R. A. Jensen and H. Rouse. 1950. Diffusion of submerged jets. *ASCE Transactions* 115:639-664.

Albright, L. D. 1976. Air flow through hinged baffle slotted inlets. *Transactions of the ASAE* 19(4):728-735.

Albright, L. D. 1989. Slotted inlet baffle control based on inlet jet momentum numbers. *Transactions of the ASAE* 32(5):1764-1768.

Anderson, D. A., J. C. Tannehill, and R. H. Pletcher. 1984. *Computational Fluid mechanics and heat transfer*. Hemisphere Publishing Co., New York, NY.

Awbi, H. B. and A. A. Setrak. 1986. Numerical solution of ventilation air jet. *Proc. 5th Int. Symp. On the Use of Computers for Environmental Engineering Related to Buildings*. Bath, UK. July, 1986, PP.236-46.

Awbi, H. B. 1991. *Ventilation of buildings*. Chapman & Hall, London.

ASHRAE. 1993. *ASHRAE Handbook: Fundamentals*. American society of Heating, Refrigeration and Air-Conditioning Engineers, Atlanta, GA.

Barber, E. M., S. Sokhansanj and W. P. Lampman. 1982. Stability of airflow patterns in ventilated airspaces. ASAE Paper No. 82-4551. St. Joseph, MI.

Baturin. V. V. 1972. *Fundamentals of Industrial Ventilation*. 3rd edition. Pergamon Press, Oxford, U.K.

Berckmans, D., J. M. Randall, D. Van Thielen, and V. Goedseels. 1993. Validity of the Ar in ventilating commercial livestock buildings. *J. Agric. Engng. Res.* 56:239-251.

Bodman, G. R. 1976. Non-mechanical ventilation of animal housing facilities. ASAE Paper No. 76-4041. St. Joseph, MI.

Chen, C. J. and W. Rodi. 1980. *Vertical turbulent buoyant jets-a review of experimental data.* Pergamon Press Ltd., Oxford, England.

Christianson, L. L., G. L. Riskowski, J. S. Zhang and R. Koca. 1988. Predicting air velocity at the pig level. In *Proceedings of the third international livestock environment symposium.* Toronto, Canada.

Fissore, A. and G. Liebecq. 1990. Experimental study of air jets pathways in large slot ventilated spaces. In *Room Vent '90,* Proc. 2nd international conference on engineering aero- and thermodynamics of ventilated rooms, session D2. Oslo, Norway, 13-15 June.

Fissore, A. A. and G. A. Liebecq. 1991. A simple empirical model for predicting velocity distributions and comfort in a large slot-ventilated space. *ASHRAE Transactions* 97(2):1087-1095.

Forthmann, E. 1934. Turbulent jet expansion. National Advisory Comittee for Aeronautics, Techanical Memorandum No. 789.

Fox, R. W. and A. T. McDonald. 1973. *Introduction to fluid mechanics.* John Wiley & Sons, Inc., New York, NY.

Franklin, G. F., J. D. Powell and M. L. Workman. 1990. *Digital control of dynamic systems.* 2nd edition. Addison-Wesley Publishing Co., Inc., Reading, MA.

Hanzawa, H., A. K. Melikow, and P. O. Fanger. 1987. Airflow characteristics in the occupied zone of ventilated spaces. *ASHRAE Transactions* 93(1):524-539.

Hinze, J. O. 1975. *Turbulence.* 2nd edition McGraw-Hill, Inc., New York, NY.

Jin, Y. and J. R. Ogilvie. 1990. Near floor air speeds from center slot air inlets in swine barns. ASAE Paper No. 90-4004. St. Joseph, MI.

Jin, Y. and J. R. Ogilvie. 1992. Airflow characteristics in the floor region of a slot ventilated room (isothermal). *Transactions of the ASAE* 35(2):695-702.

Kaul, P., W. Maltry, H. J. Muller and V. Winter. 1975. Scientific-technical principles for the control of the environment in livestock houses and stores. Translation 430. Brit. Soc. Res. Agric. Eng., N.I.A.E., Silsoe, England.

Kays, W. M. and M. E. Crawford. 1980. *Convective Heat and Mass Transfer*. McGraw-Hill, Inc., New York, NY.

Koestel, A. 1955. Paths of horizontally projected heated and chilled air jets. *Transactions ASHVE* 61:213-232.

Launder, B. E. and W. Rodi. 1981. The turbulent wall jet. *Progressing Aerospace Sci.* 19:81-128.

Leonard J. J. and J. B. McQuitty. 1986a. Archimedes number criteria for the control of cold ventilation air jets. *Canadian Agricultural Engineering* 28:117-123.

Leonard, J. J. and J. B. McQuitty. 1986b. The use of Archimedes number in the design of ventilation systems for animal housing. *Proc. Conference on Agricultural Engineering* 1986, Institution of Engineers, Camberra, Australia.

Leonard J. J. and J. B. McQuitty. 1988. Air mixing in a mechanically ventilated room. *Canadian Agricultural Engineering*. 30:185-189.

Li, Z. H., J. S. Zhang, A. M. Zhivov and L. L. Christianson. 1993. Characteristics of diffuser air jets and airflow in the occupied regions of mechanically ventilated rooms-a literature review. *ASHRAE Transactions* 99(1):1119-1127.

Liepmann, H. W. and J. Laufer. 1947. Investigation of free turbulent mixing. NACA TN1257.

Liu, Q., S. J. Hoff., and D. S. Bundy. 1995. A comparison of three proposed ventilation criteria. ASAE Paper No. 95-4642. St. Joseph, MI.

Myers, G. E., J. J. Schauer and R. H. Eustis. 1963. Plane turbulent wall jet flow development and friction factor. *ASME Journal of Basic Engineering* 47-54.

Moog, W. 1981. Room flow tests in a reduced-scale. *ASHRAE Transactions* 87(4):1162-1181.

Mullejans H. 1966. The similarity between non-isothermal flow and heat transfer in mechanically ventilated rooms. BRISA. Translation 202. Heating and Ventilating Research Association, Bracknell, UK.

Murphy, G. 1950. *Similitude in Engineering*. Ronald Press Co., New York, NY.

Nevins, R. G. 1976. *Air diffusion dynamics-theory, design and applications*. Business News Publishing Co., Birmingham, MI.

Nielsen, P.V. 1976. Flow in air-conditioned rooms-Model experiments and numerical solutions of the flow equations. English translation of Ph.D. dissertation. Technical University of Denmark, Lyngby, Denmark.

Nielsen, P. V., A. Restivo and J. H. Whitelaw. 1978. The Velocity characteristics of ventilated rooms. *J. of Fluids Eng.* 100(9):291-298.

Nielsen, P. V., A. Restivo and J. H. Whitelaw. 1979. Buoyancy-affected flows in ventilated rooms. *Numerical Heat Transfer* 2:115-127.

Nielsen, P. V. 1988. Numerical prediction of air distribution in rooms-status and potentials. In *Building Systems: Room Air and Air Contaminant Distribution*, ed. L. L. Christianson, 31-38, ASHRAE, Atlanta, GA.

Ogilvie, J. R., E. M. Barber and J. M. Randall. 1990. Floor air speeds and inlet design in swine ventilation systems. *Transactions of the ASAE* 33(1):255-259.

Pai, S. 1954. *Fluid dynamics of jets*. D. Van Nostrand Co., Inc., Toronto, Canada.

Parczewski K. I. and P. N. Renzi. 1963. Scale model studies of temperature distributions in internally heated enclosures. *ASHRAE Transactions* 69:453-463.

Pattie, D. R. and W. R. Milne. 1966. Ventilation airflow patterns by use of models. *Transactions of the ASAE* 9(5):646-649.

Rajaratnam, N. 1976. *Turbulent jets*. Elsevier Scientific Publishing Co., Amsterdam, Netherlands.

Randall, J. M. and V. A. Battams. 1979. Stability criteria for airflow patterns in livestock buildings. *J. of Agri. Engng. Res.* 24(3):361-374.

Rousseau, A. N. and L. D. Albright. 1996. An alternative kinematic similarity criterion for slot-ventilated enclosures. *Transactions of the ASAE* 38(6):1887-1889.

Schlichting, H. 1979. *Boundary-Layer Theory*. McGraw-Hill, Inc., New York, NY.

Schwarz, W. H. and W. P. Cosart. 1961. The two-dimensional turbulent wall jet. *J. of Fluid Mechanics* 10(4):481-495.

Shepherd, D. G. 1965. *Elements of fluid mechanics*. Brace & World, Harcourt, NY.

Sigalla, A. 1958. Measurements of skin friction in a plane turbulent wall jet. *J. of the Royal Aeronautical Society* 6:873-877.

Smith, M. R. 1965. Ventilating Characteristics of slotted inlets for livestock buildings. Unpublished Ph. D. dissertation. Iowa State University. Ames, IA.

Smith, M. R. and T. E. Hazen. 1968. Similitude study of Ventilation-inlet configuration. *Transactions of the ASAE* 11(2):218-225,235.

Szucs, E. 1980. *Similitude and Modeling.* Elsevier Scientific Publishing Co., Amsterdam, Netherlands.

Tennekes, H. and J. L. Lumley. 1972. *A First Course in Turbulence.* MIT Press, Cambridge, MA.

Thorshauge, J. 1982. Air-velocity fluctuations in the occupied zone of ventilated spaces. *ASHRAE Transactions* 88(2):753-764.

Timmons, M.B. 1979. Experimental and numerical study of air movement in slot-ventilated enclosures. Unpublished Ph.D. disserttion. Cornell University, Ithaca, NY.

Timmons, M. B., L. D. Albright, R. B. Furry and K. E. Torrance. 1980. Experimental and numerical study of air movement in slot-ventilated enclosures. *Transactions of the ASAE* 86(1):221-239.

Timmons, M. B. and G. Baughman. 1981. Similitude analysis of ventilation by stack effect from an open ridge livestock structure. *Transactions of the ASAE* 14:1030-1034.

Timmons, M. B. 1984. Use of physical models to predict the fluid motion in slot-ventilated livestock structures. *Transactions of the ASAE* 27(2):502-507.

Tuve, G. L. 1953. Air velocities in ventilating jets. *ASHVE Transactions* 59:261.

Wang J. and J. R. Ogilvie. 1994a. Design guidelines for airflow patterns in slot-inlet rooms: non-isothermal. ASAE Paper No. 94-4534. St. Joseph, MI.

Wang, J. and J. R. Ogilvie. 1994b. Design guidelines for floor velocity distribution in slot-inlet ventilated buildings. ASAE Paper No. 94-4536. St. Joseph, MI.

White, F. M. 1991. *Viscous fluid flow.* 2nd edition. McGraw-Hill, Inc., New York, NY.

Yao, W. Z., L L. Christianson and A. J. Muehling. 1986. Air movement in neutral pressure swine buildings-similitude theory and test results. ASAE Paper No. 86-4532, St. Joseph, MI.

Young, D. F. 1994. *Similitude, Modeling, and Dimensional Analysis in Engineering.* Unpublished Lecture Notes and Problems for Em584 in Iowa State University.

Yu, H. and S. J. Hoff. 1994. Validation of the momentum ratio concept for isothermal airflow similarity in a ceiling slot-ventilated enclosure. ASAE Paper No. 94-4582. St. Joseph, MI.

Zhang, J. S., L. L. Christianson and G. L. Riskowski. 1991. Effect of diffuser air velocity profiles on scaling methods for predicting room air motion. ASAE Paper No. 91-4558. St. Joseph, MI.

Zhang, J. S. 1991. A fundamental study of two dimensional room ventilation flows under isothermal and non-isothermal conditions. Unpublished Ph.D. dissertation. University of Illinois at Urbana-Champaign, Urbana, IL.

Zhang, J. S., G. J. Wu and L. L. Christianson. 1993. A new similitude modeling technique for studies of nonisothermal room ventilation flows. *ASHRAE Transactions*: 99(1):129-138.

ACKNOWLEDGMENTS

I would like to express my sincere appreciation to my advisor, Dr. Steven J. Hoff, for his special guidance, support, advise, encouragement, and friendship. He always gave me help and encouragement whenever I needed it. His enthusiasm and dedication to guide a student and conduct research are a standard model worth following.

I would also like to express my gratitude to my special committee, Dr. Dwaine S. Bundy, Dr. Gregory M. Maxwell, Dr. Ron M. Nelson, Dr. Joseph M. Prusa, and Dr. Richard J. Smith for their time, efforts, patience, and interests. They always gave me their hands whenever I met problems and asked their help.

Many people in the Agricultural and Biosystems Engineering Department have made significant contribution to this project. Especially Dr. Qianbao Liu, when he studied in the Department who provided me much suggestion and discussion to solve the problems of the project; Marc P. Lott, the technician of the Department, his enthusiasm helped me to solve the problems I met in my experiments; Mark E. Oberreuter and Todd Van Hal, the graduate student and undergraduate student who helped me construct the experimental facilities.

Thanks are also extended to all those who helped me at Iowa State University. I also appreciate the National I-Lan Institute of Agriculture and Technology of Republic of China who provided me the opportunity to study for my doctoral degree.

Finally, I would like to thank my mother and my wife, they give me their love and care in my life. My wife also helped me in the experiments and typed the final report.